UNIVERSITÀ DEGLI STUDI DI TRIESTE

DIPARTIMENTO DI ELETTROTECNICA, ELETTRONICA ED INFORMATICA

XX Ciclo del
Dottorato di Ricerca in
Ingegneria dell'Informazione
(Settore scientifico-disciplinare: ING-INF/03)

TESI DI DOTTORATO

Beamforming Techniques for Wireless Communications in Low-Rank Channels: Analytical Models and Synthesis Algorithms

Dottorando
MASSIMILIANO COMISSO

Coordinatore
Chiar.mo Prof. Alberto Bartoli
(Università degli Studi di Trieste)

Tutore
Chiar.mo Prof. Fulvio Babich
(Università degli Studi di Trieste)

Relatore
Chiar.mo Prof. Lucio Manià
(Università degli Studi di Trieste)

Correlatore
Chiar.mo Prof. Roberto Vescovo
(Università degli Studi di Trieste)

Summary

The objective of this thesis is discussing the application of multiple antenna technology in some selected areas of wireless networks and fourth-generation telecommunication systems. The original contributions of this study involve, mainly, two research fields in the context of the emerging solutions for high-speed digital communications: the mathematical modeling of distributed wireless networks adopting advanced antenna techniques and the development of iterative algorithms for antenna array pattern synthesis. The material presented in this dissertation is the result of three-year studies performed within the Telecommunication Group of the Department of Electronic Engineering at the University of Trieste during the course of Doctorate in Information Engineering.

In recent years, an enormous increase in traffic has been experienced by wireless communication systems, due to a significant growth in the number of users as well as to the development of new high bit rate applications. It is foreseen that in the near future this trend will be confirmed. This challenging scenario involves not only the well established market of cellular systems, but also the field of emerging wireless technologies, such as WiMAX (Worldwide interoperability for Microwave Access) for wireless metropolitan area networks, and Wi-Fi (Wireless Fidelity) for wireless local area networks, mobile ad-hoc networks and wireless mesh networks. The rapid diffusion of architectures adopting an ad-hoc paradigm, in which the network infrastructure is partially or totally absent and that can be deployed using low-cost self-configuring devices, has further enlarged the number of systems that have to coexist within a limited frequency spectrum. In such evolving environment, the development of interference mitigation methods to guarantee the communication reliability, the implementation of proper radio resource allocation schemes for managing the user mobility as well as for supporting multimedia and high speed applications, represent the most relevant topics. Classic approaches are focused on the use of the time-frequency resources of the propagation channel. However, to satisfy the increasing demand of network capacity, while guaranteeing at the same time the necessary levels in the quality of the offered services, operators and manufacturers must explore new solutions.

In this scenario, the exploitation of the spatial domain of the communication channel by means of multiple antenna systems can be a key improvement for enhancing the spectral efficiency of the wireless systems. In a rich scattering environment, the use of multiple antennas enables the adoption of diversity and spatial multiplexing techniques for mitigating and, respectively, exploiting multipath fading effects. In propagation environments characterized by small angular spreads, the combination of antenna arrays and beamforming algorithms provides the possibility to suppress the undesired sources and to receive the signals incoming from the desired ones. This leads to an increase of the signal to interference plus noise ratio at the receiver that can be exploited to produce relevant benefits in terms of communication reliability and/or capacity. A proper design of the medium access control layer of the wireless network can enable the simultaneous exchange of packets between different node pairs as well as the simultaneous reception of packets from multiple transmitters at a single node. Switched-beam antennas, adaptive antennas (also referred to as smart antennas), and phased-antenna arrays represent some of the available beamforming techniques that can be applied to increase the overall system capacity and to mitigate the interference, in a scenario where several different technologies must share the same frequency spectrum.

In the context of distributed wireless networks using multiple antenna systems, the core of this thesis is the development of a mathematical model to analyze the performance of the network in presence of multipath fading, with particular reference to a scenario in which the signal replicas incoming at the receiver are confined within a small angle and are characterized by small relative delays. This propagation environment, referred to as *low-rank*, is the typical operating scenario of smart antennas, which necessitate high spatial correlation channels to work properly. The novel aspects of this study are represented by the theoretical and numerical modeling of the sophisticated adaptive antennas in conjunction with a detailed description of the channel statistics and of the IEEE 802.11 medium access control scheme. A theoretical model providing a more realistic perspective may be desirable, considering that, at present, not only cost and competition issues, but also too optimistic expectations, as compared to the first measurements on the field, have induced the wireless operators to delay the adoption of smart antenna technology.
The presented analysis includes the most relevant elements that can influence the network behavior: the spatial channel model, the fading statistic, the network topology, the access scheme, the beamforming algorithm and the antenna array geometry. This last aspect is numerically investigated considering that the size of the user terminal represents a strict constraint on the number of antennas that can be deployed on the device, and so the maximization of the performance be-

comes related to the geometrical distribution of the radiators. In ad-hoc and mesh networks, the typical communication devices, such as laptops, palmtops and personal digital assistants require compact and cheap antenna structures as well as beamforming algorithms easy to implement. In particular, the low-cost characteristics have guaranteed a wide popularity to wireless mesh technology, which have encouraged the birth of a new social phenomenon, known as *wireless community networks*, whose objective is the reduction of the Internet access cost.
The adoption of multi-antenna systems is the purpose of the IEEE 802.11n amendment, which, however, not considering modifications of the medium access control layer, provides higher bit rates for the single link, but does not allow simultaneous communications between different couples of nodes. This aspect must be taken into account together with the fact that, nowadays, IEEE 802.11x represents the leading family of standards for wireless local communications, and enhancement proposals have to pay careful attention to the backward compatibility issues. The mathematical model presented in this thesis discusses the suitable parameter settings to exploit advanced antenna techniques in 802.11-based networks when the access scheme supports multiple communications at the same time, maintaining a realistic description for the antenna patterns and the channel behavior.

The presentation of two new iterative algorithms for antenna array pattern synthesis represents the core of the last part of this dissertation. The proposed solutions are characterized by implementation simplicity, low computational burden and do not require the modification of the excitation amplitudes of the array elements. These advantages make the presented algorithms suitable for a wide range of communication systems, while matching also the inexpensiveness of mesh and ad-hoc devices. In particular, phase-only synthesis techniques allow the adoption of a cheaper hardware, including only phase shifters, which are available at a reasonable price, while avoiding the use of the more expensive power dividers.
The first presented algorithm employs the spatial statistic of the channel for properly placing the pattern nulls, in order to suppress the undesired power incoming from a given angular interval. This solution exploits the improved knowledge of the spatial properties of the propagation environment for enhancing the interference suppression capabilities at the transmitter and receiver sides. The second algorithm is a phase-only technique that is able to generate multiple nulls towards the undesired directions and multiple main lobes towards the desired ones. This method provides the possibility to perform spatial multiplexing adopting low-cost electronic components.

The thesis is organized in three parts. The first one provides the background material and represents the basics of the following arguments, while the other two parts are dedicated to the original results developed during the research activity.

With reference to the first part, the fundamentals of antenna array theory are briefly summarized in the first chapter. The most relevant aspects of the wireless propagation environment are described in the second chapter, focusing on the characteristics of the spatial domain in a low-rank scenario. The third chapter presents a classification of the different multiple antenna techniques according to the channel properties and provides an overview of the most common beamforming algorithms. The fourth chapter introduces the most significant aspects of the distributed wireless networks, presenting the main open issues and the current proposals for the exploitation of the potential offered by antenna array systems.
The second part describes the original results obtained in the mathematical modeling of ad-hoc and mesh networks adopting smart antennas in realistic propagation scenarios. In particular, the fifth chapter presents the theoretical analysis to evaluate the number of simultaneous communications that can be sustained by a distributed wireless network using adaptive antennas in presence of multipath. The sixth chapter extends this model to switched-beam antennas, while addressing the mobility aspects and discussing the cost-benefit tradeoff that is related to the use of multiple antenna techniques in today's wireless networks. A detailed throughput-delay analysis is performed in the seventh chapter, where the impact of advanced antenna systems on 802.11-based networks is investigated using a Markov chain model. The influence of the antenna array geometry is examined in the eighth chapter adopting a numerical approach based on a discrete-time simulator, which is able to take into account the details of the channel and of the antenna system behavior.
The third part describes the original results obtained in the field of antenna array pattern synthesis. The ninth chapter presents the technique developed to modify the excitation phases of an antenna array in order to reject interferers spread over an angular region according to a given spatial statistic. The tenth chapter describes the iterative algorithm for phased arrays, which is able to produce low side-lobe level patterns with multiple prescribed main lobes and nulls. Finally, the eleventh chapter summarizes the thesis contributions and remarks the most important conclusions.

The intent of the work presented hereafter is to examine the benefits that derive from the employment of smart antenna techniques from a realistic perspective, as well as to provide some useful solutions to improve the reliability of the communications and to increase the network capacity.

List of acronyms

AA	Adaptive Antenna.
ADC	Analog-to-Digital Converter.
ACK	ACKnowledgement.
AP	Access Point.
BER	Bit Error Rate.
BPSK	Binary Phase Shift Keying.
BSS	Basic Service Set.
CDMA	Code Division Multiple Access.
CFP	Contention Free Period.
CLA	Cantor Linear Array.
CMA	Constant Modulus Algorithm.
CP	Contention Period.
CPU	Central Processing Unit.
CRA	Concentric Ring Array.
CS	Carrier Sensing.
CSE	Cumulative Square Error.
CSMA	Carrier Sensing Multiple Access.
CTS	Clear To Send.
CW	Contention Window.
DA	Directional Antenna.
DC	DownConversion.
DCTS	Directional CTS.
DCF	Distributed Coordination Function.
DD	Directional DATA.
DFT	Discrete Fourier Transform.
DIFS	Distributed InterFrame Space.
DNAV	Directional NAV.
DOA	Direction Of Arrival.
DS	Distribution System.
DSP	Digital Signal Processor.
DSSS	Direct Sequence Spread Spectrum.

DWN	Distributed Wireless Network.
ECB	Efficient Coding Bound.
E-SPC	Extended-SPC.
ESPRIT	Estimation of Signal Parameters via Rotational Invariance Techniques.
ESS	Extended Service Set.
FDMA	Frequency Division Multiple Access.
FHSS	Frequency Hopping Spread Spectrum.
FIR	Finite Impulse Response.
FNBW	First Null BeamWidth.
FPGA	Field Programmable Gate Array.
GBSBM	Geometrically Based Single Bounce Macrocell.
HPBW	Half Power BeamWidth.
IBSS	Independent Basic Service Set.
ICI	InterCarrier Interference.
IF	Intermediate Frequency.
IR	InfraRed.
ISI	InterSymbol Interference.
ISM	Industrial, Scientific and Medical.
LMS	Least Mean Square.
LOS	Line Of Sight.
MAC	Medium Access Control.
MANET	Mobile Ad-hoc NETwork.
MIMO	Multiple Input Multiple Output.
MRC	Maximal Ratio Combining.
MSE	Mean Square Error.
MUSIC	MUltiple SIgnal Classification.
MVDR	Minimum Variance Distortionless Response.
NAV	Network Allocation Vector.
OCTS	Omnidirectional CTS.
OFDM	Orthogonal Frequency Division Multiplexing.
PAS	Power Azimuth Spectrum.
PC	Point Coordinator.
PCF	Point Coordination Function.
PCMCIA	Personal Computer Memory Card International Association.
PDA	Personal Digital Assistant.
PDP	Power Delay Profile.
PER	Packet Error Rate.
pdf	probability density function.
PHY	PHYsical (layer).
QAM	Quadrature Amplitude Modulation.
QPSK	Quadrature Phase Shift Keying.

RCB	Random Coding Bound.
RF	Radio Frequency.
RTS	Request To Send.
SBA	Switched-Beam Antenna.
SCM	Single Coordinate Method.
SCSMA/CN	Selective CSMA with Cooperative Nulling.
SD	Smart DATA.
SDMA	Space Division Multiple Access.
SIFS	Short InterFrame Space.
SINR	Signal to Interference plus Noise Ratio.
SLL	Side-Lobe Level.
SNR	Signal to Noise Ratio.
SPC	Single Parity Check.
SQP	Sequential Quadratic Programming.
STC	Space-Time Coding.
TDMA	Time Division Multiple Access.
TEM	Transverse ElectroMagnetic.
UCA	Uniform Circular Array.
ULA	Uniform Linear Array.
URA	Uniform Rectangular Array.
Wi-Fi	Wireless Fidelity.
WiMAX	Worldwide interoperability for Microwave Access.
WLAN	Wireless Local Area Network.
WMN	Wireless Mesh Network.

Contents

List of symbols[1]

$\mathbf{a}(\varphi)$	Antenna array steering vector in the azimuth plane.
$AF(\vartheta, \varphi)$	Antenna array factor.
$\mathcal{B}_{\mathrm{rx}}$	Receiver filter bandwidth.
b_{pl}	Number of bits of the payload.
b_{ts}	Number of bits of the training sequence.
C_{r}	Coding rate.
$CW_{i'}$	Contention window at i'-th transmission attempt.
$CW_{\min}$	Minimum contention window.
CW_{opt}	Optimum contention window.
$\mathbb{D}$	Destination node.
$\det(\cdot)$	Matrix determinant.
$\mathbb{E}\{\cdot\}$	Expectation.
$E(\mathbf{w}, \varphi)$	Antenna system field pattern in the azimuth plane.
$\mathcal{E}_k(\varphi)$	Field pattern of the k-th antenna element in the azimuth plane.
$\mathbf{E}_{\mathrm{s}}(\mathbf{r})$	Electric complex field.
$F_{\mathrm{D}}(\varphi)$	Equivalent power gain pattern in the azimuth plane.
$F_{\mathrm{T}}(r, \varphi)$	Topology function.
f^{d}	Doppler spread.
$G(\varphi)$	Antenna system power gain pattern in the azimuth plane.
G_{d}	Average equivalent power gain in the desired direction.
G_{m}	Average equivalent power gain in $[0, 2\pi]$.
G'_{m}	Average equivalent power gain outside the FNBW.
G''_{m}	Average equivalent power gain outside the HPBW.
G_{n}	Average equivalent power gain in a null.
G_{tx_1}	Transmitting equivalent power gain of the interferers in the region $\mathbb{R}_1$.
G_{tx_2}	Transmitting equivalent power gain of the interferers in the region $\mathbb{R}_2$.
$\mathbf{g}$	Weight vector for the terms of the cost function $\beth(\mathbf{w})$.
g_l	Weight for the l-th term of the cost function $\beth(\mathbf{w})$.
$\mathbf{H}_{\mathrm{s}}(\mathbf{r})$	Magnetic complex field.
$\mathbb{I}$	Generic interferer.

[1]This list contains the symbols that recur along the thesis and whose explanation is not repeated in each section where they are mentioned. Mathematical quantities without direct physical meaning and defined only for calculation purposes are not reported.

$\mathbf{I}_N$	Identity matrix with rank N.
j	Imaginary unit.
$\mathcal{L}_\mathrm{c}$	Area covered by the communication range of a node.
$\mathcal{L}_\mathrm{t}$	Area covered by the entire network.
L_max	Number of sustainable links.
M_l	Number of array pattern nulls that are necessary to suppress the l-th spread interferer.
m	Retry Limit of the 802.11 DCF.
m'	Maximum backoff stage of the 802.11 DCF.
m_N	Nakagami parameter.
N	Number of antennas.
N_CRA	Number of antennas of a CRA.
$\mathcal{N}_\mathrm{hop}$	Average number of hops between source and destination.
N_rx	Number of receiving antennas of a MIMO system.
N_tx	Number of transmitting antennas of a MIMO system.
N_UCA	Number of antennas of a UCA.
N_ULA	Number of antennas of a ULA.
N_URA	Number of antennas of a URA.
n	Number of nodes in the entire network.
n_2	Number of nodes in the region $\mathbb{R}_2$.
n_des	Number of desired sources.
n_int	Number of interferers.
n_tx	Number of transmitting sources.
P_des	Received desired signal power.
P_int	Received interference power.
P_{int_1}	Interference power received from region $\mathbb{R}_1$.
P_{int_2}	Interference power received from region $\mathbb{R}_2$.
P_{int_3}	Interference power received from region $\mathbb{R}_3$.
P_rx	Total received power.
$\bar{P}_\mathrm{rx}$	Average power at the input of the receiving antenna system.
P_tx	Transmitted power.
$P_\varphi(\varphi)$	Power Azimuth Spectrum.
p_c	Conditional collision probability.
p_outage	Outage probability.
p_tx	Transmission probability of a single node.
Q	Number of multipath components corresponding to a generic source.
$\mathcal{R}$	Bit rate for the DATA packet.
$\mathbb{R}_1$	Region of insuppressible interference.
$\mathbb{R}_2$	Region of suppressible interference.
$\mathbb{R}_3$	Region of no interference.
R_c	Communication range of a node.
$\mathcal{R}_\mathrm{c}$	Bit rate for the control packets.
$R_\mathrm{H}(\varphi)$	Radius bounding regions $\mathbb{R}_1$ and $\mathbb{R}_2$.

$R_{\mathrm{L}}(\varphi)$	Radius bounding regions $\mathbb{R}_2$ and $\mathbb{R}_3$.
R_{sd}	Average source-destination distance.
$\mathbf{R}_{\mathrm{ss}}$	Correlation matrix corresponding to the desired part of $\mathbf{x}(t)$.
R_{t}	Radius of the area occupied by the entire network.
$\mathbf{R}_{\mathrm{uu}}$	Correlation matrix corresponding to the undesired part of $\mathbf{x}(t)$.
$\mathbf{R}_{\mathrm{xx}}$	Array correlation matrix.
$\mathbf{r}$	Position vector.
r_k	Radial coordinate of the k-th array element.
$\mathrm{rank}(\cdot)$	Matrix rank.
$\mathbb{S}$	Source node.
S_{ag}	Normalized aggregate throughput.
S_{input}	Net offered traffic load.
S_{max}	Sustainable throughput.
$\mathrm{SINR}_{\mathrm{th}}$	SINR threshold in not mobile environment.
$\mathrm{SINR}_{\mathrm{out}}$	SINR at the antenna system output.
$\mathrm{sgn}(\cdot)$	Sign function.
$\mathcal{T}$	Successful packet delay.
T_{ACK}	Time required to transmit an ACK packet.
T_{CTS}	Time required to transmit a CTS packet.
T_{DATA}	Time required to transmit a DATA packet.
T_{RTS}	Time required to transmit an RTS packet.
T_{col}	Time wasted because of collision.
T_{s}	Transmitted symbol duration.
T_{succ}	Time required by a successful transmission.
t	Time variable.
$\mathrm{tr}(\cdot)$	Matrix trace.
$\vec{\mathrm{v}}$	Vector speed of a mobile node.
v_{c}	Speed of light in the free space.
W	Noise power.
$\mathbf{w}$	Vector of antenna array excitations.
$\mathbf{w}(i)$	Vector of antenna array excitations at time instant i.
w_k	Current excitation of the k-th array element.
$w_k(i)$	Current excitation of the k-th array element at time instant i.
$\mathbf{x}(i)$	Antenna input signal vector at time instant i.
$\mathbf{x}(t)$	Antenna input signal vector at time t.
$x_k(t)$	Input signal at the k-th antenna array element at time t.
$\mathbf{x}_{\mathrm{s}}(i)$	Desired part of $\mathbf{x}(i)$ at time instant i.
$\mathbf{x}_{\mathrm{u}}(i)$	Undesired part of $\mathbf{x}(i)$ at time instant i.
α	Path-loss exponent.
γ_{G}	Normalization constant for the truncated Gaussian pdf.
γ_{L}	Normalization constant for the truncated Laplacian pdf.
γ_{LMS}	Step size for the LMS algorithm.
$\gamma_{\mathrm{m_1}}$	Maximum angular spread for the ring of scatterers pdf.

γ_{m_2}	Maximum angular spread for the disk of scatterers pdf.
γ_α	Term accounting for the antenna height in the path-loss model.
$\delta^{\mathrm{K}}_{i'm}$	Kronecker delta.
ε	Permittivity of the medium.
ϑ	Zenith angle.
$\overline{\Lambda}$	Mean value of a Poisson packet arrival process.
Λ_1	Probability of packet arrival during the processing of a previous packet.
Λ_2	Probability of packet arrival in the idle state.
λ	Wavelength.
μ	Permeability of the medium.
$\epsilon_{\mathrm{num\_slots}}$	Average number of slots required for processing a packet in the 802.11 DCF.
ϵ_{slot}	Average time between two consecutive backoff time counter decrements in the 802.11 DCF.
$\epsilon_{\mathrm{succ\_slots}}$	Average number of slots required for a successful packet transmission in the 802.11 DCF.
ξ_k	Angular position of the k-th element of a UCA.
ρ_{c}	Radius of a UCA.
ρ_{l}	Interelement spacing of a ULA.
$\tilde{\varrho}_{\mathrm{act}}(r,\varphi)$	Active node density.
$\varrho_{\mathrm{DOA}}(\varphi)$	Pdf of the DOAs.
$\varrho^{l}_{\mathrm{DOA}}(\varphi)$	Pdf of the DOAs corresponding to the l-th interferer.
$\varrho_{\mathrm{FAD}}(z)$	Pdf of the envelope of the received signal.
$\tilde{\varrho}_{\mathrm{FAD}}(z)$	Pdf of the squared envelope of the received signal.
$\varrho_{\mathrm{SOU}}(r,\varphi)$	Pdf of the sources around the destination.
$\varrho_{\mathrm{TOP}}(r,\varphi)$	Pdf of the interferers around the destination.
$\varrho_{(\cdot)_r}(r)$	Marginal of the pdf $\varrho_{(\cdot)}(r,\varphi)$ with respect to r.
$\varrho_{(\cdot)_\varphi}(\varphi)$	Marginal of the pdf $\varrho_{(\cdot)}(r,\varphi)$ with respect to φ.
σ_{slot}	Slot time.
$\hat{\sigma}_\varphi$	Azimuth spread of the channel.
$\hat{\sigma}_{\varphi_l}$	Azimuth spread of the channel between the l-th source and the destination.
$\hat{\sigma}_\tau$	Delay spread of the channel.
ς	Angle between source-destination LOS and relative vector speed $\vec{\mathrm{v}}$.
Φ	Vector of array excitation phases.
ϕ_k	Excitation phase of the k-th array element.
φ	Azimuth angle.
φ_0	Mean DOA.
φ^{3dB}	HPBW in the azimuth plane.
φ^{FN}	FNBW in the azimuth plane.
φ^{d}	Desired azimuth direction.
φ^{d}_l	Desired azimuth direction corresponding to the l-th source.
φ_k	Azimuth coordinate of the k-th array element.

φ_{lq}	DOA of the q-th signal replica corresponding to l-th source.
φ^{n}	Undesired azimuth direction.
φ_l^{n}	Undesired azimuth direction corresponding to the l-th source.
Ψ_{col}	Collision probability.
Ψ_{drop}	Drop probability.
$\psi_{i',i}$	Stationary probability of being in the state (i', i).
Ψ_{succ}	Probability of successful transmission.
$\psi_{\mathrm{s}}(t)$	Stochastic process representing the backoff stage of the 802.11 DCF at time t.
Ψ_{tx}	Transmission probability.
$\psi_{\mathrm{t}}(t)$	Stochastic process representing the backoff timer of the 802.11 DCF at time t.
$\beth(\mathbf{w})$	Cost function.
$\daleth(\mathbf{w})$	Mean square norm.
$\lfloor \cdot \rfloor$	Floor function.
$\lceil \cdot \rceil$	Ceiling function.
$(\cdot)^*$	Complex conjugate.
$(\cdot)^\dagger$	Matrix pseudoinverse.
$(\cdot)^H$	Complex conjugate transpose of a vector or matrix.
$(\cdot)^T$	Transpose of a vector or matrix.

Part I

Background

Chapter 1

Fundamentals of Antenna Arrays

This chapter briefly summarizes the basic principles of antennas, explaining the mechanism of wireless electromagnetic propagation. Some fundamental definitions of antenna theory are recalled from the literature and an introduction to antenna arrays is provided together with a description of the most common array geometries.

1.1 Maxwell's equations

Wireless communications are based upon the transmission and reception of electromagnetic signals from antennas. The physics laws that describe the propagation of an electromagnetic wave are summarized by the Maxwell's equations, which can be expressed for an isotropic and homogeneous medium as [1]:

$$\nabla \bullet \mathbf{E}(\mathbf{r},t) = \frac{\rho_{\text{vol}}(\mathbf{r},t)}{\varepsilon}, \tag{1.1a}$$

$$\nabla \bullet \mathbf{H}(\mathbf{r},t) = 0, \tag{1.1b}$$

$$\nabla \times \mathbf{E}(\mathbf{r},t) = -\mu \frac{\partial \mathbf{H}(\mathbf{r},t)}{\partial t}, \tag{1.1c}$$

$$\nabla \times \mathbf{H}(\mathbf{r},t) = \varepsilon \frac{\partial \mathbf{E}(\mathbf{r},t)}{\partial t} + \mathbf{J}(\mathbf{r},t), \tag{1.1d}$$

where $\mathbf{r}$ denotes the spatial position vector, t is the time variable, $\mathbf{E}(\mathbf{r},t)$ is the electric field intensity vector, μ is the permeability of the medium, $\mathbf{H}(\mathbf{r},t)$ is the magnetic field intensity vector, ε is the permittivity of the medium, $\mathbf{J}(\mathbf{r},t)$ is the current density vector and $\rho_{\text{vol}}(\mathbf{r},t)$ is the volume charge density.
According to the mathematical meaning of the divergence operator, which measures the magnitude of a vector field's source or sink and can be viewed as a flux

density, and to the meaning of the curl operator, which shows the vector field's rate of rotation (the direction of the axis of rotation and the magnitude of the rotation), the four Maxwell's equations describe the principles of electrodynamics. The first equation (Gauss's law) states that the presence of static or dynamic charges in a given volume determines a diverging electric field, while the second one (Gauss's law for magnetism) means that there is nothing available in nature which makes a magnetic field diverge. The third equation (Faraday's law) states that a non-stationary magnetic field causes a curl in the electric field and, finally, the last equation (Ampere's law) means that a non-stationary electric field and/or a current through a medium capable of carrying a flow of electric charges determines a curl in the magnetic field.
The Faraday's and the Ampere's laws are fundamental to obtain a wave propagating in a wireless environment, where no charge and current densities are present. In this case, a stationary current density $\mathbf{J}(\mathbf{r})$ is useless, being unable to generate a space-time varying electromagnetic field. Instead, a time-varying current density $\mathbf{J}(\mathbf{r}, t)$ generates a space-time varying magnetic field $\mathbf{H}(\mathbf{r}, t)$, which, in turn, generates a space-time varying electric field $\mathbf{E}(\mathbf{r}, t)$. At this point, the electric field can produce a space-time varying magnetic field even in the absence of a current density, and so the magnetic and the electric fields are able to sustain each other.

1.2 Antenna fundamentals

An antenna is a device capable of carrying the time-varying current density that is necessary to generate the electromagnetic wave. The *IEEE Standard Definitions of Terms for Antennas*, [2], defines an antenna as "that part of a transmitting or receiving system that is designed to radiate or to receive electromagnetic waves". The antenna represents a transitional structure between free-space and a guiding device, where the guiding device is a transmission line that transports the electromagnetic energy from the transmitter to the antenna or from the antenna to the receiver [3].

1.2.1 Poynting vector

Assuming harmonic variations, the instantaneous radiated fields $\mathbf{E}(\mathbf{r}, t)$ and $\mathbf{H}(\mathbf{r}, t)$ can be expressed in terms of the complex fields $\mathbf{E}_{\mathrm{s}}(\mathbf{r})$ and $\mathbf{H}_{\mathrm{s}}(\mathbf{r})$ as:

$$\mathbf{E}(\mathbf{r}, t) = \mathrm{Re}\{\mathbf{E}_{\mathrm{s}}(\mathbf{r})e^{j\omega t}\}, \tag{1.2a}$$

$$\mathbf{H}(\mathbf{r}, t) = \mathrm{Re}\{\mathbf{H}_{\mathrm{s}}(\mathbf{r})e^{j\omega t}\}, \tag{1.2b}$$

where $j = \sqrt{-1}$ is the imaginary unit and ω is the angular frequency. The components of the complex fields produced by an antenna are directly related to the

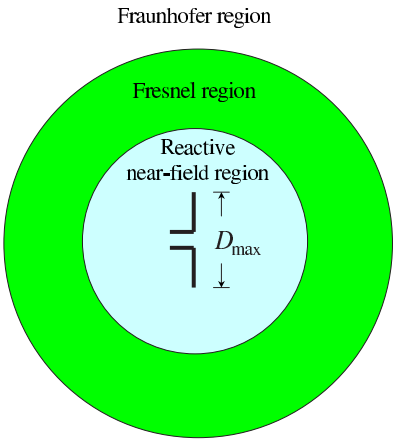

Figure 1.1: Antenna field regions.

physical properties of the antenna itself and can be derived solving the Maxwell's equations by proper mathematical and numerical techniques. The quantity used to describe the power associated to an electromagnetic field is the Poynting vector, which is defined in the sinusoidal case as:

$$\overrightarrow{\mathcal{W}}(\mathbf{r}) \triangleq \frac{1}{2}\mathbf{E}_{\mathrm{s}}(\mathbf{r}) \times \mathbf{H}_{\mathrm{s}}^{*}(\mathbf{r}), \tag{1.3}$$

where $(\cdot)^*$ denotes the complex conjugate. The real part of $\overrightarrow{\mathcal{W}}(\mathbf{r})$ represents the active power density of the field generated by the antenna, while the imaginary part of $\overrightarrow{\mathcal{W}}(\mathbf{r})$ represents the reactive power density associated to this field. Therefore, the average power radiated over a closed surface $\mathcal{M}$ surrounding the antenna can be evaluated as:

$$P_{\mathrm{rad}} = \oiint_{\mathcal{M}} \overrightarrow{\mathcal{W}}(\mathbf{r}) \bullet \mathrm{d}\mathbf{s} = \oiint_{\mathcal{M}} \frac{1}{2}\mathrm{Re}\{\mathbf{E}_{\mathrm{s}}(\mathbf{r}) \times \mathbf{H}_{\mathrm{s}}^{*}(\mathbf{r})\} \bullet \mathrm{d}\mathbf{s}. \tag{1.4}$$

1.2.2 Antenna regions

The generated electromagnetic field and the radiation properties of an antenna are related to its physical size and to the operating wavelength. The space surrounding an antenna is usually subdivided into three regions, which are defined by proper boundaries (Fig. 1.1). The first region, called the *reactive near-field* region, is bounded by the antenna surface and by the spherical surface having radius $0.62\sqrt{D_{\max}^3/\lambda}$, where $D_{\max}$ is the largest dimension of the antenna and λ

is the wavelength. This region contains the reactive energy stored in the vicinity of the antenna, while the active radiated power is negligible. The second region, called the *radiating near-field* or *Fresnel* region, is defined by the intersection of the spheres having radii $0.62\sqrt{D^3_{\max}/\lambda}$ and $2D^2_{\max}/\lambda$. In this region the radiation of active power prevails, but the angular field distribution depends on the distance from the antenna. The *far-field* or *Fraunhofer* region lies outside the sphere having radius $2D^2_{\max}/\lambda$ and represents the principal region of operation for many antennas. In the Fraunhofer region the imaginary part of the Poynting vector approaches zero much faster than its real part and so the reactive power is negligible. Besides, the electric and magnetic field components are perpendicular to each other and transverse to the radial direction of propagation $\hat{\mathbf{r}}$. Therefore, in the Fraunhofer region, $\mathbf{E}_{\rm s}(\mathbf{r})$ and $\mathbf{H}_{\rm s}(\mathbf{r})$ form a Transverse ElectroMagnetic (TEM) wave:

$$\mathbf{E}_{\rm s}(\mathbf{r}) = \eta_0 \mathbf{H}_{\rm s}(\mathbf{r}) \times \hat{\mathbf{r}}, \tag{1.5a}$$

$$\mathbf{H}_{\rm s}(\mathbf{r}) = \frac{1}{\eta_0} \hat{\mathbf{r}} \times \mathbf{E}_{\rm s}(\mathbf{r}), \tag{1.5b}$$

where $\eta_0 = \sqrt{\mu/\varepsilon} \cong 377\ \Omega$ is the intrinsic impedance of the free space.

1.2.3 Radiation properties

The radiation intensity $\mathcal{W}_{\rm u}(\vartheta, \varphi)$ is a far-field parameter that represents the radiated power per unit solid angle in a given direction defined by the zenith angle ϑ and the azimuth angle φ. This parameter can be evaluated multiplying the component of the Poynting vector in the direction of propagation by r^2:

$$\mathcal{W}_{\rm u}(\vartheta, \varphi) = r^2 \mathrm{Re}\{\overrightarrow{\mathcal{W}}(\mathbf{r}) \bullet \hat{\mathbf{r}}\}, \tag{1.6}$$

and is used to define the *antenna power gain*, which represents the ratio between the radiation intensity and the power at the input of the antenna, $P_{\rm input}$, divided by 4π:

$$\mathcal{G}(\vartheta, \varphi) \triangleq \frac{4\pi \mathcal{W}_{\rm u}(\vartheta, \varphi)}{P_{\rm input}}. \tag{1.7}$$

The antenna power gain is also given by the product between the antenna radiation efficiency $e_{\rm cd}$ and the directivity $\mathcal{D}(\vartheta, \varphi)$. In particular, the radiation efficiency accounts for the conduction and the dielectric losses, and is defined as the ratio of the radiated power to the input power:

$$e_{\rm cd} \triangleq \frac{P_{\rm rad}}{P_{\rm input}} = \frac{P_{\rm rad}}{P_{\rm rad} + P_{\rm loss}}, \tag{1.8}$$

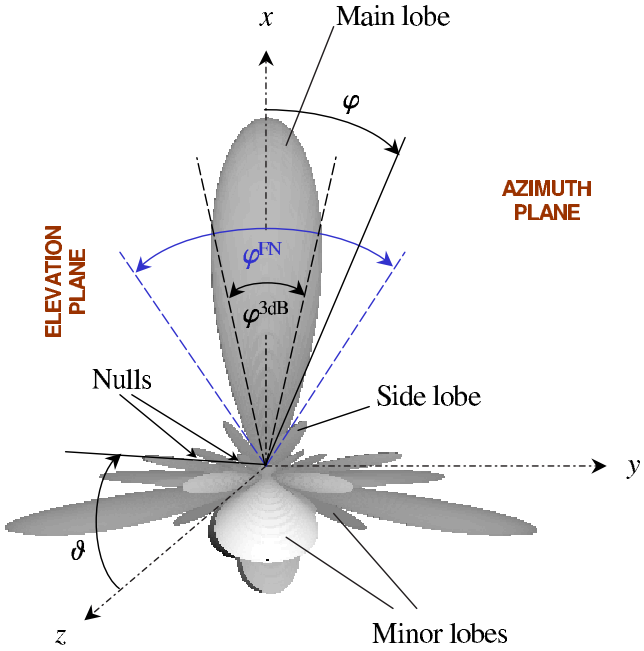

Figure 1.2: Example of radiation pattern.

where P_{loss} is the antenna power loss. Besides, the directivity is the ratio between the radiation intensity and the radiated power divided by 4π:

$$\mathcal{D}(\vartheta, \varphi) \triangleq \frac{4\pi \mathcal{W}_{\text{u}}(\vartheta, \varphi)}{P_{\text{rad}}}. \tag{1.9}$$

The radiation properties of an antenna as a function of the space coordinates are described by mathematical functions called *radiation patterns*. These functions can be adopted to represent several antenna parameters, such as radiation intensity, field strength, directivity and power gain. With reference to the example shown in Fig. 1.2, the following characterizing elements can be defined in a radiation pattern.

- *Null*: direction in which the pattern assumes very small values, ideally zero.
- *Lobe*: any angular region bounded by two nulls.
- *Main lobe*: lobe that contains the direction of maximum radiation.
- *Minor lobe*: any lobe except the main one. If the pattern assumes the maximum radiation value in unwanted directions external to the main lobe, the lobes containing these directions are called *grating lobes*.

- *Side lobe*: a minor lobe that is usually adjacent to the main lobe and occupies the same hemisphere in the direction of maximum gain.

- *Half Power BeamWidth (HPBW) or 3 dB BeamWidth*: angular region containing the direction of maximum radiation that lies between the two directions in which the radiation is one-half of this maximum. In the figure φ^{3dB} denotes the HPBW in the azimuth plane.

- *First Null BeamWidth (FNBW)*: entire angle spanned by the main lobe. The FNBW can be associated to the ability of an antenna to reject interference. In the figure φ^{FN} represents the FNBW in the azimuth plane.

- *Side-Lobe Level (SLL)*: maximum relative radiation of the highest side lobe with respect to the maximum radiation of the main lobe.

1.3 Antenna arrays

Usually the beamwidth of a single antenna element pattern is too wide for many wireless terrestrial and space applications, which, in many cases, require high gains towards certain directions [4]. Besides, a narrower HPBW (or FNBW) can be necessary for spatial filtering operations and to increase the gain in the desired directions as well as to reduce it in the undesired ones. Directional patterns can be obtained by increasing the single antenna element size or by using more radiating elements in order to form an array. In this second case the individual antennas are arranged according to a proper geometrical configuration and the current excitations of each element are synthesized to provide the desired radiation pattern. For practical purposes all radiators belonging to an array are usually chosen as identical, even if, for specific applications, antenna arrays consisting of different elements can be built. By adopting multi-antenna structures, it is possible to generate radiation patterns with multiple main beams, each with a desired beamwidth, while satisfying side-lobe level and null constraints. The synthesis process can be performed by properly selecting the number of array elements, their geometrical configuration and the interelement spacing. Besides, the radiation pattern can be electronically controlled by modifying the phase and/or the amplitude of the current excitations.
The total field radiated by an antenna array is determined by the vector addition of the individual elements. The far-field radiation properties of an antenna array can be mathematically summarized by the array steering vector:

$$\mathbf{a}(\vartheta,\varphi) \triangleq [\mathcal{E}_1(\vartheta,\varphi)e^{j\frac{2\pi v_c}{\lambda}\tau_1(\vartheta,\varphi)},...,\mathcal{E}_N(\vartheta,\varphi)e^{j\frac{2\pi v_c}{\lambda}\tau_N(\vartheta,\varphi)}]^T, \tag{1.10}$$

where $(\cdot)^T$ denotes the transpose of a vector or matrix, $\mathcal{E}_k(\vartheta,\varphi) = \sqrt{\mathcal{G}_k(\vartheta,\varphi)}$ is the k-th single element field (or amplitude) pattern, v_c is the speed of light in free space and $\tau_k(\vartheta,\varphi)$ represents the delay of a plane wave arriving from direction (ϑ,φ) and measured from the k-th element of the array with respect to the origin. The array steering vector includes both the radiation properties of each element and the geometrical characteristics of the antenna array. These characteristics determine the delay, which can be evaluated as:

$$\tau_k(\vartheta,\varphi) = \frac{\mathbf{r}_k \bullet \hat{\mathbf{r}}^\mathrm{i}}{v_\mathrm{c}}, \tag{1.11}$$

where $\mathbf{r}_k = (r_k \sin\vartheta_k \cos\varphi_k, r_k \sin\vartheta_k \sin\varphi_k, r_k \cos\vartheta_k)^T$ is the position of the k-th array element in spherical coordinates, and:

$$\hat{\mathbf{r}}^\mathrm{i} = (\sin\vartheta\cos\varphi, \sin\vartheta\sin\varphi, \cos\vartheta)^T, \tag{1.12}$$

is the unit vector of the incoming wave. According to the principle of pattern multiplication, if the individual elements are identical, the pattern produced by an array can be expressed as the product between the pattern of the single element with respect to a given reference point and the array factor:

$$AF(\vartheta,\varphi) \triangleq \sum_{k=1}^{N} w_k e^{j\frac{2\pi v_\mathrm{c}}{\lambda}\tau_k(\vartheta,\varphi)}, \tag{1.13}$$

where w_k is the complex excitation of the k-th array element. The characteristics of $AF(\vartheta,\varphi)$ can be controlled by varying the excitations, the number of elements, the interelement spacing and the geometrical configuration of the array.
When two antenna array elements are sufficiently close, the electromagnetic field radiated by one element couples into the other and vice versa. This phenomenon is called mutual coupling and depends on the interelement spacing, the radiation characteristics and the orientation of the single element. This interchange of energy complicates the array design, because mutual coupling is difficult to predict by analytical methods, but, in many scenarios, it must be taken into account because of its significant contribution [3]. In fact, mutual coupling leads to a distortion of the single element radiation pattern, which influences the resulting pattern of the entire antenna array and may lead to unprecise steering of the main lobe and the nulls. An interelement distance larger than or equal to half the wavelength is commonly considered sufficient to neglect mutual coupling effects, while, for lower distances, the distorted element patterns can be evaluated with numerical techniques.

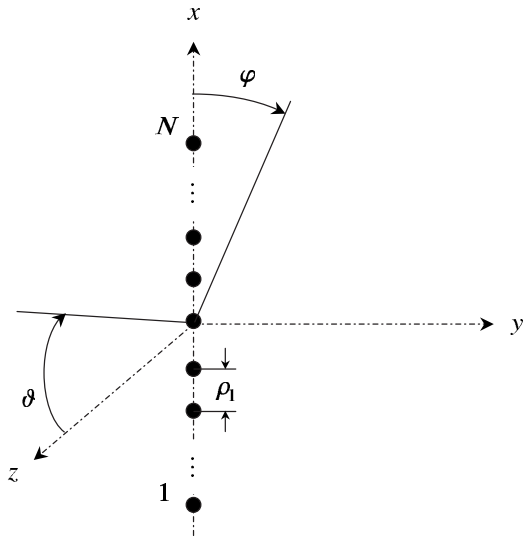

Figure 1.3: Uniform linear array.

1.3.1 Linear arrays

Usually, in the design of an antenna array, some constraints, such as the SLL, the FNBW, the HPBW and the directivity, are specified, while others, such as the phase/amplitude of the elements, the number of radiators and the geometry of the array, must be properly derived to satisfy the design requirements.
The most common and most analyzed geometry is the linear antenna array, which consists of N antenna elements displaced on a straight line. If the adjacent elements are equally spaced (Fig. 1.3), the array is referred to as a Uniform Linear Array (ULA). If, in addition, all excitations have identical amplitudes ($|w_1| = |w_1| = ... = |w_N|$) and the phase of the k-th element is increased by a constant progressive phase ι with respect to the $(k-1)$-th element, the array is referred to as a uniform array. In this particular case, the normalized array factor in the azimuth plane can be expressed as:

$$AF_{\text{norm}}\left(\vartheta = \frac{\pi}{2}, \varphi\right) = \frac{1}{N} \frac{\sin\left[\frac{N}{2}\left(\frac{2\pi\rho_{\text{l}}}{\lambda}\cos\varphi + \iota\right)\right]}{\sin\left[\frac{1}{2}\left(\frac{2\pi\rho_{\text{l}}}{\lambda}\cos\varphi + \iota\right)\right]}, \tag{1.14}$$

where ρ_{l} is the interelement spacing. The main lobe can be steered towards the desired direction by properly modifying the progressive phase shift, while a nar-

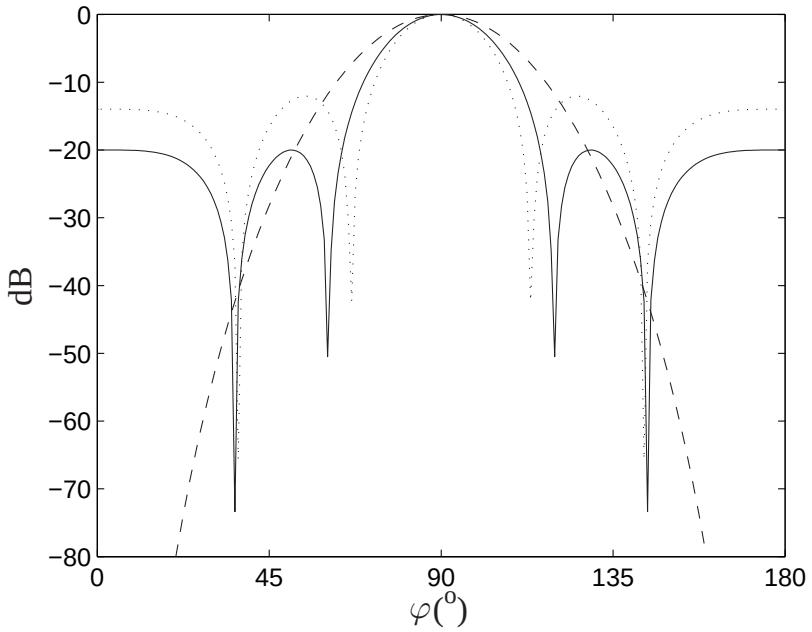

Figure 1.4: Array gain of a ULA for $N = 5$ and $\rho_l = 0.5\lambda$.
····· Uniform array – – – – Binomial array —— Dolph-Tschebyscheff array

row HPBW can be obtained by increasing N.
A limitation of uniform arrays is due to the fact that, independently of the number of elements, the ratio between the maximum of the main lobe and the maximum of the first side lobe is approximately equal to 13.5 dB. This level may be not suitable for certain applications, where more stringent constraints must be imposed on the level of the secondary lobes. In fact, to reduce the transmitted/received power outside the main lobe, the minor lobes should be as low as possible. In general, the problem of low SLL array design is substantially equivalent to the problem of designing Finite Impulse Response (FIR) digital filters in a Digital Signal Processor (DSP). Therefore, a large number of techniques have been taken from digital signal processing to produce patterns with low side lobes. These techniques perform the weighting of the array elements by adopting proper functions, such as Gaussian, Kaiser-Bessel and Blackman windows [5].
Widely adopted synthesis techniques for ULAs are the Dolph-Tschebyscheff and the binomial methods, which consider a nonuniform distribution of the excitation amplitudes. Comparing the characteristics of uniform, Tschebyscheff and binomial arrays, it can be observed that the uniform arrays provide the smallest HPBW and the highest SLL, while the binomial arrays yield the largest HPBW and the lowest SLL (Fig. 1.4). In particular, a binomial array with interelement

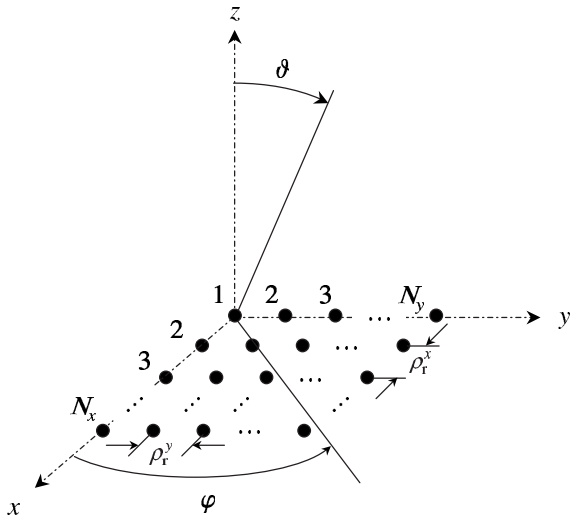

Figure 1.5: Uniform rectangular array.

spacing lower than or equal to $\lambda/2$ has no side lobes. The HPBW and the SLL of a Tschebyscheff array lie between those of binomial and uniform arrays. Besides, for a given SLL, the Dolph-Tschebyscheff arrays provide the smallest FNBW and, reciprocally, for a given FNBW, the Dolph-Tschebyscheff arrays provide the lowest possible SLL [3].
Even if ULAs are widely applied, there are scenarios in which the linear geometry is not appropriate. Other configurations must be adopted to satisfy some particular encumbrance requirements on buildings or vehicles and to provide higher performance in terms of beam scanning.

1.3.2 Rectangular arrays

Rectangular arrays are more versatile with respect to linear arrays and can be employed to obtain patterns with a lower SLL. Similarly to ULAs, proper weighting methods can be considered to further reduce the side-lobe level and the beamwidth. Besides, a rectangular configuration has the capability to perform the beam scanning in both the azimuth and the elevation planes.
As shown in Fig. 1.5, a rectangular array is obtained when the individual radiating elements are positioned along a rectangular grid. If the adjacent elements are equally spaced the array is called a Uniform Rectangular Array (URA). This configuration finds application in a wide range of systems, such as remote sens-

ing, tracking and search radar. An $N_x \cdot N_y$ URA can also be viewed as N_y linear arrays placed at distance ρ_{r}^y, where each array is formed by N_x elements with interelement spacing ρ_{r}^x. Therefore, for a progressive phase URA with uniform amplitudes, the normalized array factor can be expressed as:

$$AF_{\mathrm{norm}}(\vartheta,\varphi) = \left\{ \frac{1}{N_x} \frac{\sin\left[\frac{N_x}{2}\left(\frac{2\pi\rho_{\mathrm{r}}^x}{\lambda}\sin\vartheta\cos\varphi + \iota_x\right)\right]}{\sin\left[\frac{1}{2}\left(\frac{2\pi\rho_{\mathrm{r}}^x}{\lambda}\sin\vartheta\cos\varphi + \iota_x\right)\right]} \right\} \cdot \left\{ \frac{1}{N_y} \frac{\sin\left[\frac{N_y}{2}\left(\frac{2\pi\rho_{\mathrm{r}}^y}{\lambda}\sin\vartheta\sin\varphi + \iota_y\right)\right]}{\sin\left[\frac{1}{2}\left(\frac{2\pi\rho_{\mathrm{r}}^y}{\lambda}\sin\vartheta\sin\varphi + \iota_y\right)\right]} \right\}, \tag{1.15}$$

where ι_x and ι_y are the progressive phase shifts along the x and the y axis, respectively. When the interelement spacing is larger than or equal to half the wavelength, grating lobes can appear in the radiation pattern because of the in-phase addition of the radiated fields towards directions different from that scanned by the main lobe.

1.3.3 Circular arrays

Another commonly employed configuration is the Uniform Circular Array (UCA), in which the elements are regularly arranged on a circular ring (Fig. 1.6). The UCA is of very practical interest and is often adopted in radar and sonar systems as well as in cellular base stations. Considering a UCA of radius ρ_{c}, the normalized array factor can be expressed as:

$$AF\left(\vartheta,\varphi\right) = \sum_{k=1}^{N} w_k e^{j\frac{2\pi}{\lambda}\rho_{\mathrm{c}}\sin\vartheta\cos(\varphi-\xi_k)}, \tag{1.16}$$

where ξ_k is the angular position of the k-th element. Thanks to its high degree of symmetry the UCA is able to provide an identical HPBW towards all azimuth directions. Besides, a direct comparison between a UCA and a ULA shows that, adopting the same number of elements and the same spacing between adjacent radiators, the circular array produces narrower main beams with respect to the corresponding linear array. The performance of the circular configurations can be improved by using multiple rings in order to obtain a Concentric Ring Array (CRA). This planar geometry enables the scanning in both azimuth and elevation planes [6–7].

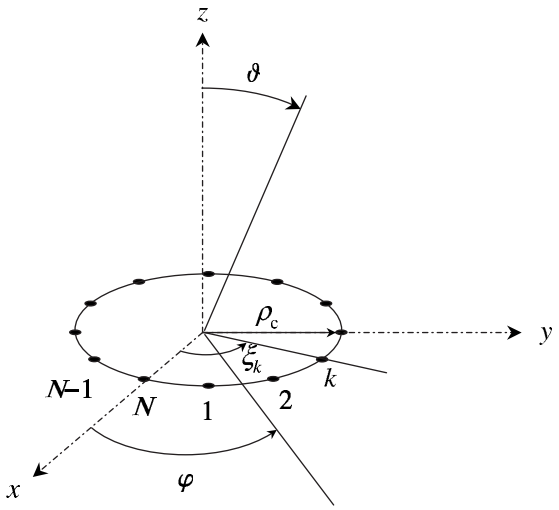

Figure 1.6: Uniform circular array.

1.3.4 Conformal arrays

ULAs, URAs and UCAs are widely adopted geometries, based upon a regular and symmetrical design. These configurations are suitable for applications in which the mounting support is able to sustain the structure and particular size or shape constraints are not present. However, in many practical scenarios, such as spacecraft, aircraft or missile applications, the mounting surface is irregular and/or the available space is limited. In these situations the array geometry must be designed to match the particular requirements of the support and so a conformal array is needed. The antenna elements can be disposed on an ellipse, on an arc, or can be placed according to more complex three-dimensional topologies, usually circularly symmetric surfaces, such as cylinders, cones or spheres [8]. In general, the patterns of the elements can be oriented towards different directions, because of the irregularity of the geometry, and so the single element pattern cannot be factored out from the total array pattern. [9].
Proper antenna elements may be required for conformal arrays, because the generic radiator may have to adhere to aerodynamic profiles. Besides, particular single element radiation patterns may be necessary to satisfy the design specifications for dedicated array topologies [10].

Chapter 2

Propagation Channel Modeling

This paper introduces the main characteristics of the wireless propagation environment and provides some basic definitions. To provide realistic models for evaluating the performance of advanced antenna array systems, particular attention is dedicated to the spatial properties of the wireless communication channel. The most important statistical distributions for the Power Azimuth Spectrum (PAS) are presented together with the classical fading models.

2.1 The wireless channel

Free-space propagation occurs when a unique direct signal path exists between a transmitter and a receiver. However, this model oversimplifies the real behavior of the wireless channel, in which obstacles and scatterers characterize the surrounding environment of two communicating nodes. Reflections, refractions, diffractions and scattering determine the presence of many signal replicas at the receiver, leading to a phenomenon referred to as multipath. Besides, the complexity of the scenario is increased by the effects due to mobility, which cause short-term fluctuations (fading) and long-term fluctuations (shadowing) of the received signal envelope. Therefore, taking into account these characteristics, the signal attenuation in a wireless propagation channel is usually schematized as the combination of three main factors: path-loss, fading and shadowing.

2.1.1 Path-loss attenuation

Path-loss attenuation is the power density reduction of an electromagnetic wave propagating through space and is mainly due to the distance between the transmitter and the receiver. However, additional environmental elements, due to location

of antennas, terrain contours, vegetation, foliage and dry, may increase the losses. The path-loss attenuation can be described by a parameterized ground model, in which the power received by a node at distance r from a transmitter is evaluated as [11]:

$$P_{\mathrm{rx}} = \frac{P_{\mathrm{tx}}\gamma_\alpha G_{\mathrm{tx}} G_{\mathrm{rx}}}{r^\alpha}, \tag{2.1}$$

where P_{tx} is the transmission power, $\alpha(> 2)$ is the path-loss exponent, γ_α accounts for the height of the transmitting and the receiving antennas with respect to the floor, G_{tx} and G_{rx} are, respectively, the transmitting and the receiving antenna system gains. The value assumed by the parameter α is chosen according to the particular attenuation characteristics of the wireless channel. A value equal to 2 models the behavior of the free space, while $\alpha = 4$ is considered adequate for a relatively lossy scenario, such as a two ray ground propagation environment. The typical value for the path-loss exponent in a dense urban environment, in presence of several buildings, ranges from 4 to 6.

2.1.2 Fading

In a multipath scenario each signal component is characterized by its amplitude, phase shift, delay and Direction Of Arrival (DOA). A fundamental metric for describing the behavior of the multipath channel is the Power Delay Profile (PDP), which provides the signal power as a function of the delay of the multipath components. Usually, in a wireless environment, the PDP has one or more peaks, whose presence indicates an inherent clustering of the delays. The information obtained from the PDP can be used to evaluate the delay spread, which is defined as:

$$\hat{\sigma}_\tau = \sqrt{\frac{\sum_{q=1}^{Q} P_{\mathrm{rx}_q}\bar{\tau}_q^2}{\sum_{q=1}^{Q} P_{\mathrm{rx}_q}} - \left(\frac{\sum_{q=1}^{Q} P_{\mathrm{rx}_q}\bar{\tau}_q}{\sum_{q=1}^{Q} P_{\mathrm{rx}_q}}\right)^2}, \tag{2.2}$$

where Q is the number of multipath components, P_{rx_q} and $\bar{\tau}_q$ are, respectively, the power level and the delay corresponding to the q-th path. The delay spread is the standard deviation of the PDP and represents a measure of the time dispersion of the channel. The widening of the channel impulse response in the time domain can lead to InterSymbol Interference (ISI), an unwanted phenomenon in which the previously transmitted symbols have influence on the currently received received one.

Another relevant feature of the wireless channel is caused by the Doppler effect, which is due to the relative motion between transmitter, receiver and obstacles. Doppler effect determines a frequency broadening of the received signal that is proportional to the relative motion speed and to the carrier frequency. By consequence, adjacent frequency channels may experience InterCarrier Interference

(ICI). Besides, the combination of multipath and mobility leads to fluctuations of the received signal envelope (multipath fading), caused by the constructive and destructive addition of the signal replicas due to the different phase shifts.
Multipath fading is defined as *flat fading* when the delay spread is much lower than the inverse of the receiver filter bandwidth $\mathcal{B}_{\mathrm{rx}}$, while it is defined as *frequency selective fading* when $\hat{\sigma}_\tau \gtrsim 1/\mathcal{B}_{\mathrm{rx}}$, namely when the delay spread is larger or close to $1/\mathcal{B}_{\mathrm{rx}}$. In the first case the multipath characteristics of the channel do not degrade the received signal quality, while in the second case amplitude and phase distortions are experienced at the receiver.
The temporal rate of change of the wireless channel is measured by the Doppler power spectrum, which provides statistical information regarding the variation of the frequency of a signal received by a mobile node traveling at a given speed. The classical approach, known as the Clarke model, assumes that the received signal comes from directions uniformly distributed in the azimuth domain. Assuming the use of a single $\lambda/2$ vertical dipole antenna, having power gain $\mathcal{G}(\vartheta = \pi/2, \varphi) = 3/2$ in the entire azimuth plane, the Doppler power spectrum for a flat fading channel is given by [12]:

$$\mathcal{S}_{\mathrm{D}}(f) = \begin{cases} \dfrac{3\bar{P}_{\mathrm{rx}}}{2\pi f^{\mathrm{d}} \sqrt{1 - \left(\dfrac{f - f_0}{f^{\mathrm{d}}}\right)^2}} & |f - f_0| < f^{\mathrm{d}} \\ 0 & \text{elsewhere} \end{cases}, \tag{2.3}$$

where $\bar{P}_{\mathrm{rx}}$ is the average received power from all multipath components, f_0 is the carrier frequency and the Doppler spread can be expressed as $f^{\mathrm{d}} = f_0|\vec{\mathrm{v}}|/v_{\mathrm{c}}$, with $\vec{\mathrm{v}}$ representing the relative vector speed. Multipath fading can also be distinguished between *fast fading* when the Doppler spread is larger or close to the inverse of the symbol duration T_{s}, and in *slow fading* when $f^{\mathrm{d}} << 1/T_{\mathrm{s}}$. Besides, if the product $\hat{\sigma}_\tau f^{\mathrm{d}}$ is lower than one, the channel is said to be *underspread*, while, if $\hat{\sigma}_\tau f^{\mathrm{d}} > 1$ it is classified as *overspread* [13].
The small-scale fluctuations of the received power, leading to fast fading, can be observed over distances in the order of half wavelength. These variations are analytically described by proper statistic distributions that characterize the envelope and the squared envelope of the received signal.

2.1.2.1 Rayleigh fading

When there is no direct path between the transmitter and the receiver, the entire received electric field is due to multipath. The in-phase component, $x_{\mathrm{I}}(t)$, and the

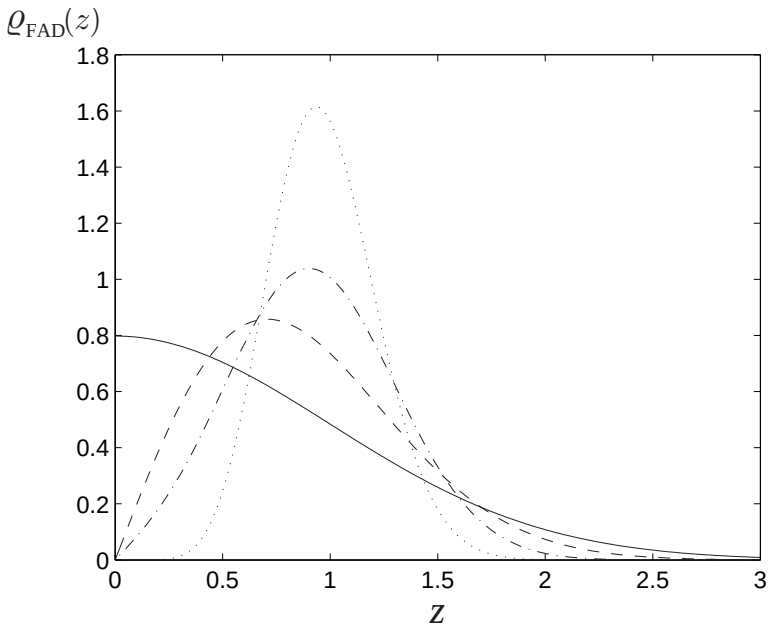

Figure 2.1: Statistics of the received signal envelope for $\bar{P}_{\mathrm{rx}} = 1$.
-·-·- Rice ($K_{\mathrm{R}} = 2$) ---- Rayleigh
····· Nakagami ($m_{\mathrm{N}} = 4$) —— Nakagami ($m_{\mathrm{N}} = 1/2$).

quadrature component, $x_{\mathrm{Q}}(t)$, of the incoming signal can be modeled as complex Gaussian random processes. These two processes have zero mean because of the absence of Line Of Sight (LOS) between transmitter and receiver. Therefore, applying a bivariate transformation, it can be proved that the statistic of the envelope $\sqrt{x_{\mathrm{I}}^2(t) + x_{\mathrm{Q}}^2(t)}$ follows a Rayleigh distribution:

$$\varrho_{\mathrm{FAD}}(z) = \begin{cases} \dfrac{2z}{\bar{P}_{\mathrm{rx}}} e^{-\frac{z^2}{\bar{P}_{\mathrm{rx}}}} & z \geq 0 \\ 0 & \text{elsewhere} \end{cases}, \tag{2.4}$$

while the statistic of the squared envelope $x_{\mathrm{I}}^2(t) + x_{\mathrm{Q}}^2(t)$ is exponential:

$$\tilde{\varrho}_{\mathrm{FAD}}(z) = \begin{cases} \dfrac{1}{\bar{P}_{\mathrm{rx}}} e^{-\frac{z}{\bar{P}_{\mathrm{rx}}}} & z \geq 0 \\ 0 & \text{elsewhere} \end{cases}. \tag{2.5}$$

Experimental studies have shown that Rayleigh fading is a proper model for heavily built-up urban environments, characterized by the presence of rich scattering

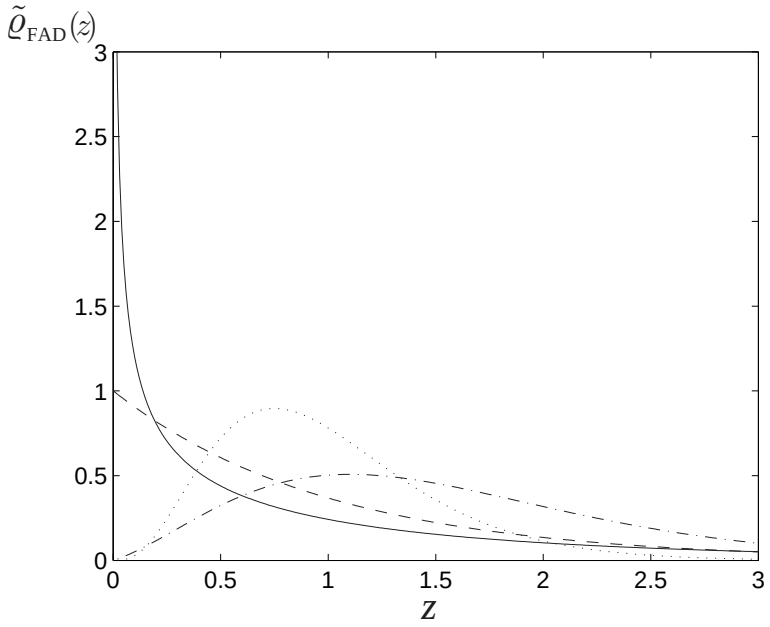

Figure 2.2: Statistics of the square of the received signal envelope for $\bar{P}_{\mathrm{rx}} = 1$.
-·-·- Rice ($K_{\mathrm{R}} = 2$) ---- Rayleigh
····· Nakagami ($m_{\mathrm{N}} = 4$) —— Nakagami ($m_{\mathrm{N}} = 1/2$).

and absence of LOS between the communicating nodes [14].

2.1.2.2 Rician fading

The Rician distribution, instead, is suitable when, in addition to the multipath components, there exists a direct path between the transmitter and the receiver. The received signal envelope is characterized by the probability density function (pdf):

$$\varrho_{\mathrm{FAD}}(z) = \begin{cases} \dfrac{2z(K_{\mathrm{R}}+1)}{\bar{P}_{\mathrm{rx}}} e^{-K_{\mathrm{R}} - \frac{(K_{\mathrm{R}}+1)z^2}{\bar{P}_{\mathrm{rx}}}} I_0\left(2z\sqrt{\dfrac{K_{\mathrm{R}}(K_{\mathrm{R}}+1)}{\bar{P}_{\mathrm{rx}}}}\right) & z \geq 0 \\ 0 & \text{elsewhere} \end{cases} \tag{2.6}$$

where $I_0(\tilde{z}) = \frac{1}{2\pi}\int_0^{2\pi} e^{-\tilde{z}\cos\varphi'}\mathrm{d}\varphi'$ is the modified Bessel function of the first kind and zero-order, and K_{R} is the Rice factor, representing the ratio between the power of the direct signal and the power of the scattered components. When $K_{\mathrm{R}} = 0$ the Rician distribution coincides with the Rayleigh distribution, while

for $K_{\mathrm{R}} \to +\infty$ the channel does not exhibit fading. In presence of Rician fading the squared envelope has a non-central chi-square distribution with two degrees of freedom:

$$\tilde{\varrho}_{\mathrm{FAD}}(z) = \begin{cases} \dfrac{K_{\mathrm{R}}+1}{\bar{P}_{\mathrm{rx}}} e^{-K_{\mathrm{R}} - \frac{(K_{\mathrm{R}}+1)z}{\bar{P}_{\mathrm{rx}}}} I_0\left(2\sqrt{\dfrac{K_{\mathrm{R}}(K_{\mathrm{R}}+1)z}{\bar{P}_{\mathrm{rx}}}}\right) & z \geq 0 \\ 0 & \text{elsewhere} \end{cases} \tag{2.7}$$

In both cases (Rayleigh and Rice) the phase of the received signal is assumed uniformly distributed in $[0, 2\pi]$.

2.1.2.3 Nakagami fading

Another commonly adopted fading statistic, derived from empirical studies, has been introduced by Nakagami [12]. This distribution describes the envelope of the received signal by a central chi-square distribution with m_{N} degrees of freedom:

$$\varrho_{\mathrm{FAD}}(z) = \begin{cases} 2\left(\dfrac{m_{\mathrm{N}}}{\bar{P}_{\mathrm{rx}}}\right)^{m_{\mathrm{N}}} \dfrac{z^{2m_{\mathrm{N}}-1}}{\Gamma(m_{\mathrm{N}})} e^{-\frac{m_{\mathrm{N}} z^2}{\bar{P}_{\mathrm{rx}}}} & z \geq 0,\ m_{\mathrm{N}} \geq 1/2 \\ 0 & \text{elsewhere} \end{cases}, \tag{2.8}$$

and the squared envelope by a Gamma density:

$$\tilde{\varrho}_{\mathrm{FAD}}(z) = \begin{cases} \left(\dfrac{m_{\mathrm{N}}}{\bar{P}_{\mathrm{rx}}}\right)^{m_{\mathrm{N}}} \dfrac{z^{m_{\mathrm{N}}-1}}{\Gamma(m_{\mathrm{N}})} e^{-\frac{m_{\mathrm{N}} z}{\bar{P}_{\mathrm{rx}}}} & z \geq 0,\ m_{\mathrm{N}} \geq 1/2 \\ 0 & \text{elsewhere} \end{cases}, \tag{2.9}$$

where m_{N} is also called the Nakagami parameter and $\Gamma(m_{\mathrm{N}}) = \int_0^{+\infty} \tilde{z}^{m_{\mathrm{N}}-1} e^{-\tilde{z}} \mathrm{d}\tilde{z}$ is the Euler gamma function. The Nakagami parameter m_{N} can be used to obtain more or less severe fading conditions with respect to the Rayleigh pdf. In particular, for $m_{\mathrm{N}} = 1$ the Nakagami distribution coincides with the Rayleigh distribution, while for $m_{\mathrm{N}} \to +\infty$ fading is absent. In essence, as m_{N} gets larger the fading conditions become less severe. The Rice distribution can be closely approximated by choosing the Nakagami parameter as a function of the Rice factor K_{R} according to $m_{\mathrm{N}} = (K_{\mathrm{R}}+1)^2/(2K_{\mathrm{R}}+1)$. Besides, with respect to the Rice distribution, the Nakagami distribution has the advantage to provide in many cases closed form analytical expressions, thanks to the absence of Bessel functions.

2.1.3 Shadowing

Slow fading is due to long-term variations of the mean value of the received signal envelope. This phenomenon is also known as large-scale fading or shadowing, because the fluctuations in the mean signal level are usually caused by the node movement in the proximity of objects, such as buildings and hills, which produce a shadow effect. Empirical studies have shown that shadowing can be described by a log-normal distribution:

$$\varrho_{\mathrm{SHA}}(z) = \begin{cases} \dfrac{1}{z\sigma_{\mathrm{S}}\sqrt{2\pi}} e^{-\frac{(\log z - z_{\mathrm{S}})^2}{2\sigma_{\mathrm{S}}^2}} & z \geq 0 \\ 0 & \text{elsewhere} \end{cases}, \tag{2.10}$$

where σ_{S}^2 and z_{S} are the mean and the variance of $\log z$, respectively. The usual value for the standard deviation σ_{S}, which is influenced by the density of the scatterers, ranges from 5 to 12 dB and have a slight dependence on frequency, but is nearly independent of the path length.

2.2 Spatial channel models

Classical models involve time and frequency domains, however, when advanced antenna array techniques are adopted, the spatial characteristics of the scattering environment have an enormous impact on the system performance. In the past years, researchers assumed that the DOAs of the received signal replicas were uniformly distributed in the entire azimuth plane. However, this hypothesis can be not realistic when referred to the uplink channel between a mobile node and a cellular base station, or considering the communication between the backbone nodes of a wireless mesh network in outdoor environment.
With reference to the spatial domain, some parameters have been defined to take into account the antenna characteristics with respect to the spatial distribution of the different signal components [15]. In a multipath environment, the signal replicas arrive at the receiver with angles that, in general, are different from the mean DOA corresponding to the direct path. The Power Azimuth Spectrum (PAS) $P_{\varphi}(\varphi)$ and the angular spread $\hat{\sigma}_{\varphi}$ are used to characterize the spatial properties of the channel in the azimuth domain. The PAS represents the power distribution along all the possible DOAs, while, from a theoretical point of view, the angular spread can be viewed as the square root of the variance of the PAS. In general, the angular spread (or azimuth spread) provides a measure of the angular dispersion

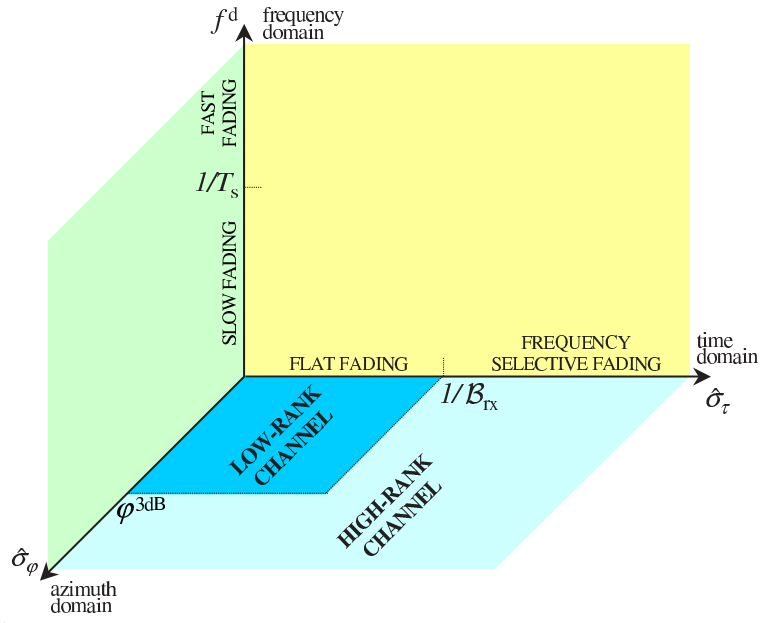

Figure 2.3: The wireless channel.

of the channel and is defined as:

$$\hat{\sigma}_{\varphi} = \sqrt{\frac{\sum_{q=1}^{Q} P_{\mathrm{rx}_q} \varphi_q^2}{\sum_{q=1}^{Q} P_{\mathrm{rx}_q}} - \varphi_0^2}, \tag{2.11}$$

where φ_q is the DOA of the q-th signal replica (having power P_{rx_q}), and

$$\varphi_0 = \frac{\sum_{q=1}^{Q} P_{\mathrm{rx}_q} \varphi_q}{\sum_{q=1}^{Q} P_{\mathrm{rx}_q}}, \tag{2.12}$$

is the mean DOA. Recalling the definition given in [15], a channel is called *low-rank* if $\hat{\sigma}_{\tau} << 1/\mathcal{B}_{\mathrm{rx}}$ (flat fading), and $\hat{\sigma}_{\varphi} << \varphi^{3\mathrm{dB}}$, while it is called *high-rank* if $\hat{\sigma}_{\tau} \gtrsim 1/\mathcal{B}_{\mathrm{rx}}$ or $\hat{\sigma}_{\varphi} \gtrsim \varphi^{3\mathrm{dB}}$ (Fig. 2.3). In a low-rank environment the spatial and temporal correlations between the signal replicas are very high and the incoming multipath components can be considered as confined within a small angle. In a high-rank environment, instead, the paths can be spread over a wide angular region, leading to a low spatial correlation. Referred to the spatial domain, this distinction depends both on the angular distribution of the DOAs and on the spacing between the antenna array elements, which influences the capabilities to discriminate the different paths.

2.2.1 Low-rank environment

A low-rank channel model basically consists of a local scattering model around the transmitting node and is associated with the LOS component. The contributions from scatterers around the receiving node and from distant scatterers are considered negligible. Therefore, the distance and the height of the receiving node with respect to the transmitting ones play a fundamental role in determining the angular spread [16–17].
The study of the azimuthal dispersion in a low-rank scenario, where the angular distribution cannot be resolved by the main lobe of the antenna radiation pattern, gets a considerable interest in the field of multiple antenna techniques. This interest is due to three main motivations.

- When the antenna array is adopted for interference suppression purposes, the main objective is to place pattern nulls towards the undesired sources. The nulls are much sharper than the main lobe and so the amount of residual interference incoming from directions different than the mean DOA have a considerable impact on the communication system performance. The statistic of the angular distribution of each undesired source provides useful information for modeling in a realistic manner the interference mitigation capabilities of the antenna system.

- Even if in a low-rank channel the main lobe of the radiation pattern is able to receive all multipath components relative to a desired source, the signal replicas are received with a lower gain as they become more distant from the mean DOA. Therefore, the PAS becomes helpful to take into account the degradation of the antenna power gain towards the directions corresponding to the desired source.

- The knowledge of the PAS in a high spatial correlation environment improves the level of accuracy of the DOA estimation algorithms, which can be much higher than the HPBW. In fact, the actual resolution accuracy is mainly limited not only by the Signal to Noise Ratio (SNR), but also by the angular spread around the mean DOA.

Several models have been developed in the literature to describe the PAS in different low-rank propagation environments [18–23]. Some of these statistics have been analytically derived adopting a geometrical approach that takes into account the displacement of the scatterers in the proximity of the transmitting node. Other statistics have been derived by curve fitting techniques applied on empirical data collected during environmental measurements. In this second case a closed form expression that describes the position of the scatterers around the transmitter is difficult to obtain and usually numerical approaches are adopted to simulate the

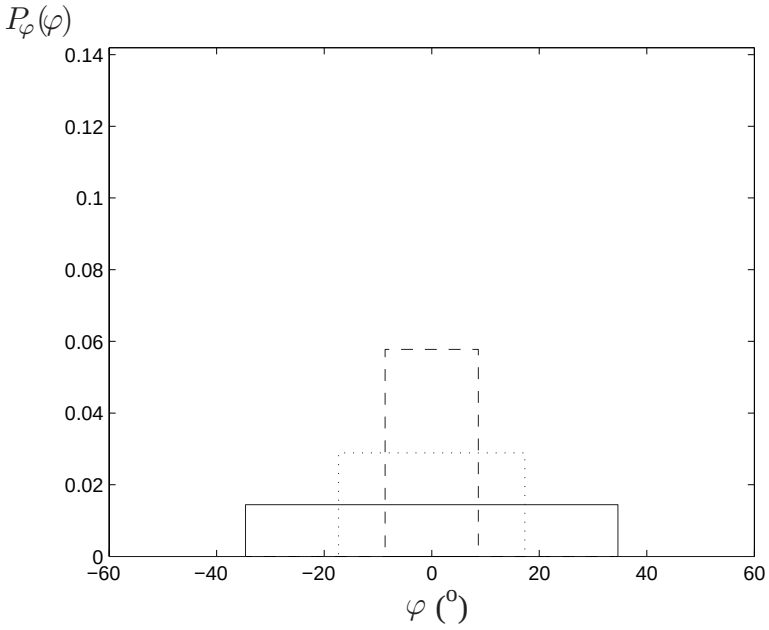

Figure 2.4: Uniform PAS for $P_{\mathrm{rx}} = 1$ and $\varphi_0 = 0$.
—— $\hat{\sigma}_\varphi = 5^o$ $(\varphi_\Delta \cong 8.7^o)$
····· $\hat{\sigma}_\varphi = 10^o$ $(\varphi_\Delta \cong 17.3^o)$
---- $\hat{\sigma}_\varphi = 20^o$ $(\varphi_\Delta \cong 34.6^o)$

channels that obey to these statistics. A brief overview of the most common distributions for the PAS is provided in the following of this subsection.

2.2.1.1 Uniform distribution

This statistic for the PAS has been proposed in [18], where it is assumed that the DOAs are uniformly distributed in the angular interval $[\varphi_0-\varphi_\Delta, \varphi_0+\varphi_\Delta]$, defined by the mean DOA and by the width $2\varphi_\Delta$. The PAS, shown in Fig. 2.4 for three values of the angular spread, is described by:

$$P_\varphi(\varphi) = \begin{cases} \dfrac{P_{\mathrm{rx}}}{2\varphi_\Delta} & |\varphi - \varphi_0| \leq \varphi_\Delta \\ 0 & \text{elsewhere} \end{cases}, \tag{2.13}$$

where P_{rx} denotes the power received from all directions and the angular spread is equal to $\varphi_\Delta/\sqrt{3}$.
In practice, distributions of scatterers that lead to a uniform distribution of the

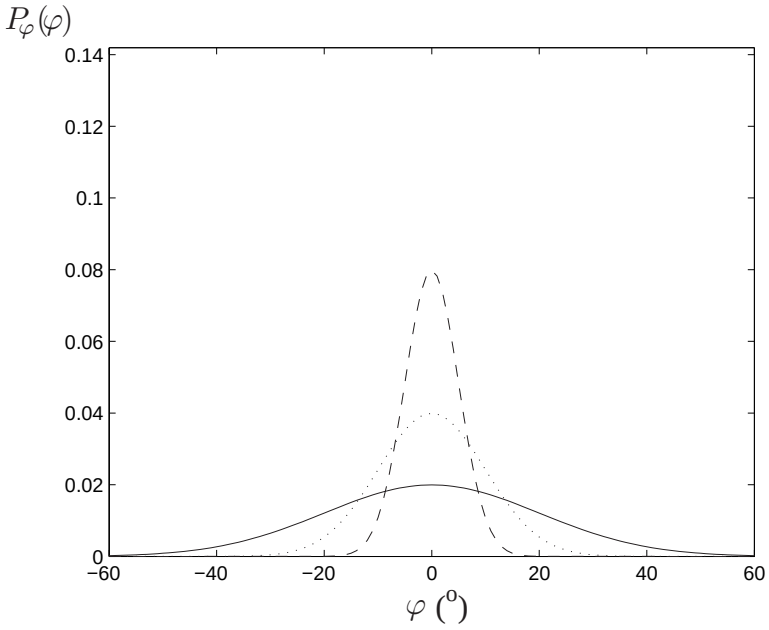

Figure 2.5: Truncated cosine PAS for $P_{\mathrm{rx}} = 1$ and $\varphi_0 = 0$.
—— $\hat{\sigma}_\varphi = 5^o$ $(\kappa = 130)$
····· $\hat{\sigma}_\varphi = 10^o$ $(\kappa = 32)$
---- $\hat{\sigma}_\varphi = 20^o$ $(\kappa = 7)$

DOAs are difficult to justify from a physical point of view. However, in some cases, this statistic is employed because it simplifies the calculations and enables the derivation of closed form analytical expressions.

2.2.1.2 Truncated cosine

The truncated cosine distribution has been derived analyzing the results obtained from channel measurements in urban areas in the early 1970's [19]. In particular, this statistic has been adopted to evaluate the correlation between two base station antennas. Analytically, the truncated cosine PAS can be described by:

$$P_\varphi(\varphi) = \begin{cases} \dfrac{P_{\mathrm{rx}}\gamma_{\mathrm{c}}}{\pi}\cos^\kappa(\varphi - \varphi_0) & |\varphi - \varphi_0| \leq \pi/2 \\ 0 & \text{elsewhere} \end{cases}, \tag{2.14}$$

where γ_{c} is a proper constant that can be obtained imposing the normalization condition $\int_{\varphi_0-\pi/2}^{\varphi_0+\pi/2} P_\varphi(\varphi) = P_{\mathrm{rx}}$, while the exponent κ determines $\hat{\sigma}_\varphi$ (Fig. 2.5).

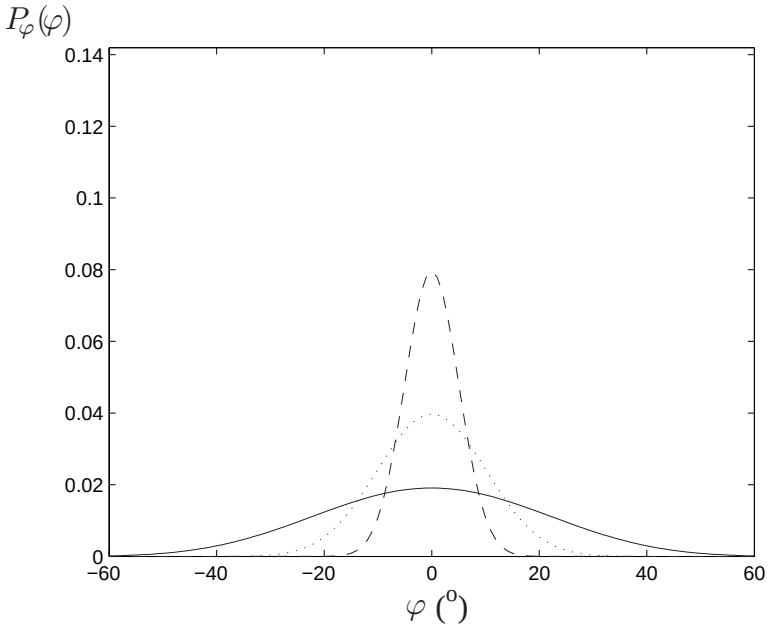

Figure 2.6: Truncated Gaussian PAS for $P_{\mathrm{rx}} = 1$ and $\varphi_0 = 0$.
—— $\hat{\sigma}_\varphi = 5^o$ ····· $\hat{\sigma}_\varphi = 10^o$ ---- $\hat{\sigma}_\varphi = 20^o$

To evaluate the desired κ value for a given angular spread, numerical techniques are usually adopted, even if, theoretically, a closed form computation is possible.

2.2.1.3 Truncated Gaussian

The use of a truncated Gaussian has been proposed in [20] in order to provide a PAS model directly related to the angular spread. This PAS is described by:

$$P_\varphi(\varphi) = \begin{cases} \dfrac{P_{\mathrm{rx}}\gamma_{\mathrm{G}}}{\sqrt{2\pi}\hat{\sigma}_\varphi} e^{-\frac{(\varphi-\varphi_0)^2}{2\hat{\sigma}_\varphi^2}} & |\varphi - \varphi_0| \leq \pi/2 \\ 0 & \text{elsewhere} \end{cases}, \tag{2.15}$$

where γ_{G} is the normalization constant. For small values of the angular spread the truncated cosine and the Gaussian distributions are very close to each other, as it can be noticed by comparing Fig. 2.5 and Fig. 2.6. The truncated cosine provides a realistic behavior for the uplink channel between a mobile node and a cellular base station, but the κ values that are required to model a low-rank environment, being in the order of 100, are not practical. The Gaussian distribution, instead, allows a closed form computation as a function of the angular spread, while representing a proper model for the PAS.

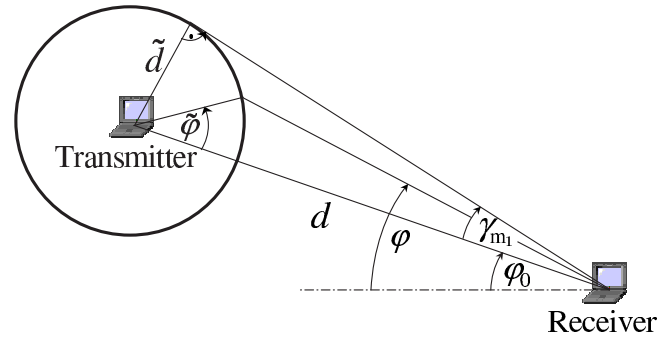

Figure 2.7: Ring of scatterers model.

2.2.1.4 Ring of scatterers

The PAS can also be derived geometrically, taking into account the displacement of the scatterers inside a region close to the transmitter.
Considering a uniform distribution of the scatterers on a circumference of radius $\tilde{d}$ surrounding the transmitting node, it can be assumed that the transmitted power is uniformly distributed in the angle $\tilde{\varphi}$ (Fig. 2.7). In particular, the power scattered by the differential element of $\tilde{\varphi}$, $\mathrm{d}\tilde{\varphi}$, can be evaluated as:

$$\mathrm{d}P = \frac{P_{\mathrm{rx}}}{2\pi}\mathrm{d}\tilde{\varphi}. \tag{2.16}$$

The angle $\tilde{\varphi}$ can be calculated by geometrical considerations from:

$$\frac{d}{\sin[\pi - \tilde{\varphi} - (\varphi - \varphi_0)]} = \frac{\tilde{d}}{\sin(\varphi - \varphi_0)}, \tag{2.17}$$

where d is the distance between the transmitter and the receiver. Defining $\gamma_{\mathrm{m}_1} = \mathrm{arcsin}(\tilde{d}/d)$, (2.17) can be written as:

$$\tilde{\varphi} = \arcsin\left[\frac{\sin(\varphi - \varphi_0)}{\sin\gamma_{\mathrm{m}_1}}\right] - (\varphi - \varphi_0), \tag{2.18}$$

to obtain $\tilde{\varphi}$ as a function of the generic azimuth DOA. The power received at the differential element of φ, $\mathrm{d}\varphi$, can be evaluated as $2\mathrm{d}P$ because, for any given azimuth, the power contribution is due to the portion of the ring facing the array and the portion on the opposite side. Therefore, the PAS can be obtained from:

$$P_{\varphi}(\varphi) = 2\frac{P_{\mathrm{rx}}}{2\pi}\frac{\mathrm{d}\tilde{\varphi}}{\mathrm{d}\varphi}, \tag{2.19}$$

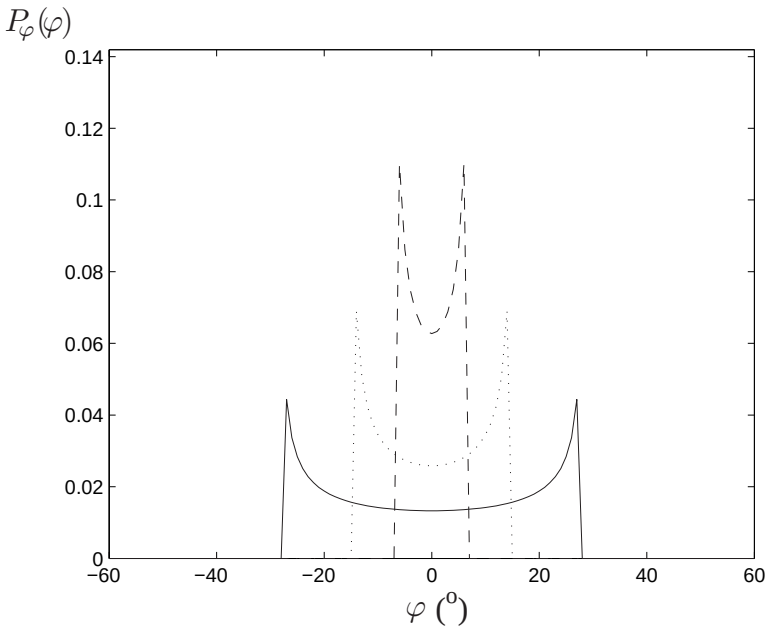

Figure 2.8: PAS corresponding to the ring of scatterers geometry for $P_{\mathrm{rx}} = 1$ and $\varphi_0 = 0$.
—— $\hat{\sigma}_\varphi = 5^o$ ($\gamma_{\mathrm{m}_1} \cong 7.3^o$)
····· $\hat{\sigma}_\varphi = 10^o$ ($\gamma_{\mathrm{m}_1} \cong 15.1^o$)
---- $\hat{\sigma}_\varphi = 20^o$ ($\gamma_{\mathrm{m}_1} \cong 28.3^o$)

which provides the following expression:

$$P_\varphi(\varphi) = \begin{cases} \dfrac{P_{\mathrm{rx}}}{\pi} \dfrac{\cos(\varphi-\varphi_0) - \sqrt{\sin^2\gamma_{\mathrm{m}_1} - \sin^2(\varphi-\varphi_0)}}{\sqrt{\sin^2\gamma_{\mathrm{m}_1} - \sin^2(\varphi-\varphi_0)}} & |\varphi-\varphi_0| < \gamma_{\mathrm{m}_1} \\ 0 & \text{elsewhere} \end{cases} \tag{2.20}$$

The PAS corresponding to the ring of scatterers presented here has been calculated adopting the process proposed in [21] for the case $\tilde{d} << d$. For small values of γ_{m_1}, (2.20) becomes:

$$P_\varphi(\varphi) = \begin{cases} \dfrac{P_{\mathrm{rx}}}{\pi\sqrt{\gamma_{\mathrm{m}_1}^2 - (\varphi-\varphi_0)^2}} & |\varphi-\varphi_0| < \gamma_{\mathrm{m}_1} \\ 0 & \text{elsewhere} \end{cases}, \tag{2.21}$$

which coincides with the expression presented in [21]. From the curves in Fig. 2.8 it can be noticed that, differently from the previous distributions, the mean DOA

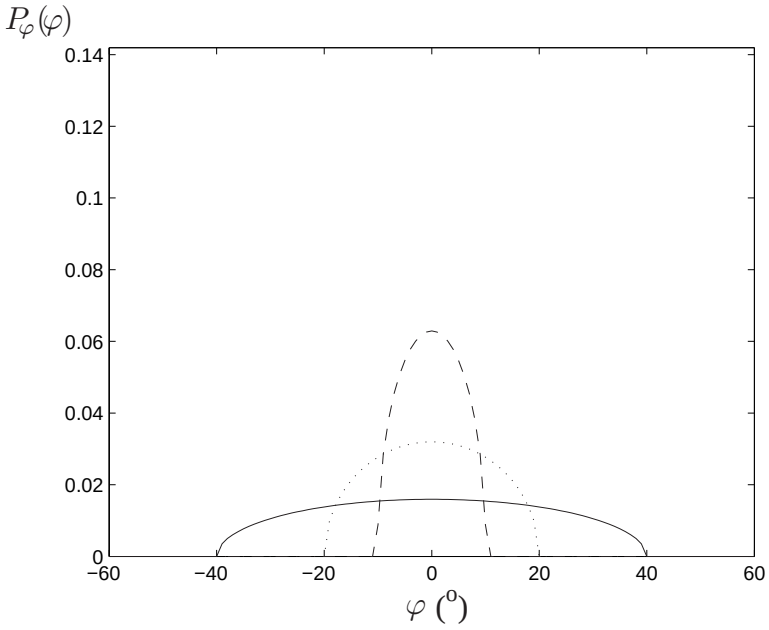

Figure 2.9: PAS corresponding to the disk of scatterers geometry for $P_{\mathrm{rx}} = 1$ and $\varphi_0 = 0$.
—— $\hat{\sigma}_\varphi = 5^o$ $(\gamma_{\mathrm{m}_2} \cong 10.1^o)$
····· $\hat{\sigma}_\varphi = 10^o$ $(\gamma_{\mathrm{m}_2} \cong 20.0^o)$
---- $\hat{\sigma}_\varphi = 20^o$ $(\gamma_{\mathrm{m}_2} \cong 40.0^o)$

is associated to the minimum power and the major contribution is given by the farther components.

2.2.1.5 Disk of scatterers

The spatial propagation model deriving from a disk of scatterers has been presented in [22] and is also known as the Geometrically Based Single Bounce Macrocell (GBSBM) channel model. The PAS is determined by the diameter of the disk surrounding the transmitter. This diameter defines a circle, called circle of influence, in which the scatterers are considered uniformly distributed. The PAS, plotted in Fig. 2.9, is described by:

$$P_\varphi(\varphi) = \begin{cases} \dfrac{2P_{\mathrm{rx}}}{\pi} \dfrac{\cos(\varphi-\varphi_0)\sqrt{\sin^2\gamma_{\mathrm{m}_2} - \sin^2(\varphi-\varphi_0)}}{\sin^2\gamma_{\mathrm{m}_2}} & |\varphi-\varphi_0| \leq \gamma_{\mathrm{m}_2} \\ 0 & \text{elsewhere} \end{cases} \tag{2.22}$$

where γ_{m_2} denotes the maximum angular shift from mean DOA.

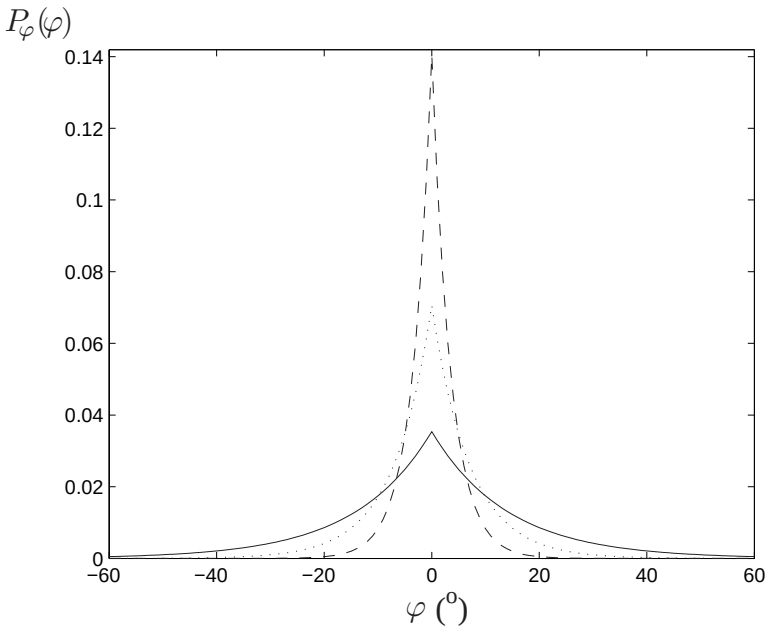

Figure 2.10: Truncated Laplacian PAS for $P_{\mathrm{rx}} = 1$ and $\varphi_0 = 0$.
—— $\hat{\sigma}_\varphi = 5^o$ ····· $\hat{\sigma}_\varphi = 10^o$ ---- $\hat{\sigma}_\varphi = 20^o$

2.2.1.6 Truncated Laplacian

Recent field measurements reveal a PAS having a Laplacian distribution around the mean DOA. The empirical data have been obtained in areas characterized by buildings ranging from four to six floors and irregular street grids, corresponding to a typical urban environment. The statistic is described by [23]:

$$P_\varphi(\varphi) = \begin{cases} \dfrac{P_{\mathrm{rx}}\gamma_{\mathrm{L}}}{\sqrt{2}\hat{\sigma}_\varphi} e^{-\frac{\sqrt{2}|\varphi-\varphi_0|}{\hat{\sigma}_\varphi}} & |\varphi-\varphi_0| \leq \gamma_{\mathrm{m_1}} \\ 0 & \text{elsewhere} \end{cases}, \tag{2.23}$$

where γ_{L} is the normalization constant. The truncated Laplacian PAS suggests that the distribution of scatterers is not uniform in area, but more energy is reflected from the regions closer to the transmitter (Fig. 2.10). As described in [21], this phenomenon may be due to a shielding effect of the scatterers that are closer to the transmitter with respect to the farther scatterers. Besides, additional propagation loss may occur due to the larger distance of these scatterers from the transmitter.

Chapter 3

Multiple Antenna Systems

This chapter introduces the main advantages of multi-antenna techniques and provides a classification, based on the wireless channel characteristics, of the different multiple antenna approaches. The fundamental concepts regarding Multiple Input Multiple Output (MIMO) systems, spatial diversity, fixed and adaptive beamforming, are presented, and some common theoretical definitions are illustrated. Besides, with particular reference to a low-rank environment, some of the most frequently adopted signal processing algorithms are recalled from the literature.

3.1 Benefits of multi-antenna systems

The recent development of high bit rate applications, such as multimedia streaming and video conferencing, together with the raised number of users, have increased the bandwidth demand in both cellular and Wireless Local Area Network (WLAN) environments. Traditionally, user communications are separated by frequency, as in Frequency Division Multiple Access (FDMA), by time, as in Time Division Multiple Access (TDMA), or by code, as in Code Division Multiple Access (CDMA) [24]. Recently, the possibility of separating the different users by space has led to the development of a new multiplexing technique, called Space Division Multiple Access (SDMA) [25]. The fundamental element of SDMA is the antenna array, whose elements are dynamically controlled to produce multiple beams towards the desired directions and nulls towards the undesired ones. The use of multi-antenna techniques, only recommended for Beyond Third Generation (B3G) cellular systems, represents a key concept in Fourth Generation (4G) systems and in WLAN scenarios for supporting higher bit rates [26]. The increased interest of researchers, operators and manufacturers in multi-antenna technologies

is due to some fundamental benefits that can be achieved in terms of quality, capacity and communication reliability [27–28].
Antenna arrays can be employed to improve the link quality by combating the effects due to multipath propagation. Alternatively, adopting multiple antennas, the different signal paths can be exploited to combat fading by spatial diversity techniques or can be used to increase the link capacity by allowing transmission of different data streams from different antennas. Therefore, the amount of traffic that can be sustained by a communication system for a given frequency bandwidth can be increased, leading to considerable spectral efficiency improvements.
Antenna arrays can also be employed to focus the energy towards certain directions and to mitigate or, adopting more sophisticated adaptive solutions, to suppress the transmission/reception towards other directions. This leads to a reduction of the transmitted/received interference and enables the spatial filtering of the incoming signals.
Wireless networks in which the topology is subdivided by cells, such as the wireless mesh networks or the classical cellular systems, may obtain large benefits from the adoption of multiple antennas. In particular, the increased coverage range, which decreases the power requirements, and the possibility to track the mobile nodes using proper non-overlapping beams, reduce the number of required handovers together with the need to deploy new base stations or mesh routers. Therefore, multi-antenna technology may have a considerable impact not only in terms of performance improvement, but also in terms of cost reduction for wireless operators.

3.2 Classification

As described in Section 2.2, the wireless propagation environment can be classified as high-rank or low-rank, depending on the angular spread of the channel, the separation between the antenna elements, the delay spread and the signal bandwidth. This interaction between the characteristics of the multipath channel and the physical properties of the antenna system determines the received signal statistics. In particular, the different multi-antenna approaches can be classified taking into account the spatial fading correlation between the signals received by the different elements of the array (Fig. 3.1). In a low correlation environment (high-rank channel) it is expected that the different multipath components provide a statistically independent behavior, which can be exploited by spatial multiplexing, to increase the bit rate, or by diversity, to improve the reliability of the communications. In particular, the objective of MIMO-spatial multiplexing is the increase of the system capacity, while spatial diversity is adopted to reduce the Bit Error Rate (BER). In a high correlation environment (low-rank channel), instead, fixed

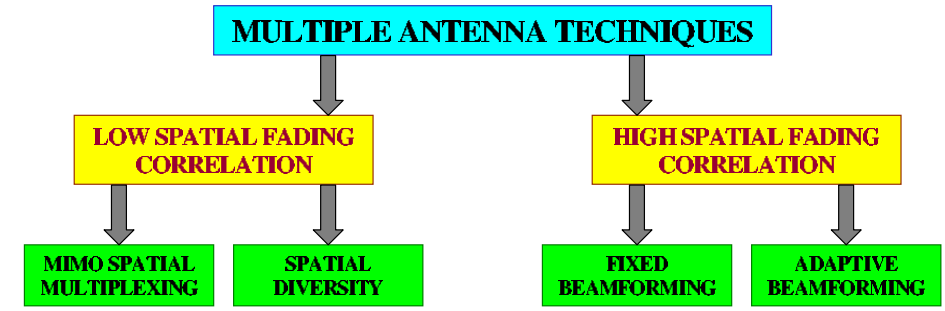

Figure 3.1: Classification of multiple antenna systems.

and adaptive beamforming techniques are adopted for maximizing the Signal to Interference plus Noise Ratio (SINR) at the antenna system output. This goal is obtained focusing the energy towards certain desired directions and mitigating or suppressing the energy towards the undesired ones.

3.3 MIMO-spatial multiplexing

MIMO systems represent one of the most promising research areas of wireless communications. The use of multiple antennas at both the receiver and the transmitter in a high-rank channel can significantly increase the link capacity, enabling the exploitation of multiple parallel radio channels in the same frequency band by separation in space. Adopting a MIMO system, the data stream from a single user is demultiplexed into N_{tx} spatial streams, corresponding to the number of transmitting antennas, and encoded into channel symbols. At the receiver side the streams are received by N_{rx} antennas and separated using proper signal processing techniques. The spectral efficiency increase that is achievable adopting MIMO technology is due to the fact that, in a rich scattering environment, the different signal paths incoming from the transmitter appear highly uncorrelated at each receiving antenna. The receiver can exploit this property to separate the signals originated from the different transmitting antennas, enabling the simultaneous reception of multiple spatial streams at the same frequency.

From the theoretical point of view the performance improvement provided by MIMO techniques can be quantified by the ergodic capacity, which is defined as the average of the maximum value of the mutual information between the transmitted and the received signal. Denote as $\mathcal{H} = [h_{kk'}]$ the $N_{\mathrm{rx}} \cdot N_{\mathrm{tx}}$ transfer channel matrix in a narrowband MIMO system, where $h_{kk'}$ is the complex path gain from the k'-th transmitting antenna to the k-th receiving antenna (Fig. 3.2). Assum-

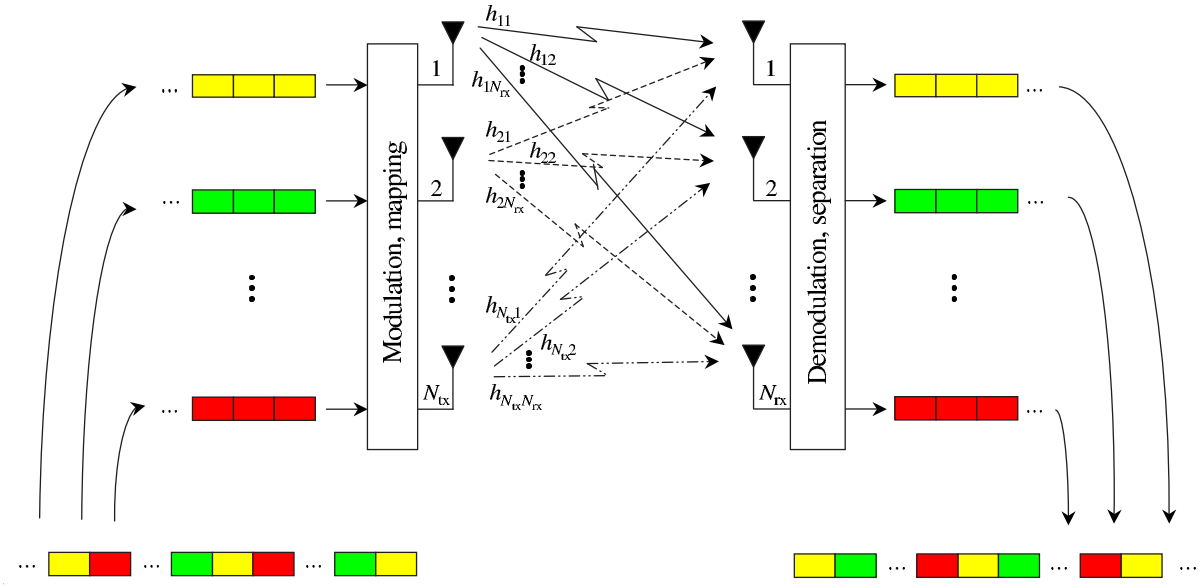

Figure 3.2: MIMO system.

ing that the coefficients of $\mathcal{H}$ are uncorrelated circularly symmetric Gaussian with zero mean and unit variance, and that the channel is unknown at the transmitter but perfectly known at the receiver, the ergodic capacity can be expressed as [29]:

$$\mathcal{C} = \mathbb{E}\left\{\log_2\left[\det\left(\mathbf{I}_{N_{\mathrm{rx}}} + \frac{\bar{P}_{\mathrm{out\_sa}}}{W}\frac{\mathcal{H}\mathcal{H}^H}{N_{\mathrm{tx}}}\right)\right]\right\}, \tag{3.1}$$

where $\mathbb{E}\{\cdot\}$ is the expectation, $\mathbf{I}_{N_{\mathrm{rx}}}$ is the identity matrix of rank N_{rx}, $\bar{P}_{\mathrm{out\_sa}}$ is the average power at the output of the generic receiving antenna and W is the noise power. Fixing the value of N_{rx} in (3.1), it can be shown that $\mathcal{H}\mathcal{H}^H/N_{\mathrm{tx}} \to \mathbf{I}_{N_{\mathrm{rx}}}$ for $N_{\mathrm{tx}} \to \infty$. Therefore, if the number of transmitting antennas is very large, the ergodic capacity approaches $N_{\mathrm{rx}}\log_2(1+\bar{P}_{\mathrm{out\_sa}}/W)$, growing linearly in the number of receiving antennas.
Instead, if N_{tx} is not very large and if $N_{\mathrm{rx}} \leq \mathrm{rank}(\mathcal{H})$, with $\mathrm{rank}(\mathcal{H})$ representing the rank of matrix $\mathcal{H}$, the ergodic capacity can be approximated in a high signal to noise ratio regime by [30]:

$$\mathcal{C} \cong N_{\mathrm{min}}\log_2\left(\frac{1}{N_{\mathrm{tx}}}\frac{\bar{P}_{\mathrm{out\_sa}}}{W}\right) + \frac{1}{\log 2}\left(\sum_{k=1}^{N_{\mathrm{min}}}\sum_{k'=1}^{N_{\mathrm{max}}-k}\frac{1}{k'} - \gamma_{\mathrm{E}}N_{\mathrm{min}}\right), \tag{3.2}$$

where $N_{\mathrm{min}} = \min(N_{\mathrm{tx}}, N_{\mathrm{rx}})$, $N_{\mathrm{max}} = \max(N_{\mathrm{tx}}, N_{\mathrm{rx}})$ and $\gamma_{\mathrm{E}} \cong 0.577$ is the Euler-Mascheroni's constant. In particular, (3.2) states that, in a rich scattering

environment, the number of available spatial streams between the transmitter and the receiver is constrained by the minimum between the number of antennas at the transmitter and at the receiver. This situation holds until the rank of the channel matrix is sufficiently high and so the signals arriving at the receiving antennas are uncorrelated. When the rank of $\mathcal{H}$ is reduced, the system capacity decreases. It is worth noticing that, even if the high-rank property of the channel is necessary to achieve a high spectral efficiency in a MIMO channel, low correlation does not guarantee high capacity with certainty. In [31], the authors prove the existence of degenerate channels, called "keyholes", in which the matrix $\mathcal{H}$ has poor rank properties even if the antennas both at the transmitter and at the receiver sides exhibit low fading correlation.

3.4 Spatial diversity

Diversity exploits the available copies of a signal to minimize fading effects and can be realized adopting different approaches. A diversity scheme can be obtained by transmitting multiple copies of the signal at intervals larger than the coherence time in order to provide time uncorrelated replicas (time diversity). Other diversity techniques exploit different polarizations (polarization diversity), different frequencies (frequency diversity), and multiple transmit and/or receive antennas (spatial diversity).
Fundamentally, a multi-antenna receiver can be implemented adopting four basic approaches: selection diversity, feedback diversity, Maximal Ratio Combining (MRC) and equal gain combining. In the first case the receiver selects the largest signal from those available at the different antenna elements, while in the second case the antenna outputs are scanned to find the highest SNR. In MRC, the signals are weighted, co-phased and summed, while in equal gain combining the signals are co-phased but summed with unity weights. Spatial receive diversity techniques, and in particular MRC, require the channel knowledge at the receiver to perform the coherent combining of the signal replicas. Instead, spatial transmit diversity can be achieved with and without channel knowledge. When the channel coefficients are known, the signal is transmitted from antennas experiencing independent fading (adopting antenna selection or weighting techniques) in order to maximize the signal power at the receiver. If no channel information is available, the signal can be transmitted from different antennas through Space-Time Coding (STC), which provides space and time diversity. One of the most efficient and simple STC techniques, employing only two transmit antennas, is the Alamouti scheme [33].
Transmit and receive diversity can be combined to obtain a diversity order equal to the product of the number of transmit and receive antennas. By consequence, the

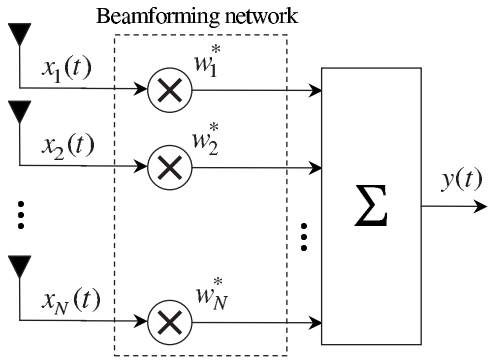

Figure 3.3: Analog beamforming.

MIMO channel provides $N_{\text{tx}}N_{\text{rx}}$ degrees of freedom that can be exploited for diversity purposes, (link quality improvement), or to perform spatial multiplexing, (link capacity increase). This imposes a tradeoff between bit rate enhancement and communication reliability. Recent research studies have addressed this topic by investigating which fraction of the degrees of freedom should be used for diversity, employing the remaining ones to improve the capacity [34–35].

3.5 Beamforming in low-rank environment

The term "beamforming" is used to denote an array processing technique for estimating one or more desired signals. The output provided by each antenna element is weighted according to a certain criterion in order to distinguish the spatial properties of a signal of interest from noise and interference. The name beamforming comes from the early forms of antenna arrays that were used to generate pencil beams, so as to receive signals from a specific direction and attenuate signals incoming from other directions. From this primary meaning related to propagation environments characterized by a low angular spread, beamforming has been extended to rich scattering scenarios and, at present, this term is used to denote the antenna processing techniques operating both in low and high-rank channels.
In a low-rank environment, depending on the level of sophistication of the adopted processing algorithm, beamforming techniques can be subdivided in two main groups: fixed beamforming and adaptive beamforming. In the first case the interference is mitigated but not suppressed and the system can be usually realized at a reasonable cost. Adaptive antennas, instead, require the adoption of complex signal processing algorithms in order to steer the main lobe towards the desired

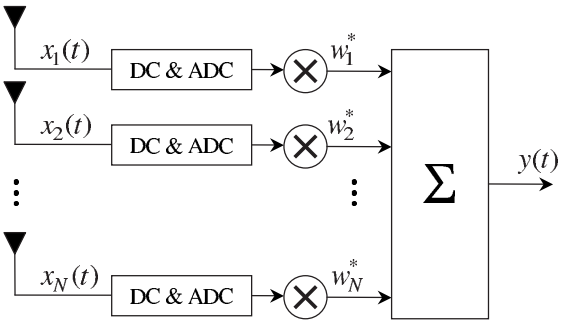

Figure 3.4: Digital beamforming.

direction and to suppress the undesired sources. This second approach leads to optimal performance, but is more expensive and needs considerable implementation efforts.
A narrowband beamformer is a processor operating on the input signals at the N antennas as a single linear combiner with coefficients equal to the antenna weights $\mathbf{w} = [w_1, ..., w_N]^T \in \mathbb{C}^{N\times 1}$. Therefore, the array output can be expressed as:

$$y(t) = \sum_{k=1}^{N} w_k^* x_k(t) = \mathbf{w}^H \mathbf{x}(t), \tag{3.3}$$

where $\mathbf{x}(t) = [x_1(t), ..., x_N(t)]^T$ is the received signal vector at the N antennas [36]. Theoretically, these weights may be applied directly at the Radio Frequency (RF) stage, realizing a beamforming network with analog devices (Fig. 3.3). This choice is rather costly due to the high quality required for the RF components. Analog beamforming needs precise phase shifters and selective power dividers. Most of the analog beamformers are used to form a unique lobe towards a desired direction, while multiple lobes are usually difficult to realize. However, considering that phase control elements are widely available and that many existing systems do not possess the capability for amplitude weighting, the use of analog phase-shifters alone represents an effective approach to simplify the hardware design [37]. Therefore, a large number of phase-only synthesis algorithms have been developed in the literature [38–43]. Inevitably, phase-only weighting provides lower performance with respect to phase-amplitude weighting. It is well known that an array of N antenna elements, in which the weights can be modified both in amplitude and phase, provides $N-1$ degrees of freedom. The one dimensional constraint regarding the desired direction reduces this number to $N-2$, which represents the number of directions that can be suppressed. In phase-only control systems this number of degrees of freedom is further reduced because of

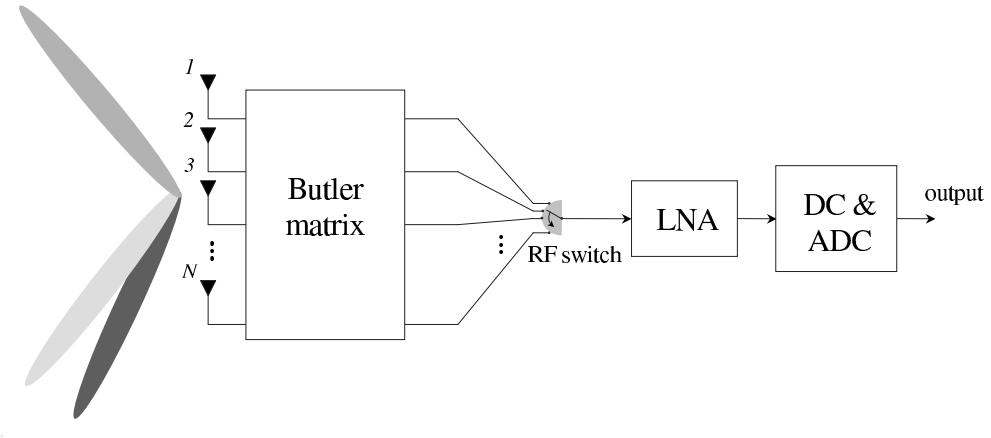

Figure 3.5: Switched-beam technique.

the constant amplitude constraint. Unfortunately, there are no theorems for the case of phase-only weighting that provide, in general, the remaining number of degrees of freedom.
From a logical point of view, the philosophy of digital beamforming is similar to that of analog beamforming in the sense that both techniques adjust the antenna weights, but using a different practical approach (Fig. 3.4). In digital beamforming the received RF signals are downconverted to Intermediate Frequency (IF) and then digitized by Analog-to-Digital Converters (ADCs). The DownConverter (DC) is adopted to simplify the digitization process, which gets more complex as the frequency increases. The availability of digital signals enables the use of a considerable number of processing algorithms [5, 36, 44–45], because the adaptation can be performed by the controlling software at a lower frequency.

3.6 Fixed beamforming

Fixed beamforming does not perform the amplitude weighting of the received signals and can be realized adopting either an analog approach (e.g. switched-beam, delay and sum) or a digital approach (e.g. beam-space beamforming).

3.6.1 Switched-beam antennas

The simplest technique for improving the performance of the system considers the use of multiple fixed beams (Fig. 3.5) [45]. Switched-Beam Antennas (SBAs) generate a finite number of radiation patterns, thus making one RF signal available

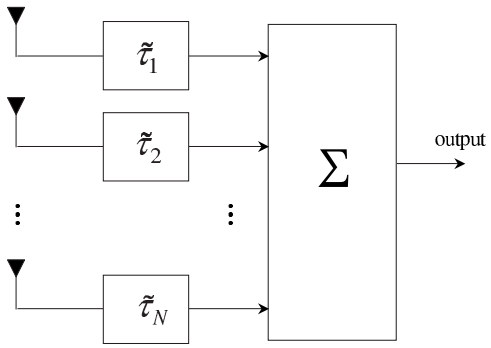

Figure 3.6: Delay and sum beamforming.

for each possible beam. The patterns are synthesized using an RF network that combines the signals received by the N antennas in order to form the different beams looking towards certain directions. The RF network (Butler matrix) is realized adopting analog phase shifters [46]. An RF switch selects, from inside the set of available outputs, the signal with the highest SINR that will be further processed by the Low Noise Amplifier (LNA) and, after downconversion, will be digitized. This technique requires only a single transmitting/reciving chain, but its performance is limited by the impossibility to perform a continuous beam and null steering.

3.6.2 Delay and sum beamforming

The most ancient form of spatial filtering that adopts an analog approach is the delay and sum beamforming, where delays are used instead of phase shifters (Fig. 3.6) [36]. For narrowband signals this scheme is substantially equivalent to switched-beam, but the delay and sum technique can also be applied to broadband signals. Depending on the delays, the antenna array isolates the signal for certain directions, but the interference is not specifically taken into account, because this scheme does not perform any amplitude weighting.

3.6.3 Beam-space beamforming

The two previous methods were both examples of analog fixed beamforming. Beam-space, instead, is a fixed beamforming technique that adopts a digital approach. Rather than directly weighting the signals incoming on the array elements, the antenna outputs can be first processed in order to produce a set of orthogonal

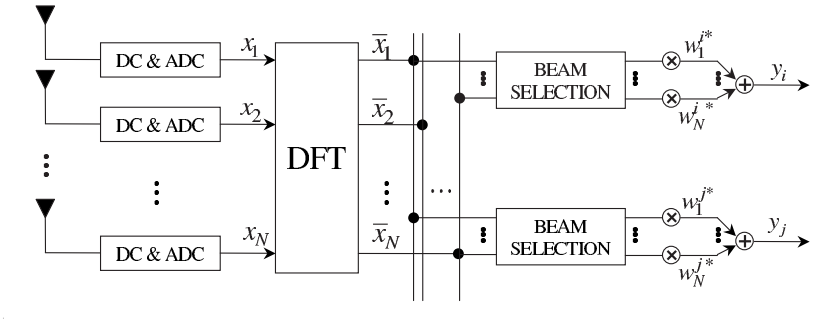

Figure 3.7: Beam-space beamforming.

multiple beams (Fig. 3.7). Assuming the use of an N elements ULA with interelement spacing ρ_1, the generic component of the array weight vector has the form:

$$e^{-j\frac{2\pi}{\lambda}\rho_1 k \sin\varphi_{k'}}, \quad k = 0, ..., N-1, \tag{3.4}$$

where the set of directions is selected according to:

$$\sin\varphi_{k'} = \frac{k'\lambda}{N\rho_1}, \quad k' = 0, ..., N-1. \tag{3.5}$$

Substituting (3.5) in (3.4), one obtains a generic Discrete Fourier Transform (DFT) element:

$$w_{k'k} = e^{-j2\pi\frac{k'k}{N}}, \quad k' = 0, ..., N-1,\ k = 0, ..., N-1. \tag{3.6}$$

The DFT outputs $\overline{\mathbf{x}} = \mathrm{DFT}_N[\mathbf{x}]$ correspond to N orthogonal directions that can be further processed (selected and weighted in phase) to provide the final desired output.

3.7 Adaptive beamforming

Adaptive Antennas (AAs) are also referred to in literature as smart antenna systems and represent advanced techniques able to maximize the SINR at the array output. They find application in environments where the spatial correlation between the signal replicas is high. The radiation pattern is dynamically controlled to perform the electrical beam steering to a desired direction, and null steering to reject interfering signals. Considering a multipath environment, where Q_l signal replicas arrive from the l-th generic source, the i-th sample of the signal received

by an N elements antenna array from n_{tx} transmitting sources can be described by:

$$\mathbf{x}(i) = \underbrace{s_0(i)\frac{1}{\tilde{\Upsilon}_0}\mathbf{a}(\varphi_0)}_{\mathbf{x}_{\mathrm{s}}(i)} + \underbrace{\sum_{l=0}^{n_{\mathrm{tx}}-1}\sum_{\substack{q=0 \text{ if } l\neq 0 \\ q=1 \text{ if } l=0}}^{Q_l-1}\frac{1}{\tilde{\Upsilon}_{lq}}s_l(i-\bar{\tau}_{lq})\mathbf{a}(\varphi_{lq}) + \tilde{\mathbf{n}}_{\mathrm{G}}(i)}_{\mathbf{x}_{\mathrm{u}}(i)}, \tag{3.7}$$

where $s_l(i)$ is the i-th sample of the signal transmitted by the l-th source, $\tilde{\Upsilon}_{lq}$ is the complex attenuation of the q-th replica of the l-th source incoming from φ_{lq} direction with delay $\bar{\tau}_{lq}$, $\mathbf{a}(\varphi_{lq})$ is the steering vector in the azimuth domain that, as described in Section 1.3, depends on the array geometry, and $\tilde{\mathbf{n}}_{\mathrm{G}}(i)$ represents the Gaussian noise vector. Without loss of generality, in (3.7), it is assumed that $l = 0$ represents the desired direction. In signal processing theory the received signal is usually decomposed in two parts, one corresponding to the desired signal, $\mathbf{x}_{\mathrm{s}}(i)$, and one including interference and noise, $\mathbf{x}_{\mathrm{u}}(i)$, which are used to define the array correlation matrices:

$$\mathbf{R}_{\mathrm{xx}} = \mathbb{E}\left\{\mathbf{x}(i)\mathbf{x}^H(i)\right\} \in \mathbb{C}^{N\times N}, \tag{3.8a}$$

$$\mathbf{R}_{\mathrm{ss}} = \mathbb{E}\left\{\mathbf{x}_{\mathrm{s}}(i)\mathbf{x}_{\mathrm{s}}^H(i)\right\} \in \mathbb{C}^{N\times N}, \tag{3.8b}$$

$$\mathbf{R}_{\mathrm{uu}} = \mathbb{E}\left\{\mathbf{x}_{\mathrm{u}}(i)\mathbf{x}_{\mathrm{u}}^H(i)\right\} \in \mathbb{C}^{N\times N}. \tag{3.8c}$$

Assuming that the processes $\mathbf{x}(t)$, $\mathbf{x}_{\mathrm{s}}(t)$, $\mathbf{x}_{\mathrm{u}}(t)$ are ergodic in the correlation matrix, (3.8) are usually approximated by their noisy estimates:

$$\mathbf{R}_{\mathrm{xx}} \cong \tilde{\mathbf{R}}_{\mathrm{xx}} = \frac{1}{\mathcal{N}_{\mathrm{as}}}\sum_{i=1}^{\mathcal{N}_{\mathrm{as}}}\mathbf{x}(i)\mathbf{x}^H(i), \tag{3.9a}$$

$$\mathbf{R}_{\mathrm{ss}} \cong \tilde{\mathbf{R}}_{\mathrm{ss}} = \frac{1}{\mathcal{N}_{\mathrm{as}}}\sum_{i=1}^{\mathcal{N}_{\mathrm{as}}}\mathbf{x}_{\mathrm{s}}(i)\mathbf{x}_{\mathrm{s}}^H(i), \tag{3.9b}$$

$$\mathbf{R}_{\mathrm{uu}} \cong \tilde{\mathbf{R}}_{\mathrm{uu}} = \frac{1}{\mathcal{N}_{\mathrm{as}}}\sum_{i=1}^{\mathcal{N}_{\mathrm{as}}}\mathbf{x}_{\mathrm{u}}(i)\mathbf{x}_{\mathrm{u}}^H(i), \tag{3.9c}$$

where $\mathcal{N}_{\mathrm{as}}$ is the number of available samples. The information contained in the correlation matrices is fundamental in digital array processing because the weight vector is estimated by methods based on the eigenanalysis of these matrices.
Adaptive antennas can be subdivided into three groups: spatial reference, temporal reference and blind techniques. This classification is performed distinguishing among the information required by the antenna system to realize the adaptation.

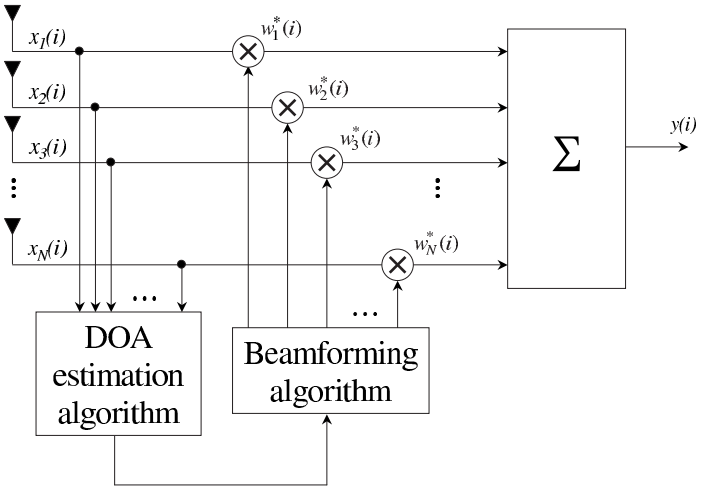

Figure 3.8: Spatial reference technique.

Spatial reference techniques use the DOAs of the incoming signals, temporal reference methods employ a reference signal, while blind techniques exploit some a priori known characteristics of the desired signal. The following subsections provide a brief description of each group of algorithms.

3.7.1 Spatial reference techniques

Spatial reference techniques perform the antenna system adaptation using the DOAs relative to the multipath components of the desired and of the interfering signals. In practice two algorithms are needed, one to estimate the DOAs and one to estimate the antenna weights (Fig. 3.8). The beamforming algorithms are developed in order to maximize the SINR at the array output, which, using the correlation matrices, can be expressed as:

$$\mathrm{SINR} = \frac{\mathbb{E}\left\{|\mathbf{w}^H \mathbf{x}_\mathrm{s}(i)|^2\right\}}{\mathbb{E}\left\{|\mathbf{w}^H \mathbf{x}_\mathrm{u}(i)|^2\right\}} = \frac{\mathbf{w}^H \mathbf{R}_{\mathrm{ss}} \mathbf{w}}{\mathbf{w}^H \mathbf{R}_{\mathrm{uu}} \mathbf{w}}. \tag{3.10}$$

It is known from the literature that the Minimum Variance Distortionless Response (MVDR) beamformer is able to maintain an undistorted array response to the desired signal while minimizing the output interference plus noise power [47]. Therefore, the problem can be reformulated as finding:

$$\min_{\mathbf{w}} \ \mathbf{w}^H \mathbf{R}_{\mathrm{uu}} \mathbf{w} \tag{3.11}$$

subject to the constraint:

$$\mathbf{w}^H \mathbf{a}(\varphi_0) = 1. \tag{3.12}$$

The solution can be calculated by means of the Lagrange multiplier method, by minimizing the function:

$$\mathcal{F}(\mathbf{w}, \gamma_{\mathcal{F}}) = \mathbf{w}^H \mathbf{R}_{\mathrm{uu}} \mathbf{w} + \gamma_{\mathcal{F}}[1 - \mathbf{w}^H \mathbf{a}(\varphi_0)]. \tag{3.13}$$

Taking the gradient and setting it to zero, one obtains the MVDR beamformer:

$$\mathbf{w}_{\mathrm{opt}} = \frac{\mathbf{R}_{\mathrm{uu}}^{-1} \mathbf{a}(\varphi_0)}{\mathbf{a}^H(\varphi_0) \mathbf{R}_{\mathrm{uu}}^{-1} \mathbf{a}(\varphi_0)}. \tag{3.14}$$

In practice, when the estimate of $\mathbf{R}_{\mathrm{uu}}$ is not available, the total array correlation matrix $\mathbf{R}_{\mathrm{xx}}$ is used to estimate the weights. In this case, the optimum weights are selected by minimizing the mean output power $\mathbf{w}^H \mathbf{R}_{\mathrm{xx}} \mathbf{w}$, while maintaining unity response in the look direction. More precisely, the optimum weight vector can be simply obtained from (3.14) by replacing $\mathbf{R}_{\mathrm{uu}}$ with $\mathbf{R}_{\mathrm{xx}}$.
The MVDR beamformer is computationally consuming because it requires the calculation of $\mathbf{R}_{\mathrm{xx}}$ and $\mathbf{R}_{\mathrm{xx}}^{-1}$ together with the estimation of the DOAs. Therefore, some techniques have been developed to reduce the computational burden. The two main approaches are the Frost and the Howells-Applebaun algorithms [48–49], which do not require the calculation of $\mathbf{R}_{\mathrm{xx}}^{-1}$ and converge to the optimum weights by recursively updating $\mathbf{w}$. However, all the beamformers based on spatial reference methods need the knowledge of the direction of arrivals of the incoming signals.

3.7.1.1 DOA estimation algorithms

The most common techniques for DOA estimation can be distinguished between spectral based and parametric algorithms. Spectral based algorithms use a function, called *pseudospectrum*, in which the maxima give an indication of the DOAs. A large number of spectral based solutions have been proposed in literature, such as the Bartlett method, the Capon estimate, the linear prediction method, the maximum entropy method and many others [5].
A simple and widely adopted technique is the MUltiple SIgnal Classification (MUSIC) algorithm, which exploits the eigenstructure properties of the array correlation matrix [36]. The method assumes that the noise at different antenna elements is uncorrelated. In general, the incident signals can be correlated, although the MUSIC algorithm becomes ineffective when this correlation becomes too high. When $n_{\mathrm{tx}} (< N)$ directions must be estimated, the space spanned by the eigenvectors of $\mathbf{R}_{\mathrm{xx}}$ can be partitioned in two orthogonal subspaces: the signal subspace $\mathbf{V}_{\mathrm{s}}$ and the noise subspace $\mathbf{V}_{\mathrm{n}}$. The signal subspace is generated by

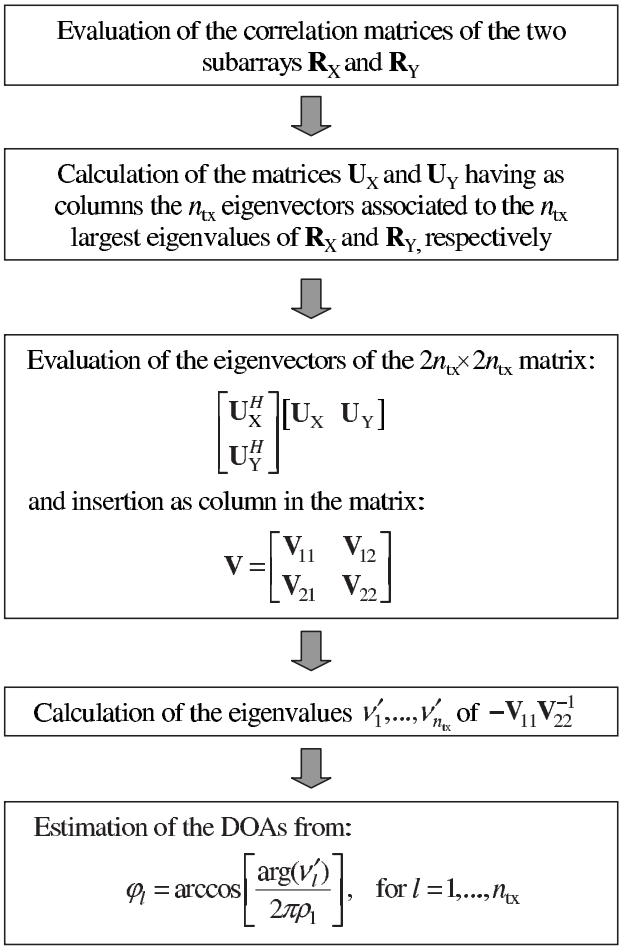

Figure 3.9: ESPRIT algorithm.

the eigenvectors associated to the n_{tx} largest eigenvalues of $\mathbf{R}_{\mathrm{xx}}$, while the noise subspace is spanned by the eigenvectors associated to the $N - n_{\mathrm{tx}}$ smallest eigenvalues of $\mathbf{R}_{\mathrm{xx}}$. The steering vectors corresponding to the directional sources are orthogonal to the noise subspace and are contained in the signal subspace. The n_{tx} DOAs are estimated by evaluating the maxima of the MUSIC pseudospectrum:

$$\tilde{\mathcal{S}}_{\mathrm{MUSIC}}(\varphi) = \frac{1}{\mathbf{a}^H(\varphi)\mathbf{V}_{\mathrm{n}}\mathbf{V}_{\mathrm{n}}^H\mathbf{a}(\varphi)}, \tag{3.15}$$

where $\mathbf{a}(\varphi)$ is usually redefined, in the DOA estimation terminology, as scanning vector. When $\tilde{\mathcal{S}}_{\mathrm{MUSIC}}(\varphi)$ has a local maximum, its denominator has a local minimum and so this method estimates the direction of arrival by searching the most

orthogonal scanning vectors $\mathbf{a}(\varphi)$ to the noise subspace. The MUSIC algorithm is characterized by a certain computational complexity, but can be applied to antenna arrays of arbitrary geometry.
Another family of algorithms for DOA estimation, alternative to spectral based techniques, adopts a parametric approach. A robust and computationally efficient algorithm is the Estimation of Signal Parameters via Rotational Invariance Techniques (ESPRIT). ESPRIT is a parametric method that exploits the rotational invariance in the signal subspace which is provided by two (sub)arrays with translational invariance structure. The array geometry must be properly chosen to make possible the selection of two subarrays having this property. For example, a ULA with N antenna elements and interelement spacing ρ_{l} can be viewed as two subarrays, where the first subarray is formed by the first $N-1$ elements and the second subarray is formed by the last $N-1$ elements. One obtains two subarrays separated by a distance ρ_{l}, where the k-th element of the first subarray and the k-th element of the second subarray form the k-th pair. The algorithm uses the correlation matrices $\mathbf{R}_{\mathrm{X}}$ and $\mathbf{R}_{\mathrm{Y}}$ of the two subarrays to estimate the DOAs. The overall procedure is briefly summarized in Fig. 3.9. The above explanation is referred to a linear geometry, however, ESPRIT can be also applied to rectangular, triangular and circular arrays [50–51].
In general, adopting spatial reference techniques, both beamforming and DOA estimation algorithms require careful array calibration in order to precisely determine the physical characteristics of the antenna system. Mutual coupling between the array elements lead to distorted single element patterns that can hardly affect the accuracy of the results.

3.7.2 Temporal reference techniques

Temporal reference techniques perform the antenna system adaption using a reference signal (training sequence) $y_{\mathrm{d}}(i)$ that is known both at the transmitter and at the receiver (Fig. 3.10). The array output $y(i)$ is subtracted from $y_{\mathrm{d}}(i)$ to generate an error $y_{\mathrm{e}}(i) = y_{\mathrm{d}}(i) - y(i)$ which is used to control the weight vector. In particular, $\mathbf{w}$ is adjusted in order to minimize the Mean Square Error (MSE) between the array output and the training sequence:

$$\mathrm{MSE} = \mathbb{E}\left\{|y_{\mathrm{e}}(i)|^2\right\} = \mathbb{E}\left\{|y_{\mathrm{d}}(i)|^2\right\} - 2\mathbf{w}^H\tilde{\mathbf{y}} + \mathbf{w}^H\mathbf{R}_{\mathrm{xx}}\mathbf{w}, \tag{3.16}$$

where $\tilde{\mathbf{y}} = \mathbb{E}\{\mathbf{x}(i)y_{\mathrm{d}}(i)\}$. The MSE surface is a quadratic function of $\mathbf{w}$ and is minimized by imposing its complex gradient with respect to $\mathbf{w}$ equal to zero:

$$\nabla_{\mathbf{w}^*}\mathbb{E}\left\{|y_{\mathrm{e}}(i)|^2\right\} = -2\tilde{\mathbf{y}} + 2\mathbf{R}_{\mathrm{xx}}\mathbf{w}, \tag{3.17}$$

which leads to the Wiener-Hopf equation for the optimal weight vector:

$$\mathbf{w}_{\mathrm{opt}} = \mathbf{R}_{\mathrm{xx}}^{-1}\tilde{\mathbf{y}}. \tag{3.18}$$

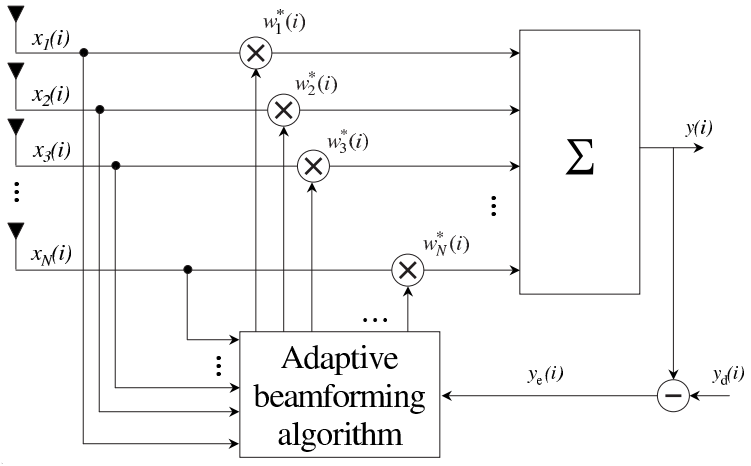

Figure 3.10: Temporal reference technique.

The complete solution of the Wiener-Hopf equation requires the computation of the inverse of the array correlation matrix $\mathbf{R}_{\mathrm{xx}}^{-1}$ and the calculation of $\tilde{\mathbf{y}}$. However, other techniques can be employed to reduce the computational burden, such as the unconstrained Least Mean Square (LMS) algorithm and the Recursive Least Square (RLS) algorithm [36].

3.7.2.1 Unconstrained LMS algorithm

The LMS algorithm is referred to as constrained LMS when the estimated weights are subjected to constraints at each iteration, while it is referred to as unconstrained LMS when the weights are not constrained at each iteration. This second option is mainly applicable when $\mathbf{w}$ is iteratively calculated exploiting a reference signal. LMS updates the weights at each iteration by estimating the gradient of the MSE quadratic error surface and then moving the weights in the opposite direction with respect to the gradient by a small quantity, which is determined by a constant called step size γ_{LMS}. This constant largely influences the convergence characteristics of the algorithm in terms of speed and closeness to the optimal solution. Unconstrained LMS uses an estimate of the gradient by replacing $\mathbf{R}_{\mathrm{xx}}$ and $\tilde{\mathbf{y}}$ with their noisy estimates available at $(i+1)$-th iteration, namely $\mathbf{x}(i+1)\mathbf{x}^H(i+1)$ and $\mathbf{x}(i+1)y_{\mathrm{d}}(i+1)$, respectively. Therefore, the weights are updated from:

$$\mathbf{w}(i+1) = \mathbf{w}(i) - \gamma_{\mathrm{LMS}}\mathbf{x}(i+1)y_{\mathrm{e}}^*(i) \tag{3.19a}$$

$$y_{\mathrm{e}}(i) = \mathbf{w}^H(i)\mathbf{x}(i+1) - y_{\mathrm{d}}(i+1) \tag{3.19b}$$

and the convergence is guaranteed if $0 < \gamma_{\mathrm{LMS}} < 1/\nu_{\max}$, where $\nu_{\max}$ denotes the maximum eigenvalue of $\mathbf{R}_{\mathrm{xx}}$. Under this condition the algorithm is stable and $\mathbf{w}$ converges to the optimum weight vector. However, for practical purposes, the following alternative (and more restrictive) condition can be applied:

$$0 < \gamma_{\mathrm{LMS}} < \frac{1}{\mathrm{tr}\,(\mathbf{R}_{\mathrm{xx}})}, \tag{3.20}$$

where $\mathrm{tr}\,(\mathbf{R}_{\mathrm{xx}})$ represents the trace of $\mathbf{R}_{\mathrm{xx}}$. This option is often preferred because the calculation of $\mathrm{tr}\,(\mathbf{R}_{\mathrm{xx}})$ is easier to perform as compared to the estimation of the eigenvalues of $\mathbf{R}_{\mathrm{xx}}$. The excess MSE produced by the LMS algorithm with respect to the theoretical minimum, corresponding to optimal solution, is mainly influenced by the minimum eigenvalue $\nu_{\min}$ of $\mathbf{R}_{\mathrm{xx}}$. As the spread of the eigenvalues increases, the highest γ_{LMS} value that guarantees the stability decreases. The selection of a too small step size results in a lower rate of convergence, while an excessively high value of γ_{LMS} leads to a rapid achievement of the solution, but the weights fluctuate inside a larger region and the excess MSE is larger. The main advantage of the LMS algorithm is its implementation simplicity, while its main drawback is the sensitivity of the convergence behavior to the eigenvalue spread.

3.7.2.2 RLS algorithm

The problem related to the influence of the eigenvalues on the convergence characteristics of the LMS algorithm is solved by the RLS algorithm, in which the gradient step size is replaced by a gain matrix $\hat{\mathbf{R}}_{\mathrm{xx}}$, which is estimated at each iteration. The RLS algorithm minimizes the Cumulative Square Error (CSE) exponentially weighted, which is defined at the i-th iteration as:

$$\mathrm{CSE}(i) = \sum_{i'=0}^{i} \gamma_{\mathrm{RLS}}^{i-i'} |y_{\mathrm{e}}(i')|^2, \tag{3.21}$$

where $\gamma_{\mathrm{RLS}} \in (0,1)$ is called the forgetting factor, as the update equation tends to deemphasize the old samples. The weights are updated using:

$$\mathbf{w}(i) = \mathbf{w}(i-1) - \hat{\mathbf{R}}_{\mathrm{xx}}^{-1}(i)\mathbf{x}(i)y_{\mathrm{e}}^{*}(i-1), \tag{3.22}$$

where, the gain matrix at i-th iteration is estimated as:

$$\hat{\mathbf{R}}_{\mathrm{xx}}^{-1}(i) = \begin{cases} \dfrac{1}{\tilde{\gamma}_{\mathrm{RLS}}}\mathbf{I}_N & i = 0 \\ \dfrac{1}{\gamma_{\mathrm{RLS}}}\left[\hat{\mathbf{R}}_{\mathrm{xx}}^{-1}(i-1) - \dfrac{\hat{\mathbf{R}}_{\mathrm{xx}}^{-1}(i-1)\mathbf{x}(i)\mathbf{x}^{H}(i)\hat{\mathbf{R}}_{\mathrm{xx}}^{-1}(i-1)}{\gamma_{\mathrm{RLS}} + \mathbf{x}^{H}(i)\hat{\mathbf{R}}_{\mathrm{xx}}^{-1}(i-1)\mathbf{x}(i)}\right] & i > 0 \end{cases}, \tag{3.23}$$

and $\tilde{\gamma}_{\mathrm{RLS}} > 0$. As compared to the LMS algorithm, the RLS approach presents a higher complexity, but provides a higher speed of convergence and performs better in flat fading channels [53].
With respect to spatial reference techniques, temporal reference techniques require the use of a reference signal. This leads to an increased overhead during packet transmission, because a preamble must be added to the packet payload to allow the adaptation process. However, using temporal reference algorithms, a precise characterization of the physical antenna system is not required. In fact, mutual coupling effects among the array elements are transparently handled during the adaptation routine and the estimation of the distorted single element radiation patterns is not necessary.

3.7.3 Blind techniques

Temporal reference systems require synchronization and demodulation before performing the weight adaptation, whereas spatial reference systems need DOA estimation and very strictly calibrated hardware. Blind techniques, instead, do not necessitate training sequences or any information regarding the physical antenna system, because they are based on the a priori knowledge of some characteristics of the desired signal. The most common algorithm adopting the blind approach is the Constant Modulus Algorithm (CMA) [54]. This algorithm operates on the principle that the amplitude of the communication signal is distorted by interference and multipath fading. Otherwise, the signal should have a constant envelope. The CMA tries to restore this envelope in an average sense by minimizing the following cost function:

$$\mathcal{F}_{\mathrm{CMA}}(\mathbf{w}) = \frac{1}{2}\mathbb{E}\left\{[|y(i)|^2 - y_0^2]^2\right\}, \tag{3.24}$$

where y_0 represents the desired amplitude in absence of interference and the antenna system output $y(i)$ is a function of $\mathbf{w}$. The minimization of (3.24) can be performed adopting the LMS approach that leads to the following iterative solution for the beamforming weight vector:

$$\mathbf{w}(i+1) = \mathbf{w}(i) - \gamma_{\mathrm{LMS}}\mathbf{x}(i+1)y(i)[|y(i)|^2 - y_0^2]. \tag{3.25}$$

It can be observed that, defining the error term as $y_{\mathrm{e}}(i) = y^*(i)[|y(i)|^2 - y_0^2]$, (3.25) becomes equal to the update equation of the LMS algorithm expressed by (3.19a). The two conditions which may lead to stop the adaptation are $|y(i)| = y_0$, representing the desired convergence, and $|y(i)| = 0$. This second case is not a practical problem, since the system noise moves the weight vector away from this unstable zero gradient point [28]. The main drawback of CMA is that, in an hostile

fading environment, the algorithm may incorrectly select an interferer having the same envelope of the desired signal.

Chapter 4

Distributed Wireless Networks

This chapter introduces the fundamental characteristics of a distributed wireless network, focusing on the impact of multiple antennas on the system behavior. A brief description of the widely diffused IEEE 802.11 standard for WLANs is provided, with particular reference to the medium access control layer. Besides, a short overview of the research literature that analyzes the theoretical aspects related to the adoption of beamforming techniques in Distributed Wireless Networks (DWNs) is presented.

4.1 General concepts

In recent years, there has been an increased interest in the design of DWNs for indoor and outdoor operations, given their self-configuring capabilities and their lower installation cost with respect to the infrastructured networks. DWNs include the well known Mobile Ad-hoc NETworks [55] (MANETs) as well as the lately introduced Wireless Mesh Networks (WMNs) [56], and the application domain involves data, voice and video transmission. WMNs and MANETs are characterized by the lack of a wired infrastructure, as is required in cellular environment through the deployment of base stations. Besides, both kinds of networks adopt a multi-hop approach. The generic node is able to communicate directly with any other node that resides within its transmission range, but, in order to exchange packets with nodes residing beyond this range, the presence of intermediate relays is required to forward the messages hop by hop.
Even if many common aspects exist between MANETs and WMNs, some key differences can be highlighted. In a MANET, nodes can be considered substantially identical (Fig. 4.1), while, in a WMN, nodes can be classified in two groups: the mesh routers, forming the backbone WMN, and the mesh clients, forming the client WMN (Fig. 4.2). Mesh routers and MANET nodes may be laptops or

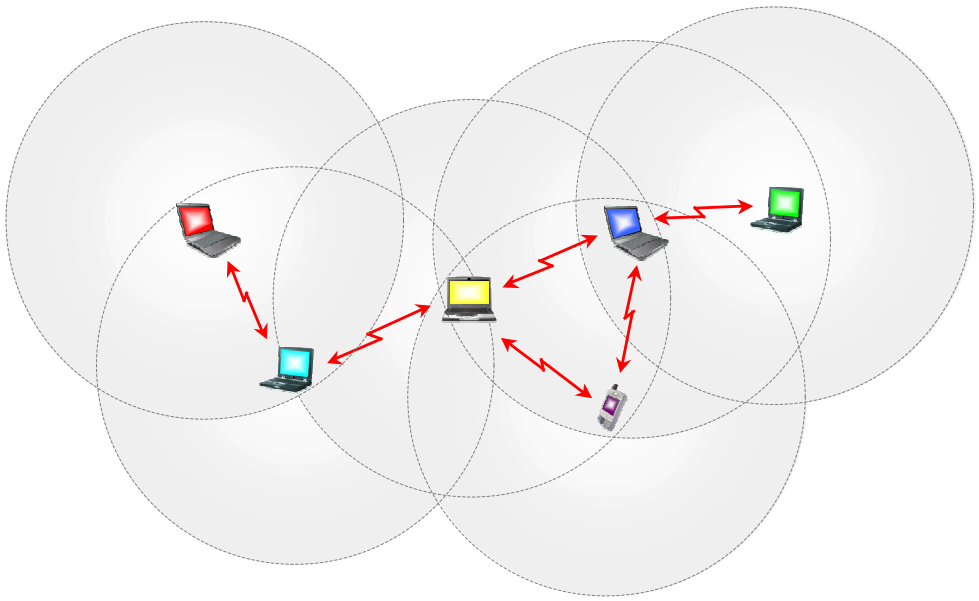

Figure 4.1: Ad-hoc network.

Personal Digital Assistants (PDAs) with a wireless board, and must have routing capabilities to perform packet forwarding. A mesh router provides multiple virtual or physical interfaces to manage the communications with both the mesh clients and the other mesh routers. Besides, the backbone nodes can be equipped with multiple radios to increase the available bandwidth resources. However, in this case, co-channel interference remains a limiting factor even if the frequency channels are non-overlapping. Another fundamental difference between MANETs and WMNs is that, in a MANET, nodes are mobile and power saving is mandatory, while in a backbone WMN the nodes have a limited mobility and energy saving is not a fundamental concern.
Even if MANETs and WMNs have different constraints in terms of mobility and power saving, a fundamental topic for both kinds of networks is the increase of the network throughput and the improvement of communication reliability.
Over the past twenty years, DWNs have been adopted for seamless internetworking in areas without pre-existing communication infrastructures, finding application in military and disaster recovery environments. However, the recent introduction of new standards and technologies, such as Bluetooth [57] and IEEE 802.11 [58], has largely increased the interest of manufacturers and operators for the civil application of distributed networks. The rapid diffusions of wireless devices among users, from cell phones to portable laptops, increases the demand

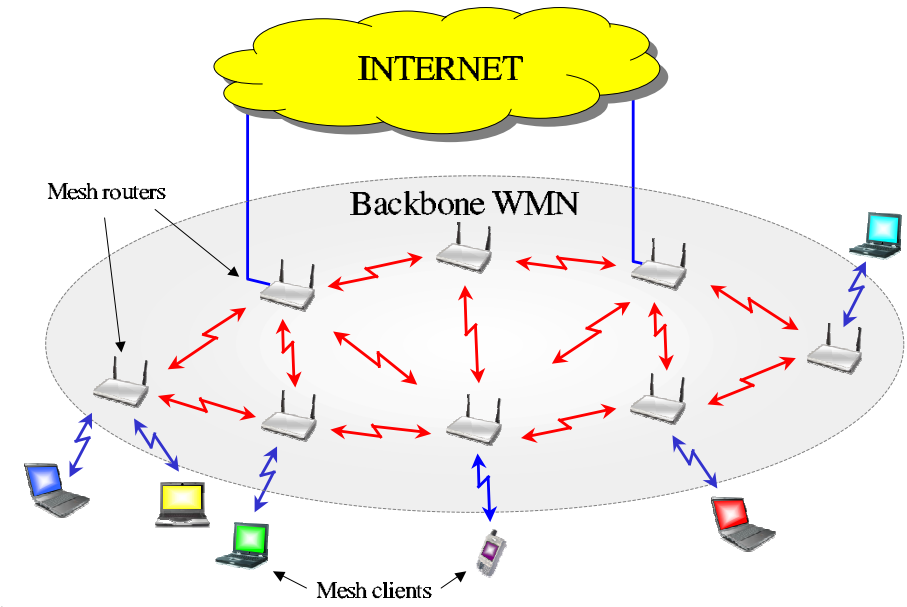

Figure 4.2: Wireless mesh network.

of wireless services in personal, local, campus and metropolitan areas. The deployment of WMNs represents a low-cost opportunity to support temporary occurrences, such as conferences, concerts and sport events, as well as to guarantee permanent services, including enterprise networking, broadband home networking, building automation, community networks, etc.

4.2 IEEE 802.11

The most widely adopted standard for DWNs is the IEEE 802.11, which provides detailed specifications for the Medium Access Control (MAC) and the PHYsical (PHY) layers of WLANs. The legacy version, [58], approved in 1997, has been successively extended by different task groups, providing a set of WLAN standards that are globally denoted by the term 802.11x. Some extensions have been developed to increase the available rate [59–61], while other amendments concern Quality of Service (QoS) support [62] and security improvement [63]. Further proposals, regarding the communication in high mobility environment, fast roaming, WMN management and throughput enhancement, are in phase of study or are already present in draft format.
The 802.11 legacy version operates at 2.4 GHz and adopts two spread spectrum techniques to transmit the data frames over the medium: the Direct Sequence

Spread Spectrum (DSSS) and the Frequency Hopping Spread Spectrum (FHSS). Together with these RF technologies, the standard provides the possibility to communicate by InfraRed (IR). However, this option has not been considered in the successive extensions of 802.11 because IR PHY requires LOS and cannot pass through walls, issues which restrict it to small indoor environments.

4.2.1 Transmission rates

The nominal bit rates provided by the RF PHY of the legacy 802.11 are 1 and 2 Mbits/s obtained using Binary Phase Shift Keying (BPSK) and Quadrature Phase Shift Keying (QPSK) modulations. The 802.11b amendment provides two additional bit rates equal to 5.5 and 11 Mbits/s, while the 802.11g reaches the 54 Mbits/s employing the Orthogonal Frequency Division Multiplexing (OFDM) technique. The same rates of the 802.11g are available in the 5.8 GHz band by adopting the 802.11a PHY layer extension. Both 802.11a and 802.11g can operate at several bit rates, varying from 6 to 54 Mbits/s, but, since the transmitter power is limited (100 mW in Europe and 1 W in USA), the transmission range decreases when the bit rate increases. The different rates are obtained selecting the proper transmission mode, which is defined by the combination between the modulation scheme and the coding rate of the adopted convolutional encoder.
At present, the Task Group n is working on the final version of the 802.11n extension that is expected to be approved in 2009 [26]. This further amendment combines MIMO and OFDM technologies to support nominal rates in the order of 300÷600 Mbits/s, depending on the number of antennas employed at the transmitter/receiver sides and on the richness of the scattering environment [64–65].

4.2.2 Architecture

The basic element of an 802.11 WLAN is the Basic Service Set (BSS), which represents a set of nodes that communicate with each other. If there is no connection to a wired network, the BSS is called Independent BSS (IBSS) and the nodes, which can be mobile, are able to exchange information adopting multi-hop approach. An IBSS is often formed without pre-planning and the wireless connections are maintained for only as long as the WLAN is needed. Therefore, an IBSS is defined as an ad-hoc network. When there is an Access Point (AP), the BSS is called infrastructure BSS. In this case, if a node has to communicate with another node of the same BSS, the communication is sent first to the AP and then from the AP to the destination node. Two BSSs that are too far to communicate directly can be connected by an abstract medium called Distribution System (DS). The DS enables the communications between APs of different BSSs, guarantees the forwarding of frames to mobile nodes moving from a BSS to another, and exchanges

information with the wired network. The union of the DS and of the connected BSSs is called Extended Service Set (ESS). The ESS and all of its mobile nodes appear to all external equipments as a single MAC layer network with physically stationary nodes. The legacy 802.11 does not guarantee the connection to a node exiting from an ESS and entering in another one. This problem is addressed in the 802.11s extension, which defines the procedure for coordinating different ESSs in order to form a WMN.
The 802.11 protocol provides two fundamental methods to access the medium: the Distributed Coordination Function (DCF), which manages the communications in ad-hoc networks, and the Point Coordination Function (PCF), which supports the centralized network operations.
A temporal structure, called *Superframe* is subdivided in two periods, the Contention Free Period (CFP), in which the PCF operates, and the Contention Period (CP), in which the DCF does. The beginning and the durations of the CFP and of the CP are decided by a Point Coordinator (PC), usually the AP, and are communicated to all nodes by proper beacon frames. The PCF is useful for time bounded traffic, but consumes much bandwidth, because, for each source-destination communication, two transmissions must be performed (source-AP and AP-destination).

4.2.3 The 802.11 DCF

The 802.11 DCF is a random access scheme based on the Carrier Sensing Multiple Access with Collision Avoidance (CSMA/CA) protocol and working on best effort basis for asynchronous data transfer. Two access mechanisms are provided by the DCF: a basic access mechanism and a Request To Send/Clear To Send (RTS/CTS) one.

4.2.3.1 Basic access

The basic access is a two way handshaking method in which the correct reception of the DATA packet is communicated to the source by sending an ACKnowledgement (ACK) packet. The access procedure can be summarized as follows.
A source node having in its buffer a DATA packet ready for transmission monitors the channel. At the first transmission attempt, if the channel is sensed idle for a Distributed InterFrame Space (DIFS) time, the node immediately transmits, while, if the channel is sensed busy during the DIFS, the node goes on monitoring. When the channel is sensed idle for a DIFS, the source generates a random backoff interval in a discrete time to reduce the collision probability with other competing nodes. The backoff time is given by the product between the slot time σ_{slot} and a random integer selected in the interval $[0, CW_{\min} - 1]$, where $CW_{\min}$

is the minimum Contention Window (CW). If the number of contending nodes is high, many nodes monitor the channel and may access immediately once the medium is sensed idle. The random backoff that each node has to wait reduces the probability that two nodes transmit simultaneously. Both σ_{slot} and $CW_{\min}$ are specified by the standard and depend on the adopted physical layer technology. In particular, σ_{slot} is set equal to the time required by a node to detect the transmission of a packet by any other node. The slot time accounts for the time needed to switch from the receiving to the transmitting state, for the time to signal to the MAC layer the state of the channel and for the propagation delay.
The generated backoff time is inserted in a reverse counter that is decremented if the channel persists in the idle state, frozen if the medium is sensed busy and reactivated when the channel is sensed idle for a DIFS or an Extended InterFrame Space (EIFS). In particular, the node waits for a DIFS if no collision has been detected during the busy period, while it waits for an EIFS(>DIFS) if a collision has been detected. When the backoff counter reaches the zero value the packet is transmitted (at the beginning of the corresponding slot time).
In order to confirm the correct DATA reception, an ACK is sent back by the destination to the source after a Short InterFrame Space (SIFS<DIFS). If the source does not receive the ACK within timeout, a retransmission is scheduled. In this case the retransmission counter is updated, the contention window is doubled and a new backoff is generated. In particular, at each failed attempt, the contention window is doubled up to a maximum value $CW_{\max} = 2^{m'} CW_{\min}$, where m' represents the maximum backoff stage. Further retransmissions are attempted until the maximum number of retransmissions $m(\geq m')$, called Retry Limit, is reached and the packet is discarded.
The four interframe spaces involved in the 802.11 standard are carefully selected to provide an implicit prioritization mechanism. In particular, the SIFS is chosen as the smallest one in order to provide the highest priority to the ongoing communications. The Point coordination function Inter Frame Space (PIFS), used by the AP, is equal to a SIFS plus a slot time and, being lower than the DIFS, which is equal to SIFS+$2\sigma_{\text{slot}}$, guarantees higher priority to the AP with respect to the other contending nodes.

4.2.3.2 RTS/CTS access

The 802.11 DCF provides an additional four-way handshaking mechanism for packet transmission, called RTS/CTS (Fig. 4.3). In this case a source having a packet awaiting transmission follows the same rules explained above for the basic access, but, instead of the DATA packet, the source preliminarily transmits an RTS packet. If the destination receives the RTS correctly, it responds, after a SIFS, with a CTS packet. The source is allowed to transmit its DATA packet only if the CTS is

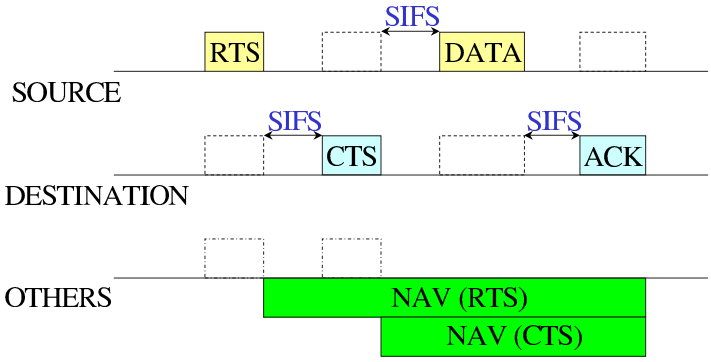

Figure 4.3: RTS/CTS access mechanism.

correctly received. RTS and CTS are short frames that carry information regarding the length of the packet to be transmitted. This information can be read by any listening node and exploited to update the Network Allocation Vector (NAV). The NAV is a value that indicates to a node the amount of time that remains before the medium becomes available again. The detection of just one packet among the RTS and the CTS reduces the hidden terminal problem, a phenomenon occurring when a node is hidden from either the source or the destination.
The RTS/CTS mechanism is very effective in terms of system performance mainly when large packets are considered. Assuming a perfect channel sensing by each node, a collision may occur only when two or more packets are transmitted within the same slot time. Adopting the basic access for large DATA packets, a collision leads to a considerable waste of time, while, employing the RTS/CTS mechanism, the collision involves only the shorter RTS/CTS packets and so less time is wasted.

4.3 DWNs and advanced antenna techniques

The 802.11 DCF is designed assuming the use of a single antenna at each node, therefore, by using the standard access scheme, a high performance level cannot be guaranteed for the interfered communication. The presence of undesired sources represents a worthy problem to address, because in recent years the level of interference has been considerably increased, especially in the unlicensed Industrial, Scientific and Medical (ISM) band (900 MHz, 2.4 GHz and 5.8 GHz), due to the large number of technologies sharing the same frequency range. For example, in the 2.4 GHz band, several standards, such as IEEE 802.11b/g/n, Bluetooth, IEEE 802.16a and HomeRF, and many devices, such as microwave ovens, have to coexist. Besides, the limited resources of the wireless channel are, in

practice, further decreased by the propagation environment that is affected by multipath and fading. These problems, together with the growing demand for supporting higher bit rates, have raised the interest of the research community on multiple antenna techniques.
The adoption of multiple antennas is able to provide a large performance improvement and so the introduction of MIMO systems at the PHY layer of the 802.11 standard is the objective of the efforts of the Task Group n. However, the complete exploitation of the potential offered by diversity techniques and MIMO systems in high-rank environment, and of fixed and adaptive beamforming in low-rank environment, requires the modification of the 802.11 MAC layer as well as the design of novel and efficient SDMA schemes. Several MAC protocols have been proposed in the literature to exploit the capabilities of multi-antenna technology. These access schemes can be classified according to the characteristics of the antenna system adopted at PHY layer that, in turn, depend on the spatial properties of the propagation environment.
The diversity approach is considered in [66–70], while 802.11 DCF modifications to support MIMO systems are proposed in [71–75]. In the first case the throughput improvement is obtained by increasing the reliability of the single communication link, while, in the second case, the MAC protocols are designed to support the simultaneous transmission of multiple data streams. This latter approach requires a tradeoff between throughput improvement and interference reduction [71–72].
The large part of the MAC protocols proposed in the literature for DWNs adopting multiple antennas assumes a low-rank environment and is designed to operate with sectorized, switched-beam, directional and adaptive antennas [76–112]. As described in the previous chapter, beamforming techniques increase the SINR at the array output and allow each node of the network to communicate in presence of a larger interference power. To exploit the larger immunity against the undesired sources, the access schemes are developed to enable the possibility that different node pairs communicate simultaneously. However, the novel mechanisms that can be conceived to reach this objective may generate problems due to the directionality of the communications. The following paragraphs summarize these problems and briefly describe the main proposals for exploiting advanced antenna techniques in DWNs.

4.3.1 MAC layer problems

The most common drawbacks that can be encountered in a DWN using fixed and adaptive beamforming are due to hidden and exposed terminals, deafness, muteness and suicide ACK. Some of these problems are already present when the communications are performed in omnidirectional operating mode, while others appear when the packet exchange is directional. These new problems put

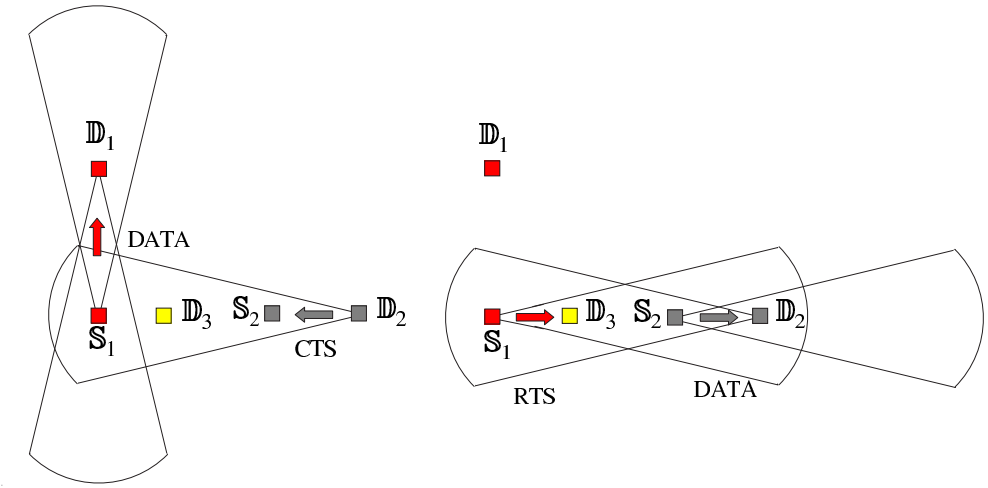

Figure 4.4: Hidden terminal due to unheard RTS.

in evidence that the introduction of advanced antenna systems does not immediately guarantee higher performance, but requires proper optimization techniques at MAC layer.

4.3.1.1 Hidden terminal due to unheard RTS/CTS

In the omnidirectional antenna case the effects due to hidden terminal can be considerably mitigated, even if not completely removed, by adopting the RTS/CTS exchange. However, if the packets are not transmitted in omnidirectional operating mode, new kinds of hidden terminal may occur: the hidden terminal due to unheard RTS/CTS and the hidden terminal due to asymmetry of gain [77–78].
A possible scenario in which the first situation may occur is shown in Fig. 4.4. The source $\mathbb{S}_1$ is transmitting a DATA packet to the destination $\mathbb{D}_1$ in beamforming operating mode[1]. Besides, $\mathbb{S}_1$ has placed a null towards $\mathbb{S}_2$ and $\mathbb{D}_2$ to suppress their interference. During the communication between $\mathbb{S}_1$ and $\mathbb{D}_1$ the destination $\mathbb{D}_2$ transmits a CTS packet to $\mathbb{S}_2$, which cannot be received by $\mathbb{S}_1$ (Fig. 4.4a). If $\mathbb{S}_1$ and $\mathbb{D}_1$ finish their communication while that between $\mathbb{S}_2$ and $\mathbb{D}_2$ is still in progress, and if $\mathbb{S}_1$ has a packet for another destination $\mathbb{D}_3$ (lying in the same direction of the pair $\mathbb{S}_2$-$\mathbb{D}_2$), a collision may occur between the RTS packet sent by $\mathbb{S}_1$ and the DATA packet that $\mathbb{D}_2$ is trying to receive from $\mathbb{S}_2$ (Fig. 4.4b).
This phenomenon, called hidden terminal due to unheard RTS/CTS, puts in evi-

[1]The term “beamforming operating mode” is adopted in this thesis to indicate the use of directional, adaptive, switched-beam and phased-array systems.

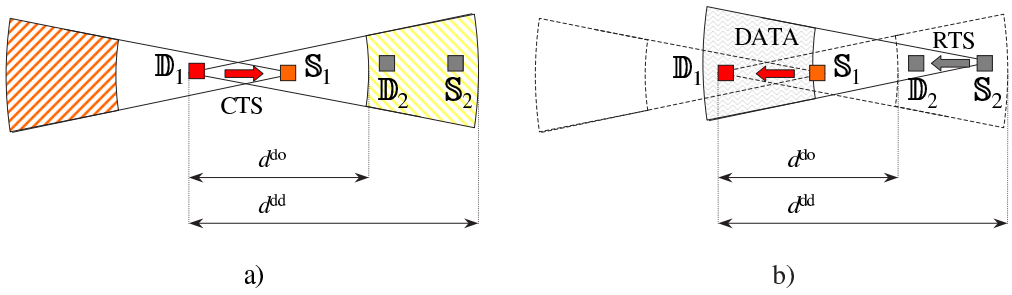

Figure 4.5: Hidden terminal due to asymmetry of gain.

dence that the exploitation of the spatial domain using only directional communications may increase the collision probability in certain scenarios.

4.3.1.2 Hidden terminal due to asymmetry of gain

This situation may occur in a DWN when the antenna gain towards the desired direction in beamforming operating mode and the antenna gain in omnidirectional operating mode are different. In this case, the communication range between two nodes depends on the state of their antenna systems: the distance d^{dd} that can be reached when both nodes operate in a beamforming mode is larger than the distance d^{do} that can be reached when one node adopts a directional approach and the other operates in omnidirectional mode. This difference may lead to the situation described by Fig. 4.5.
The node $\mathbb{S}_2$ is in the idle state and senses the channel in omnidirectional operating mode. Therefore, $\mathbb{S}_2$ is not able to receive the directional CTS transmitted by $\mathbb{D}_1$ to $\mathbb{S}_1$, because the distance between $\mathbb{D}_1$ and $\mathbb{S}_2$ is larger than d^{do} (Fig. 4.5a). While $\mathbb{D}_1$ is receiving the DATA packet from $\mathbb{S}_1$, a packet for $\mathbb{D}_2$ arrives in the transmission buffer of $\mathbb{S}_2$. $\mathbb{S}_2$ performs a directional carrier sensing in the $\mathbb{S}_1$-$\mathbb{D}_1$ direction and senses the channel as idle, because the transmission is directed from $\mathbb{S}_1$ towards $\mathbb{D}_1$. However, when $\mathbb{S}_2$ transmits the directional RTS towards $\mathbb{D}_2$ a collision occurs because both $\mathbb{D}_1$ and $\mathbb{S}_2$ are operating in beamforming mode, namely with the highest gain.
This scenario shows that two nodes may be out of each other's range when at least one of the two is idle, but the same nodes may be within range when they are both operating in beamforming mode.

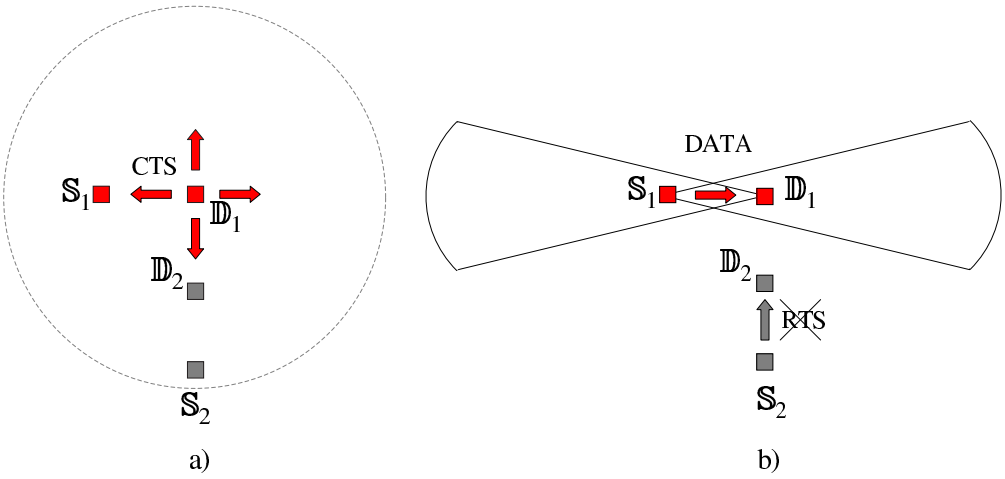

Figure 4.6: Exposed terminal.

4.3.1.3 Exposed terminal

The exposed terminal is a typical problem of DWNs that is also present when all communications are performed in omnidirectional operating mode. The main consequence of this phenomenon is an underutilization of the available spatial channel resources.
Fig. 4.6 shows a possible scenario involving directional communications. The destination $\mathbb{D}_1$ transmits an omnidirectional CTS for the source $\mathbb{S}_1$ (Fig. 4.6a). This control packet is also received by the idle node $\mathbb{S}_2$, which now knows the duration of the communication and can update its virtual carrier sensing information. Besides, during the DATA/ACK exchange between $\mathbb{S}_1$ and $\mathbb{D}_1$, a packet for $\mathbb{D}_2$ arrives at the transmission buffer of $\mathbb{S}_2$. Exploiting the virtual carrier sensing information, $\mathbb{S}_2$ may decide to delay the RTS transmission towards $\mathbb{D}_2$ in order to avoid collisions. However, as shown in Fig. 4.6b, the pairs $\mathbb{S}_1$-$\mathbb{D}_1$ and $\mathbb{S}_2$-$\mathbb{D}_2$ may send packets simultaneously without destroying the reciprocal communications. In practice, instead of avoiding a collision, the source $\mathbb{S}_2$ wastes a transmission opportunity.

4.3.1.4 Deafness

A typical drawback due to directional communication in distributed environment is deafness, which occurs when a source tries to send packets to a destination that is already involved in a communication with another node. In Fig. 4.7a the node $\mathbb{S}_1$ is sending a DATA packet to $\mathbb{D}_1$, while the source $\mathbb{S}_2$ is transmitting an omnidirectional RTS to inform the neighbors about its intention to send a packet to $\mathbb{D}_2$.

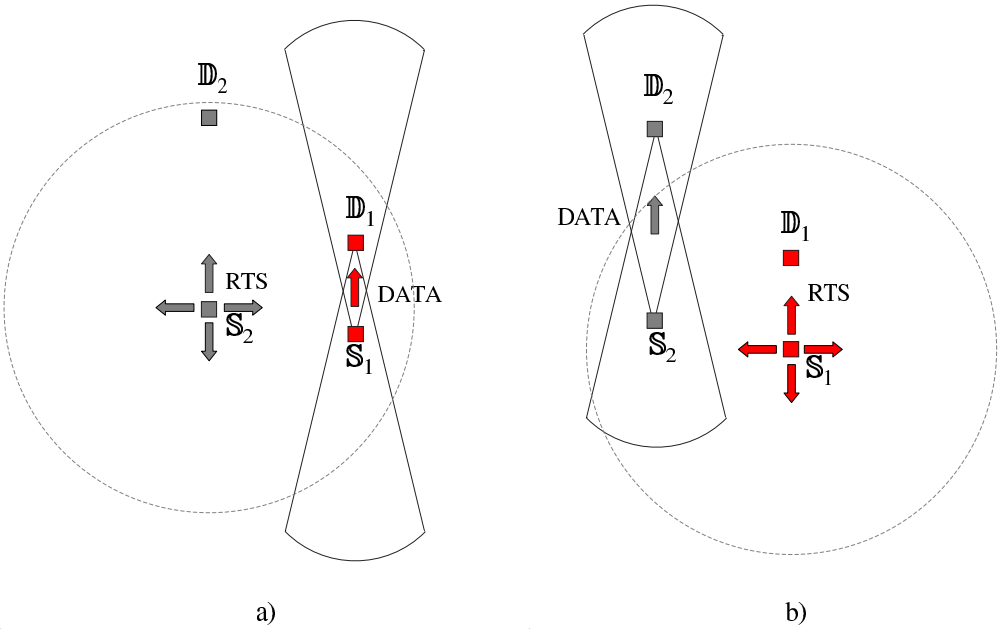

Figure 4.7: Deafness.

$\mathbb{S}_1$ is unable to hear this RTS that, however, does not destroy the current communication because $\mathbb{D}_1$ has placed a null towards $\mathbb{S}_2$. When the $\mathbb{S}_1$-$\mathbb{D}_1$ exchange is finished, deafness may occur if $\mathbb{S}_1$ has a packet for $\mathbb{S}_2$ in its transmission buffer. In fact, in this case, $\mathbb{S}_1$ sends an RTS that cannot be received by $\mathbb{S}_2$ (Fig. 4.7b). Besides, $\mathbb{S}_1$ is unaware of the ongoing communication between $\mathbb{S}_2$ and $\mathbb{D}_2$. Therefore, $\mathbb{S}_1$ assumes that the lack of the CTS response is due to collisions and goes on transmitting the RTS packet after each failed attempt. This situation may continue until the Retry Limit is reached and so the DATA packet is discarded.
The main consequences of deafness are packet losses and an increase of the level of interference, due to the useless transmission of RTS packets, which may inhibit other nodes from accessing the medium.

4.3.1.5 Muteness

Muteness is the inability of a node to transmit due to insufficient information regarding channel occupation. Assume that the RTS/CTS packets are transmitted in omnidirectional operating mode, while the DATA/ACK exchange is performed in beamforming operating mode (Fig. 4.8a). The destination $\mathbb{D}_2$ is in direct radio range of both $\mathbb{S}_1$ and $\mathbb{D}_1$, while the source $\mathbb{S}_2$ has no information about the communication between $\mathbb{S}_1$ and $\mathbb{D}_1$. On the other hand, $\mathbb{S}_1$ and $\mathbb{D}_1$ can receive the

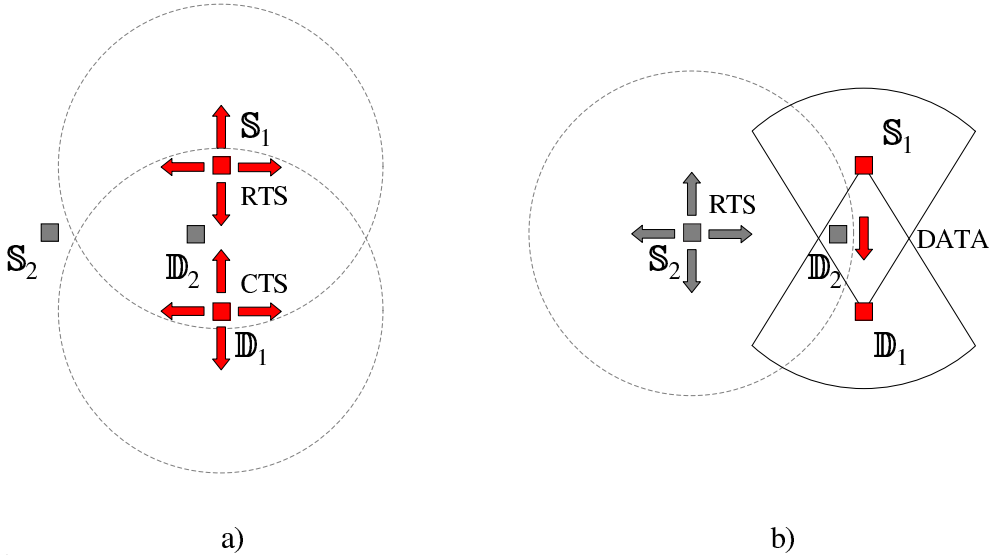

Figure 4.8: Muteness.

control packets transmitted by $\mathbb{D}_2$. This information allows the source $\mathbb{S}_1$ to know exactly when the channel is idle and thus it has a good probability of capturing the medium after each successful packet transmission. Instead, $\mathbb{S}_2$ is forced to randomly discover when the communication between $\mathbb{S}_1$ and $\mathbb{D}_1$ is silent. Therefore, $\mathbb{S}_2$ continuously tries to contend for access by sending RTS packets to $\mathbb{D}_2$, which usually defers the response because of $\mathbb{S}_1$-$\mathbb{D}_1$ activity (Fig. 4.8b). Besides, after each unsuccessful attempt, $\mathbb{S}_2$ doubles the contention window until its maximum value and backs off for an exponentially increasing amount of time. This scenario leads to a situation in which the node $\mathbb{S}_1$ captures the channel almost continuously, while the node $\mathbb{S}_2$, experiencing muteness, can communicate only when an exchange has been completed by $\mathbb{S}_1$-$\mathbb{D}_1$. The consequences of muteness, which can occur also when all communications are performed in omnidirectional operating mode, are unfairness and waste of resources due to the increased level of interference caused by the continuous transmission of the RTS packets [84].

4.3.1.6 Suicide ACK

In many practical scenarios multiple antennas can be more easily deployed on the APs, while technological limitations as well as cost considerations make it more difficult to equip small mobile nodes with advanced antenna systems. Therefore, employing SDMA technique, an AP may be able to simultaneously transmit multiple packets to different mobile nodes that, conversely, adopt an omnidirectional

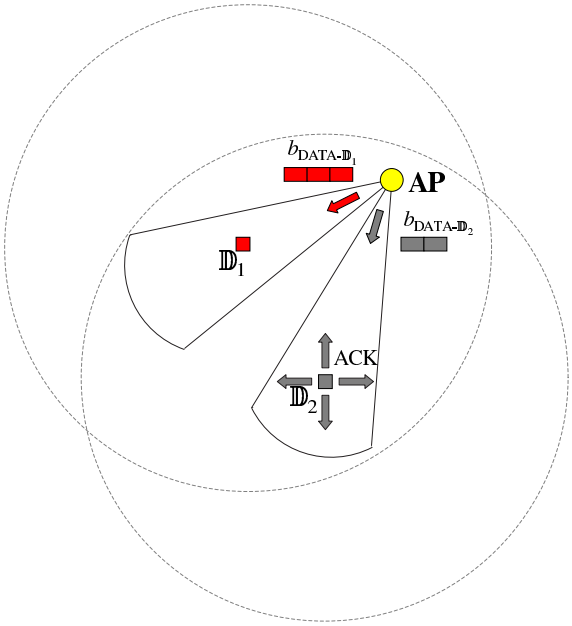

Figure 4.9: Suicide ACK.

approach. In such a scenario the suicide ACK may occur.
As shown in Fig. 4.9, the AP is sending at the same time a DATA packet to the destination $\mathbb{D}_1$, containing $b_{\text{DATA}-\mathbb{D}_1}$ bits, and a DATA packet to the destination $\mathbb{D}_2$, containing $b_{\text{DATA}-\mathbb{D}_2}$ bits. In general, the two packets can have different size. In this particular example $b_{\text{DATA}-\mathbb{D}_1}$ is larger than $b_{\text{DATA}-\mathbb{D}_2}$ and so the transmission towards $\mathbb{D}_2$ finishes when the transmission towards $\mathbb{D}_1$ is in progress. According to the 802.11 MAC protocol, $\mathbb{D}_2$ sends the ACK to the AP after a SIFS. The ACK is received by the AP, but collides with the packet destined to $\mathbb{D}_1$, because $\mathbb{D}_1$ is equipped with a unique antenna and is unable to suppress the undesired source.
The suicide ACK represents a problem arising when simultaneous uplink and downlink transmissions must be performed. Statistically, the smaller frames have a higher probability of being acknowledged, and so unfairness may arise [76,113].

4.3.2 MAC layer proposals

The access schemes designed to support beamforming in DWNs that can be found in literature are usually extensions of the 802.11 DCF. Novel approaches and sophisticated mechanisms are proposed by the different authors to solve some of the problems just itemized, as well as to increase the throughput of the entire network.

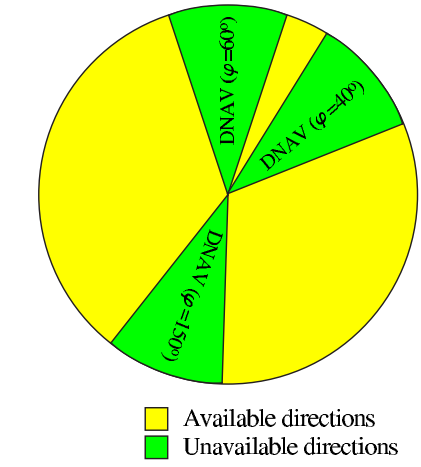

Figure 4.10: Directional NAV.

4.3.2.1 Directional NAV

A considerable performance improvement can be reached employing a directional virtual carrier sensing mechanism, called Directional NAV (DNAV), which has been deeply analyzed in [96] and also adopted in the access schemes proposed in [78–79, 81, 87, 95, 111].
The DNAV is associated with a direction, corresponding to the estimated DOA of the received signal, and a width, which depends on the antenna beamwidth (Fig. 4.10). Multiple DNAVs can be set for a node that maintains a unique timer for each DNAV and updates the direction, the width and the expiration time when the physical layer provides newer information regarding the channel occupation in the considered direction. With respect to the omnidirectional NAV used in the 802.11 DCF, the DNAV allows the access scheme to determine direction-specific channel availability, providing more precise information for resource management optimization.

4.3.2.2 Synchronous communications

The asynchronous nature of the 802.11 DCF may lead to considerable transmission delays and other phenomena, such as the ACK suicide. To combat these drawbacks, some authors propose the adoption of a partially synchronous approach [76, 91, 100].
The MAC protocol described in [91], specifically designed to reduce the packet delay, is based on a mechanism that maps the spatial channels generated by the

antenna system into logical channels. When the mapping procedure is completed, the communications are performed synchronously using proper beacon frames. Each beacon frame provides a certain transmission opportunity that enables a source to transmit for a certain amount of time (burst transmission).
In [76] the synchronous approach is adopted to avoid the suicide ACK. The communication channel is subdivided in two subchannels. The first one, in which the communications are asynchronous, is used for the omnidirectional RTS/CTS exchange, while the second subchannel, in which the communications are synchronous, is employed for the DATA/ACK exchange. Besides, in the second subchannel, both space-division and time-division multiplexing are performed to enable multiple simultaneous synchronized transmissions from the AP to the destination nodes. To avoid the suicide ACK, the ACK packets are transmitted during a slot time in a position that is selected larger than the maximum length of the DATA packet.

4.3.2.3 Tones

The use of tones reduces the hidden terminal and the deafness phenomena [80,85]. Tones are essentially sinusoids with sufficient spectral separation that do not contain information bits and thus do not require demodulation. They are only detected through energy estimation. To enable the use of tones the channel must be subdivided in two subchannels: the data channel, where the four way handshake is performed, and the control channel, where the tone is transmitted.
The access scheme proposed in [85] has been developed to address hidden terminal due to unheard RTS/CTS. In this case the tones are transmitted by the source and the destination on the control channel during the entire duration of the communication. A potential hidden terminal, sensing the control channel, is able to detect the ongoing dialogue and avoid transmission. A drawback of this protocol is that, if the tones are transmitted in beamforming operating mode, deafness may occur.
The protocol proposed in [80], called ToneDMAC (Fig. 4.11), adopts a directional RTS/CTS exchange to improve spatial reuse and considers the use of tones for specifically addressing deafness. Each tone-frequency identifies a unique node, enabling each neighbor to determine the sender of a given tone. After the directional RTS/CTS exchange, the source and the destination transmit omnidirectional out-of-band tones to inform the neighbor that the communication is completed. Besides, from tone reception, a neighbor can deduce that the possible previous failures in contacting the source or the destination were due to deafness and not to network congestion. When this neighbor detects a tone transmitted by its intended destination it sets the backoff counter to zero and generates another backoff with the minimum contention window. Differently from [85], in

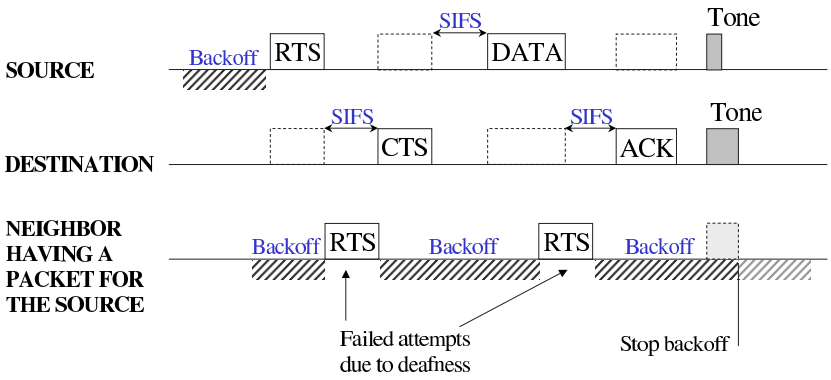

Figure 4.11: Time line for ToneDMAC protocol.

this case tones need not be transmitted simultaneously during DATA packet transmission/reception and so multiple transceivers are not necessary.

4.3.2.4 Multiple RTS packets

The reduction of deafness, exposed terminal and hidden terminal problems require the use of efficient mechanisms to identify the location of the neighbor nodes together with proper algorithms for exploiting the acquired information. To reach these objectives some authors propose the use of multiple directional RTS packets [87, 100].
In [87], the space surrounding each node is subdivided in a certain number of sectors that depends on the beamwidth of the radiation pattern generated by the antenna system. A source having a data packet ready for transmission sends an RTS packet for each sector. More precisely, the RTS packets are sent in beamforming operating mode, consecutively and in a circular way, until the area around the source is completely scanned. Each directional RTS contains a field that specifies the sector that will be used during the subsequent DATA transmission and the sector from which the RTS itself is currently transmitted. The generic neighbor inserts this information in a location table, containing the identifier of the node that has been heard, the sector employed by this node, and the sector from which this node is seen. The combined use of the location table and of the DNAV enables the neighbor to decide if its intended communication will interfere or not, so reducing the hidden terminal problems due to unheard RTS/CTS and the effects related to the exposed terminal.

4.3.2.5 Longer handshake

Some authors introduce new control packets in the handshake to enable spatial multiplexing [105], or to guarantee higher protection against interference [104]. The receiver initiated handshake presented in [105] aims to improve the performance of the bottleneck nodes by using SDMA. The destination transmits periodically an omnidirectional Ready-To-Receive packet that is employed by each neighbor to steer its main lobe towards the destination. The subsequent RTS/CTS negotiation involves the maximum allowed length of the DATA packet. Besides, each RTS packet, transmitted by the generic source, contains the particular training sequence that identifies the source itself and is used by the destination to form the corresponding receiving beam. The employment of different training sequences for different neighbors enables the generation of multiple beams for multiple sources together with the use of successive interference cancellation algorithms to distinguish the different packets.
A six way handshake is presented in [104] for protecting the DATA packet reception from ongoing and potential future interference. Two further omnidirectional control packets are introduced after the RTS/CTS exchange. These packets are transmitted by all the neighbors having heard the RTS and/or the CTS, and are used by the source and the destination for beamforming operations. More precisely, the destination transmits to the source the training sequence, which, differently from [105], is unique for all the nodes of the network, while the other neighbors transmit generic sequences of bits different from the training one. Adopting a temporal reference algorithm the source is able to steer the main lobe towards the destination and to place the nulls towards the neighbors. The same operation is then performed by the destination. In this protocol all transmissions are performed in omnidirectional operating mode, while the DATA and ACK receptions are performed in beamforming operating mode. This approach does not exploit the spatial domain at the maximum level, but, assuming a perfect physical carrier sensing, it solves almost completely the deafness and the hidden terminal problems.

4.3.3 Theoretical approaches

The MAC protocols proposed in literature are usually developed to increase the network throughput and/or to satisfy specific requirements, but from these particular applications it is difficult to quantify the actual improvement that can be achieved employing advanced antenna systems in DWNs. Besides, a detailed performance analysis becomes more laborious when realistic channel conditions and detailed models for the antenna radiation pattern must be taken into account. Therefore, theoretical models are necessary to investigate from a more general

point of view the potential offered by multi-antenna systems in order to obtain useful criteria that can be applied in MAC protocol design.
The milestone for the theoretical studies on the capacity of wireless networks is the paper of Gupta and Kumar [114]. In this work the authors prove that in a multi-hop DWN, where n identical nodes are randomly placed on a planar disk of unit area and each source randomly selects the destination, the per-node throughput decreases as a function of $O(\mathcal{R}/\sqrt{n \log n})$ under a noninterference protocol, where $\mathcal{R}$ is the maximum bit rate of the single node. This scaling law is the consequence of the multi-hop nature of DWNs and of the random policy adopted to access the shared medium, which imposes a limitation to the number of simultaneous transmissions that can be performed at any time. The former characteristic implies that, for each packet generated by a source, a growing number of relay nodes are involved in forwarding the packet to the destination. The fundamental implication of this analysis is the intrinsic limitation in terms of scalability, which generates doubts regarding the feasibility of large DWNs. This issue is deeply studied in [115], where the authors argue that the possibility to design large ad-hoc networks depends on the locality of the traffic patterns.
The theoretical analysis presented in [114], is extended in [116] to include the use of advanced antenna systems. The authors show that, using an adaptive array with N antenna elements, the per-node throughput can be increased by a factor $N - 2$, corresponding to the number of suppressible interferers. Besides, in [117], the same authors present an interesting performance analysis of a directional MAC protocol using realistic antenna radiation patterns. In particular, this study evaluates the number of communications that can be simultaneously performed in an ad-hoc network using directional antennas.
A further extension of [114] is proposed in [118] to include directional transmissions and receptions. In this paper the authors prove that, if the product between the beamwidths of the transmitting/receiving antennas decreases asymptotically as fast as $1/n$, large multi-hop DWNs may be feasible. The analysis proposed in [118] states that, from the theoretical point of view, the spatial filtering capabilities of directional antennas may slow down the reduction of the per-node throughput due to the increase of the number of nodes. However, adopting an antenna array, narrow beamwidths can be obtained using a large number of antenna elements or increasing the interelement spacing. Therefore, large ad-hoc networks require the employment of cumbersome antenna systems on mobile nodes, which, from a practical perspective, is really difficult to realize.
An interesting and somewhat surprising result is obtained in [119], where it is proved that the capacity of an ad-hoc network with a large number of nodes can be increased by exploiting the mobility of the nodes. The authors show that, adopting a proper scheduling policy, delay tolerant applications may benefit from the movement of the relay nodes. The positive effects of mobility on the capacity of

wireless networks are confirmed by the model developed in [120], where it is also proved that, when variable-rate transmission is allowed, the capacity increases in presence of time-varying flat fading. Besides, in [120], the authors analyze the benefits derived from the use of multiple antenna systems, showing that successive interference cancellation is more effective when the number of available bit rates is large.
A statistical approach for estimating the network capacity in the omnidirectional case is adopted in [121], where the authors employ the pdf of the SINR to characterize the per-node throughput in presence of shadowing and fading. The proposed model, useful to analyze the influence of the physical layer parameters on the capacity, shows that the decrease of the path-loss exponent leads to a decrease of the performance, while the particular fading statistic has a small influence.
The benefits of directional antennas and DNAV on the throughput of a DWN are analyzed in [122], where authors also investigate the impact of realistic antenna radiation patterns on the IEEE 802.11 DCF. The influence of directional transmission is also studied in [123], where a cross-layer analytical approach including shadowing and fading is described.

Original Results

Part II

Advanced Antenna Systems for Distributed Wireless Networks in Low-Rank Environment

Chapter 5

Simultaneous Communications in DWNs Using Adaptive Antenna Arrays

---

This chapter describes an analytical model for evaluating the number of simultaneous communications that can be sustained by a distributed wireless network in which the nodes are equipped with adaptive antennas. The presented mathematical framework adopts realistic models for the antenna radiation pattern and the channel behavior, and is able to take into account the network topology and the characteristics of the MAC protocol in the spatial domain. The model is employed to investigate the impact of the spatial channel model and of the angular spread on network performance. Besides, the analysis is used to examine how the number of simultaneous communications is influenced by the transmission policy of the control and of the data packets, ruled at MAC layer.[1]

5.1 Introduction

From the literature overview presented in Subsection 4.3.3, it can be observed that the available theoretical models for the evaluation of the capacity of a DWN using multiple antennas do not include the effects due to the spatial channel characteristics. Some studies investigate the impact of Directional Antennas (DAs) on network performance adopting realistic models for the physical layer and the propagation environment [122–123]. However, few papers consider the use of

[1]The content of this chapter is based on F. Babich, M. Comisso, and L. Manià, "Sustainable Simultaneous Communications in Ad-Hoc Networks Using Smart Antenna Systems," ACM Wireless Networks, accepted for publication [172,180].

AAs from a pure analytical point of view [116, 120], while taking into account detailed models for the antenna radiation patterns and the network topology.
The objective of this chapter is to present a mathematical framework for the estimation of the potential offered by smart antennas to increase the network utilization in a realistic low-rank environment. The proposed method may be used to assess and compare the limiting performance of different antenna systems and access schemes. The analysis takes into consideration the antenna radiation pattern, the network topology, the spatial channel model, the channel angular spread and the characteristics of the access scheme in the spatial domain. The main goal is the investigation of the impact of the transmission policy of the packets, ruled at MAC layer, on network performance.

5.2 Definitions and assumptions

The analyzed scenario is a DWN with n identical nodes equipped with AAs. The area occupied by the entire network is a circle of radius R_{t}, where a generic source $\mathbb{S}$ selects a destination $\mathbb{D}$ among the nodes inside its coverage range R_{c} (single-hop scenario). The topology area $\mathcal{L}_{\mathrm{t}} = \pi R_{\mathrm{t}}^2$ is chosen larger than $\mathcal{L}_{\mathrm{c}} = \pi R_{\mathrm{c}}^2$ in order to take into account the total interference received by $\mathbb{D}$ from all the nodes belonging to the network.
The analytical model presented in this chapter is used to derive the number of *sustainable links* of a DWN, $L_{\max}$, which is intended as *the maximum number of couples of nodes that can communicate at the same time in the area* $\mathcal{L}_{\mathrm{c}}$.
The number of sustainable links, being related to the area defined by coverage range, and not by the area of the entire topology, can be viewed, in a geometrical sense, as a sort of density of communications in a cell of area $\mathcal{L}_{\mathrm{c}}$. This density is influenced by the antenna gains and by the channel angular spread as well as by the position of the nodes. In particular, $L_{\max}$ provides an ideal information regarding the potential offered by adaptive arrays in a distributed environment. The number of sustainable links is derived with the specific purpose to obtain a quantity accounting for all elements present in the spatial domain, but not dependent on the time details of the scheduler. This approach allows to investigate the achievable performance without the constraints that are unavoidable when a specific backoff mechanism is adopted.
As it will be shown in Chapter 6, more specific investigations can be performed employing $L_{\max}$ in order to analyze the influence of other elements of the communication system, such as the modulation scheme and the channel coding technique. Besides, the ideality introduced assuming the maximization of the number of simultaneous communications, which presupposes a perfect scheduling, can be successively removed and the details of a realistic scheduling policy can be

added to the model. As a result, the classic performance figures, such as the successful packet delay, the aggregate throughput and the drop probability, can be consequently obtained once the number of sustainable links is established. This analysis will be performed in Chapter 7, investigating the behavior of an 802.11 network in multi-hop environment.

5.2.1 MAC layer assumptions

Following most of the access schemes proposed in literature, it is assumed that the MAC layer employs the RTS/CTS/DATA/ACK access mechanism to manage node communications [76–106, 111–112]. This choice provides more robustness against the hidden terminal and the deafness phenomena (not considered in this study). Even if the basic access can also be modified to include smart antennas [110], the RTS/CTS access guarantees that a larger quantity of position information is available at each node [124].
The presented analytical model is developed assuming that each node (always) uses its adaptive array in reception, but no assumption is made for the transmission policy of the DATA packet, which can be smart or directional. Moreover, no assumption is made for the transmission of the CTS packet, which can be performed in omnidirectional operating mode (OCTS) or in the directional one (DCTS). An effective use of AAs requires the knowledge of the positions of $\mathbb{S}$ and of each interferer $\mathbb{I}$ in order to perform the beam steering towards the desired direction and the null steering towards the undesired ones. This information can be acquired using DOA estimation algorithms, as in [110], or, in presence of multipath, the required radiation patterns can be created employing temporal reference techniques with proper training sequences [104,112]. The availability of these features allows one to assume that the destination $\mathbb{D}$ be able to distinguish between the position of the source $\mathbb{S}$ and the position of each interferer $\mathbb{I}$. The updating of the radiation patterns is obtained at a cost of a higher overhead that, however, does not influence the number of sustainable links, which is independent of the length of the headers.

5.2.2 PHY layer assumptions

At physical layer, the parameterized ground model for the path-loss attenuation is described by (2.1), where the transmission power P_{tx} is considered equal for all sources. Multipath will be added to the model in the next section.
The coverage range of a node is obtained fixing the noise power W and imposing that, in absence of interference, the SINR at antenna system output be equal to a

threshold $\mathrm{SINR}_{\mathrm{th}}$. Therefore, W and R_{c} are related by:

$$W = \frac{P_{\mathrm{tx}}\gamma_{\alpha} \cdot 1 \cdot 1}{\mathrm{SINR}_{\mathrm{th}} R_{\mathrm{c}}^{\alpha}}, \tag{5.1}$$

where, being the maximum of the transmitter/receiver radiation pattern steered in the desired direction, the normalized gains are equal to one. From (5.1), it immediately follows that:

$$R_{\mathrm{c}} = \left(\frac{P_{\mathrm{tx}}\gamma_{\alpha}}{\mathrm{SINR}_{\mathrm{th}} W} \right)^{\frac{1}{\alpha}}. \tag{5.2}$$

The choice of an ON/OFF criterion to establish packet reception represents a simple method to distinguish successful and unsuccessful transmissions that maintains the analytical tractability of the model [104, 125–126].

5.3 Multipath model and equivalent gains

As described in Chapter 2, in a multipath scenario each signal replica reaches the receiver with different amplitude, phase, delay and DOA. In particular, in the azimuth domain, the PAS and the angular spread are used to characterize the channel. The pdf of the DOAs, $\varrho_{\mathrm{DOA}}(\varphi)$, can be simply obtained normalizing the PAS to the power received from all multipath components:

$$\varrho_{\mathrm{DOA}}(\varphi) = \frac{P_{\varphi}(\varphi)}{P_{\mathrm{rx}}}, \tag{5.3}$$

and $\hat{\sigma}_{\varphi}^2$ can be viewed as the variance of the normalized PAS. The analytical expressions of the statistical distributions considered in this study for $\varphi_0 = 0$ are summarized in Table 5.1 and the corresponding graphs are plotted in Fig. 5.1.
The adopted smart antenna system is a UCA of N omnidirectional antenna elements, where the distance between two adjacent radiators is selected equal to half wavelength. The synthesis that provides the array weight vector $\mathbf{w}$ is performed using the unconstrained LMS algorithm with a training sequence of 512 bits. Besides, this reference power gain pattern is relative to a scenario in which $N - 2$ interferers are uniformly placed in the azimuth plane. Using the notation described in Section 1.3, the generated power gain pattern is expressed as:

$$G(\varphi) = \left| \sum_{k=1}^{N} w_k e^{j\frac{2\pi}{\lambda}\rho_{\mathrm{c}}\cos(\varphi - \xi_k)} \right|^2, \tag{5.8}$$

and is considered normalized with respect to its maximum. In presence of multipath the increase of $\hat{\sigma}_{\varphi}$ causes a decrease of the spatial correlation between the

	$\varrho_{\mathrm{DOA}}(\varphi)$
Truncated Gaussian [20]	$\begin{cases} \frac{\gamma_{\mathrm{G}}}{\sqrt{2\pi}\hat{\sigma}_{\varphi}} e^{-\frac{\varphi^2}{2\hat{\sigma}_{\varphi}^2}} & \lvert\varphi\rvert \leq \pi/2 \\ 0 & \text{elsewhere} \end{cases}$. (5.4)
Ring of scatterers [21]	$\begin{cases} \frac{\cos\varphi - \sqrt{\sin^2\gamma_{\mathrm{m}_1} - \sin^2\varphi}}{\pi\sqrt{\sin^2\gamma_{\mathrm{m}_1} - \sin^2\varphi}} & \lvert\varphi\rvert < \gamma_{\mathrm{m}_1} \\ 0 & \text{elsewhere} \end{cases}$. (5.5)
Disk of scatterers [22]	$\begin{cases} \frac{2\cos\varphi\sqrt{\sin^2\gamma_{\mathrm{m}_2} - \sin^2\varphi}}{\pi\sin^2\gamma_{\mathrm{m}_2}} & \lvert\varphi\rvert \leq \gamma_{\mathrm{m}_2} \\ 0 & \text{elsewhere} \end{cases}$. (5.6)
Truncated Laplacian [23]	$\begin{cases} \frac{\gamma_{\mathrm{L}}}{\sqrt{2}\hat{\sigma}_{\varphi}} e^{-\frac{\sqrt{2}\lvert\varphi\rvert}{\hat{\sigma}_{\varphi}}} & \lvert\varphi\rvert \leq \pi/2 \\ 0 & \text{elsewhere} \end{cases}$. (5.7)

TABLE 5.1: NORMALIZED PAS OF THE DIFFERENT CHANNEL MODELS.

signal replicas. By consequence, in the radiation pattern, the main lobe cannot be precisely steered and the nulls cannot be precisely placed. To account for these phenomena, the real power gain pattern $G(\varphi)$ is substituted by the function:

$$F_{\mathrm{D}}(\varphi) \triangleq \int_0^{2\pi} G(\varphi')\varrho_{\mathrm{DOA}}(\varphi' - \varphi)\mathrm{d}\varphi', \tag{5.9}$$

obtained from combining the normalized power gain pattern in absence of multipath with the DOA statistic. The physical meaning of $F_{\mathrm{D}}(\varphi)$, which in the following will be called the *equivalent power gain pattern*, derives from the fact that each signal replica incoming from direction φ' has a fraction of energy (described by the normalized PAS) that is weighted by the corresponding value of gain in the same direction, represented by $G(\varphi')$. The function $F_{\mathrm{D}}(\varphi)$ is useful to model the fact that a signal replica incoming from an undesired LOS direction φ is received with the gain corresponding to the null, but other replicas of the same signal, incoming from $\varphi' \neq \varphi$, are received with higher gains. Similar arguments hold for the case where φ represents a desired direction.

The equivalent power gain pattern can be employed to define the average equivalent power gains in presence of multipath. In general, the gain in a null, G_{n}, in a real smart antenna system is not zero and depends on the number of interferers, the physical antenna system, the length of the training sequence, etc. In this study the G_{n} value is statistically evaluated running $\mathcal{N}_{\mathrm{ar}} = 2000$ adaptive routines, where the position of the interferers is randomly generated in each realization. In particular, G_{n} is calculated as the average value of gain in each null φ_l^{n} (corresponding

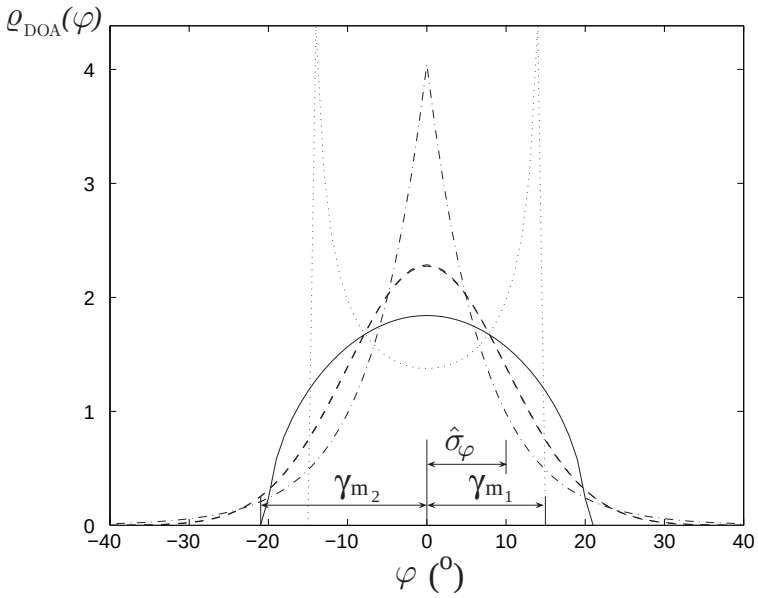

Figure 5.1: Normalized PAS of the different channel models for $\hat{\sigma}_{\varphi} = 10^{o}$.
---- Truncated Gaussian [20] ..... Ring of scatterers [21]
—— Disk of scatterers [22] -·-·- Truncated Laplacian [23]

to the l-th interferer) for all the realizations $G^{l'}(\varphi)$ and for all the nulls:

$$G_{\mathrm{n}} = \frac{1}{\mathcal{N}_{\mathrm{ar}}(N-2)} \sum_{l'=1}^{\mathcal{N}_{\mathrm{ar}}} \sum_{l=1}^{N-2} \int_{0}^{2\pi} G^{l'}(\varphi') \varrho_{\mathrm{DOA}}(\varphi' - \varphi_{l}^{\mathrm{n}}) \mathrm{d}\varphi'. \tag{5.10}$$

It is also useful to define the average values of $F_{\mathrm{D}}(\varphi)$ in $[0, 2\pi]$:

$$G_{\mathrm{m}} = \frac{1}{2\pi} \int_{0}^{2\pi} F_{\mathrm{D}}(\varphi) \mathrm{d}\varphi, \tag{5.11}$$

and outside the FNBW of $G(\varphi)$:

$$G'_{\mathrm{m}} = \frac{1}{2\pi - \varphi^{\mathrm{FN}}} \int_{\varphi^{\mathrm{FN}}/2}^{2\pi - \varphi^{\mathrm{FN}}/2} F_{\mathrm{D}}(\varphi) \mathrm{d}\varphi. \tag{5.12}$$

Observing that the transmission pattern is updated using the information acquired during packet reception, (5.10)-(5.12) can be considered not only as average receiving gains, but also as average transmission gains. Accordingly, the gains in the desired direction, assumed equal to 0^{o} without loss of generality, are evaluated

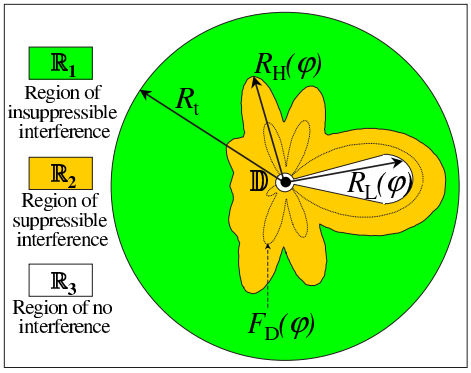

Figure 5.2: Interference regions.

as:

$$G_{\mathrm{tx_d}} = G_{\mathrm{rx_d}} = G_{\mathrm{d}} = \int_0^{2\pi} G(\varphi')\varrho_{\mathrm{DOA}}(\varphi')\mathrm{d}\varphi' = F_{\mathrm{D}}(\varphi = 0^o), \tag{5.13}$$

where $G_{\mathrm{tx_d}}$ is the transmitting gain of the source $\mathbb{S}$ towards the destination $\mathbb{D}$ and $G_{\mathrm{rx_d}}$ is the receiving gain of $\mathbb{D}$ towards $\mathbb{S}$. In the following the transmitting and the receiving equivalent gains in the desired direction will be considered as equal. It is worth noting that the scenario corresponding to absence of multipath can be derived, as a particular case, choosing $\varrho_{\mathrm{DOA}}(\varphi) = \delta^{\mathrm{D}}(\varphi)$, where $\delta^{\mathrm{D}}(\varphi)$ is the Dirac delta function.

5.4 Interference model

This section introduces the interference model for a generic destination node $\mathbb{D}$ during the reception of a DATA packet, by adopting the hypotheses and the definitions described in the previous sections.
The space surrounding $\mathbb{D}$ is subdivided into three regions, the region of insuppressible interference, $\mathbb{R}_1$, the region of suppressible interference, $\mathbb{R}_2$, the region of no interference, $\mathbb{R}_3$ [117]. These regions are identified by three radial distances, R_{t}, $R_{\mathrm{H}}(\varphi)$ and $R_{\mathrm{L}}(\varphi)$ (Fig. 5.2). In order to improve the readability of the figure, the R_{t} value used in the plot is much smaller than its real value and only the regions relative to a single destination $\mathbb{D}$ are shown. When the CTS packet is transmitted in omnidirectional operating mode, $R_{\mathrm{H}}(\varphi)$ describes a circumference of radius R_{c}, while, when the CTS packet is transmitted in beamforming operating mode (DCTS case), $R_{\mathrm{H}}(\varphi)$ depends on $F_{\mathrm{D}}(\varphi)$ (this case is depicted in the figure). The equivalent pattern $F_{\mathrm{D}}(\varphi)$, defined in (5.9), is calculated using the

radiation pattern $G(\varphi)$, which is created by the smart antenna system of $\mathbb{D}$ during the reception of the RTS packet from $\mathbb{S}$ and which is used to receive the DATA packet. The real pattern and hence the equivalent one are strictly dependent on the position of the closer interferers.
In $\mathbb{R}_1$ (region of insuppressible interference) a node is too far from $\mathbb{D}$ to correctly receive the CTS packet and does not have useful information to reduce its transmitting gain G_{tx_1} towards $\mathbb{D}$. Therefore, these nodes can interfere both with the main and the minor lobes (direct interference). A node in $\mathbb{R}_2$ (region of suppressible interference) is able to receive correctly the CTS and is aware of the communication of $\mathbb{D}$. If the MAC protocol provides a protection mechanism, this node can reduce the interference towards $\mathbb{D}$ by controlling its transmission gain G_{tx_2} in $\mathbb{D}$'s direction. This objective can be obtained, for example, placing a null towards $\mathbb{D}$ or employing the DNAV. The nodes inside the region defined by $R_{\mathrm{L}}(\varphi)$ are considered not active because they are too close to $\mathbb{D}$ and their traffic is considered blocked by the physical CS. The region of no interference $\mathbb{R}_3$ is the union of the area covered by $R_{\mathrm{L}}(\varphi)$ and of the area outside R_{t}, which represents the region outside the topology where nodes are not present.
The function $R_{\mathrm{H}}(\varphi)$ depends on R_{c} and on the equivalent pattern of $\mathbb{D}$ during the transmission of the CTS. Therefore, $R_{\mathrm{H}}(\varphi)$ is determined by the effectiveness of $\mathbb{D}$ in protecting its own reception. The range $R_{\mathrm{L}}(\varphi)$ is also a function of G_{tx_2}, so it is influenced by the effectiveness of the generic $\mathbb{I}$ in protecting $\mathbb{D}$'s reception. By consequence, $R_{\mathrm{L}}(\varphi)$ and $R_{\mathrm{H}}(\varphi)$ depend not only on the characteristics of the channel and of the antenna system, defined at physical layer, but also on the way of employing the antenna system, ruled at MAC layer.
According to the adopted channel model, the interference received by $\mathbb{D}$ from each of the three regions in presence of multipath can be calculated as a function of the number of sustainable links as:

$$P_{\mathrm{int}_1} = \int_0^{2\pi} \int_{R_{\mathrm{H}}(\varphi)}^{R_{\mathrm{t}}} \frac{P_{\mathrm{tx}}\gamma_\alpha G_{\mathrm{tx}_1}}{r^\alpha} F_{\mathrm{D}}(\varphi)\tilde{\varrho}_{\mathrm{act}}(r,\varphi) r \mathrm{d}r\mathrm{d}\varphi, \tag{5.14a}$$

$$P_{\mathrm{int}_2} = \int_0^{2\pi} \int_{R_{\mathrm{L}}(\varphi)}^{R_{\mathrm{H}}(\varphi)} \frac{P_{\mathrm{tx}}\gamma_\alpha G_{\mathrm{tx}_2}}{r^\alpha} \tilde{F}_{\mathrm{D}}(\varphi, L_{\max})\tilde{\varrho}_{\mathrm{act}}(r,\varphi) r \mathrm{d}r\mathrm{d}\varphi, \tag{5.14b}$$

$$P_{\mathrm{int}_3} = 0, \tag{5.14c}$$

where $\tilde{\varrho}_{\mathrm{act}}(r,\varphi)$ is the active node density, which is a function of the spatial distribution of the nodes, and:

$$\tilde{F}_{\mathrm{D}}(\varphi, L_{\max}) = \begin{cases} \dfrac{(N-2)G_{\mathrm{n}} + F_{\mathrm{D}}(\varphi)(2L_{\max} - N)}{2L_{\max} - 2} & L_{\max} \geq \dfrac{N}{2} \\ G_{\mathrm{n}} & L_{\max} < \dfrac{N}{2} \end{cases}. \tag{5.15}$$

The power P_{int_1} is evaluated using (2.1) and considering that $\mathbb{D}$ and $\mathbb{I}$ (in $\mathbb{R}_1$) can interfere with any equivalent gain $F_{\text{D}}(\varphi)$. The power P_{int_3} is calculated observing that no interference incomes from region $\mathbb{R}_3$. The power P_{int_2}, instead, must be determined taking into account the smart antenna system characteristics, the SINR requirements at the receiver and the channel conditions. This leads to a more complex expression. The destination $\mathbb{D}$ can detect the undesired sources in $\mathbb{R}_2$ and, moreover, these sources are aware of the presence of $\mathbb{D}$. By consequence, P_{int_2}, in (5.14b), is calculated taking into account that the smart antenna system can place a maximum of $N-2$ nulls towards the undesired sources, but, in some scenarios, this potential may be not completely exploited because of bad channel conditions or too stringent requirements on the SINR. Function $\tilde{F}_{\text{D}}(\varphi, L_{\max})$ takes into account this difference. Even if $N-2$ degrees of freedom are available, the number of communicating nodes in the region $\mathbb{R}_2$ may be higher, equal or lower than $N-2$. Therefore, the unknown $L_{\max}$ must be evaluated distinguishing between two different cases: high number of sustainable links ($L_{\max} \geq N/2$) and low number of sustainable links ($L_{\max} < N/2$).

5.5 Sustainable links

5.5.1 High number of sustainable links

This subsection evaluates the number of sustainable links of the network when $L_{\max} \geq N/2$. In this case, as stated by (5.15), $N-2$ directions of interference are received with an equivalent gain equal to $G_{\text{n}} << 1$, but the other directions of interference, in general, cannot be suppressed and may be received with any gain. In the sole region $\mathbb{R}_2$, the communicating nodes can be distinguished between suppressed interferers and not suppressed (but "tolerable") interferers. Assuming that the network can sustain $L_{\max}$ simultaneous communications in the area $\mathcal{L}_{\text{c}}$, there are $2L_{\max}$ active nodes in $\mathbb{R}_2$. These $2L_{\max}$ active nodes include $\mathbb{D}$ and its source $\mathbb{S}$, therefore the number of active interferers is $2L_{\max}-2$ and the number of unsuppressed interferers in $\mathbb{R}_2$ becomes equal to $2L_{\max}-2-(N-2) = 2L_{\max}-N$. By consequence, for $L_{\max} \geq N/2$, (5.14b) becomes implicitly defined by the number of sustainable links $L_{\max}$ (still unknown).
The active node density, in (5.14), is given by:

$$\tilde{\varrho}_{\text{act}}(r, \varphi) = n_{\text{tx}} \varrho_{\text{TOP}}(r, \varphi), \tag{5.16}$$

corresponding to the product between the number of transmitting nodes (namely active nodes) in the network and the pdf of the spatial distribution of the nodes around $\mathbb{D}$, defined as $\varrho_{\text{TOP}}(r, \varphi)$. This pdf is related to the network topology and,

for calculation purposes, is rewritten in this form:

$$\varrho_{\mathrm{TOP}}(r,\varphi)=\frac{1}{\pi R_{\mathrm{t}}^2}\begin{cases} F_{\mathrm{T}}(r,\varphi) & r\in[0,R_{\mathrm{t}}],\varphi\in[0,2\pi] \\ 0 & \text{elsewhere}\end{cases}, \tag{5.17}$$

where $\int_0^{2\pi}\int_0^{R_{\mathrm{t}}} F_{\mathrm{T}}(r,\varphi)r\mathrm{d}r\mathrm{d}\varphi=\pi R_{\mathrm{t}}^2$. In the following, $F_{\mathrm{T}}(r,\varphi)$ will be called the *topology function*. Using (5.14)-(5.17) for $L_{\max}\geq N/2$ and performing some algebra, the total power received by $\mathbb{D}$ from all the undesired sources can be evaluated as:

$$P_{\mathrm{int}}=\sum_{i=1}^{3}P_{\mathrm{int}_i}=\frac{n_{\mathrm{tx}}P_{\mathrm{tx}}\gamma_\alpha}{\pi R_{\mathrm{t}}^2}\mathcal{I}, \tag{5.18}$$

where:

$$\mathcal{I}=\mathcal{I}(L_{\max})=G_{\mathrm{tx}_1}\chi_1+\frac{(N-2)G_{\mathrm{n}}G_{\mathrm{tx}_2}}{2(L_{\max}-1)}\chi_2+\frac{G_{\mathrm{tx}_2}(2L_{\max}-N)}{2(L_{\max}-1)}\chi_3, \tag{5.19}$$

and:

$$\chi_1=\int_0^{2\pi}\int_{R_{\mathrm{H}}(\varphi)}^{R_{\mathrm{t}}}\frac{F_{\mathrm{D}}(\varphi)}{r^{\alpha-1}}F_{\mathrm{T}}(r,\varphi)\mathrm{d}r\mathrm{d}\varphi, \tag{5.20a}$$

$$\chi_2=\int_0^{2\pi}\int_{R_{\mathrm{L}}(\varphi)}^{R_{\mathrm{H}}(\varphi)}\frac{F_{\mathrm{T}}(r,\varphi)}{r^{\alpha-1}}\mathrm{d}r\mathrm{d}\varphi, \tag{5.20b}$$

$$\chi_3=\int_0^{2\pi}\int_{R_{\mathrm{L}}(\varphi)}^{R_{\mathrm{H}}(\varphi)}\frac{F_{\mathrm{D}}(\varphi)}{r^{\alpha-1}}F_{\mathrm{T}}(r,\varphi)\mathrm{d}r\mathrm{d}\varphi. \tag{5.20c}$$

Defining as $\varrho_{\mathrm{SOU}}(r,\varphi)$ the pdf of the sources around $\mathbb{D}$ in the area $\mathcal{L}_{\mathrm{c}}$, the average distance between $\mathbb{S}$ and $\mathbb{D}$ can be calculated as:

$$R_{\mathrm{sd}}=\int_0^{R_{\mathrm{c}}}\varrho_{\mathrm{SOU}_r}(r)r\mathrm{d}r, \tag{5.21}$$

where:

$$\varrho_{\mathrm{SOU}_r}(r)=r\int_0^{2\pi}\varrho_{\mathrm{SOU}}(r,\varphi)\mathrm{d}\varphi, \tag{5.22}$$

is the marginal of $\varrho_{\mathrm{SOU}}(r,\varphi)$ with respect to r. It is worth to remark that, in this chapter, the objective is to calculate the number of one-hop communications that can be performed simultaneously, regardless of the fact that these communications concern packet forwarding or packet delivery. The multi-hop scenario will be introduced in Chapter 7, once the single-hop behavior of the network has been

established.
From (2.1), the desired signal power can be evaluated as:

$$P_{\mathrm{des}} = \frac{P_{\mathrm{tx}}\gamma_{\alpha}G_{\mathrm{tx_d}}G_{\mathrm{rx_d}}}{R_{\mathrm{sd}}^{\alpha}} = \frac{P_{\mathrm{tx}}\gamma_{\alpha}G_{\mathrm{d}}^{2}}{R_{\mathrm{sd}}^{\alpha}}, \tag{5.23}$$

where G_{d} is defined in (5.13). By consequence, using (5.18) and (5.23), the SINR at the antenna system output can be calculated as:

$$\mathrm{SINR}_{\mathrm{out}} = \frac{P_{\mathrm{des}}}{P_{\mathrm{int}} + W} = \frac{P_{\mathrm{tx}}\gamma_{\alpha}G_{\mathrm{d}}^{2}}{R_{\mathrm{sd}}^{\alpha}\left[\dfrac{n_{\mathrm{tx}}}{\pi R_{\mathrm{t}}^{2}}P_{\mathrm{tx}}\gamma_{\alpha}\mathcal{I}(L_{\max}) + W\right]}, \tag{5.24}$$

where W is given by (5.1). Defining the maximum number of nodes that can simultaneously transmit in the entire network (while maintaining the output SINR above the SINR threshold) as $n_{\mathrm{tx}}^{\max}$, the number of sustainable links and $n_{\mathrm{tx}}^{\max}$ are related by:

$$L_{\max} = \frac{n_{\mathrm{tx}}^{\max}}{\pi R_{\mathrm{t}}^{2}}\frac{\pi R_{\mathrm{c}}^{2}}{2}, \tag{5.25}$$

according to the definition of $L_{\max}$ given in Section 5.2. Adopting the ON/OFF criterion to establish packet reception, the DATA packet is considered received by $\mathbb{D}$ if $\mathrm{SINR}_{\mathrm{out}}$ is higher than $\mathrm{SINR}_{\mathrm{th}}$. By consequence, using (5.1) and (5.25), equation (5.24) can be rewritten as:

$$\mathrm{SINR}_{\mathrm{th}} = \frac{G_{\mathrm{d}}^{2}}{R_{\mathrm{sd}}^{\alpha}\left[\dfrac{2L_{\max}\cdot\mathcal{I}}{\pi R_{\mathrm{c}}^{2}} + \dfrac{1}{\mathrm{SINR}_{\mathrm{th}}R_{\mathrm{c}}^{\alpha}}\right]}, \tag{5.26}$$

from which, by (5.19), a simple quadratic equation is obtained:

$$L_{\max}^{2} + c_1 L_{\max} + c_2 = 0, \tag{5.27}$$

where the coefficients c_1 and c_2 are:

$$c_1 = \frac{\mathrm{SINR}_{\mathrm{th}}R_{\mathrm{sd}}^{\alpha}R_{\mathrm{c}}^{\alpha-2}\{G_{\mathrm{tx_2}}[(N-2)G_{\mathrm{n}}\chi_2 - N\chi_3] - 2G_{\mathrm{tx_1}}\chi_1\} + \pi(R_{\mathrm{sd}}^{\alpha} - R_{\mathrm{c}}^{\alpha}G_{\mathrm{d}}^{2})}{2\mathrm{SINR}_{\mathrm{th}}R_{\mathrm{sd}}^{\alpha}R_{\mathrm{c}}^{\alpha-2}(G_{\mathrm{tx_1}}\chi_1 + G_{\mathrm{tx_2}}\chi_3)}, \tag{5.28a}$$

$$c_2 = \frac{\pi(R_{\mathrm{c}}^{\alpha}G_{\mathrm{d}}^{2} - R_{\mathrm{sd}}^{\alpha})}{2\mathrm{SINR}_{\mathrm{th}}R_{\mathrm{sd}}^{\alpha}R_{\mathrm{c}}^{\alpha-2}(G_{\mathrm{tx_1}}\chi_1 + G_{\mathrm{tx_2}}\chi_3)}. \tag{5.28b}$$

The largest root of (5.27) represents the number of simultaneous communications sustainable by the network in the area $\mathcal{L}_{\mathrm{c}}$ when $L_{\max} \geq N/2$.

5.5.2 Low number of sustainable links

As described in Section 5.4, it may happen that the number of suppressible interferers becomes lower than the available degrees of freedom, $N-2$, of the physical antenna system ($L_{\max} < N/2$). In this case, even if $N-2$ degrees of freedom are theoretically available, their actual number is lower and becomes substantially equal to $2L_{\max}-2$. Therefore, in the region $\mathbb{R}_2$, there are no "tolerable" interferers and the $2L_{\max}-2$ actual degrees of freedom are used to suppress $2L_{\max}-2$ interferers, leading to $\tilde{F}_{\mathrm{D}}(\varphi, L_{\max}) = G_{\mathrm{n}}$, as stated by (5.15). Therefore, using (5.14b) for $L_{\max} < N/2$, the interference incoming from $\mathbb{R}_2$ becomes:

$$P_{\mathrm{int}_2} = \int_0^{2\pi} \int_{R_{\mathrm{L}}(\varphi)}^{R_{\mathrm{H}}(\varphi)} \frac{P_{\mathrm{tx}}\gamma_\alpha G_{\mathrm{tx}_2}}{r^\alpha} G_{\mathrm{n}} \tilde{\varrho}_{\mathrm{act}}(r,\varphi) r \mathrm{d}r \mathrm{d}\varphi. \tag{5.29}$$

By consequence, (5.19) can be simplified as:

$$\mathcal{I} = G_{\mathrm{tx}_1}\chi_1 + G_{\mathrm{n}}G_{\mathrm{tx}_2}\chi_2, \tag{5.30}$$

and becomes independent of $L_{\max}$. Substituting (5.30) in (5.26), the number of sustainable links for $L_{\max} < N/2$ can be calculated as:

$$L_{\max} = \frac{\pi(R_{\mathrm{c}}^\alpha G_{\mathrm{d}}^2 - R_{\mathrm{sd}}^\alpha)}{2\mathrm{SINR}_{\mathrm{th}} R_{\mathrm{sd}}^\alpha R_{\mathrm{c}}^{\alpha-2}(G_{\mathrm{tx}_1}\chi_1 + G_{\mathrm{n}}G_{\mathrm{tx}_2}\chi_2)}. \tag{5.31}$$

The expression defined in (5.31) represents the complementary case with respect to $L_{\max} \geq N/2$.

5.6 Topology and access scheme

This section analyzes the dependence of $L_{\max}$ on the MAC protocol characteristics in the spatial domain for a uniform distribution of the nodes and for a random distribution of the nodes.

5.6.1 Uniform distribution

The uniform distribution of the nodes in the network, described by the pdf:

$$\varrho_{\mathrm{TOP}}^{\mathrm{u}}(r,\varphi) = \begin{cases} \dfrac{1}{\pi R_{\mathrm{t}}^2} & r \in [0, R_{\mathrm{t}}], \varphi \in [0, 2\pi] \\ 0 & \text{elsewhere} \end{cases}, \tag{5.32}$$

is analyzed first, since it leads to a more tractable derivation and is widely employed in many theoretical studies [117, 127].

5.6.1.1 Omnidirectional CTS (OCTS)

The access scheme, as stated in Section 5.4, influences the radii that limit the three interference regions and the transmission gains towards $\mathbb{D}$ of the nodes lying in these regions. Using an omnidirectional CTS transmission $R_{\mathrm{H}}(\varphi)$ describes a circumference of radius R_{c}, while $R_{\mathrm{L}}(\varphi)$ can be derived from:

$$P_{\mathrm{th}} = \frac{P_{\mathrm{tx}}\gamma_{\alpha}G_{\mathrm{tx_2}}F_{\mathrm{D}}(\varphi)}{R_{\mathrm{L}}^{\alpha}(\varphi)}, \tag{5.33}$$

where $P_{\mathrm{th}} = W \cdot \mathrm{SINR}_{\mathrm{th}}$ is the receiving power threshold. Inverting (5.33) and using (5.2), the lower bound of $\mathbb{R}_2$ can be easily obtained, and the two required radii can be written as:

$$R_{\mathrm{H}}(\varphi) = R_{\mathrm{c}}, \tag{5.34a}$$

$$R_{\mathrm{L}}(\varphi) = R_{\mathrm{c}}[G_{\mathrm{tx_2}}F_{\mathrm{D}}(\varphi)]^{\frac{1}{\alpha}}. \tag{5.34b}$$

Considering that for a uniform distribution of the nodes $F_{\mathrm{T}}(r,\varphi) = 1$ in the entire azimuth plane and using (5.34), by simple calculations, (5.20) can be rewritten as:

$$\chi_1 = K\bar{K}\int_0^{2\pi} F_{\mathrm{D}}(\varphi)\mathrm{d}\varphi, \tag{5.35a}$$

$$\chi_2 = \bar{K}\int_0^{2\pi} \left\{[G_{\mathrm{tx_2}}F_{\mathrm{D}}(\varphi)]^{\alpha_1} - 1\right\}\mathrm{d}\varphi, \tag{5.35b}$$

$$\chi_3 = \bar{K}\int_0^{2\pi} \left\{[G_{\mathrm{tx_2}}F_{\mathrm{D}}(\varphi)]^{\alpha_1} - 1\right\}F_{\mathrm{D}}(\varphi)\mathrm{d}\varphi, \tag{5.35c}$$

where:

$$K = 1 - \left(\frac{R_{\mathrm{c}}}{R_{\mathrm{t}}}\right)^{\alpha-2}, \tag{5.36a}$$

$$\bar{K} = \frac{1}{(\alpha-2)R_{\mathrm{c}}^{\alpha-2}}, \tag{5.36b}$$

$$\alpha_1 = \frac{2-\alpha}{\alpha}. \tag{5.36c}$$

The transmission gain $G_{\mathrm{tx_1}}$, due to the nodes that are too far from $\mathbb{D}$ to receive the CTS, does not depend on the MAC protocol characteristics in the spatial domain. Instead, $G_{\mathrm{tx_2}}$ is influenced by the policy ruled at MAC layer for the transmission of the DATA packet. Therefore, during $\mathbb{D}$'s reception of its own DATA packet, the equivalent transmission gains of the interferers towards $\mathbb{D}$ are defined as:

$$G_{\mathrm{tx_1}} = G_{\mathrm{m}}, \tag{5.37a}$$

$$G_{\mathrm{tx_2}} = \begin{cases} G_{\mathrm{m}} & \text{DD} \\ G'_{\mathrm{m}} & \text{DD(DNAV)} \\ G_{\mathrm{n}} & \text{SD} \end{cases}, \tag{5.37b}$$

where DD, DD(DNAV) and SD stand for Directional (without DNAV), Directional with DNAV and Smart DATA transmission, respectively. The gains G_{m}, G'_{m}, G_{n} are defined in (5.11), (5.12) and (5.10), respectively. In the DD case no protection is guaranteed and any lobe can be directed towards $\mathbb{D}$. In the DD(DNAV) case the access scheme inhibits the nodes in region $\mathbb{R}_2$ to steer their main lobes towards $\mathbb{D}$. Therefore, only the minor lobes can be directed towards the destination. In the SD case the MAC policy states that the nodes in $\mathbb{R}_2$ have to place a null towards $\mathbb{D}$ to protect its communication.

5.6.1.2 Directional CTS (DCTS)

When the MAC protocol adopts a directional CTS transmission, the radii that limit the three regions can be evaluated as:

$$R_{\mathrm{H}}(\varphi) = R_{\mathrm{c}}[F_{\mathrm{D}}(\varphi)]^{\frac{1}{\alpha}}, \tag{5.38a}$$

$$R_{\mathrm{L}}(\varphi) = R_{\mathrm{c}}[G_{\mathrm{tx}_2} F_{\mathrm{D}}(\varphi)]^{\frac{1}{\alpha}}. \tag{5.38b}$$

Performing some calculations, (5.20) can be rewritten as:

$$\chi_1 = \bar{K} \int_0^{2\pi} \left\{ [F_{\mathrm{D}}(\varphi)]^{\alpha_1} + K - 1 \right\} F_{\mathrm{D}}(\varphi) \mathrm{d}\varphi, \tag{5.39a}$$

$$\chi_2 = \bar{K} \left(G_{\mathrm{tx}_2}^{\alpha_1} - 1 \right) \int_0^{2\pi} [F_{\mathrm{D}}(\varphi)]^{\alpha_1} \mathrm{d}\varphi, \tag{5.39b}$$

$$\chi_3 = \bar{K} \left(G_{\mathrm{tx}_2}^{\alpha_1} - 1 \right) \int_0^{2\pi} [F_{\mathrm{D}}(\varphi)]^{\alpha_2} \mathrm{d}\varphi, \tag{5.39c}$$

where:

$$\alpha_2 = \frac{2}{\alpha}, \tag{5.40}$$

and the possible values of G_{tx_1} and G_{tx_2} can still be described by (5.37), according to the transmission policy ruled at MAC layer.

In a scenario where the nodes are uniformly distributed in the topology area, it is intuitive to assume the same distribution for the sources inside the region covered by R_{c}, therefore:

$$\varrho_{\mathrm{SOU}}^{\mathrm{u}}(r, \varphi) = \begin{cases} \dfrac{1}{\pi R_{\mathrm{c}}^2} & r \in [0, R_{\mathrm{c}}], \varphi \in [0, 2\pi] \\ 0 & \text{elsewhere} \end{cases}, \tag{5.41}$$

and, using (5.21) and (5.22), the average distance between the source and the destination becomes equal to $2R_{\mathrm{c}}/3$.
It is worth noticing that, in the presented model, the pdf $\varrho_{\mathrm{TOP}}(r,\varphi)$, and so the function $F_{\mathrm{T}}(r,\varphi)$, describe the topology as it is viewed by $\mathbb{D}$. Assuming this pdf as uniform in the area covered by R_{t}, the marginals with respect to r and φ can be calculated as $\varrho^{\mathrm{u}}_{\mathrm{TOP}_r}(r) = 2r/R_{\mathrm{t}}^2$ and $\varrho^{\mathrm{u}}_{\mathrm{TOP}_\varphi}(\varphi) = 1/2\pi$, respectively [121]. In terms of distance, as r gets lower the probability that an interferer is closer to $\mathbb{D}$ gets lower. Therefore, the use of a uniform distribution for $\varrho_{\mathrm{TOP}}(r,\varphi)$ implies that the interferers lie at a larger distance with a higher probability. This assumption may lead to optimistic results with respect to the real behavior of a distributed wireless network.

5.6.2 Random distribution

In phase of simulation, usually, the random position of the nodes is generated using two uniform distributions for the cartesian coordinates or for the polar coordinates. However, if the number of interferers is not sufficiently high, this choice does not lead to a uniform distribution of the nodes in the topology area. To model the behavior of a random network, it is proposed to use the following pdf:

$$\varrho^{\mathrm{r}}_{\mathrm{TOP}}(r,\varphi) = \begin{cases} \dfrac{1}{2\pi R_{\mathrm{t}} r} & r \in [0, R_{\mathrm{t}}], \varphi \in [0, 2\pi] \\ 0 & \text{elsewhere} \end{cases}, \tag{5.42}$$

which leads to the topology function $F_{\mathrm{T}}(r,\varphi) = R_{\mathrm{t}}/(2r)$. It can be noticed that, considering a finite number of nodes in the network, this pdf provides more realistic results with respect to a uniform distribution in the area $\mathcal{L}_{\mathrm{t}}$. In fact, the uniform pdf is more suitable to model network scenarios in which the total number of nodes can be assumed very large, and so a direct relationship can be established between area and interference. Instead, considering a scenario in which the number of nodes in the region $\mathbb{R}_2$ and the number of antennas are of the same order of magnitude (finite and not very large), the distance of each single interferer from the destination becomes significant. The two marginals of (5.42), $\varrho^{\mathrm{r}}_{\mathrm{TOP}_r}(r) = 1/R_{\mathrm{t}}$ and $\varrho^{\mathrm{r}}_{\mathrm{TOP}_\varphi}(\varphi) = 1/2\pi$, are both uniform, and so the probability that an interferer lies at distance r from $\mathbb{D}$ is independent of r. Inserting this topology function in (5.20), and using (5.34) and (5.38) to calculate the radii in the OCTS and in the DCTS cases, respectively, two sets of expressions are obtained. These expressions are formally equal to (5.35) and (5.39), except for the values of

the constants that become:

$$K = 1 - \left(\frac{R_{\mathrm{c}}}{R_{\mathrm{t}}}\right)^{\alpha-1}, \tag{5.43a}$$

$$\bar{K} = \frac{R_{\mathrm{t}}}{2(\alpha-1)R_{\mathrm{c}}^{\alpha-1}}, \tag{5.43b}$$

$$\alpha_1 = \frac{1-\alpha}{\alpha}, \tag{5.43c}$$

$$\alpha_2 = \frac{1}{\alpha}. \tag{5.43d}$$

According to the distribution of the interferers around $\mathbb{D}$, the pdf of the sources is selected as:

$$\varrho^{\mathrm{r}}_{\mathrm{SOU}}(r,\varphi) = \begin{cases} \dfrac{1}{2\pi R_{\mathrm{c}} r} & r \in [0, R_{\mathrm{c}}], \varphi \in [0, 2\pi] \\ 0 & \text{elsewhere} \end{cases}, \tag{5.44}$$

and so, using (5.21) and (5.22), $R_{\mathrm{sd}} = R_{\mathrm{c}}/2$.

5.6.3 Refinement for Smart DATA transmission

The choice of the transmission gain of the nodes in $\mathbb{R}_2$, as stated in (5.37b), is acceptable for the cases of directional DATA transmission with and without DNAV. In the smart DATA transmission cases, instead, the choice of $G_{\mathrm{tx}_2} = G_{\mathrm{n}}$ is correct when the number of sustainable links is low ($L_{\max} < N/2$), but may lead to an overestimation of $L_{\max}$ when the number of sustainable links is high ($L_{\max} \geq N/2$). In general, it is not true that all interferers in $\mathbb{R}_2$ are able to place a null towards $\mathbb{D}$. If the number of communicating nodes in the area $\mathcal{L}_{\mathrm{c}}$ is larger than $N-2$, some nodes will necessarily interfere with a gain larger than G_{n} towards other nodes. By consequence, the assumption $G_{\mathrm{tx}_2} = G_{\mathrm{n}}$ is too optimistic for $L_{\max} \geq N/2$.
To analyze this scenario, the same arguments described in Section 5.4 can be employed. In particular, in the SD cases, the gain G_{tx_2} must be substituted by:

$$G_{\mathrm{tx}_2} = G_{\mathrm{tx}_2}(L_{\max}) = \begin{cases} \dfrac{(N-2)G_{\mathrm{n}} + (2L_{\max} - N)G'_{\mathrm{m}}}{2(L_{\max}-1)} & L_{\max} \geq \dfrac{N}{2} \\ G_{\mathrm{n}} & L_{\max} < \dfrac{N}{2} \end{cases}, \tag{5.45}$$

where, thanks to the use of the DNAV, the transmission gain towards the directions that cannot be suppressed is given by the average gain outside the main lobe G'_{m},

expressed by (5.12). Inserting (5.45) for $L_{\max} \geq N/2$ in (5.28) and (5.35) for the OCTS case (or (5.39) for the DCTS case), equation (5.27) becomes a nonlinear equation in the unknown $L_{\max}$ that can be numerically solved. For example, for $\alpha = 4$, one can obtain a sixth degree equation for a uniform distribution of nodes, or a twelfth degree equation, for the random distribution described by the pdf in (5.42). The mathematical details regarding the uniform distribution are reported in the Appendix.
To avoid cumbersome calculations, an iterative approach can be used to obtain more precise values in the SD cases for $L_{\max} \geq N/2$. The proposed iterative procedure begins from the overestimated value of the number of sustainable links, defined as $L_{\max}(0)$ and provided by the analytical model using the gain $G_{\mathrm{tx}_2}(i = 0) = G_{\mathrm{n}}$. At the first step, a new gain $G_{\mathrm{tx}_2}(1)$ is derived using (5.45) for $L_{\max} \geq N/2$ with $L_{\max} = L_{\max}(0)$. If $L_{\max}(0)$ is not an overestimation of the real $L_{\max}$ value, then $G_{\mathrm{tx}_2}(1)$ should be equal to $G_{\mathrm{tx}_2}(0)$. If not, this means that the transmission gain used to calculate the number of sustainable links is not sufficiently realistic and must be recalculated. In general, the gain $G_{\mathrm{tx}_2}(i+1)$, at the $(i+1)$-th iteration, is evaluated as:

$$G_{\mathrm{tx}_2}(i+1) = \frac{(N-2)G_{\mathrm{n}} + [2L_{\max}(i) - N]G'_{\mathrm{m}}}{2[L_{\max}(i) - 1]}, \tag{5.46}$$

using the number of sustainable links computed at the i-th iteration, $L_{\max}(i)$. This new gain is then inserted in the analytical model involving the second degree equation to compute the new value $L_{\max}(i+1)$ and so on. The iterative procedure is terminated at step $i = i_0$ when $|L_{\max}(i_0 + 1) - L_{\max}(i_0)| < \varpi_{\mathrm{SD}}$, where the threshold value ϖ_{SD} is set equal to 10^{-3}. It can be noticed that the behavior of $G_{\mathrm{tx}_2}(i)$ is not monotonous and, for some steps, it can be larger than its exact value, leading to estimations $L_{\max}(i)$ lower than the real number of sustainable links. However, the process converges to an accurate value in a small number of steps. A validation of this iterative approach will be performed in Section 5.8.

5.7 Results

The most relevant results obtained using the described model are presented in this section. All curves are derived adopting a coverage range R_{c} equal to 100 m and assuming $R_{\mathrm{t}} >> R_{\mathrm{c}}$. The receiving threshold $\mathrm{SINR}_{\mathrm{th}}$ is chosen equal to 10 dB, a suitable value for many communication systems. A more detailed investigation regarding the choice of the threshold in agreement with the modulation scheme, the channel coding technique, the size of the packet and the packet error rate will be performed in the next chapter.

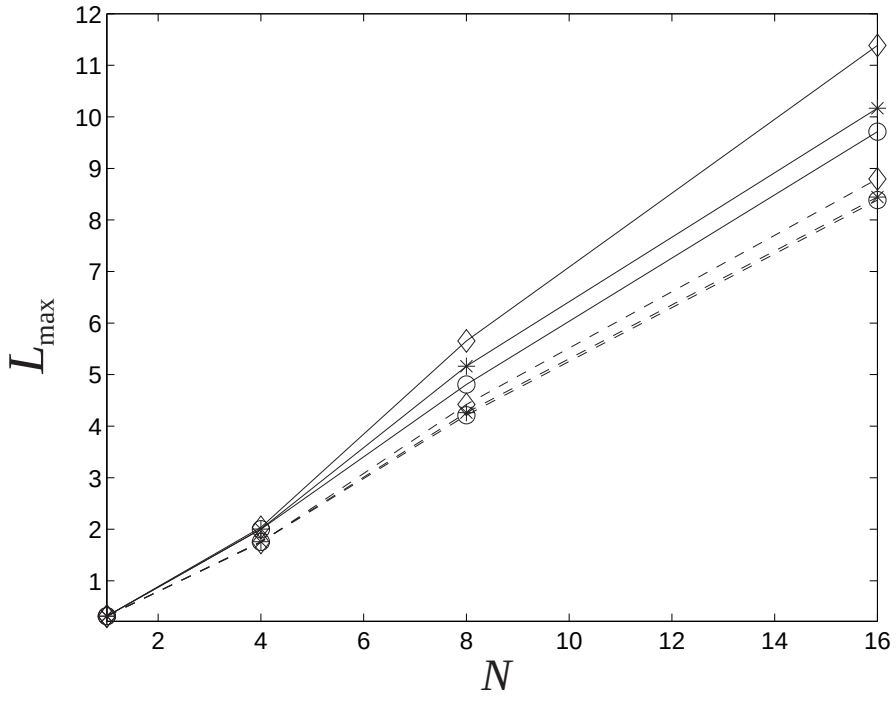

Figure 5.3: Sustainable links as a function of the number of antennas for a uniform distribution of the nodes in absence of multipath ($\hat{\sigma}_{\varphi} = 0^{o}$).
—◇— OCTS-SD - -◇- - DCTS-SD
—∗— OCTS-DD(DNAV) - -∗- - DCTS-DD(DNAV)
—○— OCTS-DD - -○- - DCTS-DD

5.7.1 Packet transmission policy

The influence of the MAC protocol characteristics in the spatial domain on the number of sustainable links can be inferred from Figg. 5.3-5.6, which are obtained choosing $\alpha = 4$ and the GBSBM channel model, corresponding to the disk of scatterers pdf, to account for the azimuth spread of the channel [22].
Fig. 5.3 shows the number of sustainable links in absence of multipath for a uniform distribution of the nodes and of the sources. The best performance can be reached when adaptive arrays are used not only in reception, but also in transmission and in conjunction with the omnidirectional CTS. The use of a directional NAV reduces the direct interference and increases the performance of the directional transmission mainly in the OCTS case. In the DCTS case, instead, the virtual carrier sensing mechanism seems less effective because little position information is available and so a lower number of nodes is aware of the ongoing communications.

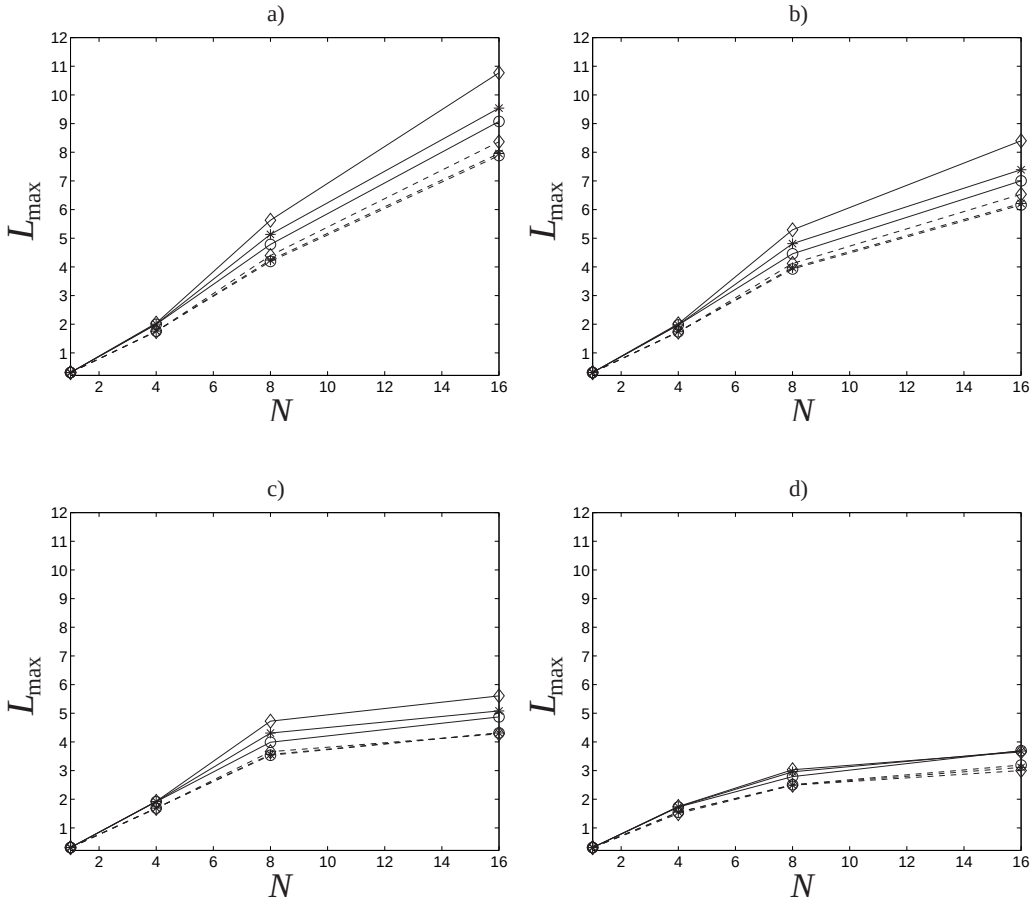

Figure 5.4: Sustainable links as a function of the number of antennas for a uniform distribution of the nodes and using the disk of scatterers pdf:
a) $\hat{\sigma}_\varphi = 1^o$, b) $\hat{\sigma}_\varphi = 3^o$, c) $\hat{\sigma}_\varphi = 5^o$, d) $\hat{\sigma}_\varphi = 10^o$.
—◇— OCTS-SD - -◇- - DCTS-SD
—∗— OCTS-DD(DNAV) - -∗- - DCTS-DD(DNAV)
—○— OCTS-DD - -○- - DCTS-DD

In general, a comparison between the cases corresponding to the same transmission policy of the DATA packet, but using a different policy for CTS transmission, shows that the adoption of an omnidirectional CTS provides better results with respect to the DCTS. It can be observed that, using a directional CTS, more transmissions are allowed, but fewer nodes are informed about the current communications and a larger interference is present in the network. Therefore, the use of omnidirectional control packets, enhancing the possible cooperation between the nodes, enables a larger number of simultaneous communications.

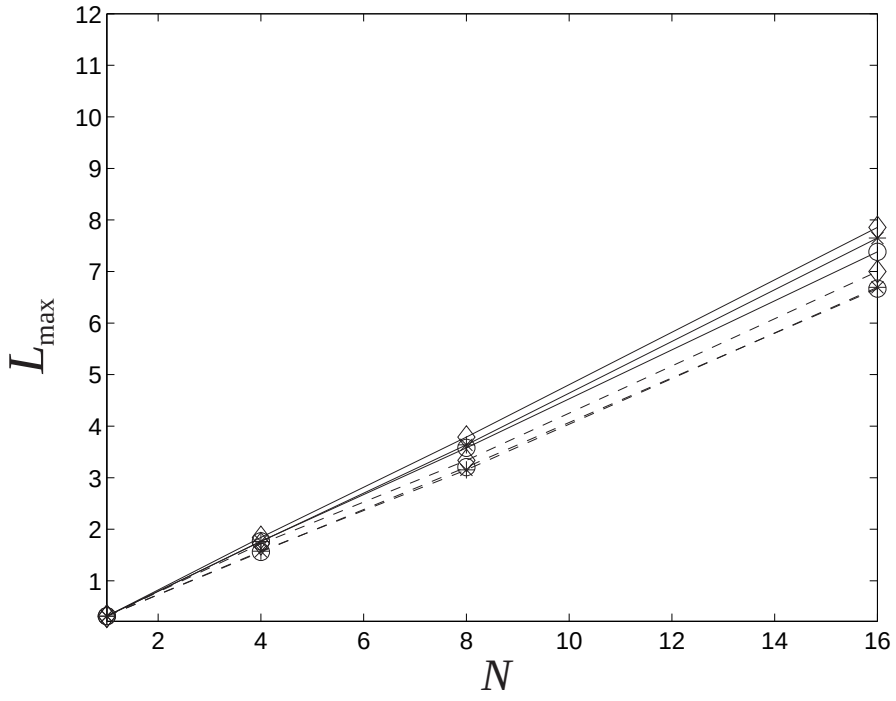

Figure 5.5: Sustainable links as a function of the number of antennas for a random distribution of the nodes in absence of multipath ($\hat{\sigma}_{\varphi} = 0^{o}$).
—◇— OCTS-SD --◇-- DCTS-SD
—∗— OCTS-DD(DNAV) --∗-- DCTS-DD(DNAV)
—○— OCTS-DD --○-- DCTS-DD

5.7.2 Angular spread and topology

The decrease of $L_{\max}$ as a function of the angular spread of the channel, shown in Fig. 5.4, confirms the sensitivity of the network behavior to the spatial decorrelation of the signals. Moreover, when the angular spread values become closer to the beamwidth of the antenna radiation pattern ($\hat{\sigma}_{\varphi} = 5^{o}$ or $\hat{\sigma}_{\varphi} = 10^{o}$, and $N = 16$), the increase in the number of antennas leads to a small performance improvement.
$L_{\max}$ experiences a considerable decrease in the second analyzed topology, where the nodes are randomly distributed (Fig. 5.5). With respect to the uniform distribution of the nodes, in this case all nodes can be closer to the destination, but the lower value of the average source-destination distance does not sufficiently compensate the larger closeness of the interferers. Moreover, even if the angular spread is low, the six analyzed MAC transmission policies behave similarly (Fig. 5.6). It seems that the level of sophistication of the access scheme in the spa-

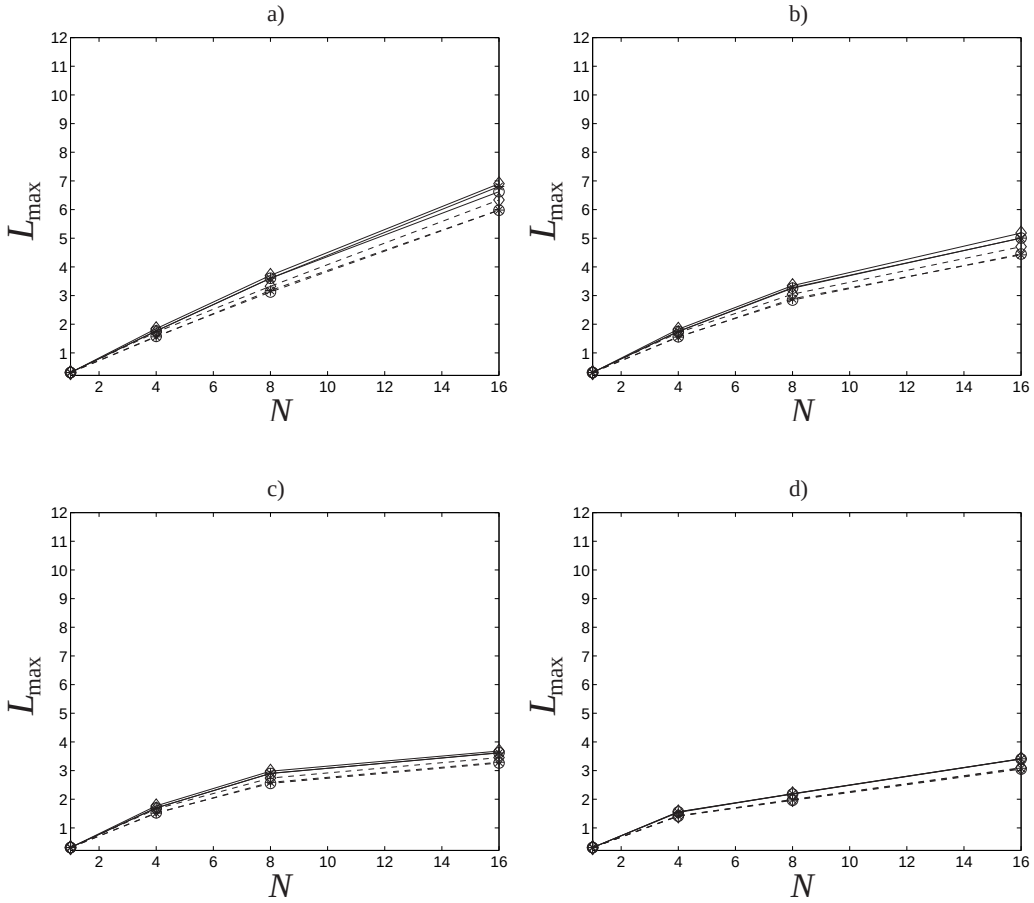

Figure 5.6: Sustainable links as a function of the number of antennas for a random distribution of the nodes and using the disk of scatterers pdf:
a) $\hat{\sigma}_\varphi = 1^o$, b) $\hat{\sigma}_\varphi = 3^o$, c) $\hat{\sigma}_\varphi = 5^o$, d) $\hat{\sigma}_\varphi = 10^o$.
—◇— OCTS-SD - -◇- - DCTS-SD
—∗— OCTS-DD(DNAV) - -∗- - DCTS-DD(DNAV)
—○— OCTS-DD - -○- - DCTS-DD

tial domain can partially increase the number of sustainable links, but the physical characteristics of the network play the decisive role in determining the performance. This behavior suggests that, in a scenario where the nodes are not mobile, such as a backbone WMN, the planning of the network topology may represent a key element for exploiting the capabilities of AAs.
The results obtained for both distributions of the nodes show that, with respect to the case where the signals are not subject to multipath, the performance degradations in a realistic outdoor environment, where $5^o \leq \hat{\sigma}_\varphi \leq 15^o$ [23], are in

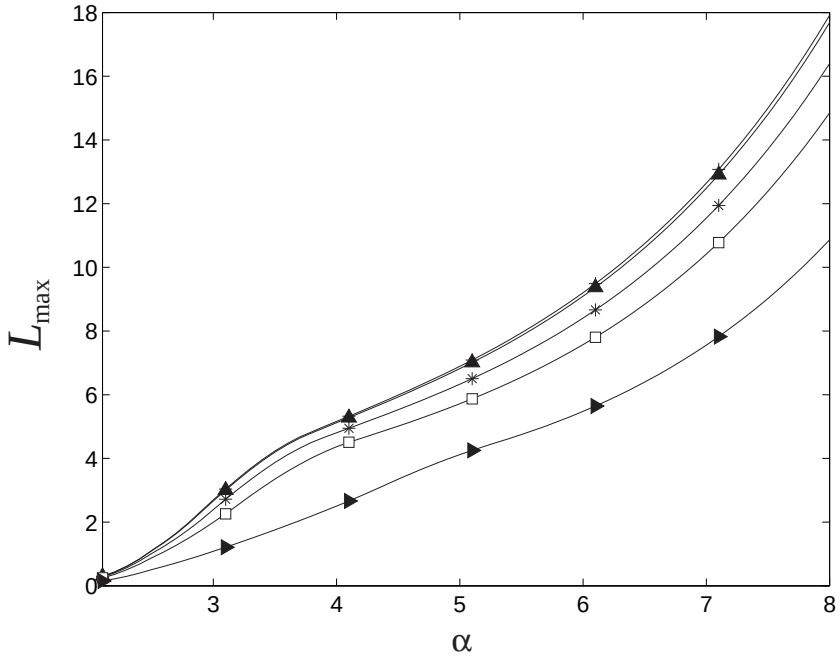

Figure 5.7: Sustainable links as a function of the path-loss exponent in the OCTS-DD(DNAV) case.
$\hat{\sigma}_\varphi = 0^o$ $\hat{\sigma}_\varphi = 1^o$ $\hat{\sigma}_\varphi = 3^o$ $\hat{\sigma}_\varphi = 5^o$ $\hat{\sigma}_\varphi = 10^o$

the order of 15%, 45% and 60% for $N = 4$, $N = 8$ and $N = 16$ antennas, respectively. Therefore, not only encumbrance and cost considerations, but also the real characteristics of the network scenario, lead to conclude that a low number of antennas may be sufficient for a device operating in a practical DWN.

5.7.3 Path loss and spatial channel model

The influence of the path-loss exponent α on the number of sustainable links for the OCTS-DD(DNAV) case is shown in Fig. 5.7. The increase of $L_{\max}$ as a function of α is due to the larger signal attenuation, which leads to a decrease of the interference power received by the generic destination. This behavior may seem in disagreement with the results presented in [117] for directional antennas, where the increase of α leads to a decrease of the capacity. Instead, the different conclusions are simply due to a slight difference in the analyzed scenarios. In the presented model, as stated by (5.2), the communication range $R_{\rm c}$, and so the average source-destination distance $R_{\rm sd}$, are decreasing functions of α. By consequence, for fixed values of transmission power and noise, they are modified according to

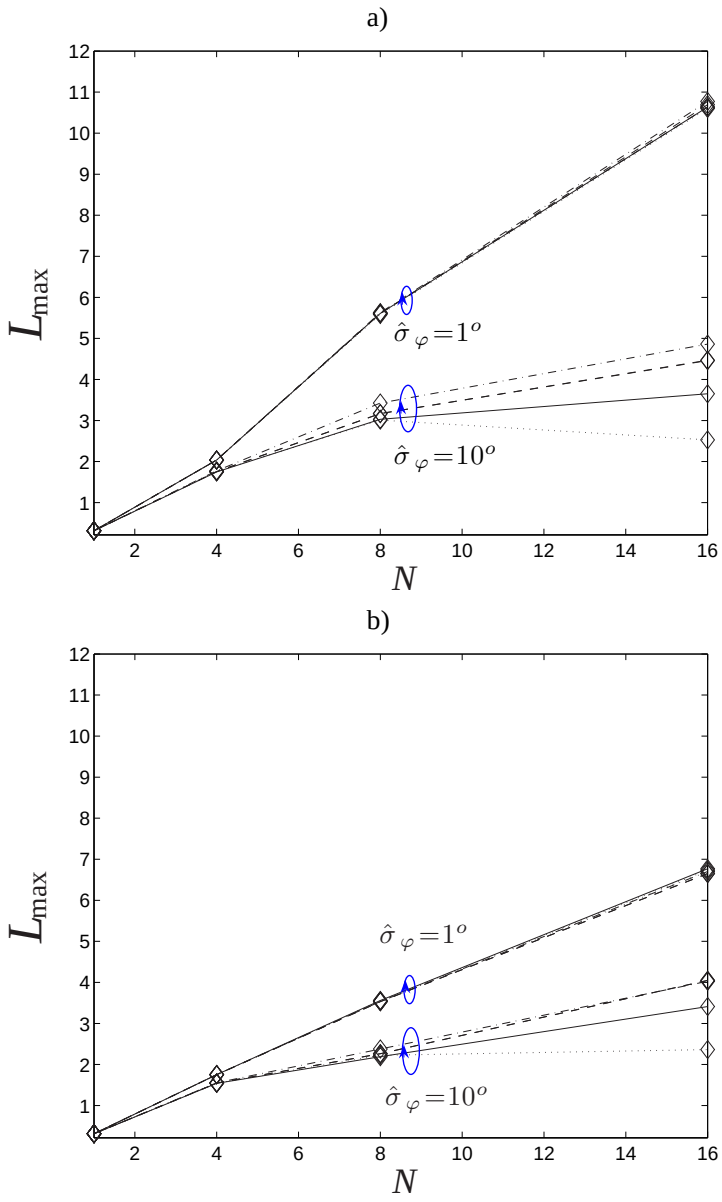

Figure 5.8: Sustainable links as a function of the number of antennas adopting different spatial channel models for the OCTS-SD case:
a) uniform distribution of the nodes, b) random distribution of the nodes.
--◇--Truncated Gaussian ····◇···· Ring of scatterers
—◇— Disk of scatterers -·◇·- Truncated Laplacian

the propagation environment. Therefore, the desired signal power is not affected by a larger attenuation, but the number of simultaneous communications are confined within a smaller area. Instead, in [117], the communication range is fixed and the increase of the path-loss exponent determines a strong decrease of the desired signal power, leading to a lower number of simultaneous communications.
Keeping the variance $\hat{\sigma}_{\varphi}^2$ constant, the presented analytical model is also employed to analyze the influence of the normalized PAS on the number of sustainable links. To this end, the constants γ_{m_1} and γ_{m_2}, in (5.5) and (5.6), respectively, are numerically evaluated for a given angular spread. Fig. 5.8, obtained for $\alpha = 4$ in the OCTS-SD case, shows that the influence of the spatial channel model becomes important for large values of N and $\hat{\sigma}_{\varphi}$. Besides, the curve corresponding to the ring of scatterers distribution puts in evidence that, in some scenarios, the increase in the number of antennas may lead to a performance reduction. The values obtained using the truncated Laplacian and the ring of scatterers seem to behave respectively as an upper and a lower limitation for $L_{\max}$. This can be intuitively justified, observing that, for the truncated Laplacian, the main energy contribution is given by the components closer to the mean DOA, while, for the ring of scatterers, the main energy is carried by the paths that are more distant from the mean DOA (Fig. 5.1). Therefore, in the first case, the main energy contributions are close to the null or to the maximum of the receiving radiation pattern, while the opposite happens in the second case.

5.8 Model validation

The results provided by the analysis are verified, for the OCTS-SD case, employing Network Simulator 2 (*ns-2*, release 2.29.3), a discrete-event network simulator developed at Berkeley National Laboratory [128].
The first simulation scenario involves a highly symmetrical environment, where the n nodes of the entire topology are subdivided in cells of radius R_{c}, each one containing n_2 nodes. In each cell the destinations and the sources are disposed on two concentric circumferences, whose radii are chosen qual to $R_{\mathrm{c}}/3$ and R_{c} (Fig. 5.9). The central cell is surrounded by six other identical cells and, therefore, it is the most significant one, being subjected to the largest interference. At the i-th step of the simulation $n_2(i) = 2i$ nodes are present in each cell. Using the gains G_{m}, G'_{m}, G_{d} and G_{n}, the $\mathrm{SINR}_{\mathrm{out}}$ value is calculated at each destination of the central cell. If, at the i-th step, at least one destination experiences a $\mathrm{SINR}_{\mathrm{out}}$ lower than $\mathrm{SINR}_{\mathrm{th}}$, the simulated value of $L_{\max}$ is assumed equal to $n_2(i-1)/2$. It is worth noticing that, in this case, the values derived by the simulations are necessarily integers. This scenario is compared with the theoretical results obtained assuming the uniform distribution of the nodes.

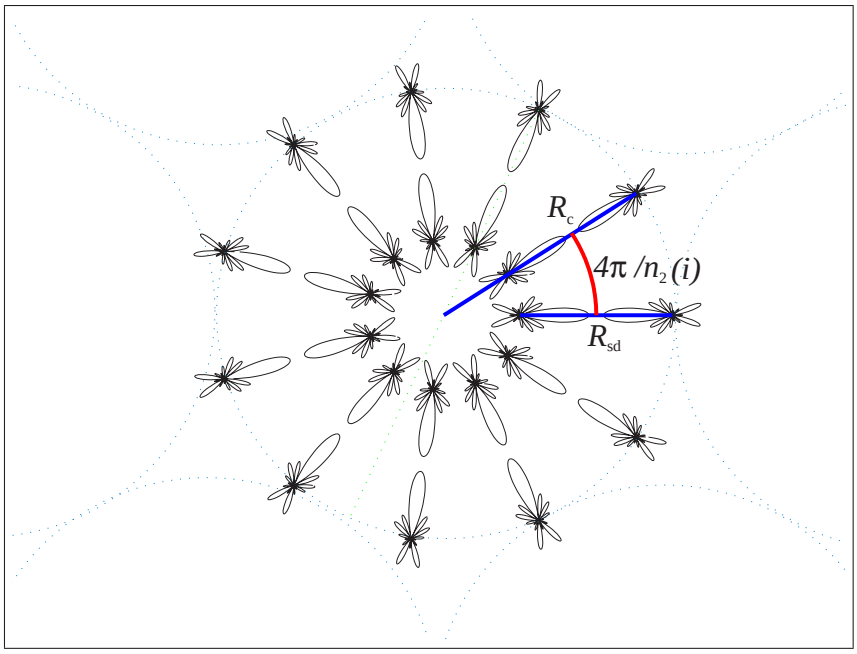

Figure 5.9: First simulation scenario. The destinations lie in the inner ring, while the sources in the outer one.

The second scenario involves a random distribution of the nodes. The position of each destination is determined, according to (5.42), using two uniformly distributed random variables, in $[0, 2\pi]$ and in $[0, R_t]$, which generate the polar coordinates with respect to the center of the topology. Similarly, the position of each source is selected using two other uniformly distributed random variables, in $[0, 2\pi]$ and in $[0, R_c]$, which generate the polar coordinates with respect to the proper destination. The reception of a packet is established adopting the threshold criterion and $L_{\max}$ is evaluated in the area $\mathcal{L}_c$, placed at the center of the topology. The simulations are repeated for different values of the total number of nodes and averaged over 100 different topologies.
The good agreement between the theoretical and the simulated values (Table 5.2), confirms the accuracy of the presented model. Analytical and simulation results confirm that adaptive antennas can largely improve the number of simultaneous communications sustainable by the network, even using a small number of antenna elements.
Finally, Table 5.3 shows the comparison between the exact calculation of $L_{\max}$, performed using the nonlinear equations reported in the Appendix, and the iterative approach described in Subsection 5.6.3 for the SD cases. The values, obtained for a uniform distribution of the nodes with $\alpha = 4$ and $\hat{\sigma}_\varphi = 0^o$, reveal that the

	Uniform distribution					
	$N = 4$		$N = 8$		$N = 16$	
	A	S	A	S	A	S
$\hat{\sigma}_\varphi = 0^o$	2.04	2.00	5.65	6.00	11.38	12.00
$\hat{\sigma}_\varphi = 1^o$	2.04	2.00	5.63	6.00	10.77	11.00
$\hat{\sigma}_\varphi = 3^o$	2.02	2.00	5.29	5.00	8.40	8.00
$\hat{\sigma}_\varphi = 5^o$	1.93	2.00	4.72	5.00	5.61	5.00
$\hat{\sigma}_\varphi = 10^o$	1.75	1.00	3.03	3.00	3.65	4.00
	Random distribution					
	$N = 4$		$N = 8$		$N = 16$	
	A	S	A	S	A	S
$\hat{\sigma}_\varphi = 0^o$	1.84	1.85	3.79	3.60	7.86	7.27
$\hat{\sigma}_\varphi = 1^o$	1.84	1.82	3.70	3.60	6.90	6.91
$\hat{\sigma}_\varphi = 3^o$	1.82	1.82	3.50	3.51	5.18	5.77
$\hat{\sigma}_\varphi = 5^o$	1.70	1.76	2.90	3.14	3.62	4.48
$\hat{\sigma}_\varphi = 10^o$	1.56	1.55	2.18	2.45	3.40	3.36

TABLE 5.2: ANALYTICAL (A) AND SIMULATED (S) $L_{\max}$ IN THE OCTS-SD CASE.

approximated solution converges to the exact one in a small number of steps i_0. An absolute error in the order of 10^{-4} can be reached for $i_0 \leq 8$.

5.9 Summary

A mathematical model to evaluate the performance of a distributed wireless network using smart antennas as a function of the channel and antenna parameters has been presented in this chapter. The model can be usefully applied for com-

	$L_{\max}(N = 4)$	$L_{\max}(N = 8)$	$L_{\max}(N = 16)$
OCTS-SD (exact)	2.0378	5.6535	11.3843
OCTS-SD (approximated)	2.0379($i_0 = 4$)	5.6536($i_0 = 6$)	11.3844($i_0 = 8$)
DCTS-SD (exact)	2.4341	5.8927	10.4674
DCTS-SD (approximated)	2.4340($i_0 = 5$)	5.8927($i_0 = 6$)	10.4673($i_0 = 7$)

TABLE 5.3: COMPARISON BETWEEN EXACT AND APPROXIMATED $L_{\max}$ FOR A UNIFORM DISTRIBUTION OF THE NODES IN ABSENCE OF MULTIPATH.

parison purposes, in scenarios that require comparison between different spatial statistics, topologies and packet transmission policies.
The results obtained from the analysis show that the choice of an omnidirectional CTS transmission leads to better performance than the directional one and, for large values of the angular spread, the performance becomes more dependent on the channel statistic in the spatial domain. Besides, despite the level of sophistication of the antenna system and of the MAC protocol, the network behavior is largely determined by the physical characteristics of the network and the channel. More precisely, the number of simultaneous communications sustainable by a distributed wireless network is largely influenced by the angular spread and the topology, and, in certain environments, the use of a large number of antennas at each node may lead to noticeable benefits only if the spatial correlation between the signal replicas is sufficiently high. Otherwise, the employment of arrays with many elements may be useless or even counterproductive.

Chapter 6

Multi-Antenna and Channel Coding Techniques for Wireless Mesh Routers

---

The objective of this chapter is the comparison of the low-cost switched-beam antennas with the more expensive adaptive antennas in a wireless mesh network scenario. The analysis is performed together with some considerations regarding the advantages and the practical possibilities of employing multi-antenna systems on mesh routers. The mathematical framework developed in Chapter 5 for a DWN using adaptive arrays is extended to include switched-beam antennas and mobility effects. Besides, in this chapter, the relationship between multiple antenna techniques and coded modulations is investigated, in order to determine the combination of antenna system and channel coding technique that may offer the best performance.[1]

6.1 Introduction

As described in Section 4.1, a WMN is a DWN having dynamic self-organizing and self-configuring capabilities, in which the nodes can be classified in two groups: the mesh clients, which can be mobile, and the mesh routers, forming the backbone of the WMN. The study presented hereafter models the behavior of this second group of nodes.
To guarantee the connectivity between the mesh routers, a proper topology plan-

[1]The content of this chapter is based on F. Babich, M. Comisso and L. Manià, 'Performance Comparison of Advanced Antenna Systems for Wireless Mesh Routers in an Outdoor Environment,' submitted to International Journal of Wireless and Mobile Computing [173,174,181].

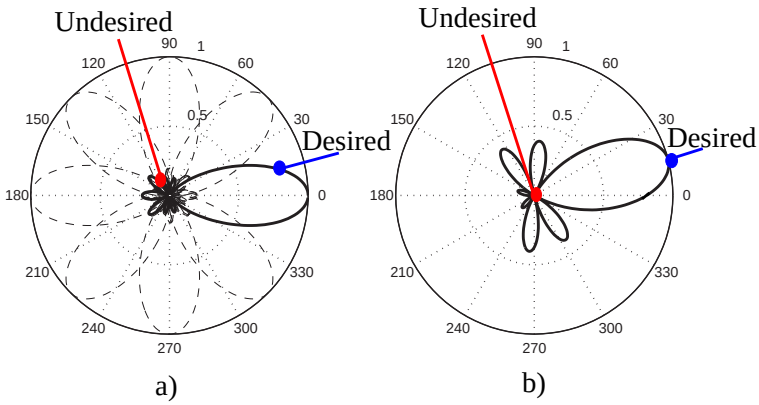

Figure 6.1: Typical power gain patterns: a) SBA, b) AA.

ning of the backbone is necessary. This planning leads to a scenario in which the neighboring mesh routers are often in LOS. Besides, the mesh routers can have to operate in outdoor environment, where the spatial correlation between the signal replicas can be sufficiently high to enable the use of switched-beam, directional and adaptive antennas. Moreover, the backbone nodes are usually fixed devices that can be connected to a feeding network and, therefore, their operations are not constrained by battery life. By consequence, in mesh routers, the use of multiple antenna systems seems a feasible improvement to reduce the interference and to increase the network capacity.
The antenna array of each router can be exploited using different processing techniques that determine the so called “level of intelligence” of the entire antenna system. As described in Section 3.6.1, SBAs have limited capabilities in interference suppression, while AAs are able to perform the electrical beam steering to a desired direction, and null steering to reject undesired signals. On the other hand, switched-beam are cheap systems, while adaptive arrays require more expensive hardware. These differences introduce a tradeoff between cost and performance.

6.2 Sustainable links of SBAs in WMNs

The theoretical model developed in the previous chapter is extended to SBAs in order to compare the performance of the two multi-antenna techniques. To better explain the choices performed in the development of the analysis, the main differences between SBAs and AAs are emphasized in Fig. 6.1, which provides an example of the typical behavior of the two antenna systems in an interference scenario. The power gain patterns reported in the figure, derived assuming a de-

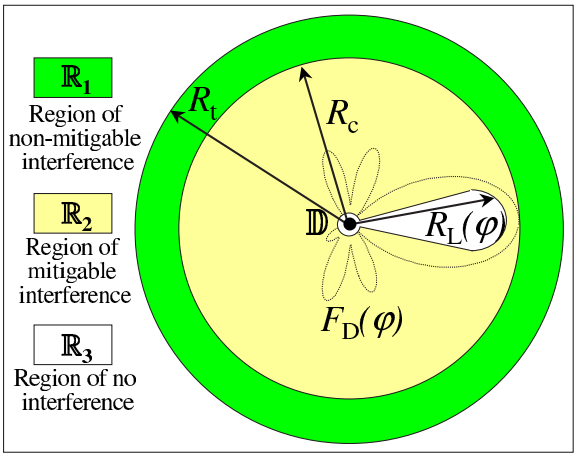

Figure 6.2: Interference regions in the SBA case.

sired direction $\varphi^{\mathrm{d}} = 15^o$ and an undesired one $\varphi^{\mathrm{n}} = 108^o$, are obtained using a UCA having $N = 8$ antenna elements and spacing between adjacent radiators equal to $\lambda/2$. With respect to AAs, in SBAs the direction of maximum gain and the position of the nulls cannot be varied with continuity. In fact, switched-beam is a multi-antenna technique in which the transmitting/receiving radiation pattern is selected among a finite number of available radiation patterns. In practice, this behavior of SBAs leads to a simplification of the calculations required to obtain the number of sustainable links.

The comparison between SBAs and AAs is limited to the OCTS case and to the uniform distribution of the nodes, two conditions that, as described in the previous chapter, lead to the largest number of simultaneous communications. Besides, the extension of the analysis to switched-beam antennas is performed assuming the use of the DNAV in order to obtain better performance also when SBAs are adopted [96]. According to these choices, the interference regions can be modeled as shown in Fig. 6.2, and the interference power received by the destination $\mathbb{D}$ from each of three regions during the reception of the DATA packet can be evaluated as:

$$P_{\mathrm{int}_1} = \frac{n_{\mathrm{tx}}}{\pi R_{\mathrm{t}}^2} \int_0^{2\pi} \int_{R_{\mathrm{c}}}^{R_{\mathrm{t}}} \frac{P_{\mathrm{tx}} \gamma_\alpha G_{\mathrm{m}} F_{\mathrm{D}}(\varphi)}{r^\alpha} r \mathrm{d}r \mathrm{d}\varphi, \tag{6.1a}$$

$$P_{\mathrm{int}_2} = \frac{n_{\mathrm{tx}}}{\pi R_{\mathrm{t}}^2} \int_{\frac{\varphi^{3\mathrm{dB}}}{2}}^{2\pi - \frac{\varphi^{3\mathrm{dB}}}{2}} \int_{R_{\mathrm{L}}(\varphi)}^{R_{\mathrm{c}}} \frac{P_{\mathrm{tx}} \gamma_\alpha G''_{\mathrm{m}} F_{\mathrm{D}}(\varphi)}{r^\alpha} r \mathrm{d}r \mathrm{d}\varphi, \tag{6.1b}$$

$$P_{\mathrm{int}_3} = 0, \tag{6.1c}$$

where G_{m} is calculated using (5.11), the equivalent power gain pattern $F_{\mathrm{D}}(\varphi)$ is defined in (5.9), the radius bounding the region $\mathbb{R}_3$ can be evaluated as:

$$R_{\mathrm{L}}(\varphi) = R_{\mathrm{c}}[G''_{\mathrm{m}} F_{\mathrm{D}}(\varphi)]^{\frac{1}{\alpha}}, \tag{6.2}$$

and:

$$G''_{\mathrm{m}} = \frac{1}{2\pi - \varphi^{3\mathrm{dB}}} \int_{\frac{\varphi^{3\mathrm{dB}}}{2}}^{2\pi - \frac{\varphi^{3\mathrm{dB}}}{2}} F_{\mathrm{D}}(\varphi)\mathrm{d}\varphi, \tag{6.3}$$

is the average power gain outside the HPBW. The desired signal power can still be calculated employing (5.23), where the transmitting/receiving power gain in the desired direction for the SBA case becomes:

$$G_{\mathrm{d}} = \frac{1}{\varphi^{3\mathrm{dB}}} \int_{-\frac{\varphi^{3\mathrm{dB}}}{2}}^{\frac{\varphi^{3\mathrm{dB}}}{2}} F_{\mathrm{D}}(\varphi)\mathrm{d}\varphi. \tag{6.4}$$

It can be noticed that, in general, using SBAs, the gain in the desired direction is not equal to one even if $F_{\mathrm{D}}(\varphi) = G(\varphi)$ (absence of multipath). In fact, the maximum of the gain function cannot be steered with continuity, because the pattern is chosen in a set having a finite number of elements.
Following the same procedure described in Subsection 5.5.1 for evaluating the output SINR, one can obtain an equation that is formally equal to (5.26), with:

$$\mathcal{I} = G_{\mathrm{m}}\chi'_1 + G''_{\mathrm{m}}\chi'_2, \tag{6.5}$$

and:

$$\chi'_1 = K\bar{K} \int_0^{2\pi} F_{\mathrm{D}}(\varphi)\mathrm{d}\varphi, \tag{6.6a}$$

$$\chi'_2 = \bar{K} \int_{\frac{\varphi^{3\mathrm{dB}}}{2}}^{2\pi - \frac{\varphi^{3\mathrm{dB}}}{2}} \left\{[G''_{\mathrm{m}} F_{\mathrm{D}}(\varphi)]^{\alpha_1} - 1\right\} F_{\mathrm{D}}(\varphi)\mathrm{d}\varphi, \tag{6.6b}$$

where K, $\bar{K}$ and α_1 are defined in (5.36) for a uniform distribution of the nodes in the OCTS case. Finally, substituting (6.5) in (5.26) and manipulating, the number of sustainable links of a backbone WMN in which the nodes employ SBAs can be evaluated as:

$$L_{\max} = \frac{\pi(R_{\mathrm{c}}^{\alpha} G_{\mathrm{d}}^2 - R_{\mathrm{sd}}^{\alpha})}{2\mathrm{SINR}_{\mathrm{th}} R_{\mathrm{sd}}^{\alpha} R_{\mathrm{c}}^{\alpha-2} (G_{\mathrm{m}}\chi'_1 + G''_{\mathrm{m}}\chi'_2)}. \tag{6.7}$$

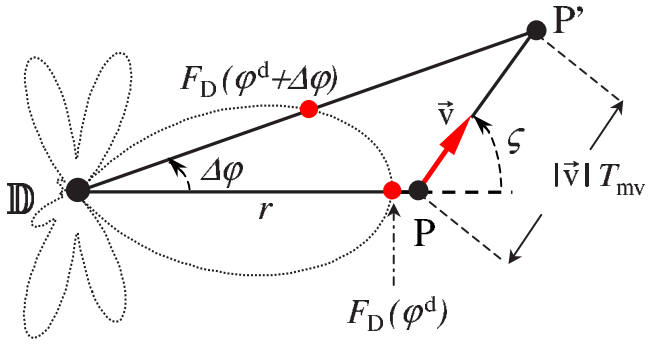

Figure 6.3: Model for the source movement.

6.3 Mobility effects

The mesh routers are usually fixed devices and so the communication channel between the backbone nodes can be modeled without considering mobility issues. Conversely, the wireless interface of a mesh router that manages the communications with the mesh clients can experience the typical effects due to a mobile environment: the change of the network topology and the presence of fading.

6.3.1 Modification of the topology

The change of the network topology can be geometrically modeled as shown in Fig. 6.3. The figure is relative to a desired direction φ^{d}, however, the modeling process is similar when referred to an undesired direction. As described in Section 5.4, the receiving pattern of the destination $\mathbb{D}$ is synthesized during the reception of the RTS packet from the source $\mathbb{S}$. Therefore, the remaining part of the handshake is performed with a pattern that cannot be updated. The time interval during which $\mathbb{D}$ can experience problems due to the movement of $\mathbb{S}$ lies between the reception of the last bit of the RTS packet until the reception of the last bit of the DATA packet. According to the 802.11 standard, this time interval is given by:

$$T_{\mathrm{mv}} = \mathrm{SIFS} + T_{\mathrm{CTS}} + \mathrm{SIFS} + T_{\mathrm{DATA}}, \tag{6.8}$$

where T_{CTS} and T_{DATA} are the times required to transmit the CTS and the DATA packets, respectively. During T_{mv}, the source, initially at distance r from $\mathbb{D}$, moves from a position P to a position P' with a relative vector speed $\vec{\mathrm{v}} = |\vec{\mathrm{v}}|e^{j\varsigma}$. This movement leads to a modification of the mean DOA, from the initial value φ^{d} to

the value $\varphi^{\mathrm{d}} + \Delta\varphi$, where:

$$\Delta\varphi = \Delta\varphi(r) = \arcsin\left[\frac{|\vec{\mathrm{v}}|T_{\mathrm{mv}}\sin\varsigma}{\sqrt{r^2 + (|\vec{\mathrm{v}}|T_{\mathrm{mv}})^2 - 2r|\vec{\mathrm{v}}|T_{\mathrm{mv}}\cos\varsigma}}\right], \tag{6.9}$$

considering that the distance traveled by the node during T_{mv} is $|\vec{\mathrm{v}}|T_{\mathrm{mv}}$. At the end of the communication, the equivalent gain becomes $F_{\mathrm{D}}(\varphi^{\mathrm{d}} + \Delta\varphi)$, which, in general, is lower than $F_{\mathrm{D}}(\varphi^{\mathrm{d}})$. For a null, instead, the new gain $F_{\mathrm{D}}(\varphi^{\mathrm{n}} + \Delta\varphi)$ is larger than $F_{\mathrm{D}}(\varphi^{\mathrm{n}})$). Therefore, taking into account the network topology, the average equivalent power gains in a null and in the desired direction can be recalculated in presence of mobility as:

$$G_{\mathrm{n}} = \int_0^{R_{\mathrm{t}}} F_{\mathrm{D}}[\varphi^{\mathrm{n}} + \Delta\varphi(r)]\varrho_{\mathrm{TOP}_r}(r)\mathrm{d}r, \tag{6.10a}$$

$$G_{\mathrm{d}} = \int_0^{R_{\mathrm{c}}} F_{\mathrm{D}}[\varphi^{\mathrm{d}} + \Delta\varphi(r)]\varrho_{\mathrm{SOU}_r}(r)\mathrm{d}r. \tag{6.10b}$$

where $\varrho_{\mathrm{TOP}_r}(r)$ and $\varrho_{\mathrm{SOU}_r}(r)$ are the marginals with respect to r of the pdf of the interferers $\varrho_{\mathrm{TOP}}(r,\varphi)$ and the pdf of the sources $\varrho_{\mathrm{SOU}}(r,\varphi)$, respectively.

6.3.2 Fading

The main cause of performance degradation in a DWN is the power fluctuation of the desired signal. As described in [126], for a given coded modulation technique, fixing the Packet Error Rate (PER) and the packet size, the fading effects can be taken into account by modifying the receiving threshold $\mathrm{SINR}_{\mathrm{th}}$. In a micromobility scenario the average value of the receiving threshold can be assumed constant and equal to the $\mathrm{SINR}_{\mathrm{th}}$ value assigned in absence of mobility. To improve communication reliability in presence of fading, the receiving threshold in a mobile environment, $\mathrm{SINR}_{\mathrm{th\_m}}$, may be modified to meet the outage requirement, the probability of which, p_{outage}, is related to the fading statistic. Accordingly, $\mathrm{SINR}_{\mathrm{th\_m}}$ can be evaluated as:

$$\mathrm{SINR}_{\mathrm{th\_m}} = \frac{\mathrm{SINR}_{\mathrm{th}}}{\bar{z}}, \tag{6.11}$$

where, for a given p_{outage} value, $\bar{z}$ can be derived from:

$$p_{\mathrm{outage}} = \Pr\{z \le \bar{z}\} = \int_0^{\bar{z}} \tilde{\varrho}_{\mathrm{FAD}}(z)\mathrm{d}z, \tag{6.12}$$

which depends on the pdf of the squared envelope of the received signal. In this chapter, $\tilde{\varrho}_{\mathrm{FAD}}(z)$ is modeled adopting the Nakagami distribution, which is expressed by the Gamma density in (2.9).

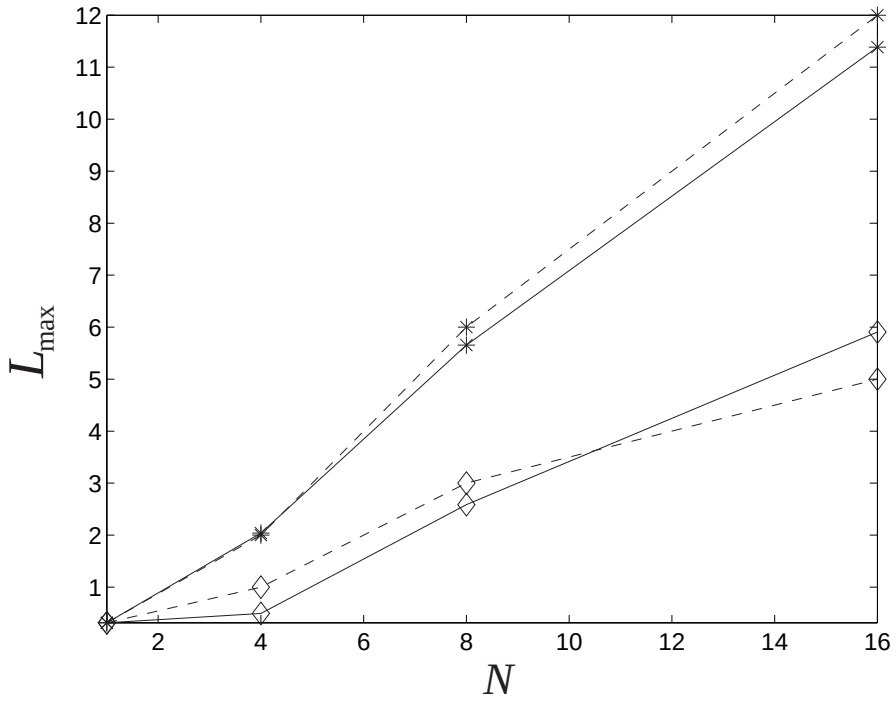

Figure 6.4: Sustainable links as a function of the number of antennas.
—◇— SBA (Analysis) --◇-- SBA (Simulation)
—∗— AA (Analysis) --∗-- AA (Simulation)

The choice of a criterion based on the outage probability allows the negotiation between the number of accepted communications and the probability of successful transmission.

6.4 Results in not mobile environment

This section investigates the network behavior in absence of mobility. Therefore, the illustrated performance is relative to the wireless interfaces of the mesh routers employed to manage the communications between the backbone nodes of the WMN. The results are obtained assuming $\alpha = 4$, $R_{\mathrm{c}} = 100$ m, $R_{\mathrm{t}} >> R_{\mathrm{c}}$, $\mathrm{SINR}_{\mathrm{th}} = 10$ dB and modeling the DOA statistic with a truncated Laplacian pdf. The physical antenna system is a UCA having $N = 8$ omnidirectional elements and spacing between adjacent radiators equal to $\lambda/2$. In the SBA case $G(\varphi)$ is modeled by the square modulus of the array factor of a UCA with uniform amplitude excitations [129], while, in the AA case, $G(\varphi)$ is modeled as described

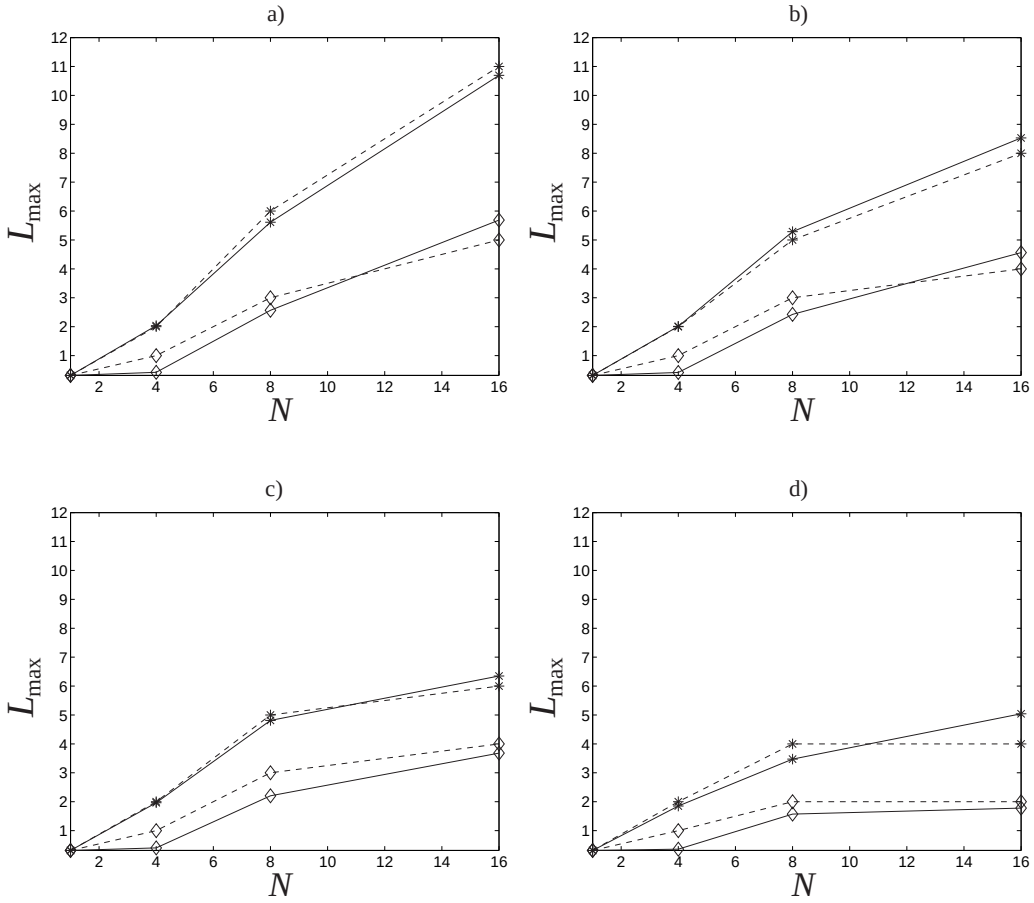

Figure 6.5: Sustainable links as a function of the number of antennas:
a) $\hat{\sigma}_{\varphi} = 1^{o}$, b) $\hat{\sigma}_{\varphi} = 3^{o}$, c) $\hat{\sigma}_{\varphi} = 5^{o}$, d) $\hat{\sigma}_{\varphi} = 10^{o}$.
—◇— SBA (Analysis) --◇-- SBA (Simulation)
—∗— AA (Analysis) --∗-- AA (Simulation)

in Section 5.3. Both reference patterns are obtained assuming $\varphi^{\mathrm{d}} = 0^{o}$, without loss of generality, and the results relative to the use of AAs are referred to the OCTS-SD case. Besides, the values provided by the analysis are compared with the simulations, which are performed adopting the network scenario presented in Section 5.8 (Fig. 5.9).

Fig. 6.4 and Fig. 6.5 show the number of sustainable links of the backbone WMN as a function of the number of antennas for different angular spread values. Both analysis and simulation reveal that, even if AAs reach the largest values of $L_{\max}$, SBAs can provide a large performance improvement too with respect to the omnidirectional antenna case. In all considered channel conditions the value of $L_{\max}$

obtained using AAs is approximately twice the value obtained employing SBAs. Intuitively, one could expect that, as the angular spread gets larger, the two antenna systems tend to perform similarly. In fact, for large values of $\hat{\sigma}_{\varphi}$, the nulls are really imprecisely placed, not existing a unique DOA for each interferer and, therefore, the interference suppression capabilities of AAs should become almost useless. Instead, adaptive arrays still behave better than switched-beam antennas. This is due to the ability of AAs to maximize the SINR at the array output also in severe channel conditions, which represents, from a signal processing point of view, the main advantage of these advanced systems. This behavior can also be inferred from the formulas obtained during the analysis. A comparison between (6.7) and (5.31) for $G_{\mathrm{tx}_1} = G_{\mathrm{m}}$ and $G_{\mathrm{tx}_2} = G_{\mathrm{n}}$, reveals that the two expressions for evaluating $L_{\max}$ are formally similar and that the interference incoming from the region of insuppressible interference is also modeled by the same expression,[2] because χ_1' in (6.6a) and χ_1 in (5.35a) are equal. Instead, the undesired power received from the region of mitigable interference is different in the two cases. When SBAs are adopted, the undesired power is an increasing function of G_{m}'', while, using AAs, it is an increasing function of $G_{\mathrm{n}}^2 (< G_{\mathrm{m}}'')$.
Fig. 6.5c,d can also be used to quantify the theoretical advantages provided by multi-antenna systems in a realistic low-rank environment ($5^o \leq \hat{\sigma}_{\varphi} \leq 15^o$) [23]. Remembering the parameter settings assumed at the beginning of this section, the interference range of a node using an omnidirectional antenna can be approximately calculated as [130]:

$$R_{\mathrm{i}} = \sqrt[4]{\mathrm{SINR}_{\mathrm{th}}} R_{\mathrm{c}} \cong 1.78 R_{\mathrm{c}}. \tag{6.13}$$

Considering (optimistically) that one communication can be performed in each circle of area πR_{i}^2, the number of sustainable links in the omnidirectional case can be approximated by:

$$L_{\max}(N = 1) = \frac{\pi R_{\mathrm{c}}^2}{\pi R_{\mathrm{i}}^2} \cong 0.32, \tag{6.14}$$

and the spatial reuse is possible only when the couples of communicating nodes are sufficiently sparse. Instead, even considering the worst simulated scenario ($\hat{\sigma}_{\varphi} = 10^o$ and $N = 4$), $L_{\max}$ becomes equal to one, using SBAs, and equal to two, using AAs. These values determine an increase in the number of sustainable links by a factor 3 and a factor 6, respectively.

[2] It is worth noticing that this does not imply that the received interference power from $\mathbb{R}_1$ is equal in the two cases, because the reference power gain $G(\varphi)$ and hence the equivalent power gain $F_{\mathrm{D}}(\varphi)$ are still different for an AA and a SBA.

6.5 Model application: multiple antennas and channel coding

This section shows a further application of the presented analytical model, which is used to investigate the relationship between multiple antenna techniques and coded modulations. The objective is to determine the combinations of channel coding technique and antenna system that may offer the best performance.

6.5.1 Coding techniques

Coded modulation techniques have been widely employed to improve the communication reliability. In Wi-Fi environment, the convolutional codes have been adopted in the widely diffused IEEE 802.11a/g physical layer standards [59,61]. However, more efficient solutions have been developed by coding theory, such as turbo codes [131], Low Density Parity Check (LDPC) codes [132], and Single Parity-Check (SPC) codes [133,134]. In particular, the employment of the LDPC codes has been considered in the 802.11n physical layer draft extension of the 802.11 standard for WLANs as a non-mandatory improvement [26].
A brief description of the coding techniques that will be analyzed in this section is provided in the following paragraphs.

6.5.1.1 Convolutional codes

The IEEE 802.11a/g physical layer extensions support eight bit rates, varying from 6 to 54 Mbits/s, which are obtained selecting the proper mode, namely the modulation scheme and the coding rate C_{r}. Four modulations are supported: BPSK, QPSK, 16 and 64 Quadrature Amplitude Modulation (QAM). These schemes are combined with different coding rates. The 802.11a/g standard extensions adopt a convolutional encoder that uses a generator polynomial $(133, 171)_8$ of rate 1/2. Some bits of the sequence, derived employing this rate, can be omitted at the transmitter side by puncturing, in order to obtain the code rates 2/3 and 3/4.
Usually, in the wireless boards, the working mode can be fixed in order to provide a desired transmission rate or can be adaptively updated accounting for the channel conditions. In both cases, for each bit rate, the threshold $\mathrm{SINR}_{\mathrm{th}}$ is usually considered the fundamental parameter for selecting the working mode according to the payload size and to the required PER [125–126, 135].

6.5.1.2 Efficient codes

A considerable performance improvement may be obtained by replacing the convolutional codes with more efficient coding techniques. Define *efficient code* a

C_{r}	$\mathcal{N}_{\mathrm{SPC}}^{\mathrm{r}}$	$\mathcal{N}_{\mathrm{SPC}}^{\mathrm{c}}$	$\mathcal{N}_{\mathrm{SPC}}^{\mathrm{p}}$
1/2	200	8	8
3/4	107	15	5
2/3	133	12	6

TABLE 6.1: PARAMETER VALUES ADOPTED FOR THE E-SPC CODES.

channel coding technique the performance of which is within 1 dB from the limiting performance that can be estimated through the Random Coding Bound (RCB), representing a theoretical upper bound to the probability of decoding error [136]. For a given length of the data block, the PER curve corresponding to the RCB, and the PER curve achievable adding 1 dB to the RCB, named in this study as the *Efficient Coding Bound* (ECB), describe a region in which the performance of the efficient codes lies. Actually, many commonly adopted coding techniques, such as turbo codes or LDPC codes, are efficient, given that their performance is within 1 dB from the RCB.

6.5.1.3 Extended-Single Parity-Check codes

Multiple Serial and Parallel Concatenated SPC (M-SPC) codes have been proposed in [134]. Data are arranged in matrix with $\mathcal{N}_{\mathrm{SPC}}^{\mathrm{r}}$ rows and $\mathcal{N}_{\mathrm{SPC}}^{\mathrm{c}}$ columns. The encoder produces $\mathcal{N}_{\mathrm{SPC}}^{\mathrm{p}}$ parity columns, operating on the original data and on $\mathcal{N}_{\mathrm{SPC}}^{\mathrm{p}}$-1 permuted versions (of the data in the parallel encoder, and of the data and the previous parities in the serial one). The code rate is:

$$C_{\mathrm{r}} = \frac{\mathcal{N}_{\mathrm{SPC}}^{\mathrm{c}}}{\mathcal{N}_{\mathrm{SPC}}^{\mathrm{c}} + \mathcal{N}_{\mathrm{SPC}}^{\mathrm{p}}}, \tag{6.15}$$

while the block size is given by $\mathcal{N}_{\mathrm{SPC}}^{\mathrm{r}}(\mathcal{N}_{\mathrm{SPC}}^{\mathrm{c}} + \mathcal{N}_{\mathrm{SPC}}^{\mathrm{p}})$. These codes show an excellent performance for high rates, such as $C_{\mathrm{r}} = 3/4$. In [137], an improved version is proposed, namely Extended-SPC (E-SPC), which includes a parity row and is capable of achieving an acceptable performance also for lower rates. The $\mathcal{N}_{\mathrm{SPC}}^{\mathrm{r}}$, $\mathcal{N}_{\mathrm{SPC}}^{\mathrm{c}}$ and $\mathcal{N}_{\mathrm{SPC}}^{\mathrm{p}}$ values used to obtain the three coding rates adopted in the 802.11a/g extensions are shown in Table 6.1.

6.5.2 Performance figure and design parameters

Convolutional codes, efficient codes and E-SPC codes are compared in this chapter combining their employment with AAs and SBAs. The performance figure

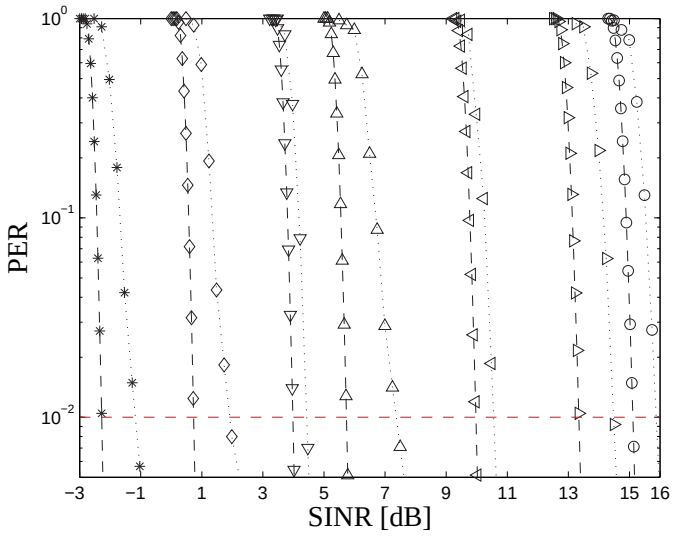

Figure 6.6: PER for 200 bytes payload.
---- RCB ····· E-SPC
∗ mode 1 ◊ mode 3 ▽ mode 4 △ mode 5 ◁ mode 6 ▷ mode 7 ○ mode 8

used to analyze the code behavior is the *sustainable throughput*, a quantity derived from the number of sustainable links that is defined as:

$$S_{\max} = L_{\max} \cdot \mathcal{R} \cdot (1 - p_{\text{outage}}). \tag{6.16}$$

$S_{\max}$, taking into account the nominal bit rate $\mathcal{R}$ and the SINR($\geq \text{SINR}_{\text{th}}$) required to sustain this rate (that influences also $L_{\max}$), is used in this study to evaluate the efficiency of the particular coded modulation technique. The sustainable throughput represents an aggregate quantity accounting for the total information exchanged in the area covered by the communication range of a node, when all the communications are simultaneously performed using the same bit rate.
This investigation compares the best performance that may be achieved by adopting convolutional codes, with the best performance one may obtain by adopting the E-SPC codes. Besides, all performance evaluations are compared with the limiting performance that is achieved by adopting the RCB threshold. A packet payload of 200 bytes is adopted, and the threshold values, SINR_{th}, are derived assuming a PER equal to 1%. For the convolutional encoder adopted in the 802.11a standard the thresholds are set according to [126]. For the RCB and the E-SPC codes SINR_{th} can be derived from Fig. 6.6, which is obtained from Matlab simulations. Finally, to delimit the efficient code region, the ECB thresholds are set adding 1 dB to the RCB ones. The adopted thresholds are summarized in

				$\mathrm{SINR_{th}}$ (dB)			
Mode	$\mathcal{R}$ (Mbits/s)	**Modulation**	C_r	RCB	ECB	E-SPC	Convolutional
1	6	BPSK	1/2	-2.3	-1.3	-1.1	2.0
2	9	BPSK	3/4	not considered			
3	12	QPSK	1/2	0.7	1.7	2.0	5.0
4	18	QPSK	3/4	4.0	5.0	4.5	7.5
5	24	16-QAM	1/2	5.7	6.7	7.4	9.5
6	36	16-QAM	3/4	10.0	11.0	10.6	13.5
7	48	64-QAM	2/3	13.3	14.3	14.5	16.0
8	54	64-QAM	3/4	15.1	16.1	15.9	19.0

TABLE 6.2: $802.11\mathrm{a/g}$ MODES AND THRESHOLD VALUES IN ABSENCE OF MOBILITY.

Table 6.2. Observe that mode 2 is not considered, given that it provides worse performance than mode 3 for all channel conditions [135].
It is worth noticing that this study aims to compare the $S_{\max}$ values that may be achieved by using the different combinations of antenna system and channel coding technique. The examined scenario does not consider SINR variations, as in adaptive modulation and coding. Instead, the analysis is performed assuming that the working pairs operate at the minimum SINR value ($\mathrm{SINR_{th}}$) that allows them to employ the relevant mode. For the different system set-ups, the performance is evaluated as a function of the antenna and of the channel parameters, such as the number of radiating elements and the angular spread.

6.5.3 Results

6.5.3.1 Not mobile environment

Fig. 6.7 and Fig. 6.8 show the number of sustainable links and the sustainable throughput achievable by each mode using AAs and SBAs, respectively. The results, obtained using the 802.11a/g convolutional encoder, are derived in absence of mobility for $\hat{\sigma}_\varphi = 10^o$.
In the AA case, mode 5, corresponding to $\mathcal{R} = 24$ Mbits/s, achieves the largest $S_{\max}$ values. Differently, SBAs behave better using the modes corresponding to the lower bit rates and, in particular, using mode 3. These different characteristics may be explained considering the different capabilities of the two antenna systems. The use of a higher modulation scheme in conjunction with a convolutional code requires a higher SINR to operate efficiently. AAs are able to pro-

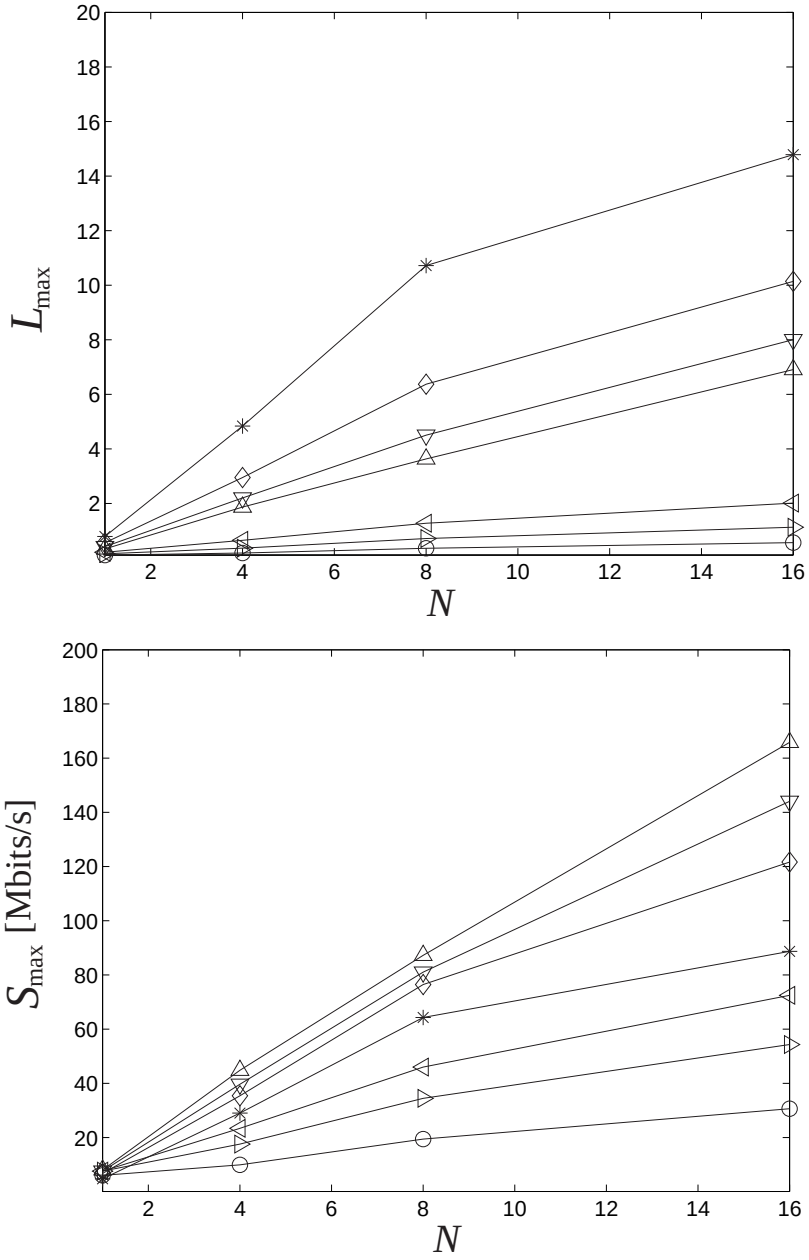

Figure 6.7: Sustainable links and sustainable throughput of a backbone WMN using AAs and convolutional coding as a function of the number of antennas for $\hat{\sigma}_{\varphi} = 10^{o}$.
$*$ mode 1 $\Diamond$ mode 3 $\triangledown$ mode 4 $\triangle$ mode 5 $\triangleleft$ mode 6 $\triangleright$ mode 7 $\circ$ mode 8

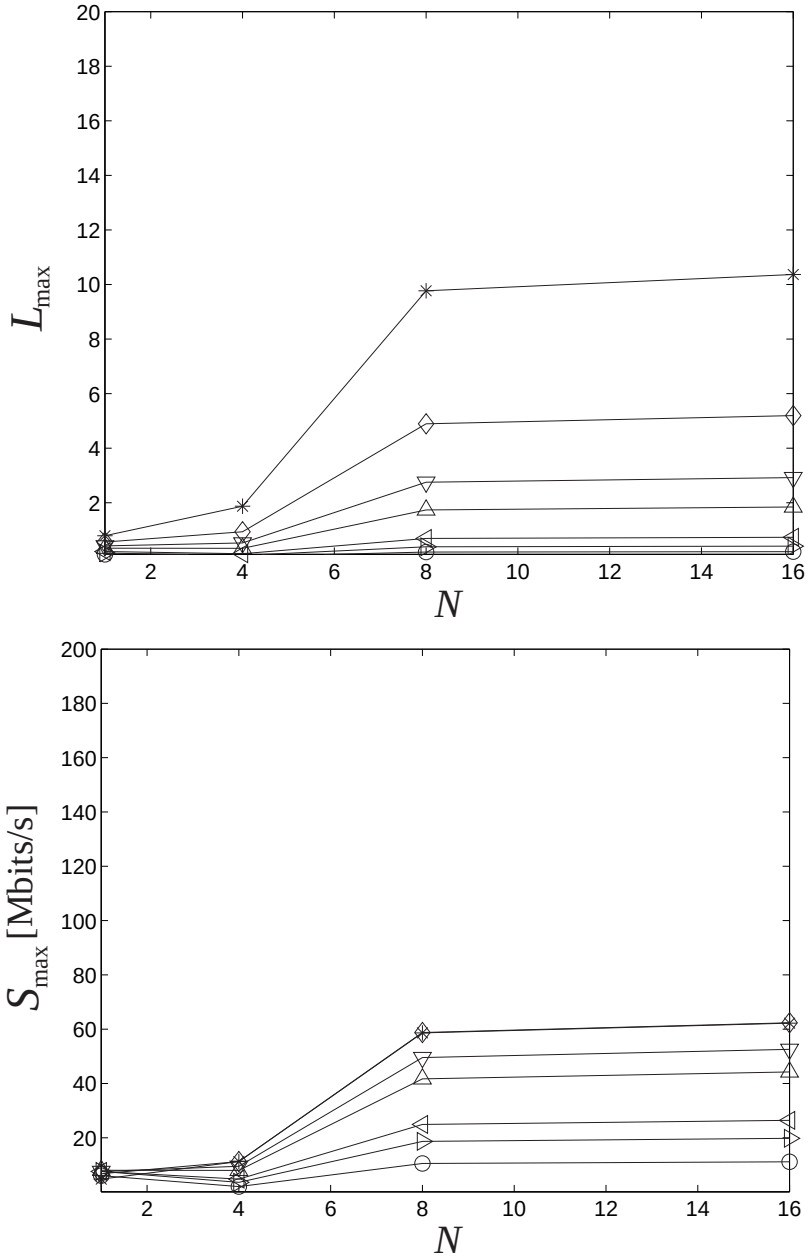

Figure 6.8: Sustainable links and sustainable throughput of a backbone WMN using SBAs and convolutional coding as a function of the number of antennas for $\hat{\sigma}_{\varphi} = 10^{o}$.
$*$ mode 1 $\Diamond$ mode 3 $\triangledown$ mode 4 $\triangle$ mode 5 $\triangleleft$ mode 6 $\triangleright$ mode 7 $\circ$ mode 8

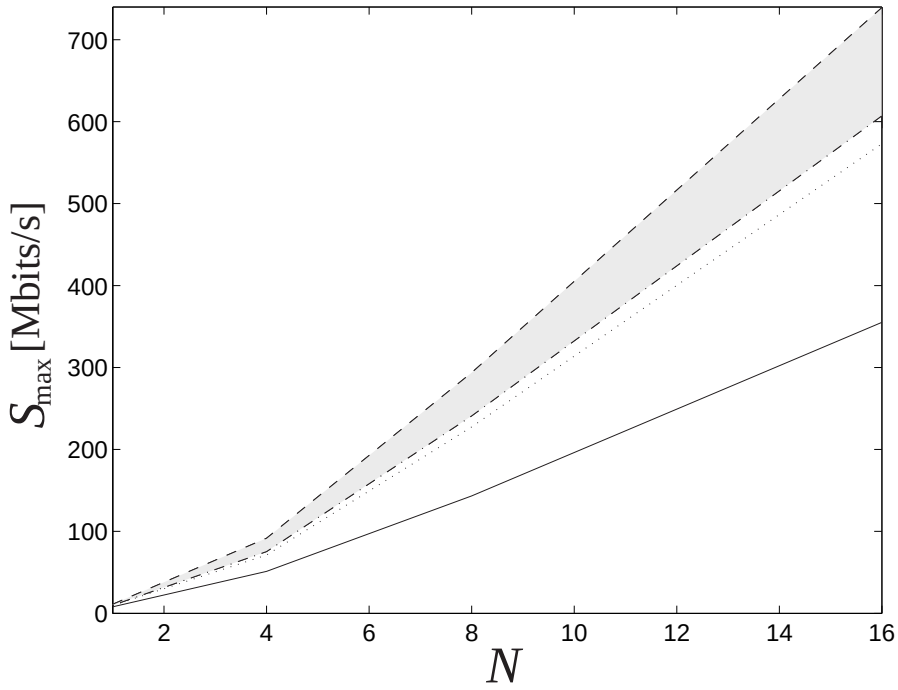

Figure 6.9: Sustainable throughput of a backbone WMN using AAs as a function of the number of antennas for $\hat{\sigma}_{\varphi} = 0^o$.
---- RCB -·-·- ECB ····· E-SPC —— Convolutional

vide the required values of SINR for some higher modes, while SBAs have more limited capabilities and work better with the lower modes. Besides, employing switched-beam antennas, a larger number of sustainable links leads, usually, to a larger sustainable throughput, while, employing adaptive arrays, the relationship between $L_{\max}$ and $S_{\max}$ is less immediate. In particular, in this case, the mode

	AA		SBA	
	mode	$L_{\max}(N = 8, \hat{\sigma}_{\varphi} = 0^o)$	mode	$L_{\max}(N = 8, \hat{\sigma}_{\varphi} = 0^o)$
RCB	3	24.47	3	22.00
ECB	3	20.08	3	17.48
E-SPC	3	18.96	1	33.31
Convolutional	5	5.97	3 or 1	8.19 or 16.38

TABLE 6.3: BEST MODE AND NUMBER OF TRANSMITTERS FOR EACH CODING TECHNIQUE AND FOR EACH ANTENNA SYSTEM.

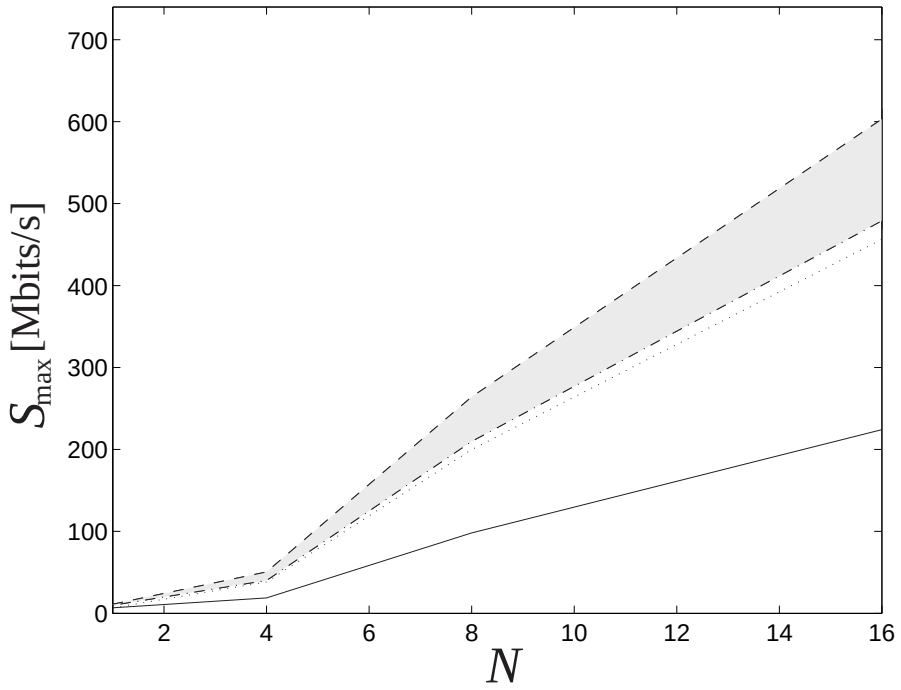

Figure 6.10: Sustainable throughput of a backbone WMN using SBAs as a function of the number of antennas for $\hat{\sigma}_{\varphi} = 0^o$.
---- RCB -·-·- ECB ····· E-SPC —— Convolutional

that maximizes the number of allowed users, does not maximize the sustainable throughput.
The results concerning E-SPC codes, RCB and ECB are shown in Fig. 6.9 for AAs and in Fig. 6.10 for SBAs. In the figures, the shaded area identifies the efficient code region, bounded by the limiting performance obtained with the RCB and the ECB. To limit the number of figures not all results are reported, but, for each combination of coding technique and antenna system, the mode providing the largest performance is selected (Table 6.3). From the results it can be observed that, using codes that are more efficient than the convolutional ones, the lower modes behave better, even if AAs are employed. Besides, adopting the convolutional codes, the performance improvement that can be obtained increasing the number of antennas is lower as compared to the other channel coding techniques. However, for a not too large value of N, the combined use of AAs and convolutional codes may provide a performance that is reasonably close to the efficient code one in the SBA case. Observe that, for both antenna systems, the sustainable throughput obtained by using the E-SPC codes is very close to the efficient code region.

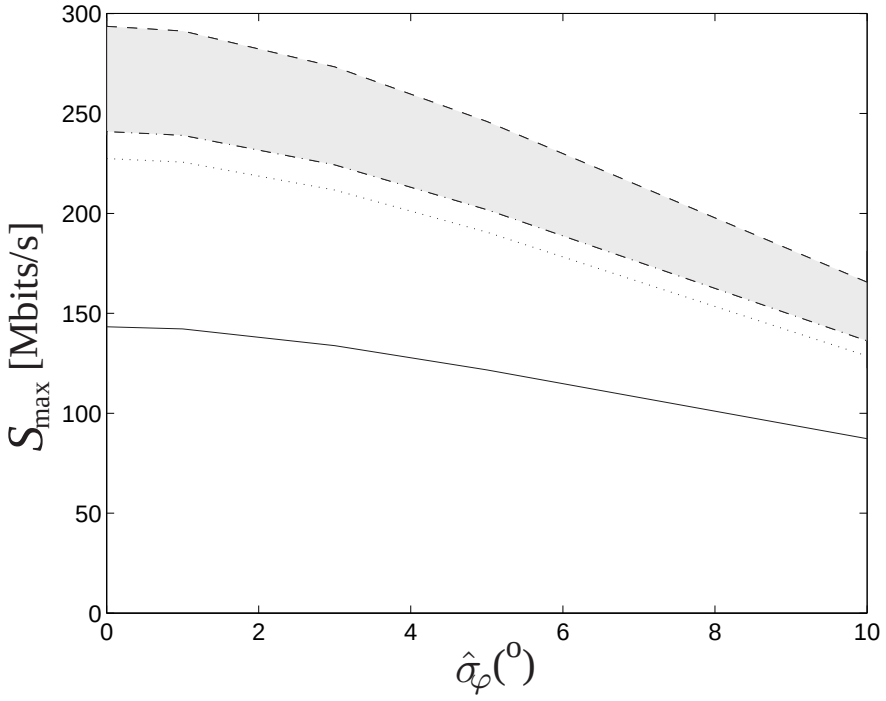

Figure 6.11: Sustainable throughput of a backbone WMN using AAs as a function of the angular spread for $N = 8$ antennas.
---- RCB -·-·- ECB ····· E-SPC —— Convolutional

Besides, the $L_{\max}$ values reported in Table 6.3 for $N = 8$ and $\hat{\sigma}_\varphi = 0^o$ show that the lower modes are associated with a larger number of transmissions. It is also interesting to observe that, in some cases, some modes can provide almost the same values of $S_{\max}$, as it happens for the modes 1 and 3 for the Convolutional-SBA combination, giving the possibility to choose between a larger number of transmitters or a higher rate value. Recalling that, in the considered scenario, the transmission power is assumed constant, a larger number of transmitters leads to more radiated (and consumed) power in the entire network. Therefore, adopting the Convolutional-SBA combination, mode 3 seems preferable from the point of view of the global power budget, while mode 1 provides a better fairness.
As one can expect, when $\hat{\sigma}_\varphi$ increases, the performance of the entire system decreases (Figg. 6.11-6.12). In general, both multi-antenna techniques experience a degradation of their interference mitigation capabilities and a lower gain in the desired direction. However, by comparing the slope of the AA plots with the SBA ones, it can be observed that, even if AAs still perform better than SBAs, the sustainable throughput of the former system is more sensitive to the channel angular

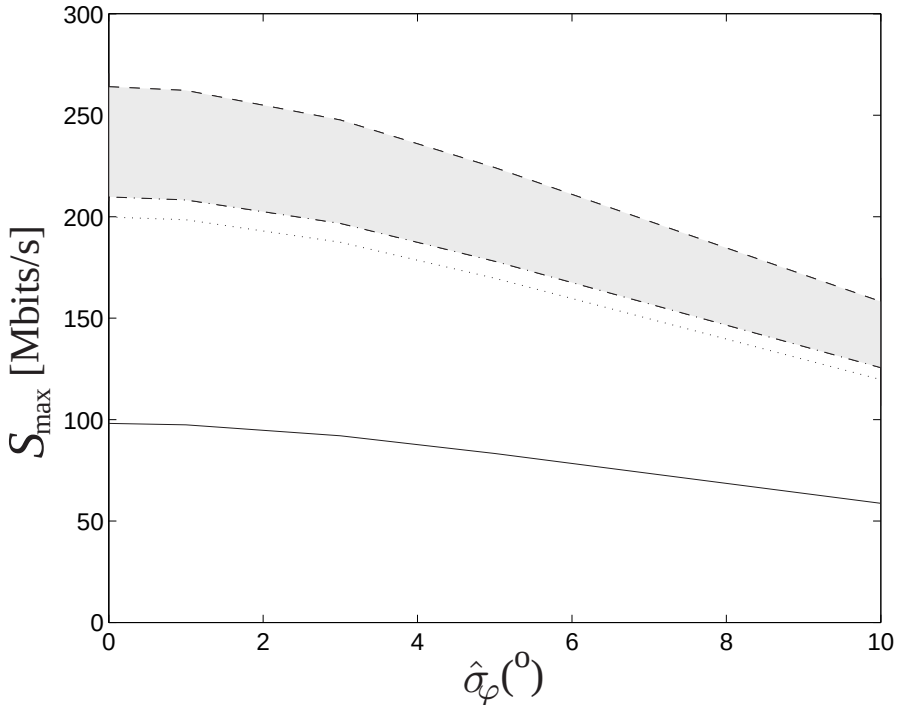

Figure 6.12: Sustainable throughput of a backbone WMN using SBAs as a function of the angular spread for $N = 8$ antennas.
---- RCB -·-·- ECB ····· E-SPC —— Convolutional

spread. This different degradation can be explained recalling that the performance of AAs is related to the interference nulling capabilities, which depend on the spatial correlation between the signal replicas. Other results, obtained adopting a 5% PER and 20 bytes payload, evidence an analogous behavior.

6.5.3.2 Mobile environment

Fig. 6.13 shows the system performance in presence of Nakagami fading for $m_{\mathrm{N}} = 1$, corresponding to Rayleigh fading. The thresholds in Table 6.2 are modified according to (6.11)-(6.12). It can be observed that, in the SBA case and for each channel coding technique, the mode providing the largest performance remains the same for all the values of the outage probability. In the Convolutional-AA and in the E-SPC-AA cases, instead, the optimal mode depends on p_{outage}. This fact explains the irregular behavior of the two curves. In these two cases the markers are used to define the first and the last value of p_{outage} for which a

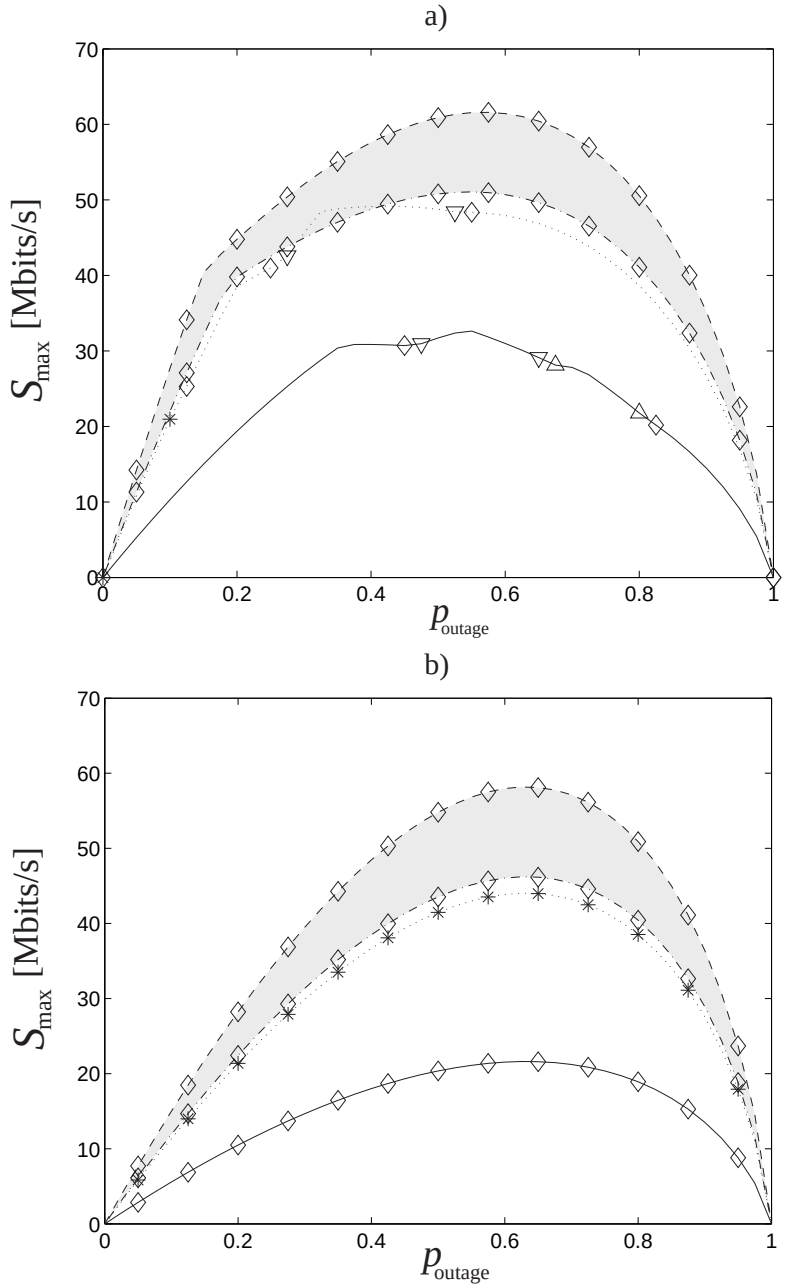

Figure 6.13: Sustainable throughput as a function of the outage probability for $N = 8$ antennas and $\hat{\sigma}_{\varphi} = 10^{o}$ in presence of Rayleigh fading: a) AAs, a) SBAs.
– – – – RCB – · – · – ECB ····· E-SPC —— Convolutional
$*$ mode 1 $\Diamond$ mode 3 $\triangledown$ mode 4 $\triangle$ mode 5 $\triangleleft$ mode 6 $\triangleright$ mode 7 $\circ$ mode 8

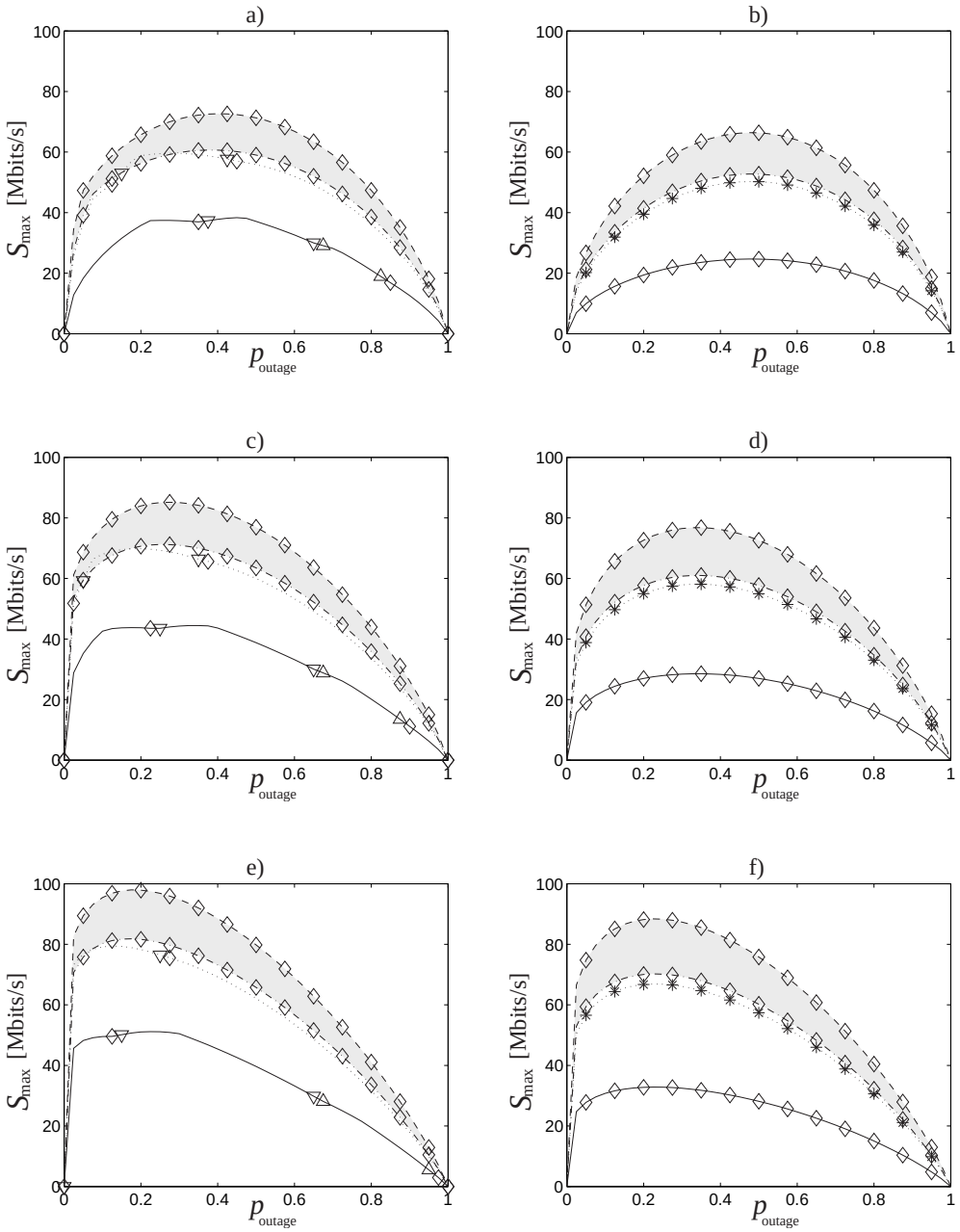

Figure 6.14: Sustainable throughput as a function of the outage probability for $N = 8$ antennas and $\hat{\sigma}_\varphi = 10^o$ in presence of Nakagami fading:
a) AAs with $m_{\mathrm{N}} = 2$, b) SBAs with $m_{\mathrm{N}} = 2$, c) AAs with $m_{\mathrm{N}} = 4$,
d) SBAs with $m_{\mathrm{N}} = 4$, e) AAs with $m_{\mathrm{N}} = 8$, f) SBAs with $m_{\mathrm{N}} = 8$.
– – – – RCB –·–·– ECB ····· E-SPC —— Convolutional
$*$ mode 1 $\Diamond$ mode 3 $\triangledown$ mode 4 $\triangle$ mode 5 $\triangleleft$ mode 6 $\triangleright$ mode 7 $\circ$ mode 8

given mode is used. For example, adopting the Convolutional-AA combination, the largest performance for $0.675 \leq p_{\text{outage}} \leq 0.800$ can be obtained adopting the rate $\mathcal{R} = 24$ Mbits/s (mode 5). For each combination of channel coding technique and antenna system, an optimal value of the outage probability may be determined, leading to the maximum sustainable throughput. Observe that, being AAs able to provide a larger SINR at the receiver output, they maintain satisfactory performance for lower values of p_{outage} with respect to SBAs. This behavior suggests that, for systems employing AAs, an aggressive approach where a larger number of communications is allowed may be adopted. Instead, a conservative approach seems more suitable for exploiting the SBA capabilities. Also in the mobile scenario the E-SPC code performance is close to the efficient code region, and, for some p_{outage} values, E-SPC codes can be included in the set of efficient codes. Observe that, in the mobile scenario and for large angular spread values, similar performance can be obtained adopting efficient coding technique regardless of the sophistication of the antenna system.
Finally, Fig. 6.14 shows the system behavior in presence of Nakagami fading for different values of the Nakagami parameter m_{N}. It can be noticed that the performance gap between convolutional codes and ECs becomes more evident as the Nakagami parameter gets larger. Besides, for larger m_{N} values the optimal p_{outage} value decreases, while the corresponding $S_{\max}$ value increases. This behavior can be intuitively confirmed observing that, as m_{N} increases, the variance of the Nakagami distribution get lower, leading to less severe fading conditions.

6.6 Considerations

Despite the advantages provided by multiple antenna systems, so far these technologies have been substantially neglected by wireless operators [138], even if their adoption seems very likely in the next two-five years [139,140].
This delay is due to many practical reasons. As described in Section 4.3.1, at MAC layer, the use of multiple antennas may originate difficulties due to deafness, suicide ACK, muteness, exposed and hidden terminal. These problems must be addressed in the design phase [124], taking into account that a commercially appreciable MAC protocol has to maintain the backward compatibility with the widely employed 802.11 standard. Besides, in some scenarios, the employment of multiple antennas can degrade the performance, when the MAC/routing layers are not properly modified and cross-layer optimization techniques are not used [141].
From the theoretical point of view, analysis and simulation of multi-antenna systems employing too idealized models for the antenna pattern, the channel behavior and the network topology may lead to optimistic results that can differ from the actual values [142].

Other fundamental issues are related to the hardware complexity. In this context SBAs and AAs have different requirements. A SBA includes a beamforming network, usually realized adopting phase shifters, and a beam selection processor. Instead, a smart antenna system requires RF/IF converters, fast ADC and Digital-to-Analog (DAC) converters, as well as a certain number of high-performance Digital Signal Processors (DSPs) and/or Field Programmable Gate Arrays (FPGAs). Therefore, to adopt smart antennas, expensive hardware devices and considerable implementation efforts are unavoidable [143]. Nowadays, the cheaper hardware required by SBAs makes them more suitable for a system-on-a-chip realization. As a consequence, some chipsets implementing the switched-beam antenna technology are already available at a reasonable cost [144]. This simpler multi-antenna technique may be more attractive for wireless operators, given that some backward compatible MAC protocols adopting SBAs have been already proposed in the literature [76]. However, some hybrid antenna systems, aiming to contain cost and complexity by adopting an adaptive approach in azimuth plane and a switched-beam approach in the elevation plane, have been presented recently [145]. These research efforts may favor the maturation and the subsequent adoption of the adaptive arrays for portable devices within few years.
Summarizing, the theoretical and numerical results demonstrate that adaptive antennas are preferable in terms of performance, mainly when not efficient coding techniques are adopted and/or the propagation environment is characterized by low angular spread values. However, cost and complexity considerations suggest the adoption of switched-beam antennas first. By exploiting all the capabilities of this simpler technique, a significant performance improvement may also be obtained, still keeping the low-cost characteristics of the mesh routers. The use of a cheaper antenna system in a practical backbone WMN may be a first step towards the full adoption of the most efficient multi-antenna technologies.

Chapter 7

Throughput-Delay Analysis of 802.11 DWNs Using Beamforming Techniques

Purpose of this chapter is to evaluate the aggregate throughput and the successful packet delay that can be achieved by a DWN using switched-beam, directional and adaptive antennas in a multi-hop scenario. The concept of sustainable links, introduced in the previous chapters, and a detailed model for the behavior of the DCF are employed to determine the performance of an 802.11-based network adopting advanced antenna techniques. The characteristics of the 802.11 backoff mechanism are analyzed using a Markov chain model that enables the investigation of the performance in saturated and non-saturated traffic conditions. Besides, suitable 802.11 MAC layer parameter settings, able to exploit smart, directional and switched-beam antenna capabilities, are also discussed.[1]

7.1 Introduction

The characteristics of the 802.11 backoff scheme, described in Section 4.2.3, have been deeply analyzed in the seminal paper of Bianchi [146], in which a Markov chain model is adopted to study the DCF behavior in saturated traffic conditions. Moving from this first study, several and detailed extensions have been developed in the literature [147–155]. In particular, a model including a finite Retry Limit m is presented in [147], where, in addition, the authors consider the general case

[1]The content of this chapter is based on F. Babich and M. Comisso, 'Throughput and Delay Analysis of 802.11-Based Wireless Networks Using Smart and Directional Antennas,' IEEE Transactions on Communications, accepted for publication [175,182].

in which m can be different from the maximum backoff stage m'. The effects of channel errors are analyzed in [148–149], while the effectiveness of the RTS/CTS access is investigated in [150]. A detailed evaluation of the packet delay is performed in [151], taking into account transmission errors due to fading and noise. Further extensions to non-saturated traffic conditions are presented in [154–155] and [152–153], where authors consider the case of heterogeneous traffic sources. All these studies are focused on the omnidirectional antenna case and so they assume that a unique communication can be performed inside the interference range of a node. However, in presence of advanced antenna systems, it becomes interesting to investigate how the 802.11 scheduler behaves when multiple simultaneous communications are allowed. Therefore, in this chapter, the Markov chain model presented in [146–151] is extended to the multi-antenna case.
The presented extension employs the concept of sustainable links to calculate, in saturated and non saturated traffic conditions, the classic performance figures of a DWN, such as the aggregate throughput and the successful packet delay. The number of sustainable links, summarizing the number of simultaneous communications that can be performed in a given region according to the characteristics of the antenna system, the topology and the channel, can be viewed as a detailed measure of the potentially available network resources. Combining this measure with an accurate model for the backoff mechanism of the DCF, a realistic framework can be obtained for analyzing the actual impact of beamforming techniques on an 802.11 distributed wireless network.
This chapter presents the model for the backoff mechanism, according to the 802.11 DCF specifications that have been summarized in Section 4.2.3.

7.2 Markov chain model

The analysis is subdivided in two parts. First, the access procedure of a source adopting the 802.11 DCF in non saturated traffic conditions is modeled adopting a Markov chain. Then, the aggregate throughput, the successful packet delay and the drop probability are derived using the number of sustainable links. The first part of the analysis is performed in this section.
Defining as $\psi_{\mathrm{s}}(t)$ and $\psi_{\mathrm{t}}(t)$ the stochastic processes representing, respectively, the backoff stage and the backoff timer at time t, the bi-dimensional process $\{\psi_{\mathrm{s}}(t), \psi_{\mathrm{t}}(t)\}$ is modeled by the Markov chain shown in Fig. 7.1, where p_{c} is the conditional probability that the source encounters a collision, $CW_{i'}$ is the contention window size at the i'-th transmission attempt:

$$CW_{i'} = \begin{cases} 1 & i' = -1 \\ 2^{i'} CW_{\min} & 0 \leq i' \leq m' \\ 2^{m'} CW_{\min} & m' < i' \leq m \end{cases}, \tag{7.1}$$

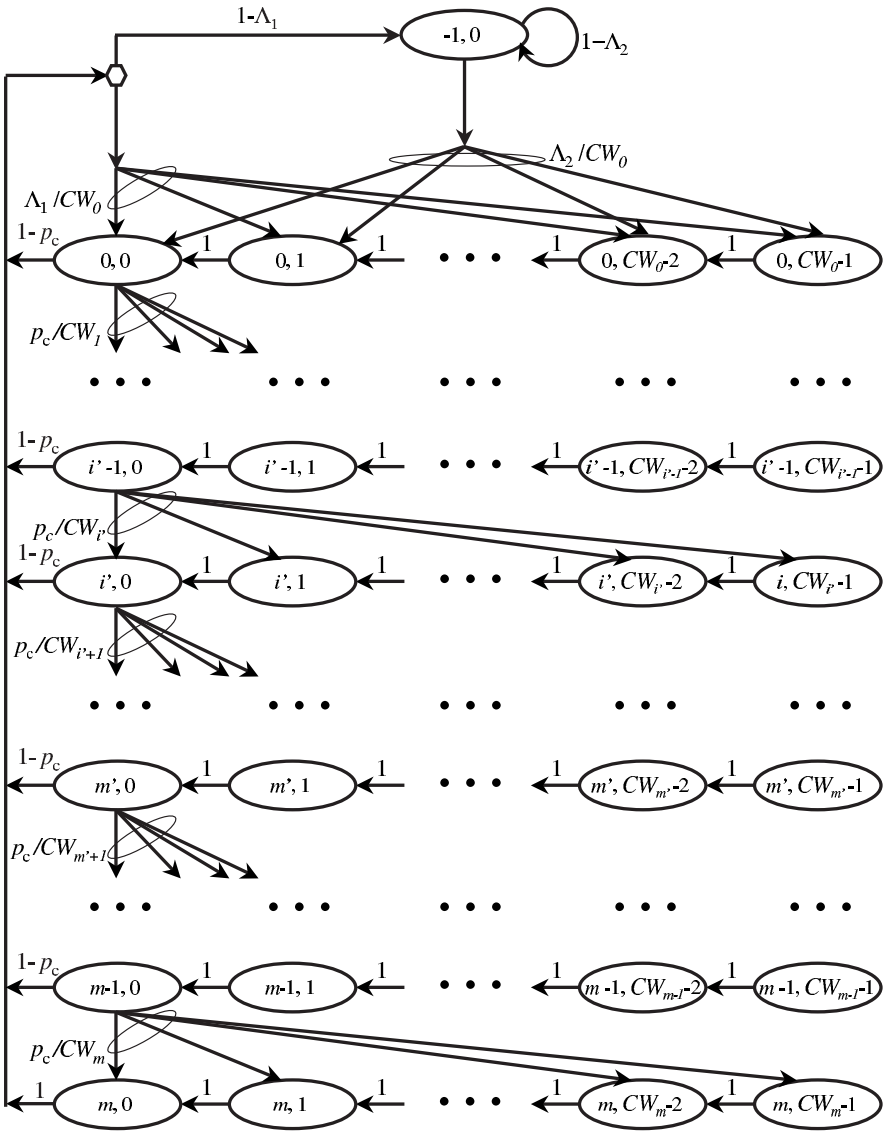

Figure 7.1: Markov chain model.

being $CW_{-1} = 1$ defined for calculation purposes and being CW_0 equal to the minimum contention window $CW_{\min}$. In the presented model, once the source $\mathbb{S}$ has successfully transmitted a packet or has discarded it after the last possible retransmission attempt, a new packet is awaiting transmission in the source buffer with probability Λ_1. The state $(-1, 0)$ is the idle state, where $\mathbb{S}$ lies if no packets are present in the buffer. When the node is in the idle state a new packet arrives

with probability Λ_2. Both Λ_1 and Λ_2 depend on the arrival rate and on the time evolution of the chain. In particular, Λ_1 accounts for the overall time spent by the source for transmitting the previous packet, while Λ_2 is influenced only by the average time between two backoff decrements. The hexagon in Fig. 7.1 does not represent a state, but simply a switch in which time is not spent.
The transition probabilities of the chain are:

$$\begin{cases} \Pr\{i', i | i', i+1\} = 1 & i \in [0, CW_{i'} - 2] \\ & i' \in [0, m] \\ \Pr\{i', i | i' - 1, 0\} = p_{\mathrm{c}}/CW_{i'} & i \in [0, CW_{i'} - 1] \\ & i' \in [1, m] \\ \Pr\{-1, 0 | -1, 0\} = 1 - \Lambda_2 & \\ \Pr\{-1, 0 | i', 0\} = [1 - p_{\mathrm{c}}(1 - \delta^{\mathrm{K}}_{i'm})](1 - \Lambda_1) & i' \in [0, m] \\ \Pr\{0, i | i', 0\} = [1 - p_{\mathrm{c}}(1 - \delta^{\mathrm{K}}_{i'm})]\Lambda_1/CW_0 & i \in [0, CW_0 - 1] \\ & i' \in [0, m] \\ \Pr\{0, i | -1, 0\} = \Lambda_2/CW_0 & i \in [0, CW_0 - 1] \end{cases}, \quad (7.2)$$

where i represents the remaining number of slots before backoff expiration and:

$$\delta^{\mathrm{K}}_{i'm} = \begin{cases} 1 & i' = m \\ 0 & \text{elsewhere} \end{cases},$$

is the Kronecker delta. As in [146–147, 150], the first equation in (7.2) accounts for the decrement of the backoff timer during the beginning of a slot time, while the second one models a collision at the i'-th transmission attempt. The third equation models the persistence in the idle state. The fourth equation takes into account the source behavior in the case of empty transmission buffer that can occur after a success within the $(m-1)$-th attempt or when the maximum number of retransmissions is reached. The fifth equation models the behavior of $\mathbb{S}$ in the case of nonempty transmission buffer after a successful transmission within the $(m-1)$-th attempt or when the maximum number of retransmissions is reached. Finally, the last equation models the packet arrival when the source is in the idle state.
The stationary distribution of the chain:

$$\psi_{i',i} = \lim_{t \to \infty} \Pr\{\psi_{\mathrm{s}}(t) = i', \psi_{\mathrm{t}}(t) = i\}, i' \in [-1, m], i \in [0, CW_{i'} - 1], \quad (7.3)$$

can be calculated observing that [146]:

$$\psi_{i',0} = p_{\mathrm{c}}\psi_{i'-1,0} \Rightarrow \psi_{i',0} = p_{\mathrm{c}}^{i'}\psi_{0,0}, \tag{7.4a}$$

$$\psi_{i',i} = \left(1 - \frac{i}{CW_{i'}}\right) p_{\mathrm{c}}\psi_{i'-1,0} = \left(1 - \frac{i}{CW_{i'}}\right) p_{\mathrm{c}}^{i'}\psi_{0,0}, \tag{7.4b}$$

for $0 < i' \leq m$ and $0 \leq i \leq CW_{i'} - 1$. Besides, the probability $\psi_{-1,0}$ can be obtained from:

$$\Lambda_2\psi_{-1,0} = (1 - \Lambda_1)\sum_{i'=0}^{m}[1 - p_{\mathrm{c}}(1 - \delta_{i'm}^{\mathrm{K}})]\psi_{i',0}, \tag{7.5}$$

which, using (7.4a), leads to:

$$\psi_{-1,0} = \frac{1 - \Lambda_1}{\Lambda_2}\psi_{0,0}. \tag{7.6}$$

Moreover, for $i' = 0$, $\psi_{0,i}$ can be calculated as:

$$\begin{aligned}\psi_{0,i} &= \left(1 - \frac{i}{CW_0}\right) \cdot \left\{\Lambda_2\psi_{-1,0} + \Lambda_1\sum_{i'=0}^{m}[1 - p_{\mathrm{c}}(1 - \delta_{i'm}^{\mathrm{K}})]\psi_{i',0}\right\} \\ &= \left(1 - \frac{i}{CW_0}\right)\psi_{0,0}.\end{aligned} \tag{7.7}$$

Using (7.4)-(7.7) and (7.1), the normalization condition for the stationary distribution of the chain can be manipulated as:

$$\begin{aligned}1 &= \sum_{i'=-1}^{m}\sum_{i=0}^{CW_{i'}-1}\psi_{i',i} \\ &= \sum_{i'=0}^{m}\sum_{i=0}^{CW_{i'}-1}\psi_{i',i} + \psi_{-1,0} \\ &= \sum_{i'=0}^{m}\sum_{i=0}^{CW_{i'}-1}\left(1 - \frac{i}{CW_{i'}}\right)p_{\mathrm{c}}^{i'}\psi_{0,0} + \frac{1 - \Lambda_1}{\Lambda_2}\psi_{0,0} \\ &= \psi_{0,0}\left[\sum_{i'=0}^{m}p_{\mathrm{c}}^{i'}\sum_{i=0}^{CW_{i'}-1}\left(1 - \frac{i}{CW_{i'}}\right) + \frac{1 - \Lambda_1}{\Lambda_2}\right] \\ &= \psi_{0,0}\left[\frac{1}{2}\sum_{i'=0}^{m}(CW_{i'} + 1)p_{\mathrm{c}}^{i'} + \frac{1 - \Lambda_1}{\Lambda_2}\right],\end{aligned} \tag{7.8}$$

from which, performing some algebra, one obtains the following expression for $\psi_{0,0}$:

$$\psi_{0,0}=\left\{\frac{2(1-\Lambda_1)(1-p_{\rm c})(1-2p_{\rm c})+\Lambda_2 CW_0(1-p_{\rm c})[1-(2p_{\rm c})^{m'+1}]}{2\Lambda_2(1-2p_{\rm c})(1-p_{\rm c})}+\right.$$
$$\left.+\ \frac{CW_0 p_{\rm c}(2p_{\rm c})^{m'}(1-p_{\rm c}^{m-m'})-p_{\rm c}^{m+1}+1}{2(1-p_{\rm c})}\right\}^{-1}. \tag{7.9}$$

7.3 Throughput-delay analysis

This section describes the second part of the analysis, evaluating the aggregate throughput, the successful packet delay and the drop probability of the DWN. The number of sustainable links is employed in this phase to take into account the communications that can be simultaneously performed using smart, directional and switched-beam antennas.
Defining as $p_{\rm tx}$ the transmission probability of the single source (still unknown), the probability $\Psi_{\rm tx}$ that at least one transmission occurs in a randomly chosen slot time in the region of suppressible interference $\mathbb{R}_2$, is given by:

$$\Psi_{\rm tx}=1-(1-p_{\rm tx})^{n_2}, \tag{7.10}$$

where $n_2 = nR_{\rm c}^2/R_{\rm t}^2 (\geq 2L_{\max})$ is the number of nodes (active and not active) that lie in $\mathbb{R}_2$. The probability $\Psi_{\rm succ}$ that a maximum of $\lfloor L_{\max} \rfloor$ transmissions are simultaneously successful is given by:

$$\Psi_{\rm succ}=\sum_{i''=1}^{\lfloor L_{\max}\rfloor}\Psi_{{\rm succ}_{i''}}=\frac{1}{\Psi_{\rm tx}}\sum_{i''=1}^{\lfloor L_{\max}\rfloor}\binom{n_2}{i''}p_{\rm tx}^{i''}(1-p_{\rm tx})^{n_2-i''}, \tag{7.11}$$

where $\lfloor \cdot \rfloor$ denotes the floor function, and

$$\Psi_{{\rm succ}_{i''}}=\frac{\binom{n_2}{i''}p_{\rm tx}^{i''}(1-p_{\rm tx})^{n_2-i''}}{\Psi_{\rm tx}}, \tag{7.12}$$

is the probability that exactly i'' transmissions are successful, conditioned to the fact that at least one source transmits. The probability $\Psi_{\rm col}$ that the transmission attempts collide is given by the probability that more than $\lfloor L_{\max} \rfloor$ transmissions occur at the same time:

$$\Psi_{\rm col}=\frac{1}{\Psi_{\rm tx}}\sum_{i''=\lfloor L_{\max}\rfloor+1}^{n_2}\binom{n_2}{i''}p_{\rm tx}^{i''}(1-p_{\rm tx})^{n_2-i''}. \tag{7.13}$$

Using (7.10)-(7.13), the average time interval, ϵ_{slot}, between two consecutive time counter decrements can be evaluated as:

$$\epsilon_{\text{slot}} = (1 - \Psi_{\text{tx}})\sigma_{\text{slot}} + \Psi_{\text{tx}}\Psi_{\text{succ}}T_{\text{succ}} + \Psi_{\text{tx}}\Psi_{\text{col}}T_{\text{col}}, \tag{7.14}$$

where σ_{slot} is the slot time duration, T_{succ} is the time required by a successful handshake and T_{col} is the time wasted because of collision. According to the RTS/CTS mechanism of the 802.11 DCF, these times can be evaluated as [146]:

$$T_{\text{succ}} = \text{DIFS} + T_{\text{RTS}} + T_{\text{CTS}} + T_{\text{DATA}} + T_{\text{ACK}} + 3 \cdot \text{SIFS}, \tag{7.15a}$$

$$T_{\text{col}} = \text{DIFS} + T_{\text{RTS}} + T_{\text{CTS}} + \text{SIFS}, \tag{7.15b}$$

where T_{RTS}, T_{CTS}, T_{DATA} and T_{ACK}, are the times required to transmit the RTS, CTS, DATA and ACK packets, respectively.
The average number of slots during which a data packet remains in the chain (regardless of packet successful transmission within the m-th attempt or packet discarding) is:

$$\epsilon_{\text{num\_slots}} = \sum_{i'=0}^{m} \frac{CW_{i'} - 1}{2} p_{\text{c}}^{i'}, \tag{7.16}$$

which, after some algebra, can be expressed as:

$$\begin{aligned} \epsilon_{\text{num\_slots}} = & \frac{CW_0 p_{\text{c}}(2p_{\text{c}})^{m'}(1-p_{\text{c}}^{m-m'}) + p_{\text{c}}^{m+1} - 1}{2(1-p_{\text{c}})} + \\ & + \frac{CW_0[1-(2p_{\text{c}})^{m'+1}]}{2(1-2p_{\text{c}})}. \end{aligned} \tag{7.17}$$

This value is calculated considering that, at the i'-th transmission attempt, the number of slots is an integer uniformly chosen in $[0, CW_{i'} - 1]$.
The presented model requires the calculation of four unknowns, namely p_{tx}, p_{c}, Λ_1 and Λ_2, which are related to each other and, using (7.9)-(7.17), can be numerically evaluated from the following nonlinear system of four equations:

$$\begin{cases} p_{\text{tx}} = \displaystyle\sum_{i'=0}^{m} \psi_{i',0} = \frac{1 - p_{\text{c}}^{m+1}}{1 - p_{\text{c}}} \psi_{0,0} \\ p_{\text{c}} = 1 - \displaystyle\sum_{i''=0}^{\lfloor L_{\max} \rfloor - 1} \binom{n_2 - 1}{i''} p_{\text{tx}}^{i''}(1 - p_{\text{tx}})^{n_2 - i'' - 1} \\ \Lambda_1 = 1 - e^{-\overline{\Lambda} \cdot \epsilon_{\text{num\_slots}} \cdot \epsilon_{\text{slot}}} \\ \Lambda_2 = 1 - e^{-\overline{\Lambda} \cdot \epsilon_{\text{slot}}} \end{cases} \tag{7.18}$$

The transmission probability p_{tx} is derived considering that a transmission occurs when the backoff timer reaches the zero value [146–147, 150]. The collision probability p_{c} is calculated considering that, if $L_{\max}$ simultaneous communications can be sustained in $\mathbb{R}_2$, p_{c} is given by the probability that more than $\lfloor L_{\max} \rfloor$ nodes transmit at the same time in $\mathbb{R}_2$. Therefore, the packet transmitted by the source collides if more than $L_{\max} - 1$ simultaneous transmissions are performed by the remaining $n_2 - 1$ nodes. Assuming that the packet arrival at each node is a Poisson process with mean $\overline{\Lambda}$, Λ_1 is the probability that at least one arrival occurs during the processing of the previous packet, namely $\epsilon_{\mathrm{num\_slots}} \cdot \epsilon_{\mathrm{slot}}$, and Λ_2 is the probability that at least one arrival occurs between two consecutive backoff timer decrements when $\mathbb{S}$ is in the idle state. More precisely, the calculation of Λ_1 is based on the average time that a packet remains in the chain, while the estimation of Λ_2 is based on the average slot duration. The accuracy and the possible limitations of these approximations will be discussed in the next section.
Once the values of p_{tx}, p_{c}, Λ_1 and Λ_2 are known, the performance figures of the network can be calculated. In a realistic environment, a considerable part of the simultaneous communications that can be sustained by the network are employed for packet forwarding, because, usually, the source-destination distance is larger than the coverage range of the single node. As described in [156], the pdf of the distance r between two nodes randomly placed on a circle of radius R_{t} is given by:

$$\varrho_{\mathrm{dist}}(r) = \begin{cases} \dfrac{2r}{R_{\mathrm{t}}} - \dfrac{r^2\sqrt{4R_{\mathrm{t}}^2 - r^2}}{\pi R_{\mathrm{t}}^4} - \dfrac{4r}{\pi R_{\mathrm{t}}^2} \arcsin\left(\dfrac{r}{2R_{\mathrm{t}}}\right) & r \in [0, 2R_{\mathrm{t}}] \\ 0 & \text{elsewhere} \end{cases} \tag{7.19}$$

Evaluating the average value of (7.19), the average number of hops $\mathcal{N}_{\mathrm{hop}}$ between a generic source-destination pair can be calculated as:

$$\mathcal{N}_{\mathrm{hop}} = \left\lceil \frac{1}{R_{\mathrm{c}}} \int_0^{2R_{\mathrm{t}}} r\,\varrho_{\mathrm{dist}}(r)\,\mathrm{d}r \right\rceil = \left\lceil \frac{128R_{\mathrm{t}}}{45\pi R_{\mathrm{c}}} \right\rceil, \tag{7.20}$$

where $\lceil \cdot \rceil$ denotes the ceiling function.
The main performance figure for a network is the normalized aggregate throughput S_{ag} that represents the sum of the normalized throughput of all nodes, where, in turn, the normalized throughput is the fraction of the overall transmission rate used for sending the payload bits. According to the presented model, the normalized aggregate throughput of the entire network in a multi-hop environment is evaluated as:

$$S_{\mathrm{ag}} = \frac{\Psi_{\mathrm{tx}} T_{\mathrm{pl}} \sum_{i''=1}^{\lfloor L_{\max} \rfloor} \Psi_{\mathrm{succ}_{i''}} i''}{\epsilon_{\mathrm{slot}}} \cdot \frac{R_{\mathrm{t}}^2}{R_{\mathrm{c}}^2} \cdot \frac{1}{\mathcal{N}_{\mathrm{hop}}}, \tag{7.21}$$

where $\Psi_{\mathrm{succ}_{i''}}$ can be calculated from (7.12), and $T_{\mathrm{pl}} = b_{\mathrm{pl}}/\mathcal{R}$ is the time required to send the payload bits b_{pl} at the transmission rate $\mathcal{R}$. Considering that a packet is dropped when it collides for $m+1$ times, the drop probability can be calculated as:

$$\Psi_{\mathrm{drop}} = p_{\mathrm{c}}^{m+1}, \tag{7.22}$$

Finally, the successful packet delay $\mathcal{T}$ is given by the product between the average number of slots required for a successful transmission $\epsilon_{\mathrm{succ\_slots}}$, the average time interval between two consecutive time counter decrements and the average number of hops:

$$\mathcal{T} = \epsilon_{\mathrm{succ\_slots}} \cdot \epsilon_{\mathrm{slot}} \cdot \mathcal{N}_{\mathrm{hop}}, \tag{7.23}$$

where:

$$\epsilon_{\mathrm{succ\_slots}} = \sum_{i'=0}^{m} \frac{CW_{i'} - 1}{2} \cdot \frac{p_{\mathrm{c}}^{i'} - p_{\mathrm{c}}^{m+1}}{1 - p_{\mathrm{c}}^{m+1}}, \tag{7.24}$$

is evaluated considering that only not dropped packets must be taken into account. Performing some algebra, this quantity can be rewritten as:

$$\begin{aligned} \epsilon_{\mathrm{succ\_slots}} = & \frac{p_{\mathrm{c}}^{m+1} CW_0 2^{m'} (p_{\mathrm{c}}^{m'-m} - 1) + 1}{2(1 - p_{\mathrm{c}}^{m+1})(1 - p_{\mathrm{c}})} + \frac{CW_0[1 - (2p_{\mathrm{c}})^{m'+1}]}{2(1 - p_{\mathrm{c}}^{m+1})(1 - 2p_{\mathrm{c}})} + \\ & - \frac{p_{\mathrm{c}}^{m+1}[CW_0 2^{m'}(m - m' + 2) - CW_0 - m - 1] - 1}{2(1 - p_{\mathrm{c}}^{m+1})}. \end{aligned} \tag{7.25}$$

It is worth noticing that the saturated behavior of the network for the omnidirectional antenna case, described in [147, 150], can be obtained from the proposed model by imposing $\overline{\Lambda} \to +\infty$, $R_{\mathrm{t}} = R_{\mathrm{c}}$ and $L_{\max} = 1$. Besides, imposing the further condition $m \to \infty$, one can derive the model presented in [146]. Besides, differently from [153], where the use of two probabilities is adopted for modeling the source behavior in presence of an infinite buffer, in this paper λ_1 and λ_2 are employed to model the Poisson arrival process in a source having a single place buffer.

7.4 Results

This section presents the results provided by the proposed analysis and compares the theoretical curves with the numerical ones, obtained simulating the backoff procedure of the 802.11 DCF with Matlab.

DIFS	34 μs	T_{RTS}	20 $\mu s + \dfrac{182 + b_{\mathrm{ts}}}{\mathcal{R}_{\mathrm{c}}}$
SIFS	16 μs	T_{CTS}	20 $\mu s + \dfrac{134 + b_{\mathrm{ts}}}{\mathcal{R}_{\mathrm{c}}}$
σ_{slot}	9 μs	T_{DATA}	20 $\mu s + \dfrac{294 + b_{\mathrm{pl}}}{\mathcal{R}}$
b_{pl}	8184 bits	T_{ACK}	20 $\mu s + \dfrac{134}{\mathcal{R}_{\mathrm{c}}}$
b_{ts}	512 bits	R_{c}	100 m
$\mathcal{R}$	24 Mbits/s	$\mathrm{SINR}_{\mathrm{th}}$	10 dB
$\mathcal{R}_{\mathrm{c}}$	12 Mbits/s	α	4

TABLE 7.1: SYSTEM PARAMETERS ASSUMING THE 802.11A SPECIFICATIONS FOR MODE 5.

7.4.1 Parameter settings

With reference to the model developed in the previous chapters to evaluate the number of sustainable links in the AA and SBA cases, in this section the $L_{\max}$ values are calculated considering a random distribution of the nodes, modeled using the pdf expressed by (5.42), and choosing a truncated Laplacian pdf to account for the DOA statistic. Besides, the results are referred to an omnidirectional transmission of the CTS packet (OCTS case).
Even if the adoption of Directional Antennas (DAs) in a DWN was not specifically addressed the previous chapters, it can be easily derived from the SBA and AA cases by noticing that a directional antenna is able to perform a continuous beam steering towards the desired source, but is unable to suppress the interferers. Therefore, the number of sustainable links for the DA case can be calculated using (6.7) and modeling the gain in the desired direction G_{d} according to (5.13).
The numerical results are derived combining the discrete-event Network Simulator 2 (*ns-2*) with a discrete-time simulator developed in Matlab. More precisely, the $L_{\max}$ value calculated employing *ns-2* is passed to Matlab, which performs the discrete-time simulation of the DCF by considering that $\lfloor L_{\max} \rfloor$ node pairs can be simultaneously active in a given slot time. Each simulation is stopped when 40000 packets have been processed. To improve the readability of the figures, the confidence intervals are not reported, because they are not distinguishable from the markers. The adopted parameters are chosen according to the 802.11a standard [59], and are summarized in Table 7.1, where $\mathcal{R}_{\mathrm{c}}$ is the transmission rate of the control packets, which, in general, can be lower than $\mathcal{R}$. A training sequence of length $b_{\mathrm{ts}} = 512$ bits is inserted in the RTS/CTS packets in order to perform

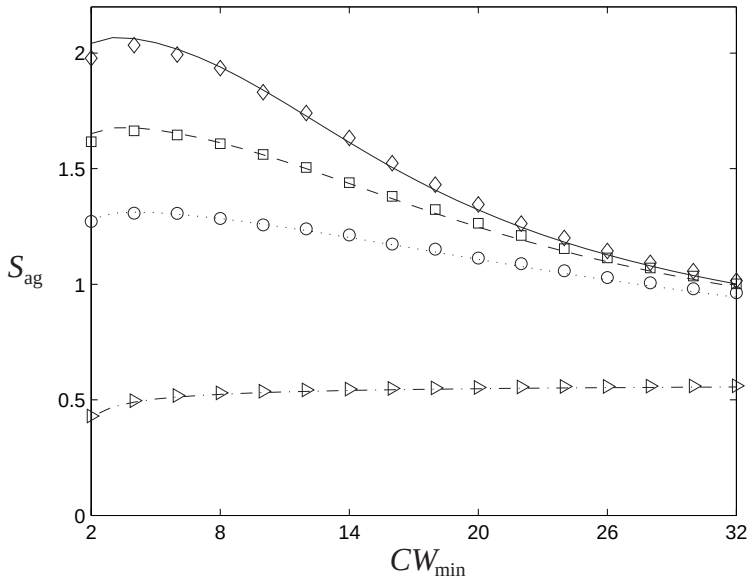

Figure 7.2: Saturation throughput as a function of the minimum contention window for $R_t = R_c$, $\hat{\sigma}_\varphi = 0^o$, $n = n_2 = 25$ and $m = m' = 6$.

—— AA (Analysis) ◊ AA (Simulation)
- - - - DA (Analysis) □ DA (Simulation)
····· SBA (Analysis) ○ SBA (Simulation)
-·-·- 802.11a (Analysis) ▷ 802.11a (Simulation)

the antenna system adaptation (of course this field is not inserted in the omni-directional case). The $\mathrm{SINR_{th}}$ value is selected taking into account the coded modulation scheme adopted by the 802.11a extension to provide the bit rate of 24 Mbits/s (mode 5) with a PER equal to 1% [126].

7.4.2 Optimum contention window

Figg. 7.2-7.3 show the saturation throughput and the successful packet delay in absence of multipath as a function of the minimum contention window for $R_t = R_c$, $n = n_2 = 25$, $m = m' = 6$ and $N = 4$ antennas (except for the 802.11a case where a unique antenna can be used). The figures prove a good agreement between analytical and numerical results, confirming that beamforming can largely reduce the packet delay and increase the network throughput even adopting not highly sophisticated multi-antenna techniques. The curves put in evidence the existence of an optimum value for the minimum contention window, CW_{opt}, for

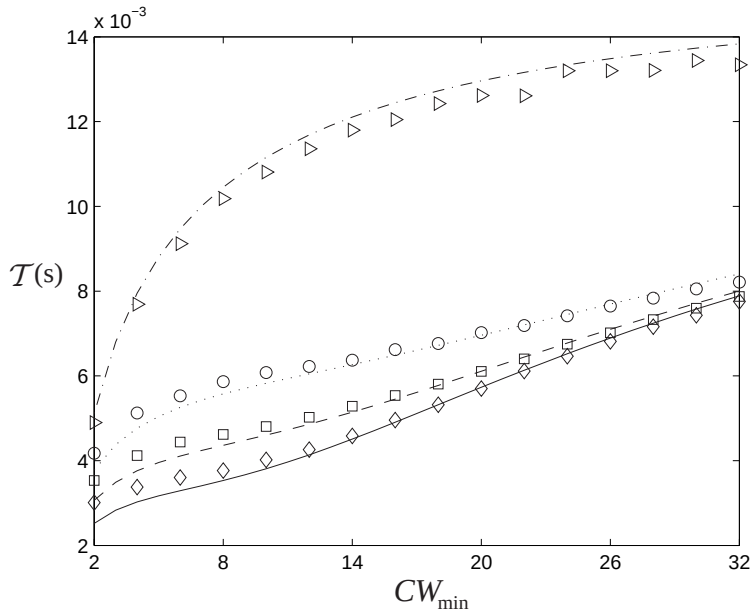

Figure 7.3: Successful packet delay as a function of the minimum contention window in saturated traffic conditions for $R_{\mathrm{t}} = R_{\mathrm{c}}$, $\hat{\sigma}_{\varphi} = 0^{o}$, $n = n_2 = 25$ and $m = m' = 6$.

—— AA (Analysis) ◊ AA (Simulation)
- - - - DA (Analysis) □ DA (Simulation)
····· SBA (Analysis) ○ SBA (Simulation)
-·-·- 802.11a (Analysis) ▷ 802.11a (Simulation)

which the throughput is maximized. In particular, $CW_{\mathrm{opt}} = 3$ in the AA case and $CW_{\mathrm{opt}} = 4$ in the DA and SBA cases. Therefore, one may conclude that, to exploit the interference mitigation capabilities of the antenna system, a smaller minimum contention window should be adopted. Besides, it can be observed that, for large values of $CW_{\min}$, the three antenna systems perform similarly, being their performance much lower than the best one. This behavior puts in evidence that an inappropriate setting of the minimum contention window for a given antenna system may be equivalent to the adoption of a simpler antenna system characterized by worse performance.

As described in [146], W_{opt} should be chosen according to the network scenario, which, for the single antenna case, is identified by the number of contending nodes. Fig. 7.4 confirms, also for the AA case, the importance of the number of stations for the setting of the optimum contention window. In the figure the bullets denote the W_{opt} values. Similarly to the omnidirectional antenna case,

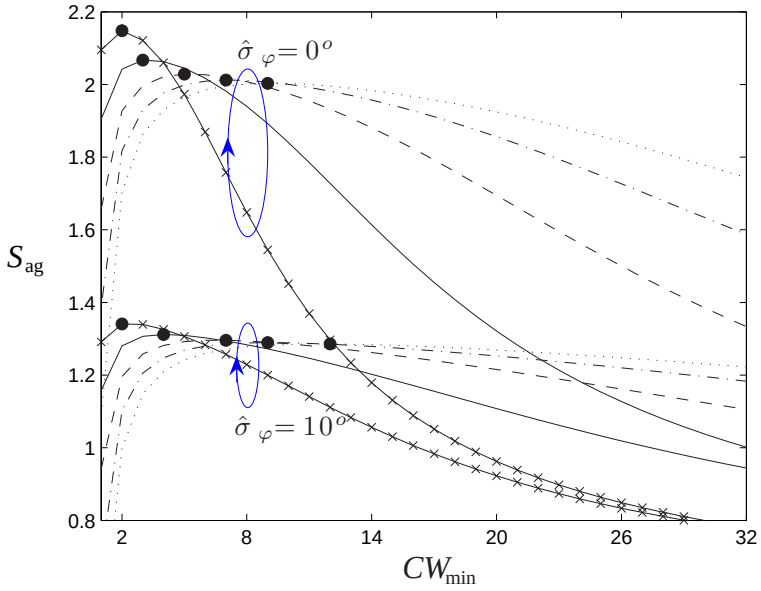

Figure 7.4: Saturation throughput as a function of the minimum contention window for different values of the angular spread and of the number of nodes in the AA case using $N = 4$ antennas.
$n_2 = 15$ $n_2 = 25$ $n_2 = 40$ $n_2 = 55$ $n_2 = 70$

W_{opt} increases as the number of contending nodes increases. Besides, the slope of the curves near the optimum value indicates that, as n_2 and $\hat{\sigma}_{\varphi}$ decrease, the throughput becomes more sensitive to the contention window size. By consequence, improper settings of W_{opt} lead to larger performance degradations when the node density is low and multipath is absent. Fig. 7.4 puts also in evidence that, when advanced antenna techniques are adopted, not only the number of contending nodes, but also the spatial characteristics of the channel are involved in the characterization of the network scenario. The markers in the figure show that the optimum throughput is very sensitive to the propagation environment, but is less sensitive to the number of nodes. Severe channel conditions, characterized by large values of the angular spread, lead to noticeable throughput reductions, and larger values of CW_{opt}. The increase of the number of contending nodes, instead, can be effectively managed by properly selecting CW_{min}, in order to mitigate the performance decrease.
Table 7.2 shows the dependence of CW_{opt} on the number of antennas and on the maximum backoff stage for the adaptive antenna case. It may be observed that a larger number of antenna elements leads to a considerable increase of through-

	$N=4$				$N=8$			
	CW_{opt}	S_{ag}	$\mathcal{T}$(ms)	$\Psi_{\text{drop}}(\%)$	CW_{opt}	S_{ag}	$\mathcal{T}$(ms)	$\Psi_{\text{drop}}(\%)$
$m=m'=1$	11	2.03	4.03	17.09	4	5.83	1.12	10.06
$m=m'=3$	7	2.03	4.58	3.95	4	5.83	1.14	0.24
$m=m'=5$	6	2.03	5.12	0.54	3	5.83	1.36	0.07
$m=m'=7$	5	2.03	5.27	0.11	3	5.83	1.38	0.01

TABLE 7.2: DEPENDENCE OF THE OPTIMUM CONTENTION WINDOW, THE AGGREGATE THROUGHPUT, THE SUCCESSFUL PACKET DELAY AND THE DROP PROBABILITY ON THE MAXIMUM BACKOFF STAGE AND ON THE NUMBER OF ANTENNAS IN THE AA CASE FOR $\hat{\sigma}_{\varphi}=0^{o}$.

put, and allows lower average delay and drop probability. The maximum backoff stage affects delay and drop probability, while the throughput may be maintained almost constant by selecting the window size properly. Considering that the characteristics of the antenna system are known, the adaptive setting of CW_{opt} in a practical scenario requires the estimation of n_2, as described in [157], and the estimation of $\hat{\sigma}_{\varphi}$. The setting of $CW_{\min}$ as a function of the angular spread may be performed manually, exploiting the approximate knowledge of the propagation scenario, for example making reference to well established models derived from measurement campaigns ($20^{o} \leq \hat{\sigma}_{\varphi} \leq 40^{o}$ in indoor environment [158], $5^{o} \leq \hat{\sigma}_{\varphi} \leq 15^{o}$ in outdoor environment [23]). The setting of $CW_{\min}$ may also be performed adopting an adaptive approach, which requires the use of proper signal processing algorithms for the estimation of $\hat{\sigma}_{\varphi}$ [159]. However, this second solution, even if more precise and able to provide optimum results, may lead to an increase of the complexity that may be not justified by the performance improvement. In fact, as shown in Fig. 7.4, small variations of $CW_{\min}$ around CW_{opt} have only minor effects on throughput, and so sub-optimal solutions may be acceptable. Sub-optimal settings may also be mandatory for managing the number of contending nodes, considering that, in many cases, the standard hardware does not allow to choose any integer value for $CW_{\min}$. As previously described, this limitation may lead to a considerable throughput decrease when the number of nodes and the angular spread are low. However, an angular spread close to zero does not represent a realistic situation in a practical 802.11 network.

7.4.3 Non saturated behavior

Fig. 7.5 and Fig. 7.6 show the aggregate throughput and the successful packet delay in non-saturated conditions as a function of the net offered load S_{input}, which

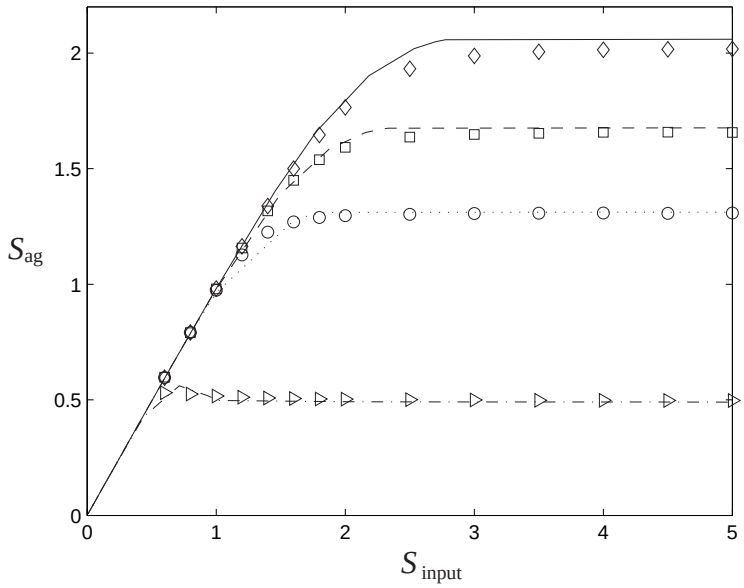

Figure 7.5: Aggregate throughput as a function of the net offered load for $R_{\text{t}} = R_{\text{c}}$, $\hat{\sigma}_{\varphi} = 0^{o}$, $n = n_2 = 25$ and $m = m' = 6$.

—— AA (Analysis) ◊ AA (Simulation)
- - - - DA (Analysis) □ DA (Simulation)
····· SBA (Analysis) ○ SBA (Simulation)
-·-·- 802.11a (Analysis) ▷ 802.11a (Simulation)

has been defined as the ratio between the aggregate throughput and the success probability.

The numerical values confirm the analytical results for the throughput behavior and the delay behavior in saturation and for low traffic load, while there are some differences in the transition zones of the delay curves, due to the slightly different models adopted in analysis and simulation. In both cases, a station is assumed to have a single place buffer in which it can store the next packet to transmit. In the analysis, the buffer content is updated only once, at the end of the previous packet transmission phase (using the average transmission duration), while, in the discrete-time simulation, the buffer content is updated regularly at each time step. For this reason, in the analysis, when the input traffic is approaching saturation, the probability of having another ready packet approaches one much faster than in simulation (a similar behavior is obtained by adopting a larger buffer in simulation, as it can be easily verified). This behavior leads to a rapid increase of the average number of slots required for a successful transmission $\epsilon_{\text{num\_slots}}$ that

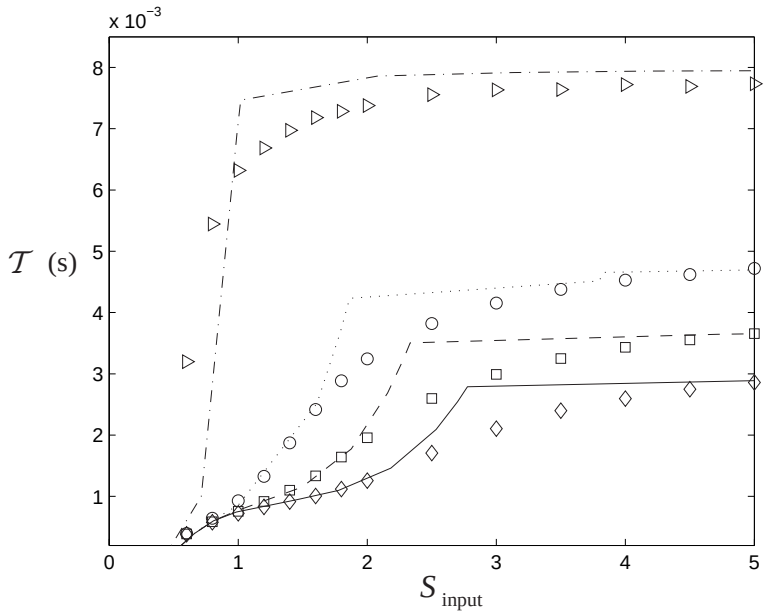

Figure 7.6: Successful packet delay as a function of the net offered load for $R_{\text{t}} = R_{\text{c}}$, $\hat{\sigma}_{\varphi} = 0^{o}$, $n = n_2 = 25$ and $m = m' = 6$.

—— AA (Analysis) ◊ AA (Simulation)
- - - - DA (Analysis) □ DA (Simulation)
····· SBA (Analysis) ○ SBA (Simulation)
-·-·- 802.11a (Analysis) ▷ 802.11a (Simulation)

determines, in turn, the fast increase of $\mathcal{T}$, as it can be inferred from (7.23). This limitation of the proposed non-saturated model does not affect the throughput, which is not dependent on $\epsilon_{\text{num\_slots}}$. A more accurate estimation of the arrival process should account for both the retransmission attempt i' and the corresponding backoff timer. This may lead to a considerable increase of complexity due to the doubling of the number of states required to analyze the single place buffer case.

7.4.4 Number of nodes

Finally, Fig. 7.7 shows the performance in saturated traffic conditions of a DWN as a function of the number of nodes. The results are obtained for a multi-hop scenario, where $R_{\text{t}} = 300$ m and $CW_{\min}$ is selected equal to 4.
As one can expect, the employment of AAs is able to provide a larger throughput and to allow the access to a larger number of nodes, while guaranteeing, at the

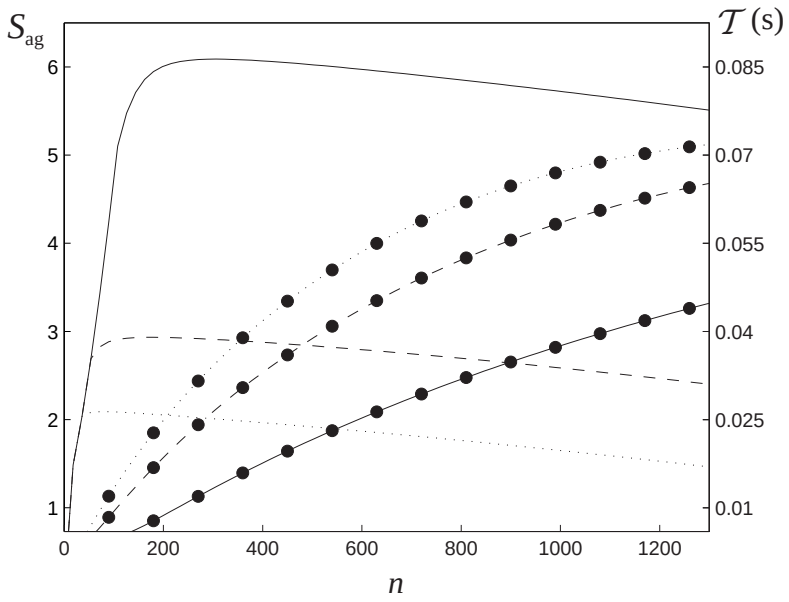

Figure 7.7: Saturation throughput and successful packet delay as a function of the number of nodes for $R_{\mathrm{t}} = 300$ m, $\hat{\sigma}_{\varphi} = 0^{o}$, $CW_{\min} = 4$ and $N = 8$.
—— Throughput (AA) - - - - Throughput (DA) ····· Throughput (SBA)
—●— Delay (AA) - -●- - Delay (DA) ···●··· Delay (SBA)

same time, a lower delay with respect to directional and switched-beam antennas. Besides, for each antenna system, there is an optimal value of the number of nodes, n_{opt}, which leads to throughput maximization. This value gets larger as the antenna system gets more sophisticated. Furthermore, comparing the successful packet delays calculated in the respective n_{opt} values of the three antenna systems, it can be observed that in optimal conditions SBAs provide a lower throughput, but are able to guarantee a lower delay with respect to directional and adaptive antennas.

7.5 Summary

The theoretical results provided in this chapter, and validated by simulations, put in evidence that an efficient exploitation of the antenna system can be obtained adopting an aggressive approach, in which the minimum contention window must be kept as low as possible in order to force the network to perform simultaneous communications. The results show that the main cause of performance degradation are due to the channel, while a larger number of contending nodes can be

managed by properly setting the 802.11 DCF parameters. The minimum contention window should be adapted to the sophistication of the antenna system, the number of contending nodes, the angular spread of the channel and the number of antennas in order to exploit the potential offered by multiple antenna techniques in terms of sustainable links.

Chapter 8

On the Influence of Array Geometry in DWNs Employing Smart Antennas

By adopting a numerical approach, this chapter investigates the influence of the geometrical configuration of the antenna array on the behavior of a DWN using smart antennas. A discrete-time simulator for the MAC/PHY layers is developed in order to evaluate the performance of the network. The study adopts a specific MAC protocol, previously proposed for ad-hoc networks, able to exploit the interferer suppression capabilities of adaptive arrays in a low-rank channel. Simulations are performed to evaluate the dependence of the aggregate throughput and of the successful packet delay on the geometry of the physical antenna system, taking into account the constraints due to the size of the terminal. Besides, it is examined how the network behavior is influenced by the training sequence length and by the speed of the mobile nodes.[1]

8.1 Introduction and array geometry description

The terminal size is one of the most important constraints for the physical antenna system design. In a distributed wireless network the nodes are usually handy devices and so cumbersome structures must be avoided. The possibility to use a multi-antenna system on a node belonging to a DWN is related not only to the size of the single radiator, but also to the displacement of the elements on the available

[1]The content of this chapter is based on F. Babich, M. Comisso, M. D'Orlando, and L. Manià, "Performance Evaluation of Distributed Wireless Networks Using Smart Antennas in Low-Rank Channel," IEEE Transactions on Communications, vol. 55, no. 7, pp. 1344–1353, Jul. 2007 [171,179].

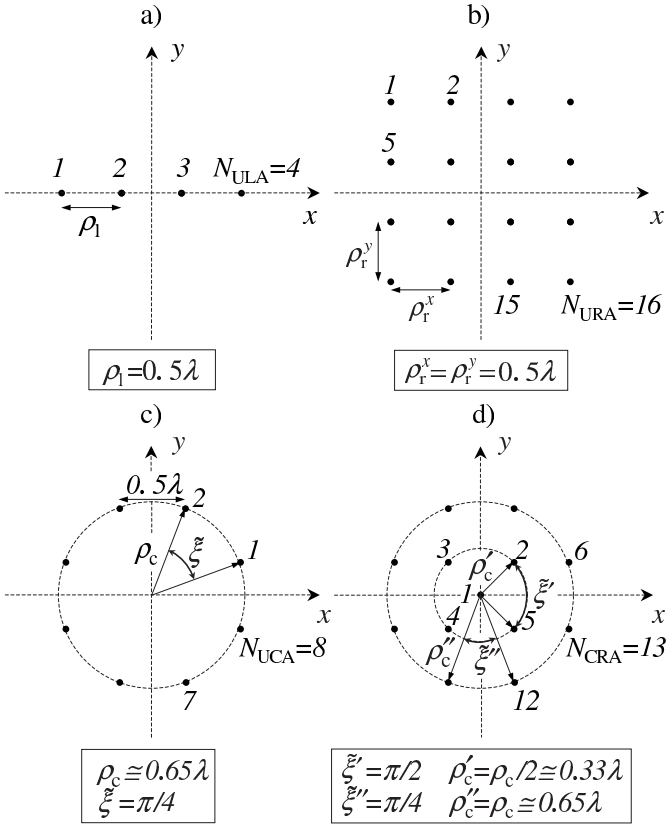

Figure 8.1: Characteristics of the analyzed array geometries:
a) ULA, b) URA, c) UCA, d) CRA.

area.

In this study, the number of omnidirectional antenna elements, N, is chosen taking into account the maximum area that the array can occupy. In particular, for each array, N is selected modeling the device as a square having an edge equal to 18 cm, which may represent the typical size of a small laptop. The size of each radiator is assumed as negligible and the operating frequency is selected equal to 2.484 GHz, corresponding to the ISM band adopted in the 802.11 legacy version and in the 802.11b/g amendments. This choice leads to a carrier wavelength λ approximately equal to 12 cm. The presented study is performed imposing the further constraint that the minimum distance between two neighboring radiators be equal to $\lambda/2 = 6$ cm in order to avoid significant mutual coupling effects.

Four different array geometries are analyzed (Fig. 8.1). The first array is a ULA with $N_{\mathrm{ULA}} = 4$ elements, spaced by $\rho_{\mathrm{l}} = \lambda/2$. The second array is a URA, having

$N_{\mathrm{URA}} = N_x \cdot N_y = 4 \cdot 4 = 16$ elements at distance $\rho_{\mathrm{r}}^x = \rho_{\mathrm{r}}^y = \lambda/2$. The third array is a UCA having $N_{\mathrm{UCA}} = 8$ elements and radius:

$$\rho_{\mathrm{c}} = \frac{\lambda}{4\sin\left(\pi/N_{\mathrm{UCA}}\right)}, \tag{8.1}$$

selected according to the constraint relative to the minimum distance between neighboring radiators. The last array is a CRA with a central radiator and two rings having respectively $N_{\mathrm{CRA}_1} = 4$ and $N_{\mathrm{CRA}_2} = 8$ elements. The CRA occupies the same area of the UCA, but is formed by $N_{\mathrm{CRA}} = 1 + N_{\mathrm{CRA}_1} + N_{\mathrm{CRA}_2} = 13$ radiators.
According to the notation of Section 1.3, the antenna system power gain in the azimuth plane is written as:

$$G(\varphi) = \left| \sum_{k=1}^{N} w_k e^{j\frac{2\pi v_{\mathrm{c}}}{\lambda}\tau_k(\varphi)} \right|^2, \tag{8.2}$$

where the weight vector $\mathbf{w} = [w_1, w_2, ..., w_N]^T$ is updated using the unconstrained LMS algorithm and the delay at the k-th antenna element, $\tau_k(\varphi)$, includes the characteristics of the array geometry. For the URA and the CRA the weights are reordered to obtain vectors instead of matrices (Fig. 8.1b,d). The order can be inferred by the numbers placed near the radiators. With reference to the adopted geometrical dimensions, the delays for the ULA, the URA, the UCA and the CRA can be calculated, respectively, as:

$$\tau_k(\varphi) = \frac{\lambda}{2v_{\mathrm{c}}}\left(k - \frac{N_{\mathrm{ULA}}+1}{2}\right)\cos\varphi, \tag{8.3}$$

$$\tau_k(\varphi) = \frac{\lambda}{2v_{\mathrm{c}}}\left[\left(\left\lceil\frac{k}{4}\right\rceil - \frac{\sqrt{N_{\mathrm{URA}}}+1}{2}\right)\cos\varphi - \left(k - 4\left\lfloor\frac{k-1}{4}\right\rfloor - \frac{\sqrt{N_{\mathrm{URA}}}+1}{2}\right)\sin\varphi\right], \tag{8.4}$$

$$\tau_k(\varphi) = \frac{\lambda}{4\sin\left(\pi/N_{\mathrm{UCA}}\right)v_{\mathrm{c}}}\cos\left[\left(k - \frac{1}{2}\right)\tilde{\xi} - \varphi\right], \tag{8.5}$$

$$\tau_k(\varphi) = \frac{\lambda}{8\sin(\tilde{\xi}/2)v_{\mathrm{c}}} \cdot \begin{cases} 0 & k = 1 \\ \cos[(2k-3)\tilde{\xi} - \varphi] & 2 \le k \le 5 \\ 2\cos\left[\left(k - \dfrac{11}{2}\right)\tilde{\xi} - \varphi\right] & 6 \le k \le N_{\mathrm{CRA}} \end{cases}, \tag{8.6}$$

where $\tilde{\xi} = 2\pi/N_{\mathrm{UCA}}$.

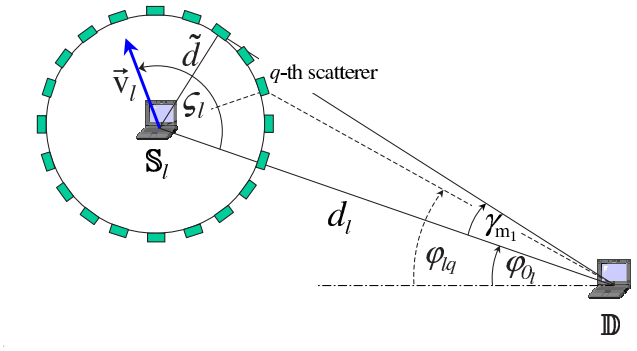

Figure 8.2: Channel model.

8.2 Signal and channel model

According to the scenario adopted for the theoretical analysis, the simulation environment is modeled assuming that, during the reception of the DATA packet, the generic destination receives the signals incoming from n_{tx} nodes, representing the number of active transmitters. This value, which includes the desired source and the interferers, depends, in practice, on the temporal evolution of the network, because of the asynchronous characteristic of the 802.11 DCF. By consequence, in the discrete-time simulator employed in this study, n_{tx} may change during the time required to receive the DATA packet. However, to avoid cumbersome notations, this dependence is not explicitly introduced in the adopted symbols.
The low-rank propagation environment is simulated using the ring of scatterers model (Paragraph 2.2.1.4). In particular, the generic l-th active source $\mathbb{S}_l$ is surrounded by $Q = 20$ scatterers that are uniformly placed along the circumference of radius $\tilde{d}$ (Fig. 8.2). The azimuth DOA φ_{lq}, corresponding to the q-th scatterer of the l-th source, and the amplitude attenuation Υ_{lq} can be calculated, by geometrical considerations, as:

$$\varphi_{lq} = \arctan\left[\frac{\tilde{d}\sin\left(\frac{2\pi}{Q}q + \varphi_{0_l}\right)}{d_l - \tilde{d}\cos\left(\frac{2\pi}{Q}q + \varphi_{0_l}\right)}\right] + \varphi_{0_l}, \tag{8.7a}$$

$$\Upsilon_{lq} = \left[\tilde{d} + \sqrt{d_l^2 + \tilde{d}^2 - 2d_l\tilde{d}\cos\left(\frac{2\pi}{Q}q + \varphi_{0_l}\right)}\right]^{\frac{\alpha}{2}}, \tag{8.7b}$$

where d_l is the distance between the l-th source and the destination, φ_{0_l} is the mean DOA with respect to $\mathbb{D}$, and $\varphi_{lq} \in]\varphi_{0_l} - \gamma_{\mathrm{m}_1}, \varphi_{0_l} + \gamma_{\mathrm{m}_1}[$, with:

$$\gamma_{\mathrm{m}_1} = \max_{0 \le l \le n_{\mathrm{tx}}} \left[\arcsin\left(\frac{\tilde{d}}{d_l}\right) \right] \simeq \max_{0 \le l \le n_{\mathrm{tx}}} \left(\frac{\tilde{d}}{d_l}\right), \tag{8.8}$$

which represents an acceptable approximation for a low-rank channel. Using (2.11) and (2.12), the angular spread relative to the l-th source can be evaluated as:

$$\hat{\sigma}_{\varphi_l} = \sqrt{\frac{\sum_{q=1}^{Q} P_{\mathrm{rx}_{lq}} \varphi_{lq}^2}{\sum_{q=1}^{Q} P_{\mathrm{rx}_{lq}}} - \left(\frac{\sum_{q=1}^{Q} P_{\mathrm{rx}_{lq}} \varphi_{lq}}{\sum_{q=1}^{Q} P_{\mathrm{rx}_{lq}}}\right)^2}, \tag{8.9}$$

where $P_{\mathrm{rx}_{lq}} = P_{\mathrm{tx}}/(Q \cdot \Upsilon_{lq}^2)$ is the power of the replica received from the direction φ_{lq} assuming a constant transmission power P_{tx} (equal for all nodes). The total signal incoming on the k-th antenna element at time t is:

$$x_k(t) = \sum_{l=1}^{n_{\mathrm{tx}}} \sqrt{P_{\mathrm{tx}}} \tilde{h}_{kl}(t) s_l(t) + \tilde{n}_{\mathrm{G}_k}(t), \tag{8.10}$$

where $s_l(t)$ is the signal transmitted by the l-th source, $\tilde{n}_{\mathrm{G}_k}(t)$ accounts for the Gaussian noise and:

$$\tilde{h}_{kl}(t) = \frac{1}{\sqrt{Q}} \sum_{q=1}^{Q} \frac{1}{\Upsilon_{lq}} e^{j\zeta_{lq} + j2\pi f_{lq}^{\mathrm{D}} t} \cdot a_{kl}^q, \tag{8.11}$$

is the channel response. In particular, ζ_{lq} is randomly selected in $[0, 2\pi]$ and:

$$f_{lq}^{\mathrm{D}} = \frac{|\vec{\mathrm{v}}_l|}{\lambda} \cos\left(\frac{2\pi}{Q} q + \varphi_{0_l} - \varsigma_l\right), \tag{8.12}$$

represents the Doppler shift relative to the q-th replica of the l-th source due to the relative speed vector $\vec{\mathrm{v}}_l = |\vec{\mathrm{v}}_l| e^{j\varsigma_l}$. Besides, in (8.11), the term $a_{kl}^q = e^{j2\pi v_{\mathrm{c}} \tau_k(\varphi_{lq})/\lambda}$ is the phase factor with which the q-th path of the signal transmitted by the source l reaches the k-th element of the array. This quantity may be viewed as a generalization of the generic component of the steering vector in presence of multipath and takes into account the geometrical characteristics of the antenna array.
The samples of the received signal vector $\mathbf{x}(i) = [x_1(i), x_2(i), ..., x_N(i)]^T$ are processed by the LMS algorithm, which updates the weight vector $\mathbf{w}$ and creates the receiving radiation pattern. Assuming that the first source is the desired one, the output SINR at the destination is evaluated as:

$$\mathrm{SINR}_{\mathrm{out}} = \frac{\sum_{q=1}^{Q} G(\varphi_{1q}) P_{\mathrm{rx}_{1q}}}{\sum_{i=2}^{n_{\mathrm{tx}}} \sum_{q=1}^{Q} G(\varphi_{lq}) P_{\mathrm{rx}_{lq}} + W}, \tag{8.13}$$

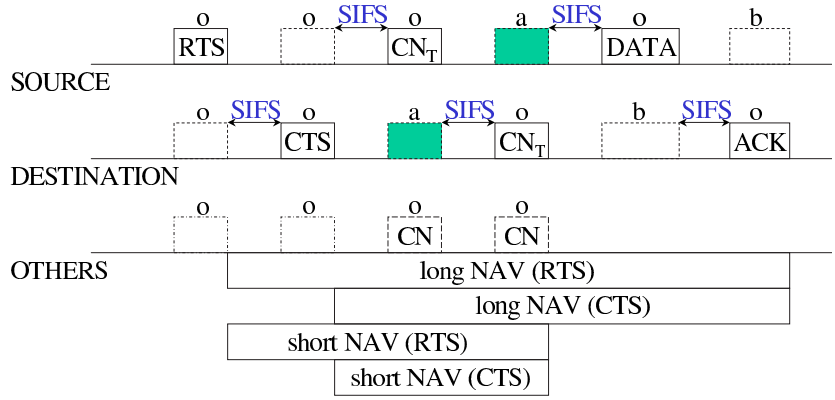

Figure 8.3: Time line for SCSMA/CN.

where $G(\varphi_{lq})$ indicates the computed smart antenna power gain in φ_{lq} direction. Assuming that an error detecting code is employed, as it is the case for the IEEE 802.11 legacy version, the correct reception of a packet during the simulation is established using the threshold $\mathrm{SINR}_{\mathrm{th}}$.

8.3 Adopted MAC protocol

As described in Section 4.3, being the 802.11 DCF designed assuming omnidirectional transmissions and receptions, it is unable to guarantee a high performance level for the interfered communication. To improve the resistance of the DWN against the undesired sources and to allow the investigation of the interference suppression capabilities of the four analyzed array geometries, the MAC protocol proposed in [104] is implemented in the simulator. A brief description of this access scheme, called Selective CSMA with Cooperative Nulling (SCSMA/CN), is given below. The symbols (o), (a) and (b), in Fig. 8.3, mean omnidirectional operating mode, adaptive phase and beamforming operating mode, respectively.
SCSMA/CN adopts a six way handshake RTS/CTS/CN/CN/DATA/ACK, in which all transmissions are omnidirectional (o), as in 802.11 DCF, but the DATA and ACK packets are received in beamforming operating mode (b). The RTS/CTS exchange (o), performed by the source and the destination, is followed by the exchange of the CN packets. This second phase involves the neighbors and is used by the source and the destination to update (a), their antenna weight vectors. The CN packets are sent (o) by the nodes that have received the RTS and/or the CTS, and have updated their omnidirectional NAVs. In particular, the nodes having a packet for the source or the destination, set a *long NAV* to avoid unnecessary

transmissions to busy stations, while the other nodes set a *short NAV* to protect the omnidirectional phase of the handshake. All the CN packets have the same length, but contain different sequences of bits. The CNs transmitted by the source and the destination (CN_T), contain the training sequence (unique for all the nodes of the network), while the CNs transmitted by the other nodes contain an arbitrary sequence, different from the training one. A collision can occur if part of the training sequence is transmitted at the same time by two or more neighboring nodes. Once the weight vectors of the antenna systems have been updated, the source and the destination transmit, respectively, the DATA and the ACK packets (o), using the computed weights to receive the ACK and the DATA packets (b). The first transmission attempt and the possible retransmissions are scheduled according to the backoff scheme of the 802.11 DCF.
In SCSMA/CN, the physical CS information collected by a neighbor is used to delay a transmission only for the duration of the omnidirectional RTS/CTS exchange between the communicating nodes, while this transmission is allowed during their DATA/ACK exchange (except for the case where the neighbor sets the long NAV). This aggressive approach is compensated by a careful protection of the receiving phase of the DATA/ACK packets. SCSMA/CN is an access scheme that tries to suppress the interference due to ongoing transmissions and, using the CN packets, it tries to avoid interference due to potential future transmissions. On one hand, the omnidirectional transmission of all involved packets produces a higher level of interference with respect to the directional transmission. This drawback becomes more evident during the exchange of the CNs that must be sent by all the neighbors. On the other hand, the omnidirectional transmission guarantees a reduction of the hidden terminal and the deafness phenomena, because the communicating nodes can be sensed more easily. Therefore, even if, with respect to other proposed access schemes [105, 111], SCSMA/CN does not completely exploit the potential offered by smart antennas in terms of throughput maximization, it largely reduces the MAC layer problems usually associated to the adoption of multiple antennas. This advantage provides a less troubled scenario for the purpose of this chapter, which is the comparison between different array geometries in terms of interference reduction.

8.4 Simulation platform

Discrete-event simulators represent powerful tools to evaluate the network performance that usually do not require long simulation time, but, unfortunately, are not able to take into account the details of the physical layer. Therefore, a discrete-time simulator has been developed in this chapter to analyze the network behavior adopting more precise models for the channel and the antenna system. Even if

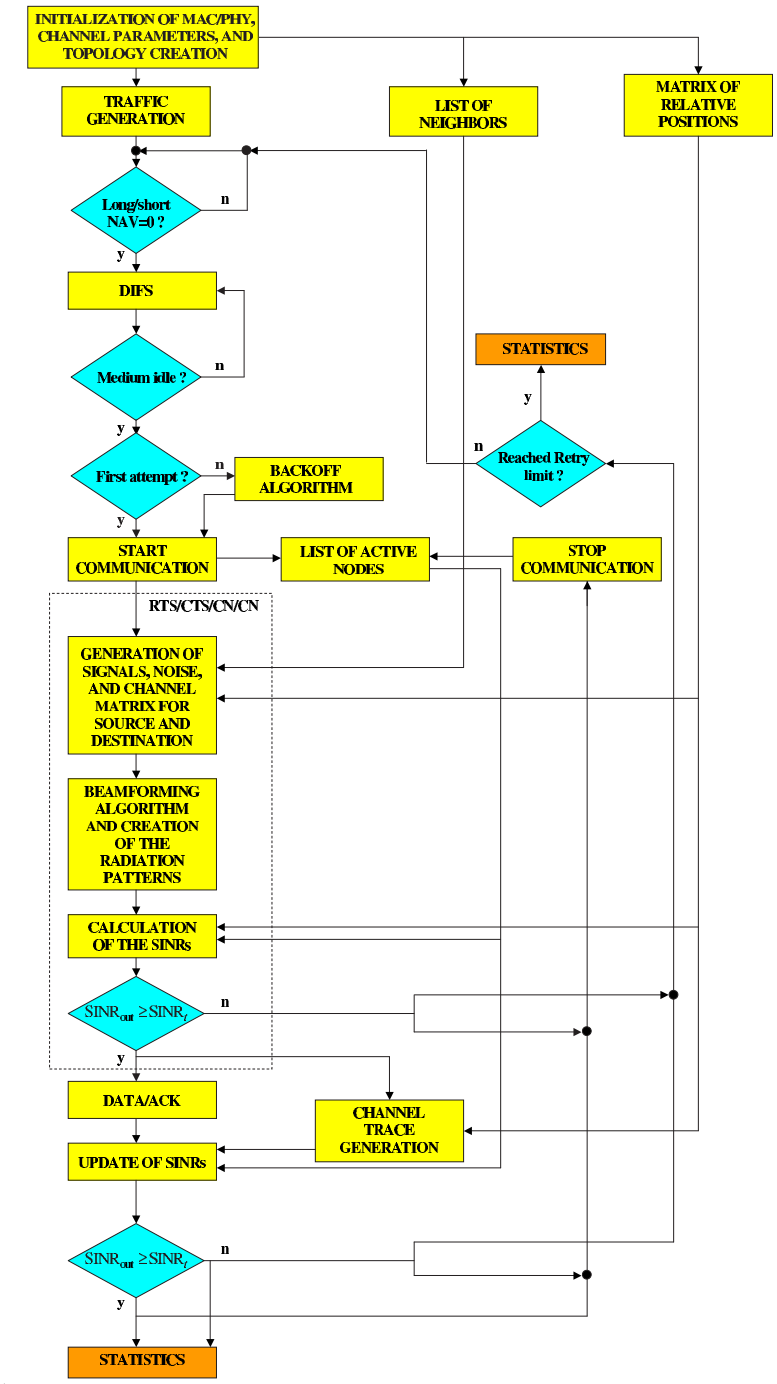

Figure 8.4: MAC/PHY discrete-time simulator.

the time required to obtain the performance becomes longer, the discrete-time approach has been preferred because it provides the possibility to have direct access to the physical layer parameters.
Fig. 8.4 shows the main components of the MAC/PHY simulator that has been implemented in Matlab. The process of initialization sets all counters to zero, fixes the desired values for the MAC/PHY and the channel parameters, and creates the network topology. Besides, the initialization process generates the list of one-hop neighbors of each node and the matrix of relative positions, which contains the distance and the angle from which each node sees the others. If the nodes are mobile these two elements are periodically updated during the simulation. The minimum adopted time step is equal to 1 μs.
Once a packet is generated, the source verifies that the long and the short NAVs have zero value, and then waits for a DIFS monitoring the channel activity. If the channel is idle the source transmits, otherwise a random backoff is generated. At the beginning of the transmission the list of active nodes is updated, the signals are generated according to the position of the neighbors (as stated by the SC-SMA/CN protocol), and the channel matrices are created according to the propagation model described in Section 8.2. The received signals are then processed by the beamforming algorithm to produce the radiation patterns of the source and of the destination. If both SINRs are larger than the receiving threshold, the communication between the two nodes is considered established. This first part simulates the omnidirectional phase of the handshake RTS/CTS/CN/CN.
The created patterns are also used to update the SINRs during the DATA/ACK exchange taking into account the activity of the network nodes. The SINR requirement is verified at the destination during the DATA transmission time, while it is verified at the source during the ACK transmission time. Mobility effects are generated assuming that the nodes move on straight trajectories. The direction of movement is randomly selected at the beginning of the simulation and then kept constant. The positions of the nodes are regularly updated and so the Doppler shifts can be different for each communication. When the DATA transmission begins, the channel simulator produces a vector of samples having the same duration of the packet transmission time. Generated packets, successes, failures, retransmissions and delays are monitored during the temporal evolution of the simulation.

8.4.1 Adopted parameters

The simulation scenario involves a DWN with $n = 25$ nodes arranged in two topologies: a random one and a regular grid. Both topologies occupy an area corresponding to a square having an edge equal to 200 m. In the regular grid the distance between neighboring nodes is 50 m and the coverage range of each node is

DIFS	50 μs	$b_{\text{PHY\_hdr}}$	192 bits
SIFS	10 μs	$b_{\text{MAC\_hdr}}$	224 bits
$CW_{\min}$	32	b_{hdr}	$b_{\text{PHY\_hdr}}$ + $b_{\text{MAC\_hdr}}$
m	7	b_{pl}	8184 bits
m'	5	b_{RTS}	160 + $b_{\text{PHY\_hdr}}$ + b_{ts}
σ_{slot}	20 μs	b_{CTS}	112 + $b_{\text{PHY\_hdr}}$ + b_{ts}
$\mathcal{R}$	1 Mbits/s	b_{DATA}	b_{hdr} + b_{pl}
$\mathcal{R}_{\text{c}}$	1 Mbits/s	b_{ACK}	112 + $b_{\text{PHY\_hdr}}$

TABLE 8.1: PARAMETER VALUES USED IN THE SIMULATIONS.

set to 95 m. The noise power can be derived from (5.1), with $\text{SINR}_{\text{th}} = 10$ dB and $\alpha = 4$. The transmission power P_{tx} is set to 100 mW, a usual value for a notebook computer or a PDA using a standard Personal Computer Memory Card International Association (PCMCIA), or a built-in Wi-Fi adapter. The packet arrival is assumed to be a Poisson process and each source selects randomly a destination among the nodes inside its coverage range.
Performance figures are the successful packet delay and the aggregate throughput, which are obtained adopting the parameters shown in Table 8.1, where b_{hdr} represents the number of bits of the header, given by the sum of $b_{\text{MAC\_hdr}}$ and $b_{\text{PHY\_hdr}}$ denoting the number of bits of the MAC and PHY headers, respectively. Besides, in the table, b_{RTS}, b_{CTS}, b_{DATA} and b_{ACK} indicate the number of bits of the RTS, CTS, DATA and ACK packets, respectively. These parameters are selected according to the DSSS physical specifications of IEEE 802.11 legacy version [58].

8.5 Results

8.5.1 Access scheme

Fig. 8.5 shows the SCSMA/CN performance in a random topology and in a regular grid topology. The curves are obtained employing the array geometries described in Section 8.1 and using a training sequence of length $b_{\text{ts}} = 512$ bits. In the figure, the horizontal and vertical lines above the curves indicate the confidence intervals at 95%, which are determined by running 10 simulations for each point.
As one can expect, SCSMA/CN is able to provide higher throughput values with respect to the omnidirectional 802.11 DCF when a proper physical antenna system is adopted. In general, the physical CS information is employed only if an omnidirectional RTS/CTS/CN/CN exchange is sensed. This approach, in which the transmission attempts are performed independently of the interference level of

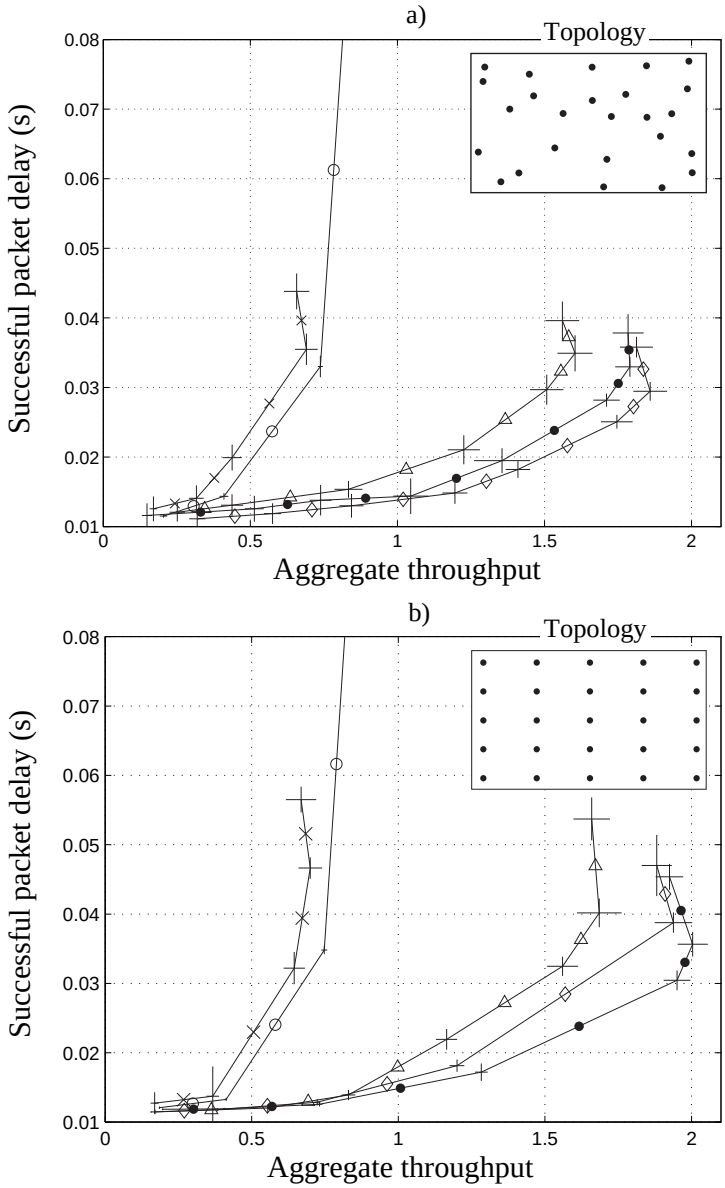

Figure 8.5: Simulated successful packet delay and aggregate throughput of IEEE 802.11 DCF and SCSMA/CN for various array geometries:
a) random topology, b) grid topology.

—×— SCSMA/CN (ULA) —△— SCSMA/CN (URA)
—●— SCSMA/CN (UCA) —◇— SCSMA/CN (CRA)
—○— IEEE 802.11 DCF

the network, is too aggressive for a ULA having only four antennas, but is effective adopting the other three array geometries. Another advantage of SCSMA/CN is the differentiation between long and short NAV, which leads to a decrease of the successful packet delay for low traffic load. In high load conditions, the finite value of the Retry Limit and the aggressiveness of the access scheme reduce the average delay for the successful packets, even if the simulations show that this improvement is obtained at a cost of a larger number of dropped packets. This behavior may be useful in real-time applications, and in scenarios in which the time constraints become more important than throughput.

8.5.2 Array geometry

Due to the limited use of CS information during the DATA/ACK exchange, the number of nodes that are authorized to communicate gets very large. In such a scenario, the network performance is mainly determined by the spatial filtering and the interference suppression capabilities of the antenna system. Among these two features, the first one depends on the FNBW and the SLL of the receiving pattern, while the second one depends on the available number of nulls as well as by their depth. In this context a key role is played by the antenna array geometry.
To emphasize the most relevant characteristics of the four geometrical configurations that are compared in this study, the typical power gain patterns generated by the four arrays for $\varphi^{\mathrm{d}} = 0^o$ in a regular grid topology are plotted in Fig. 8.6.
In both considered network topologies, the number of undesired sources that a node equipped with a ULA has to suppress is, in general, too high with respect to the number of elements of its array ($N_{\mathrm{ULA}} = 4$) and, mainly in high load conditions, the interference level is not sustainable. Moreover, φ^{FN} is large and the neighbor interferers (in terms of angle) have a high probability of lying in the region covered by the main lobe (Fig. 8.6a). Further, when the communications take place in the azimuth plane, the geometrical configuration of the radiators causes a grating lobe at 180^o with respect to the desired direction. All these drawbacks determine the poor performance of the ULA.
The higher number of elements of the URA ($N_{\mathrm{URA}} = 16$) makes this configuration more effective against interference in terms of number of available nulls as well as in terms of FNBW and SLL (Fig. 8.6b). The higher spatial filtering capabilities of the URA guarantee a more selective discrimination between desired and undesired sources, leading to higher performance. By consequence, the rectangular array receives less interference with respect to the linear one. However, the periodic arrangement of the elements of the array may create grating lobes in the radiation pattern [160]. Differently from a ULA, in which a grating lobe is always present when the communications take place in the azimuth plane, in a URA the creation or not of a grating lobe depends on the position of the desired source.

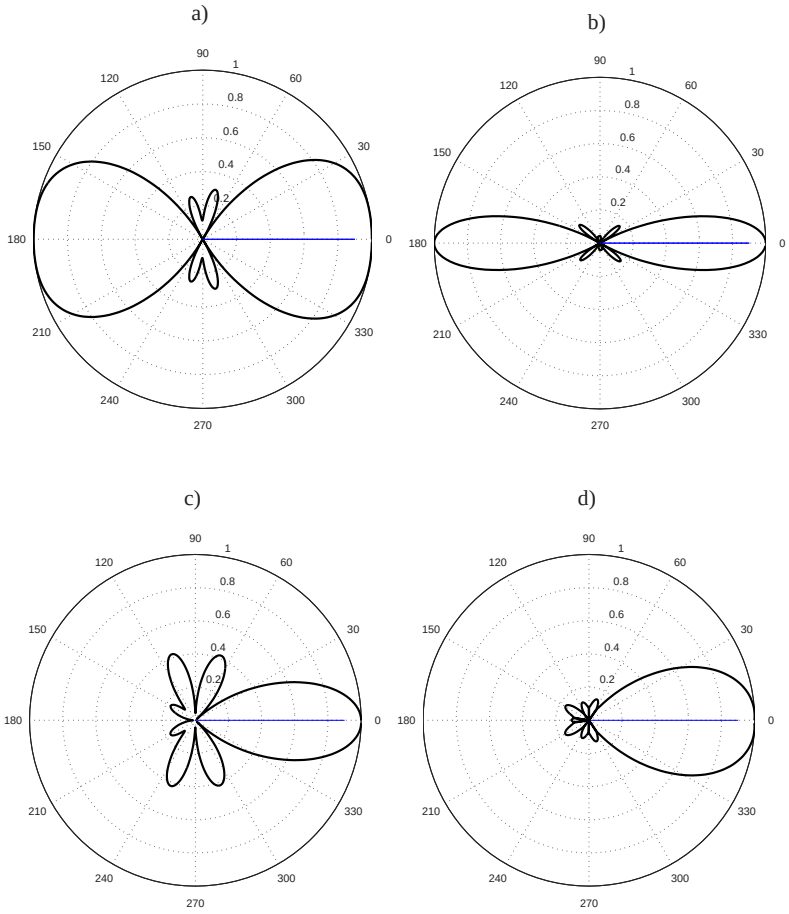

Figure 8.6: Power gain patterns in the azimuth plane:
a) ULA ($\varphi^{\mathrm{FN}} \simeq 126^o$, $\varphi^{\mathrm{3dB}} \simeq 84^o$), b) URA ($\varphi^{\mathrm{FN}} \simeq 60^o$, $\varphi^{\mathrm{3dB}} \simeq 26^o$),
c) UCA ($\varphi^{\mathrm{FN}} \simeq 86^o$, $\varphi^{\mathrm{3dB}} \simeq 36^o$), d) CRA ($\varphi^{\mathrm{FN}} \simeq 106^o$, $\varphi^{\mathrm{3dB}} \simeq 50^o$).

However, even if the rectangular configuration is less affected by this drawback, the URA seems not to be the most effective solution, given that the arbitrary scenarios in which a DWN has to operate may require the communication with nodes that lie in the same plane of the antenna array structure.
Despite the higher number of elements and the lower SLL, the performance of the URA can be lower than the performance of the geometries having a circular symmetry. In fact, given the absence of grating lobes in the azimuth plane, the systems adopting the UCA (Fig. 8.6c) and the CRA (Fig. 8.6d) may achieve a higher throughput. A direct comparison between the UCA and the CRA shows that the use of two rings does not guarantee higher immunity against interference for all network topologies. As described in [161], the concentric ring array pro-

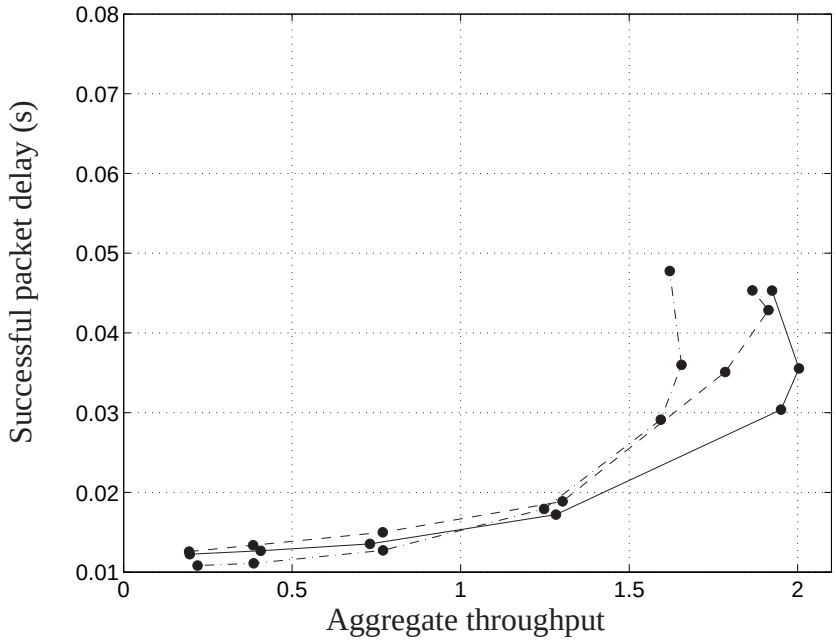

Figure 8.7: Successful packet delay as a function of the aggregate throughput for various training sequence lengths in a grid topology adopting the UCA ($\hat{\sigma}_{\varphi} = 0^{o}$). $b_{\mathrm{ts}} = 128$bits $b_{\mathrm{ts}} = 512$bits $b_{\mathrm{ts}} = 1024$bits

vides a lower SLL and a wider FNBW with respect to the uniform circular array. Actually, the inner ring of the CRA reduces the interelement spacing, leading to a wider beamwidth, but also to a reduction of the level of the minor lobes. These characteristics are advantageous in the random topology [117]. Conversely, the higher interelement spacing of the UCA causes higher side-lobe levels and a narrower beamwidth, leading to better performance in the grid topology. Therefore, the choice between a physical antenna system producing a narrow beam and a physical antenna system producing low side-lobe levels seems to be dependent on the network topology.

8.5.3 Training sequence

To determine the effects of the training sequence length on the performance of the DWN, a set of simulations is executed in the grid topology, adopting the UCA and varying the size of the CN packets (Fig. 8.7).
As shown in the figure, there is a tradeoff between the overhead introduced by using long training sequences and the interference suppression capabilities of the antenna system. The length of the training sequence has a direct impact on two

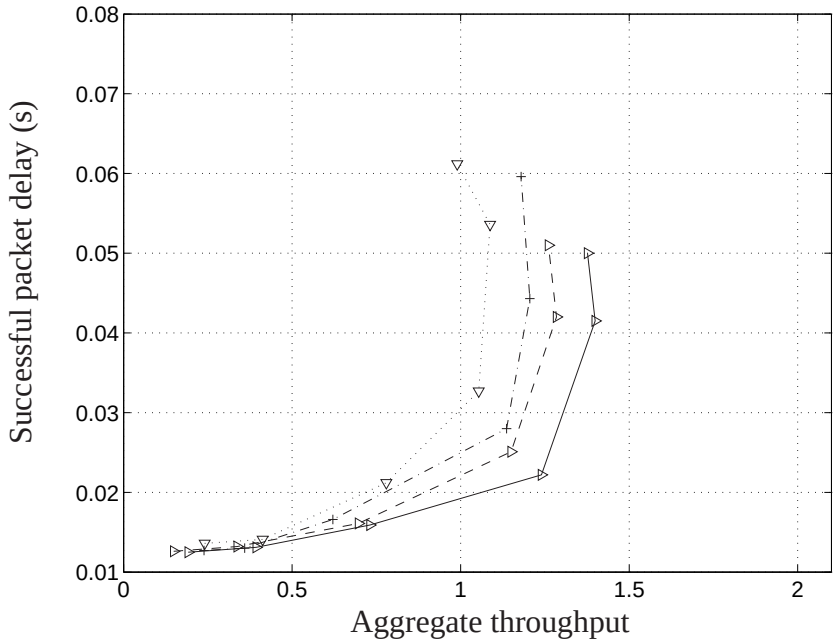

Figure 8.8: Successful packet delay as a function of the aggregate throughput in multipath fading environment adopting the UCA in a grid topology ($b_{\mathrm{ts}} = 512$ bits, $\hat{\sigma}_{\varphi} = 1^{o}$).
$|\vec{\mathrm{v}}| = 0$ km/h $|\vec{\mathrm{v}}| = 2$ km/h
$|\vec{\mathrm{v}}| = 5$ km/h $|\vec{\mathrm{v}}| = 10$ km/h

aspects of the pattern nulls: the accuracy of their steering and their depth. In particular, as the training sequence becomes longer, deeper nulls are more accurately placed. It follows that, the higher values of the successful packet delay for $b_{\mathrm{ts}} = 128$ bits and, respectively, $b_{\mathrm{ts}} = 1024$ bits, compared with the more effective length $b_{\mathrm{ts}} = 512$ bits, are due to opposite reasons. For $b_{\mathrm{ts}} = 128$ bits, the nulls are not very deep and are placed in an unprecise way. This implies that the receiving node has poor resistance against the interference, leading to an increase of the transmission failures that, in turn, increases the number of retransmissions. Conversely, for $b_{\mathrm{ts}} = 1024$ bits, deeper nulls are precisely placed. This guarantees higher immunity against interference, but the duration of the entire handshake requires longer time.

8.5.4 Multipath fading

The joint effects of multipath and mobility are shown in Fig. 8.8. The results are obtained using the UCA in the grid topology with a maximum angular spread

$\hat{\sigma}_{\varphi}^{\max} = \max_{0 \le l \le n_{\mathrm{tx}}} \hat{\sigma}_{\varphi_l} = 1^o$ and a training sequence of 512 bits.
As expected, in a single-hop scenario with a fixed bit rate, the performance decreases as the mobility increases. A higher node speed lowers the throughput, because of the faster fluctuations of the desired signal power. This degradation is emphasized by the assumption that the correct reception of a packet is established using a threshold criterion, which determines the discarding of the packet even if a single bit is received incorrectly. It is worth noting that, when an interferer falls into a deep fade, a higher SINR can be experienced by the destination, but other active nodes may produce a higher interference for a certain amount of time. By consequence, the average value of the undesired power can be considered almost constant and, in the time domain, the multipath fading experienced by the interferers does not give appreciable advantages. Instead, when the desired signal falls in a deep fade, the entire packet can be lost (unless a suitable error correcting code is used). Therefore, in the time domain, multipath fading of the desired source is harmful, while multipath fading of the interferers has negligible effects.
The maximum angular spread value that has been adopted in this set of simulations is obtained using a ring of scatterers having radius $\tilde{d} \cong 1.24$ m, which leads to a maximum delay between the signal replicas equal to $\Delta\bar{\tau}_{\max} = 2\tilde{d}/v_{\mathrm{c}} \cong 8$ ns. Therefore, being $\hat{\sigma}_{\tau} < \Delta\bar{\tau}_{\max} << T_{\mathrm{s}} = 1/\mathcal{R} = 1$ μs and $\hat{\sigma}_{\varphi}^{\max} << \varphi^{3\mathrm{dB}} = 36^o$ (Fig. 8.6c), the hypothesis of low-rank channel is largely satisfied. Besides, being the maximum Doppler spread equal to 69 Hz, the condition $f^{\mathrm{d}}\hat{\sigma}_{\tau} < 1$, for an underspread channel, is satisfied too. By consequence, the adopted propagation scenario cannot be considered particularly hostile. Despite this fact, the performance of DWNs using smart antennas are affected by interferer angular spreading (azimuth domain) and desired signal fading (time domain).

8.6 Summary

The results obtained from the discrete-time simulations put into evidence that, in a DWN using smart antennas, the geometries with circular symmetry (UCA, CRA) are more effective for reducing the interference with respect to the periodic configurations (ULA, URA). This aspect is emphasized by the adopted scenario, where the network activity takes place in the azimuth plane, which coincides with the plane where antenna arrays lie. It is not to exclude that, in a three-dimensional scenario, the URA may provide better performance thanks to its planar geometry and its higher number of radiators. However, the main conclusion that can be inferred from the presented investigation is that the better choice for the array geometry of an adaptive antenna is dependent on the network topology.
The numerical results show also that a higher throughput and a lower successful packet delay can be obtained when the length of the training sequence is selected

properly. Its value should guarantee an acceptable overhead as well as an accurate steering and a sufficient depth of the nulls.
Finally, the simulations in a mobile scenario confirm that a degradation of the performance can be present even if the propagation environment is not particularly hostile, as it is a low-rank underspread channel.

Part III

Antenna Array Synthesis Techniques

Chapter 9

Exploitation of Spatial Channel Model for Antenna Array Synthesis

This chapter presents a technique to modify the radiation pattern of an antenna array in order to reject interference in a certain angular region. This technique exploits the knowledge of the channel statistic in the azimuth domain to properly choose the position of a certain number of nulls. The method of projections is used to modify the excitation phases in order to generate the antenna array pattern. The presented algorithm requires low Central Processing Unit (CPU) time to perform the synthesis and can be applied to reject multiple undesired sources with different distributions of the DOAs.[1]

9.1 Introduction

As shown in Section 3.5, a large number of methods that consider the modification of the current excitations in amplitude and phase has been proposed in the literature in order to synthesize the radiation pattern produced by an antenna array to reject interference. However, even if the algorithms that perform both phase and amplitude weighting are able to maximize the SINR at the antenna array output, they need considerable implementation efforts and expensive hardware [138,143]. Besides, from the practical point of view, the synthesis techniques that require only the modification of the excitation phases may be preferable for many systems that are not able to perform amplitude weighting. Therefore, several phase-only algorithms have been developed to synthesize patterns satisfying side-lobe level,

[1]The content of this chapter is based on M. Comisso and R. Vescovo, "Exploitation of Spatial Channel Model for Antenna Array Synthesis," Electronics Letters, Vol. 42, No. 19, pp. 1079–1080, 14$^{\text{th}}$ Sep. 2006 [177].

beamwidth and null constraints [37–43].
An interesting theoretical analysis of the problem of SINR maximization with equal amplitude constraint is performed in [37], where the author presents two methods for phase-only adaptive nulling. A deterministic approach, suitable for linear arrays, is proposed in [38], where the Taylor expansion of the array factor is used to solve the null synthesis problem. In [39], the authors describe a genetic algorithm to modify the phases of a uniform linear array in order to place a certain number of nulls towards the undesired sources, while limiting the perturbation on the far-field pattern. A genetic technique is also adopted in [40], where a fast method is proposed to suppress the interference incoming from multiple wide angular regions. Two iterative fast methods, based on the minimization of a non-negative cost function, are described in [41]. Among the large number of possible approaches, a simple and versatile technique to update the array excitations is the method of projections [43, 162–165], which can be applied to the problem of phase-amplitude weighting as well as for amplitude-only or phase-only weighting. In the method of projections the synthesis is performed adopting an intersection approach involving proper projection operators that can be defined to satisfy the desired constraints.
As widely discussed in Section 2.2, a generic undesired source does not reach the destination from a unique DOA, but from a set of directions distributed in the angular domain. To mitigate the interference in such scenario, the classical approaches perform the array synthesis imposing a global mask [163] or a local rectangular mask [164], providing a pattern that lies below a given threshold within the interfered region. However, the recent advances in propagation channel modeling provide useful and more precise information regarding the signal statistic in the azimuth domain [19–23]. By consequence, the use of a constant threshold may be unrealistic, resulting in too severe or too weak local constraints. Besides, forming exact nulls in the pattern requires less computational time than imposing an upper bound in an angular region [43, 165].
From these considerations, it would be interesting to develop a computationally efficient algorithm able to exploit the spatial statistic of the channel for interference suppression purposes. A synthesis technique satisfying these requirements and based on the above cited method of projections is presented in the following of this chapter.

9.2 Problem formulation

With reference to a cartesian system $O(x, y, z)$, the far-field pattern of an antenna array of N elements, in the generic direction of the $x - y$ plane, can be written as

a function of the complex vector of the excitation currents $\mathbf{w}$ as:

$$E(\mathbf{w},\varphi)=\sum_{k=1}^{N} w_k \mathcal{E}_k(\varphi) e^{j\frac{2\pi}{\lambda} r_k \cos(\varphi-\varphi_k)}, \tag{9.1}$$

where, according to the notation of Section 1.3, $\mathcal{E}_k(\varphi)$ is the field pattern of the k-th array element, r_k and φ_k represent the position of the k-th radiator in polar coordinates. Assuming a mean-square norm $||.||$, defined in the space of the array patterns given by (9.1), the problem is the minimization of the distance:

$$\beth^2(\mathbf{w}) = ||E(\mathbf{w}) - E[\mathbf{w}(0)]||^2 = \int_{-\gamma_\mathrm{b}}^{\gamma_\mathrm{b}} |E(\mathbf{w},\varphi) - E[\mathbf{w}(0),\varphi]|^2 \,\mathrm{d}\varphi, \tag{9.2}$$

subject to the constraints:

$$|E(\mathbf{w},\varphi)| \le K_l \varrho^l_{\mathrm{DOA}}(\varphi), \quad \forall\varphi : \varphi^l_{\mathrm{in}} \le \varphi \le \varphi^l_{\mathrm{fin}}, \quad l=1,...,n_{\mathrm{int}}, \tag{9.3a}$$

$$|w_k| = |w_k(0)|, \qquad k=1,...,N, \tag{9.3b}$$

where $E[\mathbf{w}(0),\varphi] = E_0(\varphi)$ is the starting pattern (corresponding to iteration number 0), γ_b is a suitable constant (e.g., $\gamma_\mathrm{b}=\pi/2$ for a linear array, $\gamma_\mathrm{b}=\pi$ for a circular array), n_{int} is the number of interferers, K_l is a constant taking into account the amplitude of the l-th interferer, $\varrho^l_{\mathrm{DOA}}(\varphi)$ is the pdf of the DOA of the l-th interferer in the angular region defined by the bounds φ^l_{in} and φ^l_{fin}.

9.3 Projection operators

The basic idea of the presented method is to substitute the constraint (9.3a) by the constraint:

$$E(\mathbf{w},\varphi^{\mathrm{n}}_{l'}) = 0, \qquad l'=1,...,M, \tag{9.4}$$

with a proper selection of the positions of the $M=\sum_{l=1}^{n_{\mathrm{int}}} M_l$ nulls, where M_l denotes the number of nulls employed to suppress the l-th interferer and $\varphi^{\mathrm{n}}_{l'}$ represents the l'-th null. The problem of minimizing $\beth^2(\mathbf{w})$ subject to the constraints (9.4) and (9.3b) has been already solved in [43, 166] using the method of projections.

In general, a projector $\mathcal{P}$ over a closed nonempty subset Θ, included in a Hilbert space $\mathcal{U}$, is defined as:

$$\mathcal{P} : \mathbf{u}(\in\mathcal{U}) \to \tilde{\mathbf{u}}(\in\Theta) : ||\mathbf{u}-\tilde{\mathbf{u}}|| \le ||\mathbf{u}-\mathbf{u}'||, \ \forall\mathbf{u}'\in\Theta. \tag{9.5}$$

Therefore, the projector $\mathcal{P}$ identifies the point $\tilde{\mathbf{u}}=\mathcal{P}\mathbf{u}(\in\Theta)$ nearest to $\mathbf{u}$. If Θ is convex $\tilde{\mathbf{u}}$ is unique, while, for nonconvex sets, more than one $\tilde{\mathbf{u}}$ may exist.

In [43], the synthesis process starts from $E_0(\varphi)$ and performs a sequence of alternate projections onto the sets Θ_{null} and Θ_{mod}, containing the patterns satisfying (9.4) and (9.3b), respectively. Defining as $\Theta_{\text{AF}}(\supset \Theta_{\text{mod}} \cup \Theta_{\text{null}})$ the space of array factors that satisfy (9.1), the pattern at i-th iteration is calculated as:

$$E[\mathbf{w}(i), \varphi] = \mathcal{P}_{\text{mod}} \mathcal{P}_{\text{null}} E[\mathbf{w}(i-1), \varphi], \tag{9.6}$$

where $\mathcal{P}_{\text{mod}}$ is the projector from Θ_{AF} onto Θ_{mod}, and $\mathcal{P}_{\text{null}}$ is the projector from Θ_{AF} onto Θ_{null}. Moving from the pattern $E[\mathbf{w}(i-1), \varphi] \in \Theta_{\text{AF}}$, corresponding to the $(i-1)$-th iteration, the projector $\mathcal{P}_{\text{null}}$ identifies an element $E[\mathbf{w}^1(i), \varphi] \in \Theta_{\text{null}}$ that minimizes the distance $||E[\mathbf{w}^1(i)] - E[\mathbf{w}(i-1)]||^2$ subject to the constraint (9.4). According to [166], the excitations $\mathbf{w}^1(i)$ of the pattern obtained using the projector $\mathcal{P}_{\text{null}}$ can be evaluated as:

$$\mathbf{w}^1(i) = [\mathbf{I}_N - \tilde{\mathbf{A}}^{\dagger} \tilde{\mathbf{A}}] \mathbf{w}(i-1), \tag{9.7}$$

where $\tilde{\mathbf{A}} = [\tilde{A}_{l'k}]$, with $\tilde{A}_{l'k} = \mathcal{E}_k(\varphi^{\text{n}}_{l'}) e^{j\frac{2\pi}{\lambda} r_k \cos(\varphi^{\text{n}}_{l'} - \varphi_k)}$, and $\tilde{\mathbf{A}}^{\dagger} = (\tilde{\mathbf{A}}^H \tilde{\mathbf{A}})^{-1} \tilde{\mathbf{A}}^H$ is the pseudoinverse of matrix $\tilde{\mathbf{A}}$. The projector $\mathcal{P}_{\text{mod}}$, instead, minimizes the distance $||E[\mathbf{w}(i)] - E[\mathbf{w}^1(i)]||^2$ subject to the constraint (9.3b), where the excitations $\mathbf{w}(i)$ can be calculated as:

$$w_k(i) = |w_k(0)| e^{j \arg[w^1_k(0)]}, \qquad k = 1, ..., N, \tag{9.8}$$

and $\arg(.)$ is the argument function. The distance between the pattern synthesized at the i-th iteration $E[\mathbf{w}(i)]$ and the set Θ_{null} gets lower as i increases, leading to deeper nulls in the prescribed directions.

9.4 Exploitation of the spatial channel model

The operations performed by the projector $\mathcal{P}_{\text{null}}$ can be extended in order to impose the local masks on the starting pattern. The constraint (9.3a) can be satisfied, for the l-th interferer, by selecting the angular position of the M_l nulls to avoid that the local maxima of the side lobes of the generated pattern overcome the local mask $K_l \varrho^l_{\text{DOA}}(\varphi)$ inside the angular region bounded by φ^l_{in} and φ^l_{fin}. To simplify the description, it is assumed that the angular regions covered by local masks relative to different interferers are disjoint. However, this hypothesis does not reduce the field of application of the proposed algorithm, because the superposition of two (or more) masks leads simply to a new interference mask with a modified shape. Besides, to improve the readability of the presented expressions, the position of a generic null is indicated by $\varphi^{\text{n}}_{l,q_l}$. This notation identifies the q_l-th null relative to the l-th interferer. The subindex l accounts for the fact that M_l is,

in general, different for each interferer and so the terms $\varphi^{\mathrm{n}}_{l,q_l}$ cannot be arranged in a rectangular matrix. According to this notation and to the hypothesis of disjoint masks, the nulls can be ordered as:

$$-\pi \leq \varphi^{\mathrm{n}}_{1,1} < ... < \varphi^{\mathrm{n}}_{1,q_1} < ... < \varphi^{\mathrm{n}}_{1,M_1} < \varphi^{\mathrm{n}}_{2,1} < ... < \varphi^{\mathrm{n}}_{l,q_l} < ... < \varphi^{\mathrm{n}}_{n_{\mathrm{int}},M_{n_{\mathrm{int}}}} \leq \pi. \quad (9.9)$$

The position of the M_l nulls required to suppress the l-th interferer can be evaluated from the following system of M_l equations:

$$\begin{cases} \displaystyle\int_{\varphi^l_{\mathrm{in}}}^{\varphi^{\mathrm{n}}_{l,1}} \varrho^l_{\mathrm{DOA}}(\varphi)\mathrm{d}\varphi = \frac{1}{M_l+1} \\ \displaystyle\int_{\varphi^{\mathrm{n}}_{l,1}}^{\varphi^{\mathrm{n}}_{l,2}} \varrho^l_{\mathrm{DOA}}(\varphi)\mathrm{d}\varphi = \frac{1}{M_l+1} \\ \qquad\qquad . \\ \qquad\qquad . \\ \qquad\qquad . \\ \displaystyle\int_{\varphi^{\mathrm{n}}_{l,M_l-1}}^{\varphi^{\mathrm{n}}_{l,M_l}} \varrho^l_{\mathrm{DOA}}(\varphi)\mathrm{d}\varphi = \frac{1}{M_l+1} \end{cases} \quad (9.10)$$

Remembering that $\displaystyle\int_{\varphi^l_{\mathrm{in}}}^{\varphi^l_{\mathrm{fin}}} \varrho^l_{\mathrm{DOA}}(\varphi)\mathrm{d}\varphi = 1$, (9.10) provides the position of the nulls in order to obtain regions of equal area below the pdf. Being the pdf the derivative of the cumulative distribution function (cdf), this is equivalent to subdividing the azimuth domain of the interference in equal probability regions. This leads to concentrate the nulls where the interference is stronger and to reduce their number where the interference is weaker.
Using the notation introduced in (9.9), the system of M equations that provides the positions of the nulls required to suppress all the n_{int} interferers can be written in compact form as:

$$\int_{\varphi^{\mathrm{n}}_{l,q_l-1}}^{\varphi^{\mathrm{n}}_{l,q_l}} \varrho^l_{\mathrm{DOA}}(\varphi)\mathrm{d}\varphi = \frac{1}{M_l+1}, \qquad q_l = 1, ..., M_l\,, \;\; l = 1, ..., n_{\mathrm{int}}, \quad (9.11)$$

where $\varphi^{\mathrm{n}}_{l,0} = \varphi^l_{\mathrm{in}}$ is defined for calculation purposes. In general, this system can be numerically solved once the pdfs are known, but for some statistics the position of the nulls can be calculated in closed form. In particular, this is possible, of course, for the uniform density, but also for the widely employed truncated Laplacian pdf as well as for the ring of scatterers distribution in low-rank environment.

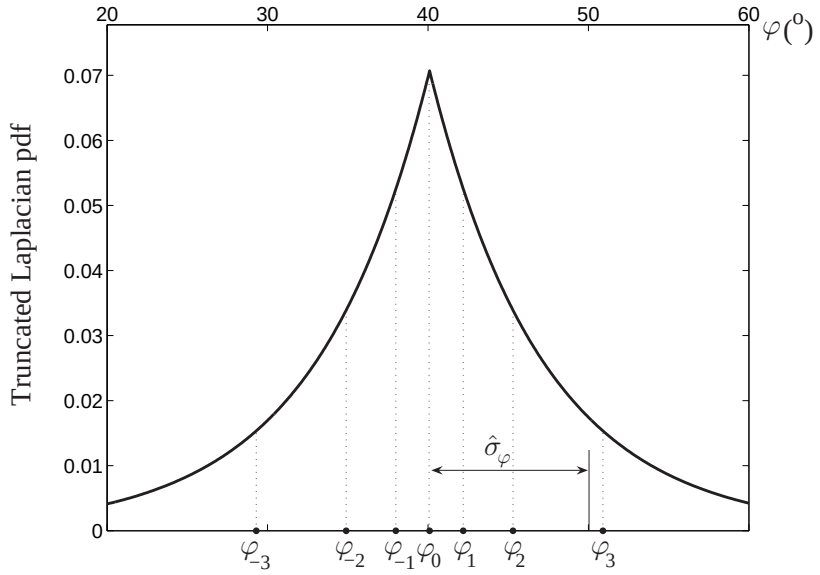

Figure 9.1: Position of the nulls for $M_1 = 7$ on a Laplacian pdf with $\hat{\sigma}_\varphi = 10^o$.

Assume $n_{\text{int}} = 1$ ($M = M_1$) and $\varphi^{\text{n}}_{1,q_1} = \varphi^{\text{n}}_q$ to simplify the notation. For the uniform pdf, the nulls are equally spaced according to:

$$\varphi^{\text{n}}_q = \varphi^1_{\text{in}} + q\,\frac{\varphi^1_{\text{fin}} - \varphi^1_{\text{in}}}{M+1}, \qquad q = 1, ..., M \tag{9.12}$$

and their displacement is equivalent to the adoption of a rectangular mask [43].
In the more realistic scenario of a truncated Laplacian distribution, the nulls can be obtained by substituting (5.7) in (9.10) with $\varphi^1_{\text{in}} = \varphi_0 - \pi/2$ and $\varphi^1_{\text{fin}} = \varphi_0 + \pi/2$. After some manipulations and exploiting the symmetry properties of this pdf, the nulls can be expressed as:

$$\varphi^{\text{n}}_q = \varphi_0 - \frac{\hat{\sigma}_\varphi}{\sqrt{2}}\,\text{sgn}(q)\log\left[1 - \frac{2|q|}{(M+1)\gamma_{\text{L}}}\right], \tag{9.13}$$

for $q = -\dfrac{M-1}{2}, ..., \dfrac{M-1}{2}$ and M odd, and:

$$\varphi^{\text{n}}_q = \varphi_0 - \frac{\hat{\sigma}_\varphi}{\sqrt{2}}\,\text{sgn}(q)\log\left[1 - \frac{2|q|-1}{(M+1)\gamma_{\text{L}}}\right], \tag{9.14}$$

for $q = -\dfrac{M}{2}, ..., -1, 1, ..., \dfrac{M}{2}$ and M even, where $\text{sgn}(.)$ is the sign function. Therefore, for a truncated Laplacian pdf, constraint (9.3a) is replaced by (9.4),

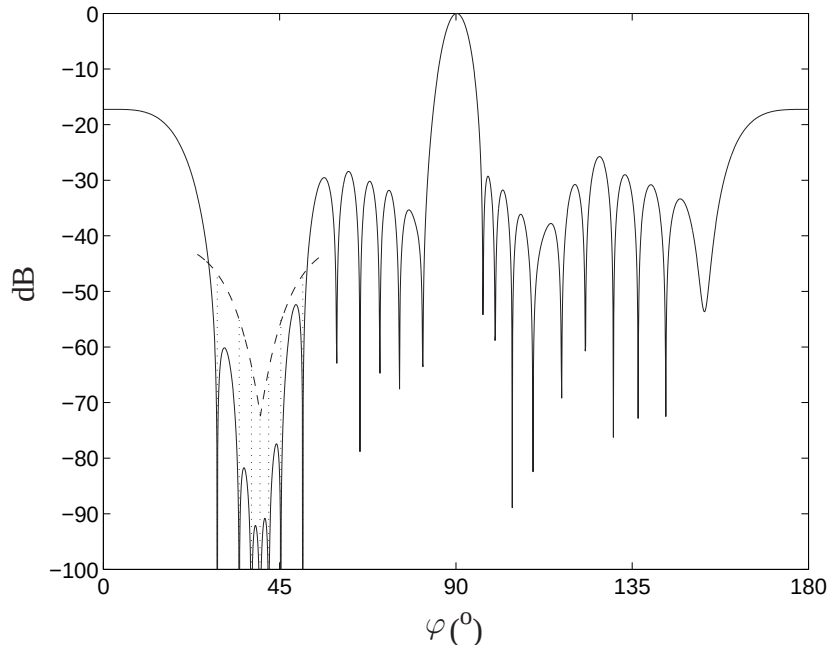

Figure 9.2: Modified power gain pattern in presence of one interferer with a Laplacian pdf with $\hat{\sigma}_{\varphi} = 10^{o}$.
---- Local mask of the interferer
—— Modified pattern

where the nulls are selected according to (9.13) or (9.14).
The nulls for the ring of scatterers distribution in a low-rank scenario can be derived using (2.21), (5.3) and (9.10) with $\varphi_{\text{in}}^{1} = \varphi_0 - \gamma_{\text{m}_1}$ and $\varphi_{\text{fin}}^{1} = \varphi_0 + \gamma_{\text{m}_1}$. Performing some algebra, one can obtain:

$$\varphi_q^{\text{n}} = \varphi_0 + \gamma_{\text{m}_1} \sin\left(q\,\frac{\pi}{M+1} + \frac{1}{2}\right), \qquad q = 1, ..., M. \tag{9.15}$$

Even if not explicitly addressed in this study, the presented method can be extended to take into account mutual coupling effects by suitably modifying each element pattern $\mathcal{E}_k(\varphi)$ in (9.1) [165].

9.5 Numerical results

The first numerical example is obtained for a uniform linear array of $N = 28$ omnidirectional elements, with interelement spacing equal to $\lambda/2$. The interference

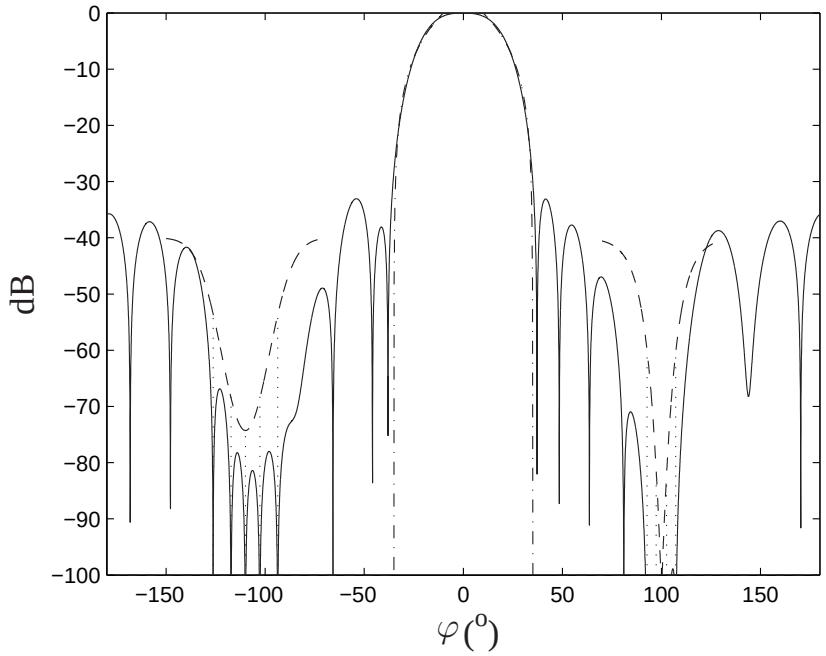

Figure 9.3: Modified power gain pattern in presence of two interferers: the first with a Gaussian pdf with $\hat{\sigma}_{\varphi_1} = 12^o$, and the second with a Laplacian pdf with $\hat{\sigma}_{\varphi_2} = 8^o$.
-·-·- Global mask for the starting pattern
- - - - Local masks of the interferers
—— Modified pattern

scenario involves a unique undesired source around the mean DOA $\varphi_0 = 40^o$ that is suppressed using $M_1 = 7$ nulls and choosing as starting point a 40 dB Chebyshev pattern. The nulls are placed according to (9.13) and the angular spread is chosen equal to 10^o (Fig. 9.1). The power gain pattern $G(\varphi) = |E(\mathbf{w}, \varphi)|^2$ is reported in Fig. 9.2. The figure shows that the lobes in the null region are shaped according to the local mask (dashed line).
The second example is obtained using a UCA of $N = 30$ omnidirectional elements, having radius equal to $\rho_c = 1.8\lambda$. The starting pattern is calculated by approximating a global mask (dash-dotted line) in the mean square sense, according to the method presented in [167]. This example involves two regions of interference, the former having a Gaussian pdf with $\hat{\sigma}_{\varphi_1} = 12^o$ around $\varphi_{0_1} = -110^o$, and the latter having a Laplacian pdf with $\hat{\sigma}_{\varphi_2} = 8^o$ around $\varphi_{0_2} = 100^o$. Fig. 9.3 shows the modified pattern, obtained employing $M_1 = M_2 = 5$ nulls to shape each region. The results reveal that the proposed technique can be employed to

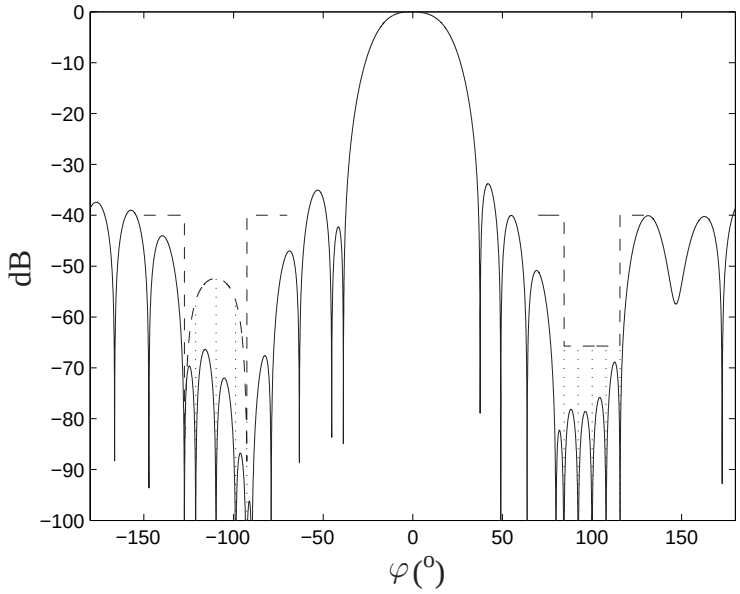

Figure 9.4: Modified power gain pattern in presence of two interferers both having a DOA statistic corresponding to the ring of scatterers with $\hat{\sigma}_{\varphi_1} = 12^o$ and $\hat{\sigma}_{\varphi_2} = 8^o$.
---- Local masks of the interferers
—— Modified pattern

simultaneously reject the interference incoming from regions with different statistics. In this case, the positions of the five nulls for the Gaussian pdf are evaluated by numerically solving (9.10).
The third example is obtained using the same parameters of the previous one, except for the pdfs of the interferers. The statistic of the first undesired source is chosen according to the ring of scatterers model and the corresponding nulls are evaluated using (9.15), while a uniform distribution is selected for the second interferer and the nulls are calculated from (9.12). The synthesized pattern, shown in Fig. 9.4, confirms that, adopting the presented method, the minor lobes can be shaped according to the local masks by controlling the density of the nulls as a function of the statistics of the interferers.

9.6 Considerations and summary

It can be noticed that the requirement at the boundaries of the dashed masks is difficult to satisfy. However, these boundaries correspond to the regions with lower

probability of incoming interference, while the regions with larger probability are effectively suppressed. An interesting advantage of the presented synthesis technique is related to the CPU time required to obtain the patterns. In particular, in the first example the excitation phases are calculated in approximately 0.91 seconds, while in the second and in the third example they are calculated in approximately 2.32 seconds. These times are obtained using a common laptop equipped with an Intel Pentium 4 processor at 2.8 GHz. Therefore, the presented method represents a fast technique to reject interference exploiting the channel statistic in the angular domain. This technique, based on the method of projections, performs the local shaping of the pattern by phase-only control. Besides, adopting antenna arrays with a sufficient number of elements, the method can be used to suppress multiple undesired sources spread over wide angular regions and with different statistical distributions.

Chapter 10

Multi-Beam and Null Synthesis of Antenna Arrays by Phase-Only Control

This chapter presents an iterative method for the synthesis of the radiation pattern produced by an antenna array of arbitrary geometry. By modifying only the excitation phases, the method is able to produce patterns with multiple prescribed main lobes and nulls, while limiting the side-lobe level. The technique is based on the minimization of a weighted cost function that takes into account multiple objectives. The presented algorithm can be easily implemented and requires a low CPU time to perform the pattern synthesis.[1]

10.1 Introduction and problem formulation

As discussed in the previous chapters, the recent adoption of the SDMA technique in several communication systems has increased the interest of the research community in the development of fast and efficient beamforming algorithms. These algorithms must be able to produce radiation patterns with multiple main lobes and multiple prescribed nulls, and, for some practical applications, should be able to perform the synthesis by controlling the sole phases of the current excitations. Among the large number of available phase-only techniques, the solutions that produce patterns with multiple main lobes are usually developed for arrays having a large number of radiators [168–169]. Recently, a phase-only method able to

[1]The content of this chapter is based on M. Comisso and R. Vescovo, "Multi-Beam Synthesis with Null Constraints by Phase Control for Antenna Arrays of Arbitrary Geometry," Electronics Letters, Vol. 43, No. 7, pp. 374–375, 29th Mar. 2007 [178].

perform multi-beam synthesis as well as null steering, and suitable for arrays with few elements, has been proposed in [42]. This technique, which enables SDMA in wireless communication networks, is based on Sequential Quadratic Programming (SQP) algorithm and is applied to ULAs.
This chapter presents a phase-only synthesis method, able to produce patterns with multiple prescribed main lobes and nulls, which can be applied to antenna arrays of arbitrary geometry. The analyzed problem can be formulated as follows. According to the reference system and the notation described in Section 9.2, the far-field pattern of an antenna array of N elements can be written as:

$$E(\mathbf{w},\varphi) = \sum_{k=1}^{N} w_k \tilde{f}_k(\varphi), \tag{10.1}$$

where $\tilde{f}_k(\varphi) = \mathcal{E}_k(\varphi) e^{j\frac{2\pi}{\lambda} r_k \cos(\varphi-\varphi_k)}$. The objective is to solve the following synthesis problem. Determine an array pattern $E(\mathbf{w},\varphi)$ such that:

- n_{des} maxima are placed in the positions $\varphi_1^{\mathrm{d}}, ..., \varphi_{n_{\mathrm{des}}}^{\mathrm{d}}$, (10.2a)
- n_{int} nulls are placed in the positions $\varphi_1^{\mathrm{n}}, ..., \varphi_{n_{\mathrm{int}}}^{\mathrm{n}}$, (10.2b)
- the gain is as low as possible in the other directions, (10.2c)
- all the excitation currents have equal amplitude, so it can be assumed $|w_1| = |w_2| = ... = |w_N| = 1$ without loss of generality. (10.2d)

10.2 Synthesis technique

In order to satisfy the requirements (10.2), it is proposed to minimize the following weighted cost function:

$$\begin{aligned} \beth^2(\mathbf{w}) \triangleq & - \sum_{l=1}^{n_{\mathrm{des}}} g_l \left| E(\mathbf{w},\varphi_l^{\mathrm{d}}) \right|^2 \\ & + g_{n_{\mathrm{des}}+1} \sum_{l,l'=1}^{n_{\mathrm{des}}} \left| E(\mathbf{w},\varphi_l^{\mathrm{d}}) - E(\mathbf{w},\varphi_{l'}^{\mathrm{d}}) \right|^2 \\ & + g_{n_{\mathrm{des}}+2} \sum_{l=1}^{n_{\mathrm{int}}} \left| E(\mathbf{w},\varphi_l^{\mathrm{n}}) \right|^2 \\ & + g_{n_{\mathrm{des}}+3} \left\| E(\mathbf{w}) \right\|^2, \end{aligned} \tag{10.3}$$

where the real non-negative numbers g_l represent the weights of the cost function and can be joined in the vector $\mathbf{g} = [g_1, ..., g_{n_{\mathrm{des}}}, g_{n_{\mathrm{des}}+1}, g_{n_{\mathrm{des}}+2}, g_{n_{\mathrm{des}}+3}]$. The

squared norm $\|E(\mathbf{w})\|^2 = \langle E(\mathbf{w}), E(\mathbf{w})\rangle$ is defined adopting the scalar product:

$$\langle \tilde{f}_k, \tilde{f}_{k'} \rangle = \int_{-\gamma_\mathrm{b}}^{\gamma_\mathrm{b}} \tilde{f}_k(\varphi)\tilde{f}^*_{k'}(\varphi)\mathrm{d}\varphi, \tag{10.4}$$

where, as described in Section 9.2, γ_b represents a constant dependent on the array geometry. The first summation in (10.3) has the aim of forming the n_des required maxima (constraint (10.2a)), the second summation imposes that the difference between the different maxima be sufficiently low, while the third and the fourth summations impose conditions (10.2b) and (10.2c), respectively. Using (10.1) and (10.4), after some manipulations the cost function can be rewritten as:

$$\begin{aligned}
\beth^2(\mathbf{w}) = & \sum_{k,k'=1}^{N} w_k w^*_{k'} \underbrace{\left[-\sum_{l=1}^{n_\mathrm{des}} g_l \tilde{f}_k(\varphi^\mathrm{d}_l)\tilde{f}^*_{k'}(\varphi^\mathrm{d}_l) \right]}_{Z^\mathrm{des}_{k'k}} \\
& + \sum_{k,k'=1}^{N} w_k w^*_{k'} \underbrace{\left\{ g_{n_\mathrm{des}+1} \sum_{l,l'=1}^{n_\mathrm{des}} \left[\tilde{f}_k(\varphi^\mathrm{d}_l) - \tilde{f}_k(\varphi^\mathrm{d}_{l'}) \right] \cdot \left[\tilde{f}_{k'}(\varphi^\mathrm{d}_l) - \tilde{f}_{k'}(\varphi^\mathrm{d}_{l'}) \right]^* \right\}}_{\tilde{Z}^\mathrm{des}_{k'k}} \\
& + \sum_{k,k'=1}^{N} w_k w^*_{k'} \underbrace{\left[g_{n_\mathrm{des}+2} \sum_{l=1}^{n_\mathrm{int}} \tilde{f}_k(\varphi^\mathrm{n}_l)\tilde{f}^*_{k'}(\varphi^\mathrm{n}_l) \right]}_{Z^\mathrm{int}_{k'k}} \\
& + \sum_{k,k'=1}^{N} w_k w^*_{k'} \underbrace{\left[g_{n_\mathrm{des}+3} \int_{-\gamma_\mathrm{b}}^{\gamma_\mathrm{b}} \tilde{f}_k(\varphi)\tilde{f}^*_{k'}(\varphi)\mathrm{d}\varphi \right]}_{Z^\mathrm{SLL}_{k'k}} \\
= & \sum_{k,k'=1}^{N} w_k w^*_{k'} Z_{k'k},
\end{aligned} \tag{10.5}$$

where $Z_{k'k} = Z^\mathrm{des}_{k'k} + \tilde{Z}^\mathrm{des}_{k'k} + Z^\mathrm{int}_{k'k} + Z^\mathrm{SLL}_{k'k}$. Imposing the equal amplitude constraint in (10.2d), the excitation currents can be written as $w_k = e^{j\phi_k}$, where ϕ_k represents the excitation phase of the k-th array element. By consequence, (10.5) can be expressed as:

$$\beth^2(\Phi) = \sum_{k,k'=1}^{N} e^{j(\phi_k - \phi_{k'})} Z_{k'k}, \tag{10.6}$$

where $\Phi = [\phi_1, ..., \phi_N]$. As the matrices $\mathbf{Z}^{\mathrm{des}} = [Z^{\mathrm{des}}_{k'k}]$, $\tilde{\mathbf{Z}}^{\mathrm{des}} = [\tilde{Z}^{\mathrm{des}}_{k'k}]$, $\mathbf{Z}^{\mathrm{int}} = [Z^{\mathrm{int}}_{k'k}]$, $\mathbf{Z}^{\mathrm{SLL}} = [Z^{\mathrm{SLL}}_{k'k}]$ are Hermitian, also the matrix $\mathbf{Z} = [Z_{k'k}]$ is Hermitian, that is, $Z_{kk'} = Z^*_{k'k}$. Therefore, $\beth^2(\Phi)$ becomes:

$$\beth^2(\Phi) = \mathrm{tr}(\mathbf{Z}) + 2\sum_{k=2}^{N}\sum_{k'=1}^{k-1} |Z_{k'k}| \cos(\phi_k - \phi_{k'} + \beta_{k'k}), \tag{10.7}$$

where $\mathrm{tr}(\mathbf{Z}) = \sum_{k=1}^{N} Z_{kk}$ is the trace of matrix $\mathbf{Z}$ and $\beta_{k'k} = \arg(Z_{k'k})$. The function $\beth^2(\Phi)$ can be minimized following the Single Coordinate Method (SCM) [41], which performs the minimization by evaluating the unknown phases sequentially. Putting into evidence the dependence from the generic phase $\phi_{\tilde{k}}$, (10.7) can be written as:

$$\begin{aligned}\beth^2(\Phi) =& \mathrm{tr}(\mathbf{Z}) + 2\sum_{k'=1}^{\tilde{k}-1} |Z_{k'\tilde{k}}| \cos(\phi_{\tilde{k}} - \phi_{k'} + \beta_{k'\tilde{k}}) + \\ &+ 2\sum_{k=\tilde{k}+1}^{N} |Z_{\tilde{k}k}| \cos(\phi_k - \phi_{\tilde{k}} + \beta_{\tilde{k}k}) + \\ &+ \digamma(\phi_1, ..., \phi_{\tilde{k}-1}, \phi_{\tilde{k}+1}, ..., \phi_N),\end{aligned} \tag{10.8}$$

where $\digamma(\phi_1, ..., \phi_{\tilde{k}-1}, \phi_{\tilde{k}+1}, ..., \phi_N)$ is a term independent of $\phi_{\tilde{k}}$. Performing some manipulations, (10.8) can be expressed as:

$$\begin{aligned}\beth^2(\Phi) =& \mathrm{tr}(\mathbf{Z}) + 2\sum_{\substack{k=1\\k\neq\tilde{k}}}^{N} |Z_{k\tilde{k}}| \cos(\phi_{\tilde{k}} - \phi_k + \beta_{k\tilde{k}}) + \\ &+ \digamma(\phi_1, ..., \phi_{\tilde{k}-1}, \phi_{\tilde{k}+1}, ..., \phi_N),\end{aligned} \tag{10.9}$$

and, for calculation purposes, rearranged as:

$$\begin{aligned}\beth^2(\Phi) =& \mathrm{tr}(\mathbf{Z}) + \sqrt{B^2_{\tilde{k}} + C^2_{\tilde{k}}} \cos(\phi_{\tilde{k}} - \tilde{\phi}_{\tilde{k}}) + \\ &+ \digamma(\phi_1, ..., \phi_{\tilde{k}-1}, \phi_{\tilde{k}+1}, ..., \phi_N),\end{aligned} \tag{10.10}$$

where:

$$B_{\tilde{k}} = 2\sum_{\substack{k=1\\k\neq\tilde{k}}}^{N} |Z_{k\tilde{k}}| \cos(\phi_k - \beta_{k\tilde{k}}), \tag{10.11a}$$

$$C_{\tilde{k}} = 2\sum_{\substack{k=1\\k\neq\tilde{k}}}^{N} |Z_{k\tilde{k}}| \sin(\phi_k - \beta_{k\tilde{k}}), \tag{10.11b}$$

$$\tilde{\phi}_{\tilde{k}} = \arg(B_{\tilde{k}} + jC_{\tilde{k}}). \tag{10.11c}$$

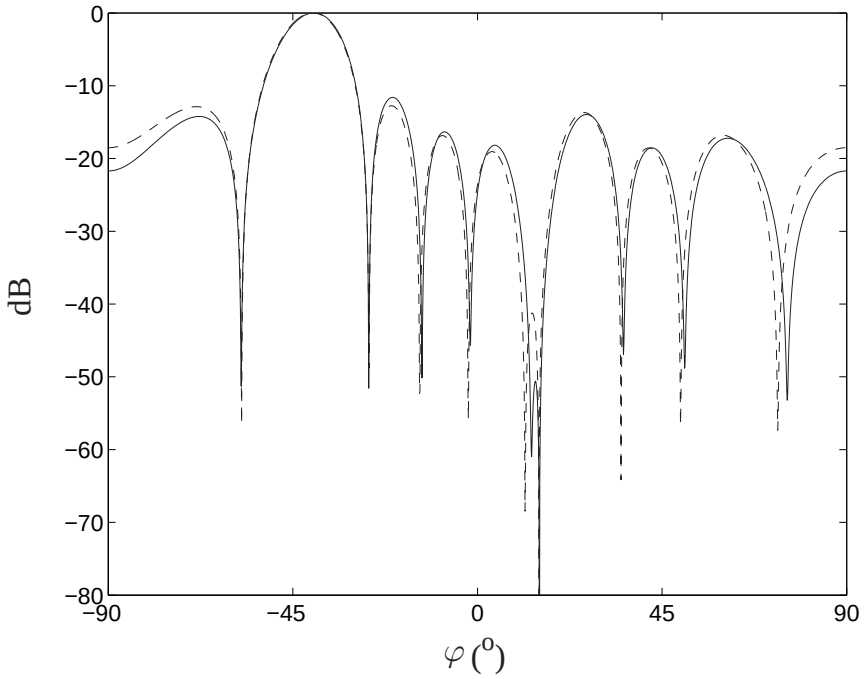

Figure 10.1: Power pattern synthesized imposing a single maximum ($\varphi_1^{\mathrm{d}} = -40^o$) and a null ($\varphi_1^{\mathrm{n}} = 15^o$) using a ULA with $N = 10$ elements.
---- SQP method using the excitation phases reported in [42]
—— Presented method with $\mathbf{g} = [1, 0, 300, 1]$

The minimum of $\beth^2(\Phi)$, as a function of $\phi_{\tilde{k}}$, is obtained for:

$$\phi_{\tilde{k}} = \pi + \tilde{\phi}_{\tilde{k}}. \tag{10.12}$$

At each step, the process is applied sequentially from $\tilde{k} = 2$ to $\tilde{k} = N$ in order to update all the excitation phases. The phase ϕ_1 is assumed as the reference phase and its value is set to zero.

10.3 Numerical results

The first numerical example refers to a ULA of $N = 10$ omnidirectional elements spaced by half wavelength. Imposing a maximum and a null, the proposed technique yields the pattern in Fig. 10.1 (solid line), which is compared to the pattern synthesized using the method described in [42]. This second method uses an SQP algorithm to form maxima and nulls in the pattern of a linear equispaced array. The pattern synthesized using the technique developed in this study shows a

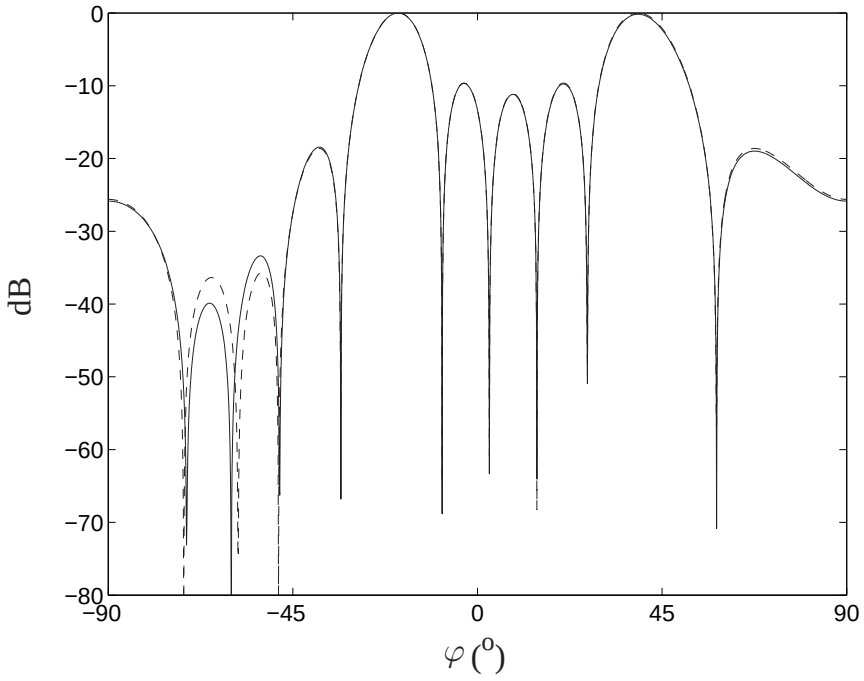

Figure 10.2: Power pattern synthesized imposing $n_{\rm des} = 2$ maxima ($\varphi_1^{\rm d} = -20^o$, $\varphi_2^{\rm d} = 40^o$) and a null ($\varphi_1^{\rm n} = -60^o$) using a ULA with $N = 10$ elements.
---- SQP method using the excitation phases reported in [42]
—— Presented method with $\mathbf{g} = [100, 100, 7, 300, 1]$

slightly lower side-lobe level in a large part of the azimuth domain with respect to the pattern derived in [42] for the same scenario. Using the presented method, the

Array element	Fig. 10.1	Fig. 10.2	Fig. 10.3
1	0^o	0^o	0^o
2	-243.3967^o	-25.7247^o	1.8244^o
3	215.5292^o	-233.9255^o	-117.9702^o
4	350.5718^o	99.6922^o	-86.8239^o
5	-274.3827^o	-108.3332^o	21.9544^o
6	-133.7257^o	-134.1755^o	37.0313^o
7	323.2568^o	17.7391^o	-72.9026^o
8	-264.3266^o	351.3101^o	-75.5418^o
9	195.8742^o	-216.6999^o	-
10	313.8894^o	117.4412^o	-

TABLE 10.1: EXCITATION PHASES OBTAINED BY THE PRESENTED METHOD.

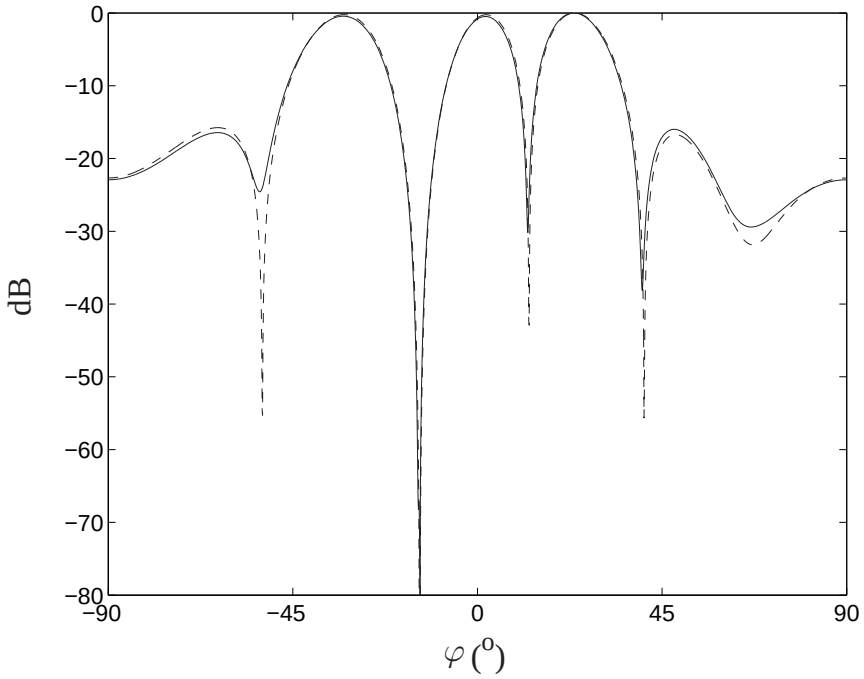

Figure 10.3: Power pattern synthesized imposing $n_{\rm des} = 3$ maxima($\varphi_1^{\rm d} = -32^o$, $\varphi_2^{\rm d} = 2^o$, $\varphi_3^{\rm d} = 22^o$) and a null ($\varphi_1^{\rm n} = -14^o$) using a ULA with $N = 8$ elements.
- - - - SQP method
—— Presented method with $\mathbf{g} = [173, 115, 115, 23, 110000, 750]$

null objective is reached imposing a sufficiently large value for the corresponding weight. The second example refers to the same array and is obtained imposing $n_{\rm des} = 2$ maxima and a single null (Fig. 10.2). It can be noticed that, employing the proposed algorithm, a deep null can be exactly placed in the required direction. Both methods perform satisfactorily when $n_{\rm des} = 3$ maxima and a single null are imposed adopting a ULA with $N = 8$ antenna elements (Fig. 10.3). This third example exploits the possibility, provided by the adopted cost function, to assign different values to the weights corresponding to the three required maxima.
The patterns in Fig. 10.1 and Fig. 10.2 (dashed lines) have been derived using the excitation phases that can be found in [42], while the pattern in Fig. 10.3 (dashed line) has been derived employing the function `fgoalattain`, which implements the SQP approach and is included in the Matlab optimization toolbox. The excitation phases obtained employing the technique presented in this chapter are given in Table 10.1 for the three synthesized patterns (solid lines). A comparison with the phase values reported in [42] shows a noticeable difference for the first considered scenario, probably due to the imprecise steering of the null.

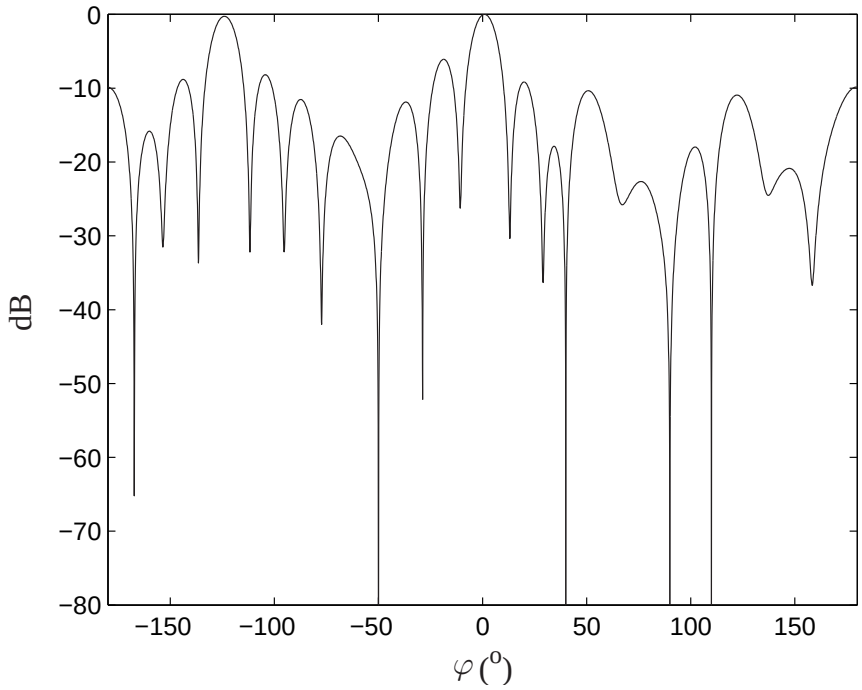

Figure 10.4: Power pattern synthesized imposing $n_{\rm des} = 2$ maxima ($\varphi_1^{\rm d} = -125^o$, $\varphi_2^{\rm d} = 0^o$) and $n_{\rm int} = 4$ nulls ($\varphi_1^{\rm n} = -50^o$, $\varphi_2^{\rm n} = 40^o$, $\varphi_3^{\rm n} = 90^o$, $\varphi_4^{\rm n} = 110^o$) using a UCA with $N = 30$ elements and employing the presented method with $\mathbf{g} = [10, 10, 7, 25000, 1]$.

Previous examples were referred to ULAs in presence of a unique interferer. However, the proposed algorithm can be applied to antenna arrays of arbitrary geometry when multiple main lobes and multiple nulls must be imposed. As a fourth example, a pattern with $n_{\rm des} = 2$ maxima and $n_{\rm int} = 4$ nulls is synthesized using a UCA with $N = 30$ equispaced omnidirectional elements and radius $\rho_{\rm c} = 1.8\lambda$ (Fig. 10.4). The figure confirms that the adopted technique is able to perform

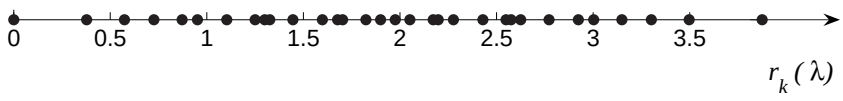

Figure 10.5: Generalized CLA array with $N = 32$ elements.

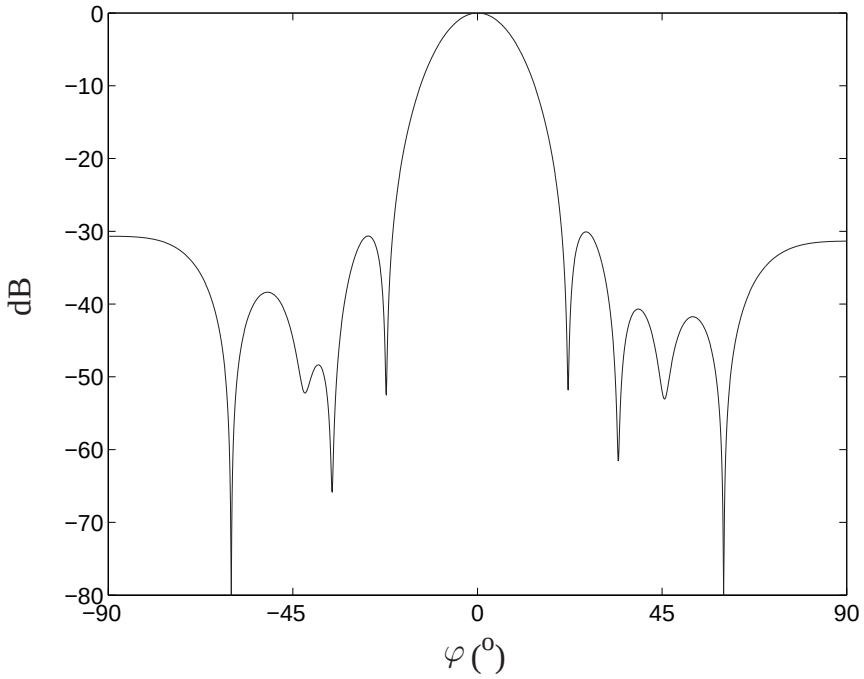

Figure 10.6: Power pattern synthesized imposing a maximum ($\varphi_1^{\mathrm{d}} = 0^o$) and $n_{\mathrm{int}} = 2$ nulls ($\varphi_1^{\mathrm{n}} = -60^o$, $\varphi_2^{\mathrm{n}} = 60^o$) using the CLA in Fig. 10.5 with $N = 32$ elements and employing the presented method with $\mathbf{g} = [1, 0, 3000, 5]$.

SDMA together with multiple interferers cancellation by phase-only control.
Using the presented technique, the weight regarding the SLL constraint ($g_{n_{\mathrm{des}}+3}$ in (10.3)) is usually kept low to reach the more stringent objectives regarding the maxima and the nulls, thus obtaining high side-lobe levels. This drawback can be mitigated by a proper choice of the array geometry. For an N elements uniform linear array, a low side-lobe level pattern can be synthesized adopting a binomial distribution of the excitation amplitudes (binomial array). However, this technique is really sensitive to small errors in the feeding network, which may lead to distorted patterns [3]. Recent studies on fractal antenna arrays show that a low side-lobe level can be obtained by employing the generalized Cantor dust with a uniform distribution of the excitation amplitudes [170]. A fifth example is obtained using a Cantor Linear Array (CLA) of $N = 32$ elements, having a scaling factor equal to 1.52 and a total length equal to 3.875λ (Fig. 10.5). The mutual coupling effect has not been considered, but it can be taken into account by suitably modifying the element patterns $\mathcal{E}_k(\varphi)$ in (10.1) [165]. Fig. 10.6 shows the pattern synthesized by using the proposed algorithm, and imposing a maximum and two symmetric nulls. It can be noticed that, while reaching the objective regarding the

Scenario	CPU time (s)
Fig. 10.1	0.24
Fig. 10.2	0.11
Fig. 10.3	0.32
Fig. 10.4	3.79
Fig. 10.6	2.47

TABLE 10.2: CPU TIMES REQUIRED TO SYNTHESIZE THE PATTERNS.

nulls, the side-lobe level is lower than -30 dB.
A further advantage of the presented solution is related to the computational burden necessary to synthesize the pattern. In fact, the proposed method is quite simple and requires low CPU time (Table 10.2). Besides, only few lines of code are necessary to implement the algorithm. In particular, the fast convergence of the proposed technique is directly related to the simple closed form computation of the phases that is performed at each iteration.

10.4 Setting of the weights

From the considered examples it can be observed that, even if the presented method requires the selection of n_{des}+3 weights for the cost function, a proper choice of such weights can be performed in few attempts by following some practical rules. In particular, the value of the weight corresponding to the nulls should be selected some orders of magnitude larger than the values of the other weights, in order to avoid possible shifts of the null positions. The adoption of different weights for different maxima becomes useful when the constraints are difficult to satisfy. In the third presented example (Fig. 10.3) four constraints ($n_{\mathrm{des}} = 3$ maxima and a null) have been imposed using an antenna array having only eight elements. In such a scenario the weight vector of the cost function $\mathbf{g}$ must be carefully selected because the number of degrees of freedom that is available is low. However, mutually equal values can be usually assigned to the n_{des} weights corresponding to the maxima, thus simplifying the use of the algorithm.

Chapter 11

Conclusions

This thesis has discussed the considerable performance improvement that can be achieved adopting multi-antenna systems as well as the degradation due to the propagation environment, proposing computationally efficient solutions for synthesizing the radiation pattern produced by an antenna array.
The presented mathematical model confirms that adaptive antennas are able to sustain a larger number of simultaneous communications with respect to directional and switched-beam techniques. However, as compared to the omnidirectional antenna case, even the use of less complex multi-antenna systems can guarantee considerable performance improvements, with the additional advantage related to the lower costs for the electronic components and the implementation. In this context, the synthesis techniques described in this study represent two examples of computationally efficient solutions to perform beamforming operations employing cheap phase shifters. The two algorithms are designed satisfying two fundamental requirements of today's communication systems: the suppression of the interference and the increase of the capacity. These objectives are obtained, in the first case, exploiting the increased knowledge of the spatial channel characteristics, and, in the second case, enabling the possibility to have multiple main lobes for spatial multiplexing operations.
Differently from a MIMO channel, in a low-rank environment multipath effects can be hardly exploited to improve the network or the single link capacity. This leads to an unavoidable degradation of the performance that can be mitigated by adopting proper countermeasures at MAC and PHY layers. The choice of the antenna array geometry, which may be dictated by encumbrance constraints, should be performed according to an efficient use of the available space on the device. The configurations having a circular symmetry show a larger versatility over the network topology and the angular spreading of the channel, as compared to the geometries characterized by a periodic displacement of the antenna elements.
The large potential offered by the antenna system at physical layer, independently

of its level of sophistication, can be quantified by the signal to interference plus noise ratio at the single node or by the number of sustainable links of the entire network. However, this potential may remain underutilized without a proper modification of the upper layers of the protocol stack. The results obtained in this thesis for a distributed wireless network prove that, at MAC layer, the theoretically available number of simultaneous communications determines a significant growth of the aggregate throughput only if the 802.11 DCF parameters are carefully selected and novel proper mechanisms, such as the directional virtual carrier sensing, are introduced. Radical modifications of the 802.11 access scheme, instead, may lead to problems of backward compatibility with the current versions of the already diffused standard. The analysis confirms the key role played by the minimum contention window, which must be set to a value able to force the coexistence of concurrent communications in order to increase the forwarded and the delivered load, while reducing the drop probability and the successful packet delay.

In the field of network modeling, an objective for future work is given by the extension of the presented mathematical framework to the 802.11e amendment. This theoretical improvement may be useful to investigate the quality of service issues in presence of multi-antenna systems. Further studies can be performed to explore adaptive solutions for the setting of the minimum contention window, which should be able to take into account the number of nodes, the angular spread and the spatial channel model. Finally, in the context of antenna array pattern synthesis, an interesting aspect to analyze may be the possibility to improve the performance of the presented algorithms adopting a power synthesis approach, in which constraints on the phase of the synthesized pattern are absent.

Appendix

Smart DATA transmission cases

This Appendix reports the complete equation for evaluating the number of sustainable links of a DWN using adaptive antennas in the SD cases for $L_{\max} \geq N/2$ (Chapter 5). The coefficients of the equation are obtained for a uniform distribution of the nodes and assuming a two-ray ground propagation model for the path-loss. The expressions are written in compact form and are valid for the omnidirectional and for the directional CTS transmission.
For $\alpha = 4$, (5.36) and (5.40) become:

$$K = 1 - \left(\frac{R_{\mathrm{c}}}{R_{\mathrm{t}}}\right)^2, \tag{11.1a}$$

$$\bar{K} = \frac{1}{4R_{\mathrm{c}}^2}, \tag{11.1b}$$

$$\alpha_1 = -\frac{1}{2}, \tag{11.1c}$$

$$\alpha_2 = \frac{1}{2}. \tag{11.1d}$$

Inserting (5.45) for $L_{\max} \geq N/2$ in (5.19) and (5.35) for the OCTS case (or in (5.39) for the DCTS the case), (5.27) becomes a sixth degree equation:

$$\sum_{i=0}^{6} c_i' L_{\max}^i = 0. \tag{11.2}$$

The exact number of sustainable links for a uniform distribution of the nodes in the SD cases is given by the largest root of (11.2). The expressions that describe

the coefficients c_i' can be written as:

$$c_0' = 4\tilde{c}_6^2, \tag{11.3a}$$

$$c_1' = 4\tilde{c}_6[\tilde{c}_5\tilde{c}_7 - 2(2\tilde{c}_6 - \tilde{c}_1)], \tag{11.3b}$$

$$\begin{aligned} c_2' =& 4[(2\tilde{c}_6 - \tilde{c}_1)^2 + \tilde{c}_5\tilde{c}_6(\tilde{c}_8 - \tilde{c}_7) + 2\tilde{c}_6(\tilde{c}_6 - 2\tilde{c}_1)] + (\tilde{c}_5\tilde{c}_7)^2 + \\ & - 2[2\tilde{c}_6(\tilde{c}_3 + \tilde{c}_5) - 2\tilde{c}_1\tilde{c}_5 - \tilde{c}_4^2]\tilde{c}_7, \end{aligned} \tag{11.3c}$$

$$\begin{aligned} c_3' =& 2[2\tilde{c}_6(\tilde{c}_3 + \tilde{c}_5) - 2\tilde{c}_1\tilde{c}_5 - \tilde{c}_4^2](\tilde{c}_7 - \tilde{c}_8) + 16[(\tilde{c}_1 + \tilde{c}_6)^2 + \tilde{c}_1\tilde{c}_6] + \\ & + 4[(\tilde{c}_3\tilde{c}_6 - \tilde{c}_1\tilde{c}_3 - \tilde{c}_1\tilde{c}_5 + \tilde{c}_2\tilde{c}_4)\tilde{c}_7 - \tilde{c}_5\tilde{c}_6\tilde{c}_8] - 2\tilde{c}_5\tilde{c}_7(\tilde{c}_3\tilde{c}_7 - \tilde{c}_5\tilde{c}_8), \end{aligned} \tag{11.3d}$$

$$\begin{aligned} c_4' =& (\tilde{c}_3\tilde{c}_7 - \tilde{c}_5\tilde{c}_8)^2 + 2\{\tilde{c}_8[2(\tilde{c}_3\tilde{c}_6 + \tilde{c}_5\tilde{c}_6 - \tilde{c}_1\tilde{c}_5) - \tilde{c}_4^2 - \tilde{c}_3\tilde{c}_5\tilde{c}_7] + \\ & + \tilde{c}_7(2\tilde{c}_1\tilde{c}_3 + \tilde{c}_2^2) - 2[(\tilde{c}_3\tilde{c}_6 - \tilde{c}_1\tilde{c}_3 - \tilde{c}_1\tilde{c}_5 + \tilde{c}_2\tilde{c}_4)(\tilde{c}_7 - \tilde{c}_8) + \\ & - 6\tilde{c}_1^2 - \tilde{c}_6^2 + 8\tilde{c}_1\tilde{c}_6]\}, \end{aligned} \tag{11.3e}$$

$$\begin{aligned} c_5' =& 2[\tilde{c}_3\tilde{c}_8(\tilde{c}_3\tilde{c}_7 - \tilde{c}_5\tilde{c}_8) + (2\tilde{c}_1\tilde{c}_3 + \tilde{c}_2^2)(\tilde{c}_8 - \tilde{c}_7)] + 8\tilde{c}_1(\tilde{c}_6 - 2\tilde{c}_1) + \\ & - 4(\tilde{c}_3\tilde{c}_6 - \tilde{c}_1\tilde{c}_3 - \tilde{c}_1\tilde{c}_5 + \tilde{c}_2\tilde{c}_4)\tilde{c}_8, \end{aligned} \tag{11.3f}$$

$$c_6' = (2\tilde{c}_1 - \tilde{c}_3\tilde{c}_8)^2 - 2\tilde{c}_2^2\tilde{c}_8, \tag{11.3g}$$

where the constants $\tilde{c}_i$ have the following meaning:

$$\tilde{c}_1 = 2\,\mathrm{SINR}_{\mathrm{th}} R_{\mathrm{c}}^2 R_{\mathrm{sd}}^4 G_{\mathrm{tx}_1} \tilde{\chi}_1, \tag{11.4a}$$

$$\tilde{c}_2 = 2\,\mathrm{SINR}_{\mathrm{th}} R_{\mathrm{c}}^2 R_{\mathrm{sd}}^4 G_{\mathrm{tx}_1} \bar{K} \tilde{\chi}_3', \tag{11.4b}$$

$$\tilde{c}_3 = 2\,\mathrm{SINR}_{\mathrm{th}} R_{\mathrm{c}}^2 R_{\mathrm{sd}}^4 G_{\mathrm{tx}_1} \bar{K} \tilde{\chi}_3'', \tag{11.4c}$$

$$\tilde{c}_4 = \mathrm{SINR}_{\mathrm{th}} R_{\mathrm{c}}^2 R_{\mathrm{sd}}^4 \bar{K}[(N-2)G_{\mathrm{n}}\tilde{\chi}_2' - N\tilde{\chi}_3'], \tag{11.4d}$$

$$\tilde{c}_5 = \mathrm{SINR}_{\mathrm{th}} R_{\mathrm{c}}^2 R_{\mathrm{sd}}^4 \bar{K} \cdot \begin{cases} N\tilde{\chi}_3'' - 2\pi(N-2)G_{\mathrm{n}} & \text{for OCTS case} \\ N\tilde{\chi}_3' - (N-2)G_{\mathrm{n}}\tilde{\chi}_2' & \text{for DCTS case} \end{cases}, \tag{11.4e}$$

$$\tilde{c}_6 = \pi(R_{\mathrm{sd}}^4 - R_{\mathrm{c}}^4 G_{\mathrm{d}} G_{\mathrm{d}}), \tag{11.4f}$$

$$\tilde{c}_7 = (N-2)G_{\mathrm{n}} - NG_{\mathrm{m}}', \tag{11.4g}$$

$$\tilde{c}_8 = 2G_{\mathrm{m}}', \tag{11.4h}$$

with:

$$\tilde{\chi}_1 = \begin{cases} K\bar{K}\displaystyle\int_0^{2\pi} F_{\mathrm{D}}(\varphi)\mathrm{d}\varphi & \text{for OCTS case} \\ \bar{K}\displaystyle\int_0^{2\pi} \left\{[F_{\mathrm{D}}(\varphi)]^{-1/2} + K - 1\right\} F_{\mathrm{D}}(\varphi)\mathrm{d}\varphi & \text{for DCTS case} \end{cases}, \tag{11.5a}$$

$$\tilde{\chi}_2' = \int_0^{2\pi} [F_{\mathrm{D}}(\varphi)]^{-1/2}\,\mathrm{d}\varphi, \tag{11.5b}$$

$$\tilde{\chi}_3' = \int_0^{2\pi} [F_{\mathrm{D}}(\varphi)]^{1/2}\,\mathrm{d}\varphi, \tag{11.5c}$$

$$\tilde{\chi}_3'' = \begin{cases} \displaystyle\int_0^{2\pi} F_{\mathrm{D}}(\varphi)\mathrm{d}\varphi & \text{for OCTS case} \\ \displaystyle\int_0^{2\pi} [F_{\mathrm{D}}(\varphi)]^{1/2}\,\mathrm{d}\varphi & \text{for DCTS case} \end{cases}. \tag{11.5d}$$

Bibliography

[1] J.D. Jackson, *Classical Electrodynamics*. New York, John Wiley and Sons, 1962.

[2] *IEEE Standard Definitions of Terms for Antennas, IEEE Std 145-1993 (Revision of IEEE Std 145-1983)*, IEEE Antennas and Propagation Society, Jun. 1993.

[3] C.A. Balanis, *Antenna Theory: Analysis and Design*. New York, John Wiley and Sons, 1997.

[4] B. Allen and M. Ghavami, *Adaptive Array Systems*. New York, John Wiley and Sons, 2005.

[5] F. Gross, *Smart Antennas for Wireless Communications with Matlab*. New York, McGraw-Hill, 2005.

[6] P. Ioannides and C.A. Balanis, "Uniform Circular Arrays for Smart Antennas," *IEEE Antennas and Propagation Magazine*, vol. 47, no. 4, pp. 192–206, Aug. 2005.

[7] ——, "Uniform Circular and Rectangular Arrays for Adaptive Beamforming Applications," *IEEE Antennas and Wireless Propagation Letters*, vol. 4, pp. 351–354, 2005.

[8] T. Haruyama, N. Kojima, I. Chiba, Y. Oh-Hashi, N. Orime and T. Katagi, "Conformal Array Antenna with Digital Beam Forming Network," in *IEEE Antennas and Propagation Society International Symposium (APS)*, vol. 2, 26-30 Jun. 1989, pp. 982–985.

[9] W.H. Kummer, "Basic Array Theory," *Proceedings of the IEEE*, vol. 80, no. 1, pp. 127–140, 1992.

[10] R. Vescovo, "Use of Directional Elements in the Null Synthesis for Arc Arrays," in *IEEE Antennas and Propagation Society International Symposium (APS)*, vol. 2, 21-26 Jun. 1998, pp. 736–739.

[11] W. Jakes, *Microwave Mobile Communications*. IEEE Press, 1974.

[12] G.L. Stuber, *Principles of Mobile Communication*. Norwell. MA, Kluwer Academic Pubblishers, 1996.

[13] E. Biglieri, J. Proakis and S. Shamai, "Fading Channels: Information-Theoretic and Communications Aspects," *IEEE Transactions on Information Theory*, vol. 44, no. 6, pp. 2619–2692, Oct. 1998.

[14] D. Chizhik, J. Ling, P.W. Wolniansky, R.A. Valenzuela, N. Costa and K. Huber, "Multiple-Input-Multiple-Output Measurements and Modeling in Manhattan," *IEEE Journal on Selected Areas in Communications*, vol. 21, no. 3, pp. 321–331, Apr. 2003.

[15] J. Fuhl, A.F. Molisch and E. Bonek, "Unified Channel Model for Mobile Radio Systems with Smart Antennas," *IEE Proceedings on Radar, Sonar and Navigation*, vol. 145, no. 1, pp. 32–40, Feb. 1998.

[16] R.B. Ertel, P. Cardieri, K.W. Sowerby, T.S. Rappaport and J.H. Reed, "Overview of Spatial Channel Models for Antenna Array Communication Systems," *IEEE Personal Communications*, vol. 5, no. 1, pp. 10–22, Feb. 1998.

[17] R. Kohno, "Spatial and Temporal Communication Theory Using Adaptive Antenna Array," *IEEE Personal Communications*, vol. 5, no. 1, pp. 28–35, Feb. 1998.

[18] J. Salz and J.H. Winters, "Effect of Fading Correlation on Adaptive Arrays in Digital Mobile Radio," *IEEE Transactions on Vehicular Technology*, vol. 43, no. 4, pp. 1049–1057, Nov. 1994.

[19] W.C.Y. Lee, "Effects on Correlation between Two Mobile Radio Base-Station Antennas," *IEEE Transactions on Communications*, vol. 21, no. 11, pp. 1214–1224, Nov. 1973.

[20] M.T. Feeney and J.D. Parsons, "Cross-Correlation between 900 MHz Signals Received on Vertically Separated Antennas in Small-Cell Mobile Radio Systems," *IEE Proceedings on Communications, Speech and Vision*, vol. 138, no. 2, pp. 81–86, Apr. 1991.

[21] T.L. Fulghum, K.J. Molnar and A.D. Hallen, "The Jakes Fading Model for Antenna Arrays Incorporating Azimuth Spread," *IEEE Transactions on Vehicular Technology*, vol. 51, no. 5, pp. 968–977, 11th Sep. 2002.

[22] P. Petrus, J.H. Reed and T.S. Rappaport, "Geometrical-Based Statistical Macrocell Channel Model for Mobile Environments," *IEEE Transactions on Communications*, vol. 50, no. 3, pp. 495–502, Mar. 2002.

[23] K.I. Pedersen, P.E. Mogensen and B.H. Fleury, "A Stochastic Model of the Temporal and Azimuthal Dispersion Seen at the Base Station in Outdoor Propagation Environments," *IEEE Transactions on Vehicular Technology*, vol. 49, no. 2, pp. 437–447, Mar. 2000.

[24] A.D. Kucar, "Mobile Radio: An Overview," *IEEE Communications Magazine*, vol. 29, no. 11, pp. 72–85, Nov. 1991.

[25] P.H. Lehne and M. Pettersen, "An Overview of Smart Antenna Technology for Mobile Heterogeneous Networks," *IEEE Communications Surveys*, vol. 2, no. 4, pp. 14–23, Fourth Quarter 1999.

[26] *IEEE Standard for Wireless LAN Medium Access Control (MAC) and PHYsical Layer (PHY) Specifications: Amendment: Medium Access Control (MAC) Enhancements for Higher Throughput*, IEEE Std 802.11n/D1.07, Dec. 2006.

[27] A. Alexiou and M. Haardt, "Smart Antenna Technologies for Future Wireless Systems: Trends and Challenges," *IEEE Communications Magazine*, vol. 42, no. 9, pp. 90–97, Sep. 2004.

[28] E. Falletti, "Applications of Adaptive Antennas in the Field of Third and Fourth Generation Wireless Communication Systems," Ph.D. dissertation, Politecnico di Torino (Italy), Dec. 2003.

[29] G.J. Foschini and M.J. Gans, "On Limits of Wireless Communications in a Fading Environment when Using Multiple Antennas," *Wireless Personal Commununications*, vol. 6, no. 3, pp. 311–335, Mar. 1998.

[30] O. Oyman, R.U. Nabar, H. Bolcskei and A.J. Paulraj, "Tight Lower Bounds on the Ergodic Capacity of Rayleigh Fading MIMO Channels," in *IEEE Global Telecommunications Conference (GLOBECOM)*, vol. 2, 17-21 Nov. 2002, pp. 1172–1176.

[31] D. Chizhik, G.J. Foschini and R.A. Valenzuela, "Capacities of Multi-Element Transmit and Receive Antennas: Correlations and Keyholes," *Electronics Letters*, vol. 36, no. 13, pp. 1099–1100, 22nd Jun. 2000.

[32] B. Holter, "On the Capacity of the MIMO Channel: A Tutorial Introduction," in *IEEE Norwegian Symposium on Signal Processing (NORSIG)*, 18–20 Oct. 2001, pp. 167—-172.

[33] S.M. Alamouti, "A Simple Transmit Diversity Technique for Wireless Communications," *IEEE Journal on Selected Areas in Communications*, vol. 16, no. 8, pp. 1451–1458, Oct. 1998.

[34] V. Tarokh, A. Naguib, N. Seshadri and A.R. Calderbank, "Combined Array Processing and Space–Time Coding," *IEEE Transactions on Information Theory*, vol. 45, no. 4, pp. 1121–1128, May 1999.

[35] L. Zheng and D.N.C. Tse, "Diversity and Multiplexing: A Fundamental Tradeoff in Multiple-Antenna Channels," *IEEE Transactions on Information Theory*, vol. 49, no. 5, pp. 1073–1096, May 2003.

[36] L.C. Godara, "Application of Antenna Arrays to Mobile Communications, Part II: Beam Forming and Direction-of-Arrival Considerations," *Proceedings of the IEEE*, vol. 85, no. 8, pp. 1193–1245, Aug. 1997.

[37] S.T. Smith, "Optimum Phase-Only Adaptive Nulling," *IEEE Transactions on Signal Processing*, vol. 47, no. 7, pp. 1835–1843, Jul. 1999.

[38] H. Steyskal, "Simple Method for Pattern Nulling by Phase Perturbation," *IEEE Transactions on Antennas and Propagation*, vol. 31, no. 1, pp. 163–166, Jan. 1983.

[39] R.L. Haupt, "Phase-Only Adaptive Nulling with a Genetic Algorithm," *IEEE Transactions on Antennas and Propagation*, vol. 45, no. 6, pp. 1009–1015, Jun. 1997.

[40] D. I. Abu-Al-Nadi, M. J. Mismar and T. H. Ismail, "Genetically Evolved Phase-Aggregation Technique for Linear Arrays Control," *Progress in Electromagnetics Research, PIER 43*, pp. 287–304, 2003.

[41] A.D. Khzmalyan and A.S. Kondrat'yev, "Fast Iterative Methods for Phase-Only Synthesis of Antenna Array Pattern Nulls," *Electronics Letters*, vol. 31, no. 8, pp. 601–602, 13^{th} Apr. 1995.

[42] M. Mouhamadou, P. Vaudon and M. Rammal, "Smart Antenna Array Patterns Synthesis: Null Steering and Multi-User Beamforming by Phase Control," *Progress in Electromagnetics Research, PIER 60*, pp. 95–106, 2006.

[43] R. Vescovo, "Null Synthesis by Phase Control for Antenna Arrays," *Electronics Letters*, vol. 36, no. 3, pp. 198–199, 3^{rd} Feb. 2000.

[44] L.C. Godara, "Applications of Antenna Arrays to Mobile Communications. I. Performance Improvement, Feasibility, and System Considerations," *Proceedings of the IEEE*, vol. 85, no. 7, pp. 1031–1060, Jul. 1997.

[45] P.H. Lehne and M. Pettersen, "An Overview of Smart Antenna Technology for Mobile Communications Systems," *IEEE Communications Surveys*, vol. 2, no. 4, pp. 2–13, Fourth Quarter 1999.

[46] H. Moody, "The Systematic Design of the Butler Matrix," *IEEE Transactions on Antennas and Propagation*, vol. 12, no. 6, pp. 786–788, Nov. 1964.

[47] J. Capon, "High-Resolution Frequency-Wavenumber Spectrum Analysis," *Proceedings of the IEEE*, vol. 57, no. 8, pp. 1408–1418, Aug. 1969.

[48] O.L. Frost III, "An Algorithm for Linearly Constrained Adaptive Array Processing," *Proceedings of the IEEE*, vol. 60, no. 8, pp. 926–935, Aug. 1972.

[49] S. Applebaum, "Adaptive Arrays," *IEEE Transactions on Antennas and Propagation*, vol. 24, no. 5, pp. 585–598, 1976.

[50] A.L. Swindlehurst and T. Kailath, "Azimuth/Elevation Direction Finding Using Regular Array Geometries," *IEEE Transactions on Aerospace and Electronic Systems*, vol. 29, no. 1, pp. 145–156, Jan. 1993.

[51] C.P. Mathews and M.D. Zoltowski, "Eigenstructure Techniques for 2-D Angle Estimation with Uniform Circular Arrays," *IEEE Transactions on Signal Processing*, vol. 42, no. 9, pp. 2395–2407, Sep. 1994.

[52] G. Long, F. Ling and J.G. Proakis, "The LMS Algorithm with Delayed Coefficient Adaptation," *IEEE Transactions on Acoustic, Speech and Signal Processing*, vol. 37, no. 9, pp. 1397–1405, Sep. 1989.

[53] J. Fernandez, I.R. Corden and M. Barrett, "Adaptive Array Algorithms for Optimal Combining in Digital Mobile Communications Systems," in *IEE International Conference on Antennas and Propagation (ICAP)*, vol. 2, 1993, pp. 983–986.

[54] D. Godard, "Self-Recovering Equalization and Carrier Tracking in Two-Dimensional Data Communication Systems," *IEEE Transactions on Communications*, vol. 28, no. 11, pp. 1867–1875, Nov. 1980.

[55] I. Chlamtac, M. Conti and J.J.-N. Liu, "Mobile Ad Hoc Networking: Imperatives and Challenges," *Ad Hoc Networks*, vol. 1, no. 1, pp. 13–64, Jul. 2003.

[56] I.F. Akyildiz, X. Wang and W. Wang, "Wireless Mesh Networks: A Survey," *Computer Networks*, vol. 47, pp. 445–487, Jan. 2005.

[57] *IEEE Standard for Wireless Medium Access Control (MAC) and Physical Layer (PHY) Specifications for Wireless Personal Area Networks (WPANs)*, IEEE Std 802.15.1, Jun. 2002.

[58] *IEEE Standard for Wireless LAN Medium Access Control (MAC) and PHYsical Layer (PHY) Specifications*, IEEE Std 802.11, Nov. 1997.

[59] *IEEE Standard for Wireless LAN Medium Access Control (MAC) and PHYsical Layer (PHY) Specifications: High-Speed Physical Layer in the 5 GHz Band*, IEEE Std 802.11a, Sep. 1999.

[60] *IEEE Standard for Wireless LAN Medium Access Control (MAC) and PHYsical Layer (PHY) Specifications: High-Speed Physical Layer Extension in the 2.4 GHz Band*, IEEE Std 802.11b, Sep. 1999.

[61] *IEEE Standard for Wireless LAN Medium Access Control (MAC) and PHYsical Layer (PHY) Specifications: Amendment 4: Further Higher Data Rate Extension in the 2.4 GHz Band*, IEEE Std 802.11g, Jun. 2003.

[62] *IEEE Standard for Wireless LAN Medium Access Control (MAC) and PHYsical Layer (PHY) Specifications: Amendment 8: Medium Access Control (MAC) Quality of Service Enhancements*, IEEE Std 802.11e, Nov. 2005.

[63] *IEEE Standard for Wireless LAN Medium Access Control (MAC) and PHYsical Layer (PHY) Specifications: Amendment 6: Medium Access Control (MAC) Security Enhancements*, IEEE Std 802.11i, Jul. 2004.

[64] *HT PHY Specification (Version 1.27)*, Enhanced Wireless Consortium, 23^{rd} Dec. 2005.

[65] M.K.A. Aziz, A.R. Nix and P.N. Fletcher, "A Study of Performance and Complexity for IEEE 802.11n MIMO-OFDM GIS Solutions," in *IEEE International Conference on Communications (ICC)*, vol. 7, 20-24 Jun. 2004, pp. 3822–3826.

[66] M. Hu and J. Zhang, "MIMO Ad Hoc Networks with Spatial Diversity: Medium Access Control and Saturation Throughput," in *IEEE Conference on Decision and Control (CDC)*, vol. 3, 14-17 Dec. 2004, pp. 3301–3306.

[67] J.C. Mundarath, P. Ramanathan and B.D. Van Veen, "NULLHOC: a MAC Protocol for Adaptive Antenna Array Based Wireless Ad Hoc Networks in Multipath Environment," in *IEEE Global Telecommunications Conference (GLOBECOM)*, 29 Nov-3 Dec. 2004, pp. 2765–2769.

[68] M. Park, R.W. Heath Jr. and S.M. Nettles, "Improving Throughput and Fairness for MIMO Ad Hoc Networks Using Antenna Selection Diversity," in *IEEE Global Telecommunications Conference (GLOBECOM)*, vol. 5, 29 Nov.-3 Dec. 2004, pp. 3363–3367.

[69] J.-S. Park, A. Nandan, M. Gerla and H. Lee, "SPACE-MAC: Enabling Spatial Reuse Using MIMO Channel-Aware MAC," in *IEEE International Conference on Communications (ICC)*, vol. 5, 16-20 May 2005, pp. 3642–3646.

[70] T. Tang, M. Park, R.W. Heath Jr. and S.M. Nettles, "A Joint MIMO-OFDM Transceiver and MAC Design for Mobile Ad Hoc Networking," in *International Workshop on Wireless Ad-Hoc Networks (IWWAN)*, 31 May-3 Jun. 2004, pp. 315–319.

[71] K. Sundaresan, R. Sivakumar, M.A. Ingram and T.-Y. Chang, "Medium Access Control in Ad hoc Networks with MIMO Links: Optimization Considerations and Algorithms," *IEEE Transactions on Mobile Computing*, vol. 3, no. 4, pp. 350–365, Oct.-Dec 2004.

[72] ——, "A Fair Medium Access Control Protocol for Ad-Hoc Networks with MIMO Links," in *Annual Joint Conference of the IEEE Computer and Communications Societies (INFOCOM)*, vol. 4, 7-11 Mar. 2004, pp. 2559–2570.

[73] K. Sundaresan and R. Sivakumar, "A Unified MAC Layer Framework for Ad-hoc Networks with Smart Antennas," in *ACM International Symposium on Mobile Ad Hoc Networking and Computing (MobiHoc)*, 24-26 May 2004, pp. 244–255.

[74] D. Wang and U. Tureli, "Cross Layer Design for Broadband Ad Hoc Network with MIMO-OFDM," in *IEEE Workshop on Signal Processing Advances in Wireless Communications (SPAWC)*, 5-8 Jun. 2005, pp. 630–634.

[75] T. Hunziker, J.L. Bordim, T. Ohira and S. Tanaka, "A CSMA/CA-Based Medium Access Scheme for Array Antenna-Enhanced Wireless Ad Hoc Networks," in *IEEE International Symposium on Wireless Communication Systems (ISWCS)*, 20-22 Sep. 2004, pp. 230–234.

[76] G. Bianchi, D. Messina, L. Scalia and I. Tinnirello, "A Space-Division Time-Division Multiple Access Scheme for High Throughput Provisioning in WLANs," in *IEEE International Conference on Communications (ICC)*, vol. 4, 16-20 May 2005, pp. 2728–2733.

[77] W.-T. Chen, T.-W. Ho and Y.-C. Chen, "An MAC Protocol for Wireless Ad-hoc Hetworks Using Smart Antennas," in *International Conference on Parallel and Distributed Systems (ICPADS)*, vol. 1, 20-22 Jul. 2005, pp. 446–452.

[78] R.R. Choudhury, X. Yang, R. Ramanathan and N.H. Vaidya, "Using Directional Antennas for Medium Access Control in Ad Hoc Networks," in *ACM International Symposium on Mobile Ad Hoc Networking and Computing (MobiHoc)*, 23-28 Sep. 2003, pp. 98–107.

[79] ——, "On Designing MAC Protocols for Wireless Networks Using Directional Antennas," *IEEE Transactions on Mobile Computing*, vol. 5, no. 5, pp. 477–491, Sep.-Oct. 2006.

[80] R.R. Choudhury and N.H. Vaidya, "Deafness: A MAC Problem in Ad Hoc Networks when using Directional Antennas," in *IEEE International Conference on Network Protocols (ICNP)*, 5-8 Oct. 2004, pp. 283–292.

[81] T. ElBatt, T. Anderson and B. Ryu, "Performance Evaluation of Multiple Access Protocols for Ad hoc Networks Using Directional Antennas," in *IEEE Wireless Communications and Networking Conference (WCNC)*, vol. 2, 16-20 Mar. 2003, pp. 982–987.

[82] N.S. Fahmy, T.D. Todd and V. Kezys, "Ad Hoc Networks with Smart Antennas Using IEEE 802.11-Based Protocols," in *IEEE International Conference on Communications (ICC)*, vol. 5, 28 Apr.-2 May 2002, pp. 3144–3148.

[83] ——, "Distributed Power Control for Ad Hoc Networks with Smart Antennas," in *IEEE Vehicular Technology Conference (VTC)*, vol. 4, 24-28 Sep. 2002, pp. 2141–2144.

[84] K.H. Grace, J.A. Stine and R.C. Durst, "An Approach for Modestly Directional Communications in Mobile Ad Hoc Networks," in *IEEE International Conference on Computer Communications and Networks (ICCCN)*, 20-22 Oct. 2003, pp. 377–384.

[85] C.-C. Shen, C. Srisathapornphat and C. Jaikaeo, "A Busy-Tone Based Directional MAC Protocol for Ad Hoc Networks," in *IEEE Military Communications Conference (MILCOM)*, vol. 2, 7-10 Oct. 2002, pp. 1233–1238.

[86] Y.B. Ko, V. Shankarkumar and N.H. Vaidya, "Medium Access Control Protocols Using Directional Antennas in Ad Hoc Networks," in *Annual Joint*

Conference of the IEEE Computer and Communications Societies (INFOCOM), vol. 1, 26-30 Mar. 2000, pp. 13–21.

[87] T. Korakis, G. Jakllari and L. Tassiulas, "A MAC Protocol for Full Exploitation of Directional Antennas in Ad-hoc Wireless Networks," in *ACM International Symposium on Mobile Ad Hoc Networking and Computing (MobiHoc)*, vol. 1, 1-3 Jun. 2003, pp. 98–107.

[88] D. Lal, R. Gupta and D.P. Agrawal, "Throughput Enhancement in Wireless Ad Hoc Networks with Spatial Channels - A MAC Layer Perspective," in *IEEE International Symposium on Computers and Communications (ISCC)*, 1-4 Jul. 2002, pp. 421–428.

[89] D. Lal, T. Joshi and D.P. Agrawal, "Localized Transmission Scheduling for Spatial Multiplexing Using Smart Antennas in Wireless Adhoc Networks," in *IEEE Workshop on Local and Metropolitan Area Networks (LAN/MAN)*, 25-28 Apr. 2004, pp. 175–180.

[90] D. Lal, V. Jain, Q.-A. Zeng and D.P. Agrawal, "Performance Evaluation of Medium Access Control for Multiple-Beam Antenna Nodes in a Wireless LAN," *IEEE Transactions on Parallel and Distributed Systems*, vol. 15, no. 12, pp. 1117–1129, Dec. 2004.

[91] T.M. Lin and J.J. Dai, "A Collision Free MAC Protocol Using Smart Antenna in Ad Hoc Networks," in *IEEE Consumer Communications and Networking Conference (CCNC)*, 5-8 Jan. 2004, pp. 301–306.

[92] K. Nagashima, M. Takata and T. Watanabe, "Evaluations of A Directional MAC Protocol for Ad Hoc Networks," in *IEEE International Conference on Distributed Computing Systems Workshops (ICDCSW)*, 2004, pp. 678–683.

[93] A. Nasipuri, Li Kai and U.R. Sappidi, "Power Consumption and Throughput in Mobile Ad Hoc Networks Using Directional Antennas," in *IEEE International Conference on Computer Communications and Networks (ICCCN)*, 14-16 Oct. 2002, pp. 620–626.

[94] A. Nasipuri, S. Ye, J. You and R.E. Hiromoto, "A MAC Protocol for Mobile Ad Hoc Networks Using Directional Antennas," in *IEEE Wireless Communications and Networking Conference (WCNC)*, vol. 3, 23-28 Oct. 2000, pp. 1214–1219.

[95] R. Ramanathan, J. Redi, C. Santivanez, D. Wiggins and S. Polit, "Ad Hoc Networking with Directional Antennas: A Complete System Solution,"

IEEE Journal on Selected Areas in Communications, vol. 23, no. 3, pp. 496–506, Mar. 2005.

[96] M. Takai, J. Martin, A. Ren and R. Bagrodia, "Directional Virtual Carrier Sensing for Directional Antennas in Mobile Ad Hoc Networks," in *ACM International Symposium on Mobile Ad Hoc Networking and Computing (MobiHoc)*, 9-11 Jun. 2002.

[97] M. Takata, K. Nagashima and T. Watanabe, "A Directional Antennas-Based Dual Mode MAC Protocol for Ad Hoc Networks," in *IEEE International Conference on Performance, Computing, and Communications (ICPCC)*, 2004, pp. 579–584.

[98] ——, "A Dual Access Mode MAC Protocol for Ad Hoc Networks Using Smart Antennas," in *IEEE International Conference on Communications (ICC)*, vol. 7, 20-24 Jun. 2004, pp. 4182–4186.

[99] M. Takata, M. Bandai and T. Watanabe, "An Extended Directional MAC for Location Information Staleness in Ad Hoc Networks," in *IEEE International Conference on Distributed Computing Systems Workshops (ICDCSW)*, 6-10 Jun. 2005, pp. 899–905.

[100] Z. Zhang, "Pure Directional Transmission and Reception Algorithms in Wireless Ad Hoc Networks with Directional Antennas," in *IEEE International Conference on Communications (ICC)*, vol. 5, 16-20 May 2005, pp. 3386–3390.

[101] ——, "DTRA: Directional Transmission and Reception Algorithms in WLANs with Directional Antennas for QoS Support," *IEEE Network*, vol. 19, no. 3, pp. 27–32, May-Jun. 2005.

[102] S. Bandyopadhyay, K. Hasuike, S. Horisawa and S. Tawara, "An Adaptive MAC Protocol for Wireless Ad Hoc Community Networks (WACNet) Using Electronically Steerable Passive Array Radiator Antenna," in *IEEE Global Telecommunications Conference (GLOBECOM)*, 25-29 Nov. 2001, pp. 2896–2900.

[103] W.T. Chen, M.S. Pan and J.J. Dai, "An Adaptive MAC Protocol for Wireless Ad Hoc Networks Using Smart Antenna System," in *IEEE Vehicular Technology Conference (VTC)*, vol. 5, 6-9 Oct. 2003, pp. 2794–2798.

[104] N.S. Fahmy and T.D. Todd, "A Selective CSMA Protocol with Cooperative Nulling for Ad Hoc Networks with Smart Antennas," in *IEEE Wireless*

Communications and Networking Conference (WCNC), vol. 1, 21-25 Mar. 2004, pp. 387–392.

[105] D. Lal, R. Toshniwal, R. Radhakrisnan, D.P. Agrawal and J. Caffery, "A Novel MAC Layer Protocol for Space Division Multiple Access in Wireless Ad Hoc Networks," in *IEEE International Conference on Computer Communications and Networks (ICCCN)*, 14-16 Oct. 2002, pp. 614–619.

[106] R. Radhakrishnan, D. Lai, J.Jr. Caffery and D.P. Agrawal, "Performance Comparison of Smart Antenna Techniques for Spatial Multiplexing in Wireless Ad Hoc Networks," in *IEEE International Symposium on Wireless Personal Multimedia Communications (WPMC)*, 27-30 Oct. 2002, pp. 168–171.

[107] H. Singh and S. Singh, "A MAC Protocol Based on Adaptive Beamforming for Ad Hoc Networks," in *IEEE International Symposium on Personal, Indoor and Mobile Radio Communications (PIMRC)*, vol. 2, 7-10 Sep. 2003, pp. 1346–1350.

[108] ——, "DOA-ALOHA: Slotted ALOHA for Ad Hoc Networking Using Smart Antennas," in *IEEE Vehicular Technology Conference (VTC)*, vol. 5, 6-9 Oct. 2003, pp. 2804–2808.

[109] ——, "Tone Based MAC Protocol for Use with Adaptive Array Antennas," in *IEEE Wireless Communications and Networking Conference (WCNC)*, vol. 2, 21-25 Mar. 2004, pp. 1246–1251.

[110] ——, "Smart-802.11b MAC Protocol for Use with Smart Antennas," in *IEEE International Conference on Communications (ICC)*, vol. 6, 20-24 Jun. 2004, pp. 3684–3688.

[111] J. Yang, J. Li and M. Sheng, "MAC Protocol for Mobile Ad Hoc Network with Smart Antennas," *Electronics Letters*, vol. 39, no. 6, pp. 555–557, 20^{th} Mar. 2003.

[112] J.Yang and J. Li, "A Novel Multiple Access Protocol for Mobile Ad Hoc Networks with Smart Antennas," in *IEEE Semiannual Vehicular Technology Conference (VTC Spring)*, vol. 3, 22-25 Apr. 2003, pp. 1768–1772.

[113] B. Jose, H. Yin, P. Mehrotra and E. Casas, "MAC layer Issues and Challenges of using Smart Antennas with 802.11," in *IEEE Vehicular Technology Conference (VTC)*, vol. 5, 6-9 Oct. 2003, pp. 3169–3173.

[114] P. Gupta and P.R. Kumar, "The Capacity of Wireless Networks," *IEEE Transactions on Information Theory*, vol. 46, no. 2, pp. 388–404, Mar. 2000.

[115] J. Li , C. Blake, D.S.J. De Couto, H.I. Lee and R. Morris, "Capacity of Ad Hoc Wireless Networks," in *ACM Annual International Conference on Mobile Computing and Networking (MobiCom)*, 01-03 Jun. 2001, pp. 61–69.

[116] A. Spyropoulos and C.S. Raghavendra, "Asymptotic Capacity Bounds for Ad-Hoc Networks Revisited: The Directional and Smart Antenna Cases," in *IEEE Global Telecommunications Conference (GLOBECOM)*, vol. 3, 1-5 Dec. 2003, pp. 1216–1220.

[117] ——, "Capacity Bounds for Ad-Hoc Networks Using Directional Antennas," in *IEEE International Conference on Communications (ICC)*, vol. 1, 11-15 May 2003, pp. 348–352.

[118] S. Yi , Y. Pei and S. Kalyanaraman, "On the Capacity Improvement of Ad Hoc Wireless Networks Using Directional Antennas," in *ACM International Symposium on Mobile Ad Hoc Networking and Computing (MobiHoc)*, 1-3 Jun. 2003, pp. 108–116.

[119] M. Grossglauser and D.N.C. Tse, "Mobility Increases the Capacity of Ad Hoc Wireless Networks," *IEEE Transactions on Networking*, vol. 10, no. 4, pp. 477–486, Aug. 2002.

[120] S. Toumpis and A.J. Goldsmith, "Capacity Regions for Wireless Ad Hoc Networks," *IEEE Transactions on Wireless Communications*, vol. 2, no. 4, pp. 736–748, Jul. 2003.

[121] R. Ebrahimrezagah and A. Mohammadi, "The Capacity of Wireless Ad Hoc Networks Using Statistical Techniques," in *IEEE International Conference on Communications (ICC)*, 11-15 Jun. 2006.

[122] M.M. Carvalho and J.J. Garcia-Luna-Aceves, "Modeling Wireless Ad Hoc Networks with Directional Antennas," in *Annual Joint Conference of the IEEE Computer and Communications Societies (INFOCOM)*, Apr 2006.

[123] Y. Wang and J.J. Garcia-Luna-Aceves, "Collision Avoidance in Single-Channel Ad Hoc Networks Using Directional Antennas," in *IEEE International Conference on Distributed Computing Systems (ICDCS)*, 19-22 May 2003, pp. 640–649.

[124] J.A. Stine, "Exploiting Smart Antennas in Wireless Mesh Networks Using Contention Access," *IEEE Wireless Communications*, vol. 13, no. 2, pp. 38–49, Apr. 2006.

[125] J. del Prado Pavon and S. Choi, "Link Adaptation Strategy for IEEE 802.11 WLAN via Received Signal Strength Measurement," in *IEEE International Conference on Communications (ICC)*, vol. 2, 11-15 May 2003, pp. 1108–1113.

[126] S. Choudhury and J.D. Gibson, "Joint PHY/MAC Based Link Adaptation for Wireless LANs with Multipath Fading," in *IEEE Wireless Communications and Networking Conference (WCNC)*, 3-6 Apr. 2006.

[127] L.-C. Wang, S.-Y. Huang and A. Chen, "On the Throughput Performance of CSMA-based Wireless Local Area Network with Directional Antennas and Capture Effect: A Cross-layer Analytical Approach," in *IEEE Wireless Communications and Networking Conference (WCNC)*, vol. 3, Mar. 2004, pp. 1879–1884.

[128] *The ns Manual (ns Notes and Documentation)*, UC Berkeley, LBL, USC/ISI, and Xerox PARC, Aug. 2006.

[129] J.I. Simoes, I. Stevanovic and A.K. Skrivervik, "Models for Simulating Switched Beam Antennas in Radio Planning," in *International Conference on Applied Electromagnetics And Communications (ICECom)*, 12-14 Oct. 2005.

[130] K. Xu, M. Gerla and S.A. Bae, "How Effective is the IEEE 802.11 RTS/CTS Handshake in Ad Hoc Networks," in *Global Telecommunications Conference (GLOBECOM)*, vol. 1, 17-21 Nov. 2002, pp. 72–76.

[131] C. Berrou and A. Glavieux, "Near Optimum Error Correcting Coding and Decoding: Turbo-Codes," *IEEE Transactions on Communications*, vol. 44, no. 5, pp. 591–600, May 1996.

[132] R.G. Gallager, "Low Density Parity-Check Codes," *IRE Transactions on Information Theory*, vol. 8, pp. 602–608, 1962.

[133] D.M. Ranking and T.A. Gulliver, "Single Parity Check Product Codes," *IEEE Transactions on Communications*, vol. 49, no. 8, pp. 1354–1362, Aug. 2001.

[134] J.S.K. Tee, D.P. Taylor and P.A. Martin, "Multiple Serial and Parallel Concatenated Single Parity-Check Codes," *IEEE Transactions on Communications*, vol. 51, no. 10, pp. 1666–1675, Oct. 2003.

[135] D. Qiao, S. Choi and K.G. Shin, "Goodput Analysis and Link Adaptation for IEEE 802.11a Wireless LANs," *IEEE Transactions on Mobile Computing*, vol. 1, no. 4, pp. 278–292, Oct.-Dec. 2002.

[136] R.G. Gallager, "The Random Coding Bound is Tight for the Average Code (Corresp.)," *IEEE Transactions on Information Theory*, vol. IT-19, pp. 244–246, Mar. 1973.

[137] F. Babich, "Design of Adaptive Systems for the Fading Channel Adopting Efficient Coded Modulations," in *IEEE International Conference on Communications (ICC)*, 11-15 Jun. 2006.

[138] F. Rayal, "Why Have Smart Antennas not yet Gained Traction with Wireless Network Operators?" *IEEE Antennas and Propagation Magazine*, vol. 47, no. 6, pp. 124–126, Dec. 2005.

[139] T. Kaiser, "When Will Smart Antennas Be Ready for the Market? Part I - results," *IEEE Signal Processing Magazine*, vol. 22, no. 2, pp. 87–92, Mar. 2005.

[140] ——, "When Will Smart Antennas Be Ready for the Market? Part II - results," *IEEE Signal Processing Magazine*, vol. 22, no. 6, pp. 174–176, Nov. 2005.

[141] J.H. Winters, "Smart Antenna Techniques and Their Application to Wireless Ad Hoc Networks," *IEEE Wireless Communications*, vol. 13, no. 4, pp. 77–83, Aug. 2006.

[142] M. Zorzi, J. Zeidler, A. Anderson, B. Rao, J. Proakis, A.L. Swindlehurst, M. Jensen and S. Krishnamurthy, "Cross-Layer Issues in MAC Protocol Design for MIMO Ad Hoc Networks," *IEEE Wireless Communications*, vol. 13, no. 4, pp. 62–76, Aug. 2006.

[143] M. Kim, "Hardware Implementation of Signal Processing in Smart Antenna Systems for High Speed Wireless Communication," Ph.D. dissertation, Department of Electrical and Computer Engineering, Yokohama National University, Yokohama, Japan, Dec. 2004.

[144] Ruckus Wireless, http://www.ruckuswireless.com/.

[145] F.E. Fakoukakis, S.G. Diamantis, A.P. Orfanides and G.A. Kyriaco, "Development of an Adaptive and a Switched Beam Smart Antenna System for Wireless Communications," in *Progress in Electromagnetics Research Symposium (PIERS)*, 22-26 Aug. 2005, pp. 276–280.

[146] G. Bianchi, "Performance Analysis of the IEEE 802.11 Distributed Coordination Function," *IEEE Journal on Selected Areas in Communications*, vol. 18, no. 3, pp. 535–547, Mar. 2000.

[147] H. Wu, Y. Peng, K. Long and S. Cheng, "A Simple Model of IEEE 802.11 Wireless LAN," in *IEEE International Conferences on Info-tech and Info-net (ICII)*, vol. 2, 29 Oct.-1 Nov. 2001, pp. 514–519.

[148] P. Chatzimisios, A.C. Boucouvalas and V. Vitsas, "Influence of Channel BER on IEEE 802.11 DCF," *Electronics Letters*, vol. 39, no. 23, pp. 1687–1688, 13th Nov. 2003.

[149] ——, "Performance Analysis of IEEE 802.11 DCF in Presence of Transmission Errors," in *IEEE International Conference on Communications (ICC)*, vol. 7, 20-24 Jun. 2004, pp. 3854–3858.

[150] ——, "Effectiveness of RTS/CTS Handshake in IEEE 802.11a Wireless LANs," *Electronics Letters*, vol. 40, no. 14, pp. 915–916, 8th Jul. 2004.

[151] Z. Hadzi-Velkov and B. Spasenovski, "Saturation Throughput - Delay Analysis of IEEE 802.11 DCF in Fading Channel," in *IEEE International Conference on Communications (ICC)*, vol. 1, 11-15 May 2003, pp. 121–126.

[152] D. Malone, K. Duffy and D. Leith, "Modeling the 802.11 Distributed Coordination Function in Nonsaturated Heterogeneous Conditions," *IEEE/ACM Transactions on Networking*, vol. 15, no. 1, pp. 159–172, Feb. 2007.

[153] K. Duffy and A.J. Ganesh, "Modeling the Impact of Buffering on 802.11," *IEEE Communications Letters*, vol. 11, no. 2, pp. 219–221, Feb. 2007.

[154] M. Ergen and P. Varaiya, "Throughput Analysis and Admission Control for IEEE 802.11a," *ACM/Kluwer Mobile Networks and Applications*, vol. 10, no. 5, pp. 705–716, Oct. 2005.

[155] G. R. Cantieni, Q. Ni, C. Barakat and T. Turletti, "Performance Analysis under Finite Load and Improvements for Multirate 802.11," *Compututer Communications*, vol. 28, no. 10, pp. 1095—-1109, Jun. 2005.

[156] S. Bates, "On Edges and Connectivity in Ad Hoc Networks," in *IEEE Global Telecommunications Conference (GLOBECOM)*, vol. 6, 29 Nov.-3 Dec. 2004, pp. 3588–3593.

[157] G. Bianchi, L. Fratta and M. Oliveri, "Performance Evaluation and Enhancement of the CSMA/CA MAC Protocol for 802.11 Wireless LANs," in *IEEE International Symposium on Personal, Indoor and Mobile Radio Communications (PIMRC)*, vol. 2, 15-18 Oct. 1996, pp. 392–396.

[158] V. Erceg et al., "TGn Channel Models," IEEE P802.11, 802.11-03/940r4, Tech. Rep., 2004.

[159] O. Besson and P. Stoica, "Decoupled Estimation of DOA and Angular Spread for Spatially Distributed Sources," in *IEEE Asilomar Conference on Signals, Systems, and Computers (ACSSC)*, vol. 1, 24-27 Oct. 1999, pp. 253–257.

[160] H. Wheeler, "The Grating-Lobe Series for the Impedance Variation in a Planar Phased-Array Antenna," *IEEE Transactions on Antennas and Propagation*, vol. 14, no. 6, pp. 707–714, Nov. 1966.

[161] R. Das, "Concentric Ring Array," *IEEE Transactions on Antennas and Propagation*, vol. 14, no. 3, pp. 398–400, May 1966.

[162] J. Gu, H. Stark and Y. Yang, "Wide-Band Smart Antenna Design Using Vector Space Projection Methods," *IEEE Transactions on Antennas and Propagation*, vol. 52, no. 12, pp. 3228–3236, Dec. 2004.

[163] O.M. Bucci, G. Franceschetti, G. Mazzarella and G. Panariello, "Intersection Approach to Array Pattern Synthesis," *Proceedings of the IEE*, vol. 137, no. 6, pp. 349–357, Dec. 1990.

[164] R. Vescovo, "Power Pattern Synthesis for Antenna Arrays with Null Constraints in the Near-Field Region," *Microwave and Optical Technology Letters*, vol. 44, no. 6, pp. 542–545, 20^{th} Mar. 2005.

[165] ——, "Null Formation with Excitation Constraints in the Pattern Synthesis for Circular Arrays of Antennas," *Electromagnetics*, vol. 21, no. 3, pp. 213–230, 1^{st} Apr. 2001.

[166] ——, "Null Control for Linear Arrays by Phase-only or Amplitude Only Modification of the Excitations," in *IEEE Antennas and Propagation Society International Symposium (APS)*, vol. 3, 11-16 Jul. 1999, pp. 2044–2047.

[167] ——, "Constrained and Unconstrained Synthesis of Array Factor for Circular Arrays," *IEEE Transactions on Antennas and Propagation*, vol. 43, no. 12, pp. 1405–1410, 1995.

[168] T.J. Peters, "Phase-Only Synthesis for Multiple Beam Phased Arrays with Element Failures," in *IEEE Antennas and Propagation Society International Symposium (APS)*, vol. 3, 18-25 Jul. 1992, pp. 1352–1355.

[169] E. Lier, D. Purdy and K. Maalouf, "Study of Deployed and Modular Active Phased-Array Multibeam Satellite Antenna," *IEEE Antennas and Propagation Magazine*, vol. 45, no. 5, pp. 34 – 45, Oct. 2003.

[170] C.P.-Baliarda and R. Pous, "Fractal Design of Multiband and Low Side-Lobe Arrays," *IEEE Transactions on Antennas and Propagation*, vol. 44, no. 5, pp. 730–739, May 1996.

List of publications

Conference proceedings

[171] F. Babich, M. Comisso, M. D'Orlando and L. Manià, "Performance Evaluation of MANETs Using Smart Antennas in Multipath Fading Environment," in 2^{nd} *IEEE International Symposium on Wireless Communication Systems (ISWCS)*, Siena (Italy), 5-7 Sep. 2005, pp. 327–331.

[172] [1]M. Comisso, F. Babich, M. D'Orlando and L. Manià, "Simultaneous Communications in Ad-Hoc Networks Using Smart Antennas in Multipath Environment," in *IEEE Global Telecommunications Conference (GLOBECOM)*, San Francisco, California (USA), 27 Nov.-1 Dec. 2006.

[173] F. Babich, M. Comisso and L. Manià, "Multi-Antenna Techniques for Wireless Mesh Networks in an Outdoor Environment," in *IEEE International Conference on Communications (ICC)*, Glasgow, Scotland (UK), 24-27 Jun. 2007, pp. 4961–4966.

[174] F. Babich and M. Comisso, "Channel Coding and Multi-Antenna Techniques for Distributed Wireless Networks," in *IEEE Global Telecommunications Conference (GLOBECOM)*, Washington, DC (USA), 26-30 Nov. 2007, pp. 4180–4184.

[175] F. Babich and M. Comisso, "Throughput Maximization in 802.11 Wireless Networks Employing Adaptive Antenna Arrays," in *IEEE International Conference on Communications (ICC)*, Beijing, China, 19-23 May 2008.

[1]Best student paper award finalist

Journal papers

[176] F. Babich, M. Comisso, M. D'Orlando and L. Manià, "Interference Mitigation on WLANs Using Smart Antennas," *Wireless Personal Communications*, vol. 36, no. 4, pp. 387–401, Mar. 2006.

[177] M. Comisso and R. Vescovo, "Exploitation of Spatial Channel Model for Antenna Array Synthesis" *Electronics Letters*, vol. 42, no. 19, pp. 1079–1080, 14$^{\text{th}}$ Sep. 2006.

[178] M. Comisso and R. Vescovo, "Multi-Beam Synthesis with Null Constraints by Phase Control for Antenna Arrays of Arbitrary Geometry," *Electronics Letters*, vol. 43, no. 7, pp. 374–375, 29$^{\text{th}}$ Mar. 2007.

[179] F. Babich, M. Comisso, M. D'Orlando and L. Manià, "Performance Evaluation of Distributed Wireless Networks Using Smart Antennas in Low-Rank Channel," *IEEE Transactions on Communications*, vol. 55, no. 7, pp. 1344–1353, Jul. 2007.

[180] F. Babich, M. Comisso and L. Manià, "Sustainable Simultaneous Communications in Ad-Hoc Networks Using Smart Antenna Systems," *ACM Wireless Networks*, accepted for publication.

[181] F. Babich, M. Comisso and L. Manià, "Performance Comparison of Advanced Antenna Systems for Wireless Mesh Routers in an Outdoor Environment," submitted to *International Journal of Wireless and Mobile Computing*.

[182] F. Babich and M. Comisso, "Throughput and Delay Analysis of 802.11-Based Wireless Networks Using Smart and Directional Antennas," *IEEE Transactions on Communications*, accepted for publication.